TECHNICAL REPORT S-68-7

ANALYSIS OF DATA FROM INSTRUMENTATION PROGRAM, PORT ALLEN LOCK

by

W. C. Sherman, Jr.
C. C. Trahan

September 1968

Sponsored by

Office, Chief of Engineers
U. S. Army

Conducted by

U. S. Army Engineer Waterways Experiment Station
CORPS OF ENGINEERS
Vicksburg, Mississippi

Destroy this report when no longer needed. Do not return it to the originator.

The findings in this report are not to be construed as an official Department of the Army position, unless so designated by other authorized documents.

TECHNICAL REPORT S-68-7

ANALYSIS OF DATA FROM INSTRUMENTATION PROGRAM, PORT ALLEN LOCK

by

W. C. Sherman, Jr.
C. C. Trahan

September 1968

Sponsored by

Office, Chief of Engineers
U. S. Army

Conducted by

U. S. Army Engineer Waterways Experiment Station
CORPS OF ENGINEERS
Vicksburg, Mississippi

ARMY-MRC VICKSBURG, MISS.

FOREWORD

This report presents the results of instrumenting Port Allen Lock to obtain engineering data for use in the analysis and design of similar structures and to determine the validity of the assumptions and procedures used to design Port Allen Lock. The instrumentation of Port Allen Lock was conducted by the U. S. Army Engineer Waterways Experiment Station (WES), Vicksburg, Mississippi, at the request of the Office, Chief of Engineers (OCE), for the U. S. Army Engineer Division, Lower Mississippi Valley (LMVD), which has overall supervision of the comprehensive program for instrumentation of Port Allen Lock. Collection and analysis of data were made under CW 030, "Prototype Analysis, Structural Behavior of Concrete Structures." WES planned the instrumentation, provided technical supervision of installation of instruments and devices, analyzed all observational data, and prepared this report.

Port Allen Lock was designed by the LMVD and was built under the supervision of the U. S. Army Engineer District, New Orleans, Louisiana. Geological studies, foundation investigation, and soils design studies were made by WES. The plan for the instrumentation was developed by WES, and the devices were installed by the New Orleans District, except for electrical measuring devices, which were installed by WES.

Calibration tests on electrical instruments and installation of the electrical measuring devices were supervised by Mr. L. M. Duke, Instrumentation Branch, WES; the field installation was supervised by Mr. R. C. Austin, Project Engineer, and Mr. C. J. Nettles, Instrumentation Engineer. Messrs. H. A. Hueseman and R. V. Bankston, New Orleans District, were also actively engaged in the supervision of installation of instruments. Laboratory tests on concrete were conducted by the Concrete Division, WES,

under the direction of Mr. E. E. McCoy. Overall supervisor of the instrumentation program was Mr. R. I. Kaufman, LMVD. Engineers at WES who were actively engaged in the investigation included Messrs. W. C. Sherman, Jr., C. C. Trahan, and D. C. Banks. Messrs. C. I. Mansur, J. D. Perrine, J. M. Duncan, and C. G. Hadjidakis, all formerly of WES, also participated in the study.

Messrs. Sherman and Trahan analyzed the data and prepared this report under the general supervision of Messrs. W. J. Turnbull and J. R. Compton, Soils Division, WES. The report was reviewed by the New Orleans District, and reviewed and approved by the LMVD and OCE prior to publication.

Directors of WES during the investigation and the preparation of this report were COL Edmund H. Lang, CE; COL Alex G. Sutton, Jr., CE; COL John R. Oswalt, Jr., CE; and COL Levi A. Brown, CE. Technical Director was Mr. J. B. Tiffany.

CONTENTS

	Page
FOREWORD	v
CONVERSION FACTORS, BRITISH TO METRIC UNITS OF MEASUREMENT	ix
SUMMARY	xi
PART I: INTRODUCTION	1
Purpose of Instrumentation Program	1
Scope of Report	1
Description of Structure	2
Construction	4
PART II: FOUNDATION DESIGN	8
Foundation Conditions	8
U-Frame Design	10
PART III: INSTRUMENTATION	25
General Plan	25
Bench Mark and Level Observations	25
Heave and Settlement Reference Points	26
Sounding Wells and Piezometers	34
Electrical Measuring Devices	35
Wall Deflection Pipes	39
PART IV: REBOUND, SETTLEMENT, AND DEFLECTION	41
Rebound and Settlement	41
Deflection of Base Slab	53
PART V: EARTH PRESSURES AND WALL MOVEMENTS	58
Sand Backfill	58
Observed Earth Pressures	58
Wall Movements	61
Earth Pressure Coefficients	62
PART VI: FOUNDATION BASE PRESSURES AND UPLIFT	65
Foundation Base Pressures	65
Comparison of Observed and Predicted Base Pressures	68
PART VII: BENDING MOMENTS IN BASE SLAB AND WALLS	70

CONTENTS

	Page
Moments Based on Applied Loads	70
Computation of Moments from Deflection	77
Moments from Internal Stresses	79
Moments Computed Using Theory of Beams On Elastic Foundations	84
PART VIII: CONCLUSIONS AND RECOMMENDATIONS	90
Conclusions	90
Recommendations	92
LITERATURE CITED	95
TABLE 1	
PLATES 1-70	
APPENDIX A: DESCRIPTION, CALIBRATION, AND INSTALLATION OF ELECTRICAL MEASURING DEVICES	A1
Electrical Measuring Devices	A1
Installation of Electrical Measuring Devices	A10
TABLES A1-A6	
APPENDIX B: DESCRIPTION, CALIBRATION, AND INSTALLATION OF WALL DEFLECTION PIPES	B1
Description and Calibration	B1
Installation of Wall Deflection Pipes	B6
TABLE B1	
APPENDIX C: RESULTS OF TESTS ON CONCRETE, REINFORCING STEEL, AND SAND BACKFILL	C1
Purpose of Tests	C1
Laboratory Tests on Concrete	C1
Tests on Reinforcing Steel	C9
Tests on Concrete Cylinders	C9
Tests on Sand Backfill	C12
TABLES C1-C6	

CONVERSION FACTORS, BRITISH TO METRIC UNITS OF MEASUREMENT

British units of measurement used in this report can be converted to metric units as follows:

Multiply	By	To Obtain
inches	2.54	centimeters
feet	0.3048	meters
yards	0.9144	meters
miles	1.609344	kilometers
square inches	6.4516	square centimeters
square feet	0.092903	square meters
cubic yards	0.764555	cubic meters
gallons	3.78533	liters
pounds	0.45359237	kilograms
tons	907.185	kilograms
kips	453.59237	kilograms
pounds per square inch	0.070307	kilograms per square centimeter
pounds per square foot	4.88243	kilograms per square meter
pounds per cubic foot	16.0185	kilograms per cubic meter
Fahrenheit degrees	5/9	Celsius or Kelvin degrees*

* To obtain Celsius (C) temperature readings from Fahrenheit (F) readings, use the following formula: $C = (5/9)(F - 32)$. To obtain Kelvin (K) readings, use: $K = (5/9)(F - 32) + 273.16$.

SUMMARY

Port Allen Lock is a reinforced concrete U-frame structure located on the west bank of the Mississippi River near Baton Rouge, La. The structure was founded at a depth of 53 ft in an abandoned channel deposit of the Mississippi River. The deposit consists primarily of silty and clayey soils extending to depths of from 100 to 150 ft. One of the most important elements in the design of the lock chamber was the assumption regarding the distribution of pressures at the base of the lock. A trapezoidal distribution of base pressures was assumed. The base pressure distribution was determined by a trial method in which the plastic and elastic deformation of the base slab and the corresponding deformation of soil foundation were computed for various assumed base pressure distributions until the desired agreement between structure and soil deformations was obtained.

At the request of the Office, Chief of Engineers, a comprehensive plan for the instrumentation of Port Allen Lock was developed to obtain engineering data for use in future analysis and design of similar structures and to determine the validity of certain assumptions and procedures used to design Port Allen Lock. The plan included the measurement of earth and hydrostatic pressures beneath the base slab and along the walls of the lock and the measurement of stresses and strains within the base slab and walls of the lock. Settlement of the lock was to be determined from observations of settlement reference points, bolts, and plates at various locations in the lock. Deflections of the walls were to be determined by means of wall deflection pipes and a deflectometer.

Engineering measuring devices were read at periodic intervals during and after construction. All devices were read for case II', a condition similar to design case II (lock completed with no water in the lock) and case III', a condition similar to design case III (maximum water level in the lock). Case I condition, in which the lock structure was assumed to be complete before placement of backfill, was not attained during construction since the backfill was brought up concurrently with the walls. The data obtained for the two conditions were analyzed and compared with design predictions.

Observed rebounds were greater than those predicted in design; observed settlements were less than those predicted in design. Settlement observations indicated that the lock settled at a uniform rate during construction, and after construction the rate of settlement decreased

sharply. Rebounds and settlements at monolith 15 were recomputed using actual observed loading conditions, which differed somewhat from those assumed for design. The recomputed rebounds were in good agreement with observed rebounds; however, the recomputed settlements were somewhat greater than observed settlements. It was concluded that for structures founded on alluvial deposits, the computed settlement would indicate the general magnitude of settlement to be expected but would not provide a sufficiently accurate estimate of the deflected shape of the base of the structure.

Observations of soil stress meters and piezometers beneath the lock chamber indicated that there were considerable differences between the observed base pressures and those based on the actual weight of the structure. The observed distributions of effective base pressures beneath the lock for cases II' and III' were in the general shape of a concave parabola, with maximum pressures occurring 40 to 50 ft from the center line of the lock. The difference between the observed base pressures (reaction) and the total structural load is attributed to frictional soil forces acting on the outer sides of the lock.

It was found that the coefficient of lateral earth pressure k varied along the height of the wall. For case II' condition, k varied from 0.6 near the top of the wall to 0.3 near the bottom of the wall. For case III', k varied from 1.2 near the top of the wall to 0.3 near the bottom. At the base of the wall, where wall movements were insignificant, k was computed to be 0.31. This value is somewhat lower than that commonly used for the coefficient of earth pressure at rest for sand, and may reflect arching effects caused by the relative settlement of the backfill with respect to the wall.

For case II', moments computed from external loads were affected considerably by the frictional forces acting at the outer sides of the lock. Computed moments in the base slab at the center of the lock were approximately one and one half times the moments computed for design. The primary reason for the discrepancy was the neglect of the frictional forces on the sides of the lock during design. The maximum steel stress for case II' was about 13,600 psi, which is high but not critical. These findings indicate that the structure performed adequately but had a factor of safety somewhat lower than that provided in design. Other computations, including the computation of moments from internal stresses and computation of deflections from moments, verified the presence of frictional forces. It was found that a reasonable estimate of the moments in the base slab could be made by assuming a uniform base pressure distribution and taking into consideration the frictional forces. For case III', frictional forces were essentially zero, and computed moments were in good agreement with moments computed for design.

Computations of base pressures and moments from theoretical consideration of a beam on an elastic foundation were in poor agreement with actual base pressures and moments computed from observed loads.

ANALYSIS OF DATA FROM INSTRUMENTATION PROGRAM
PORT ALLEN LOCK

PART I: INTRODUCTION

Purpose of Instrumentation Program

1. At the request of the Office, Chief of Engineers (OCE), a comprehensive plan for the instrumentation of Port Allen Lock was developed to obtain data on external soil loading, settlement, internal stresses and strains, etc., for use in the analysis and design of similar structures and to determine the validity of certain assumptions and procedures used to design Port Allen Lock. Plans for instrumentation of the lock were initially introduced at a conference concerning the design of U-frame locks held at the Ohio River Division Laboratories, Mariemont, Ohio, in March 1955. At this conference it was concluded that much valuable information could be derived from the observation and analysis of a carefully instrumented U-frame lock founded on typical alluvial soils. OCE subsequently directed the U. S. Army Engineer Division, Lower Mississippi Valley (LMVD), to instrument Port Allen Lock, which had been designed as a U-frame lock. Preparation of the instrumentation program, technical supervision of the installation of the devices, analysis of the data, and preparation of a final report were assigned to the U. S. Army Engineer Waterways Experiment Station (WES), Vicksburg, Miss.

Scope of Report

2. This report contains a summary of soils and foundation studies made in connection with the design of the structure, a description of the engineering measuring devices used in connection with the instrumentation program, analysis and evaluation of observations made during and after construction, and conclusions and recommendations regarding the design of Port Allen Lock and similar structures. Appendix A describes the electrical measuring devices and pertinent features of installation

of the devices. Appendix B describes the wall deflection pipes and their installation. Appendix C presents the results of field and laboratory tests on concrete, reinforcing steel, and sand backfill. Details of the design of the structure that are not included in this report can be found in reference 1. The plan of instrumentation is presented in reference 2, and detailed instructions for installing and observing the instruments are presented in reference 3. References 4 and 5 are interim reports on the instrumentation program. Information presented in the interim reports is also reported herein.

Description of Structure

3. Port Allen Lock (fig. 1) is located on the west bank of the Mississippi River about one mile* south of Port Allen, La., and just across the river from Baton Rouge, La. The lock is at the terminal of the Plaquemine-Morgan City alternate route of the Intracoastal Waterway. A general plan of the area is shown in plate 1. The lock is a reinforced concrete, U-frame structure having a usable chamber 84 ft wide by 1200 ft long, with walls 68 ft high. Most of the lock chamber has an 11.5-ft-thick base slab. A plan and profile of the lock are shown in plate 2; typical sections are shown in plate 3. A U-frame structure without piles was selected because cost estimates indicated that this type structure was more economical than other types considered. A compacted sand backfill was provided adjacent to the walls to provide reliable lateral support when the walls are subjected to loadings producing outward deflections. Collector drains behind the walls discharge at the canal end of the lock and maintain a saturation level at, or slightly above, canal water surface levels. Gates for the lock are of the horizontal frame-miter type designed for a maximum lift of 45 ft. The chamber is filled and emptied by means of 14- by 14-ft longitudinal wall culverts with side ports. Individually operated, segmental, reversed-tainter valves control the flow.

---

* A table of factors for converting British units of measurement to metric units is presented on page ix.

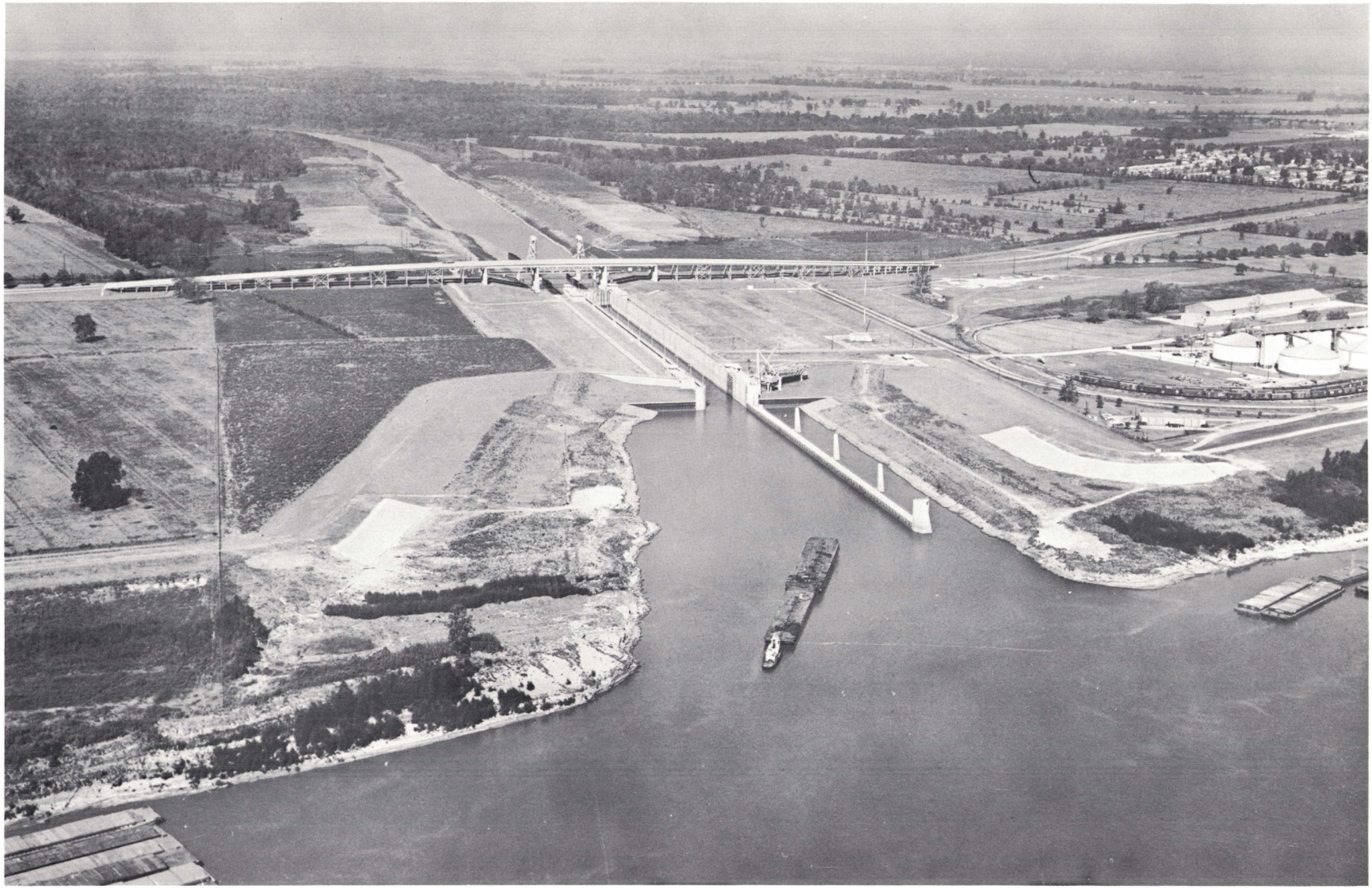

Fig. 1. Aerial view of Port Allen Lock

Construction

General construction notes

4. Port Allen Lock was constructed under the supervision of the U. S. Army Engineer District, New Orleans, La. (NOD). Excavation was initiated in February 1957, and the lock was essentially completed in September 1960 when water was first introduced into the lock. At this time, the canal west of the lock was completed for only a few hundred yards. The lock was completed on 13 April 1961. The canal excavations linking Port Allen Lock to the Intracoastal Waterways Canal were completed on 4 July 1961. The lock was placed in operation on 14 July 1961.

Excavation

5. The construction of the lock required an excavation approximately 1670 ft long and 132 ft wide at the bottom and 53 ft deep with average slopes of about 1 on 5.5. Natural ground surface in the vicinity of the lock is at approximate el 27.* The bottom of the excavation was at el -25.75 in the lock chamber and at el -32.25 at the gate bays. Excavation, which was performed by dragline and hauling equipment, was initiated in February 1957. The excavation was completed to approximate el -18 about May 1958. The final phase of excavation (excavation below approximate el -18) was accomplished just before placement of the stabilization slab. The stabilization slab was a 6-in.-thick, unreinforced concrete slab placed on the bottom of the excavation along the entire length and width of the lock to provide a firm working platform. Excavation was essentially completed in August 1958. An aerial view of the completed excavation with the base slab partially complete is shown in fig. 2.

Construction dewatering

6. Because most of the excavation was below the water table, a dewatering system was installed. The dewatering equipment consisted of a wellpoint system to control seepage from excavation slopes and a system of deep wells to lower the hydrostatic head in the deep sands that underlie

---

* All elevations are in feet referred to mean low gulf (mlg).

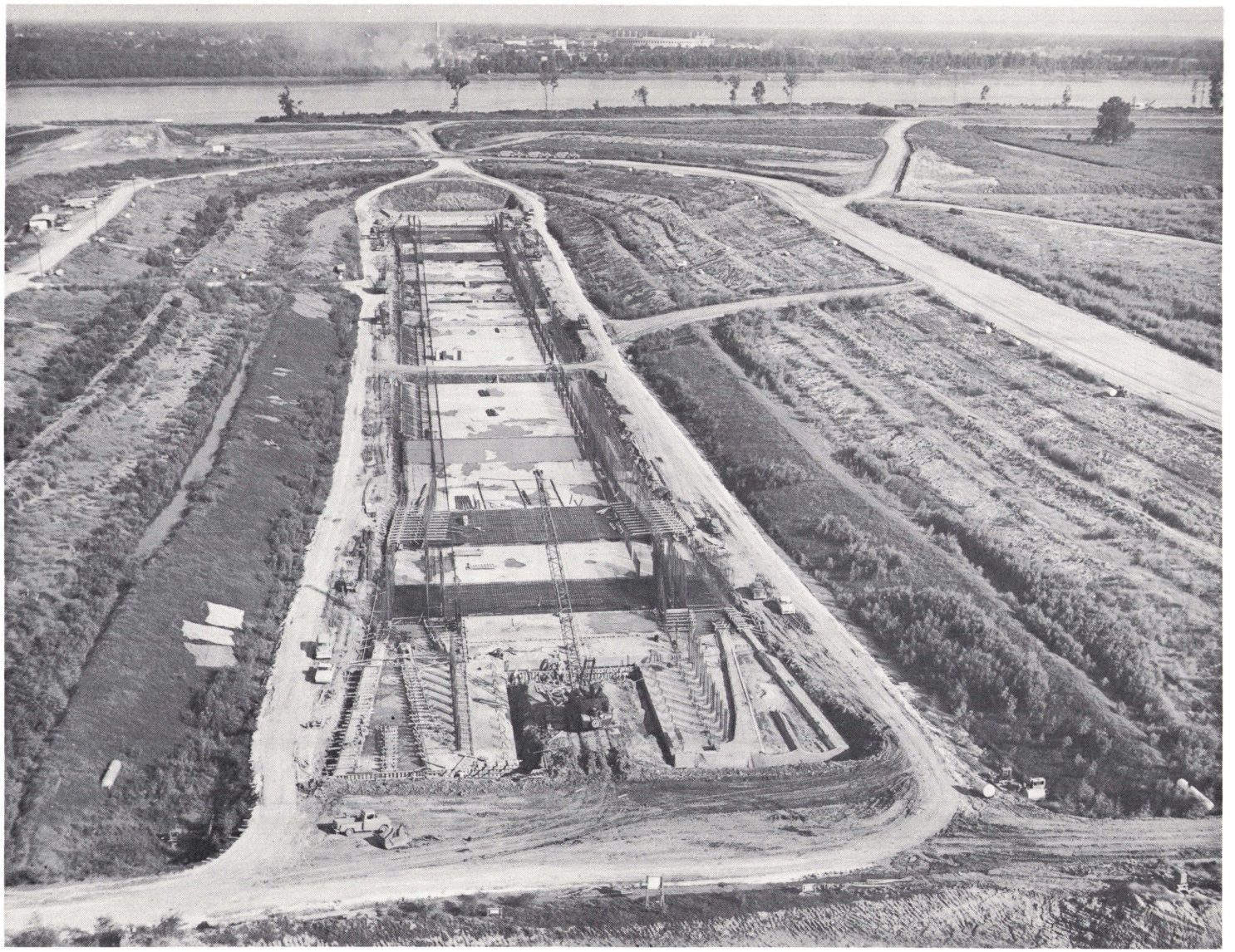

Fig. 2. Aerial view of lock during construction

the site. The wellpoint system consisted of three stages of 25-ft-long wellpoints on 12-, 10-, and 8-ft centers with the headers at el 12, -1, and -17, respectively. The deep well system consisted of 36 wood stave wells located around the top of the excavation. These wells had 10-in.-ID wood screens about 70 ft long with 3/16-in. slots, which were surrounded with 6-in.-thick gravel filters. The wells were pumped by means of deep well turbine pumps to maintain the piezometric level in the deep sand 5 ft or more below the bottom of the excavation before placement of concrete and backfill; higher piezometric levels were permissible during construction. River stages and piezometric levels in the foundation during construction are shown in plate 4. Details of the design and performance of the dewatering system have been described elsewhere.[6]

Concrete placement

7. Placement of concrete in the base slab of the lock was begun in May 1958, and the base slab was completed in November 1958. The lock walls were constructed during the period December 1958-January 1960. Placement of concrete lifts in the wall monoliths was rigidly controlled by the specifications to ensure as uniform loading of the foundation as possible. The lifts of concrete in the walls were so scheduled and placed that at no time was the elevation of the top of concrete in the wall of one monolith more than one lift above the elevation of the top of concrete in the walls of the adjacent monolith. Also, at no time was the elevation of the top of concrete in one wall of a monolith more than one lift above the elevation of the top of concrete in the opposite wall of the same monolith. Concrete operations for the lock were essentially completed in January 1960 when the last wall lift was placed.

Backfill

8. Backfill behind the lock walls consisted of a sand wedge and random backfill as shown in plate 3. Details of the placement and compaction of the sand backfill are presented in Appendix C. The random backfill, which consisted of sandy silt, silty sand, silt, and lean clay was placed in 8-in. layers and compacted with at least 6 passes of a sheepsfoot roller. In areas of modified compaction, the fill was placed in 12-in. layers and compacted with 3 passes of a crawler-type tractor.

Backfilling operations were carried on concurrently with wall construction. Generally, backfill was placed and compacted as soon as possible after the concrete had cured 14 days, except in the case of the culvert walls where no backfill was placed until the roof of the culvert had been completed. Backfill was placed simultaneously on opposite sides of lock monoliths, and the elevation of the top of backfill was kept as nearly uniform throughout the entire length of the structure as practicable. The elevations of the top of the backfill and top of the concrete in the structure at monolith 15 and piezometric levels in the sand backfill are shown in plate 4. Backfilling operations were begun in February 1959 and were completed in May 1960.

PART II: FOUNDATION DESIGN

Foundation Conditions

Site conditions

9. The lock was founded in a deposit filling an abandoned channel of the Mississippi River. The deposit, which forms a strip about 3000 ft wide adjacent and approximately parallel to the river, is composed primarily of silty and clayey soils. The area farther landward is composed of clayey backswamp deposits. These clays and silts overlie a substratum of pervious sand. A generalized soil profile along the lock center line is shown in plate 5, which shows that the lock is located within the abandoned channel deposit.

Field exploration

10. The locations of all pertinent borings made and piezometers installed in the investigation of the foundation conditions for the lock are shown in plate 1. Logs of the borings made along the center line of the lock are shown in plate 6. Borings were of the undisturbed or general sample type. Undisturbed borings in which 5-in.-diam samples were taken in cohesive materials and 3-in.-diam samples were taken in the underlying sands were made to obtain samples for determining consolidation and shear strength characteristics and values of density and permeability. General sample borings were made with cable tool and standard split-spoon samplers.

11. Piezometers were installed in the deep pervious sands along the center line of the proposed lock (at approximately right angles to the Mississippi River) in April 1955 to determine the relation between river stages and hydrostatic pressures in the deep sands. Shallow piezometers in the silty soils were installed at the same time to determine hydrostatic pressures and groundwater levels in these soils. The locations of the piezometers and piezometric data taken during 1955 are shown in plate 5. These observations indicated that the hydrostatic pressures in the deep sands reflected the river stage and that there was only a slight reduction in hydrostatic head in the deep sands landward of the river for at least 4000 ft for river stages up to el 34. From the piezometeric data, it was

concluded that the river had direct access to the substratum sands and that there was little relief due to seepage through the landside top-stratum. The piezometers in the silts overlying the sand stratum reflected the groundwater level in the area and were not so sensitive to fluctuations in river stage as those in the deep sands.

Soil conditions

12. The foundation soils at the structure proper consisted, in order of depth below the ground surface (about el 27), of 10 to 40 ft of fissured fat and lean clays underlain by about 40 to 50 ft of alternating strata of silts and sandy silts with clay strata to about el -50 to -65. Below el -50 to -65, there was a predominance of fat clays that extended to about el -70 to -130. Substratum sands with gravel having a thickness of about 70 to 130 ft underlay the silts and clays. Pleistocene silts and clays, which are very stiff and compact, were encountered approximately at el -200, about 230 ft below ground surface.

13. The water content of the zone of fat and lean clays varied from about 30 to 45 percent and averaged about 35 percent. The underlying strata of silts and sandy silts with clayey strata had water contents of about 25 to 35 percent and split-spoon resistances ranging from about 5 to 50 blows per ft. The deep clay strata below about el -65 were somewhat slickensided; water contents ranged from about 30 to 50 percent. The split-spoon resistances of the deep clays were about 10 to 35 blows per ft. The underlying sands had split-spoon resistances generally in excess of 50 blows per ft.

Laboratory tests

14. Classification and shear strength data. Classification data consisting of mechanical analysis and Atterberg limits on foundation soils beneath the lock are shown in plate 7. The wide range in plasticity characteristics and grain-size distribution of the abandoned channel deposits underlying the lock is demonstrated in this plate. Numerous shear strength tests were performed on the foundation soils for design of the excavation slopes. The data from these tests (not shown in plate 7) indicated that the undrained shear strength increases with depth, the relation

being defined approximately by a c/p ratio* of 0.30. For design purposes, the consolidated-undrained shear strength for the deposits as a whole was taken as ϕ = 25 deg , c = 0.2 ton/sq ft . The average sensitivity of the cohesive soils was about 3.

15. Consolidation tests. Consolidation tests were performed on representative samples of the silty materials, clays, and sands generally below approximate el -26 for the purpose of computing the settlement and distribution of foundation pressure beneath the lock chamber and the gate bays. The consolidation test specimens were loaded to the approximate overburden pressure, unloaded to the estimated stress after excavation for the lock, and then reloaded to obtain a recompression curve. The pressure-void ratio curves obtained for these soils are shown in plate 8; pertinent data for each sample are summarized in the tabulation in plate 8. Overburden pressures and preconsolidation pressures computed from the consolidation tests are shown in fig. 3. The clayey soils below (approximately) el -26 appear to have been consolidated under a pressure averaging about 0.7 ton/sq ft in excess of the existing overburden pressure. This relatively slight overconsolidation was considered to be the result of alternate wetting and drying of the materials during deposition. The preconsolidation pressures for the silty and sandy specimens were difficult to determine because of the very flat shape of the pressure-void ratio curves. In general, the silty materials were found to be less compressible than the clayey soils. The time rate of rebound and consolidation for typical laboratory test specimens is shown in plate 9. Test results indicated that considerable rebound and consolidation of the silts occurred instantaneously with load application, but that only about 20 to 30 percent of the consolidation of the clay strata occurred when the load was first applied.

U-Frame Design

Selection of structure type

16. Port Allen Lock was designed as a reinforced concrete U-frame

---

* Ratio of undrained shear strength to effective overburden pressure.

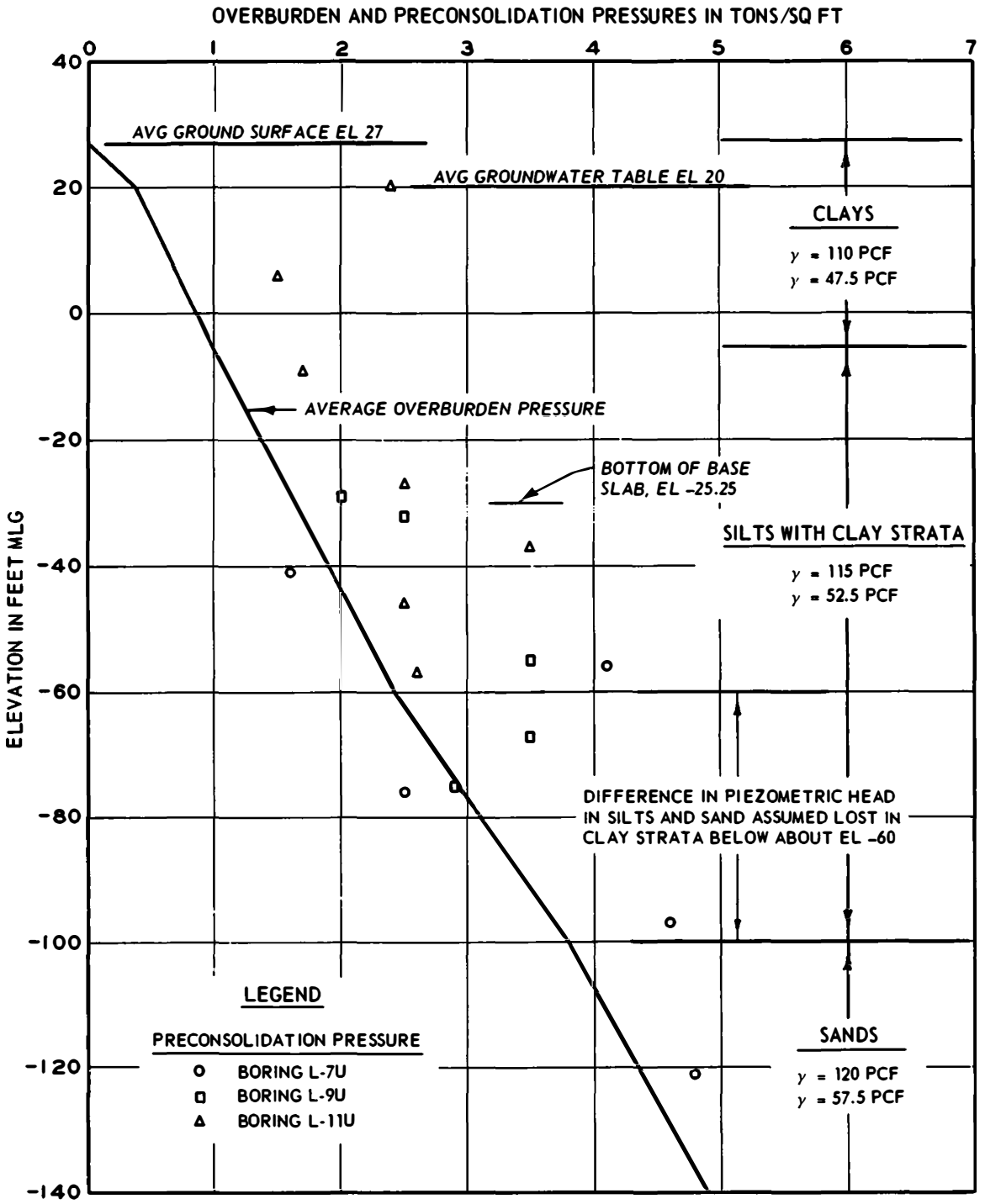

Fig. 3. Overburden and preconsolidation pressures

structure. For subsurface conditions similar to those at Port Allen Lock, a U-frame structure possesses the obvious advantages of eliminating foundation piling and elaborate foundation drainage measures. Although not a unique type of lock construction, the U-frame has not found wide acceptance in the United States, particularly where the foundation soils are relatively compressible, because of the uncertainties in estimating the magnitude and distribution of externally applied pressures.

17. Reinforced concrete, U-frame locks have been used extensively since the turn of the century on the inland waterways of Europe. The introduction of methods for dewatering deep excavations contributed to the widespread use of such structures, and the structures continue to find wide acceptance in Europe, as they are considered safer and cheaper to build than other types. Further advantages are that the chamber can be dewatered safely at any time and a more favorable support of load can be achieved than in the case of chamber walls with a separate foundation, since the structure weight is distributed over a larger area.

Design procedures for U-frame locks

18. The primary forces acting on a U-frame lock are shown in fig. 4. The base pressures oppose the downward load of the lock, which consists of the weight of lock W_C and the weight of the water inside the lock W_W, the weight of the backfill above the culverts W_B, and the vertical component of the lateral earth pressures E_V. The downward thrust W is resisted by the uplift forces u and effective foundation base pressures P. The magnitude of the uplift pressures depends on the upstream and downstream water elevations, the character of the foundation strata, and the nature and effectiveness of measures installed to control uplift pressures. Uplift pressures generally vary significantly along the length of the lock. The distribution of the effective base pressures is dependent upon complex interactions between the soil and structural elements of the lock and is the major unknown factor in design. The lateral pressures exerted on the lock walls include the water pressure in the backfill and in the lock E_W and the effective horizontal earth pressures E_H, which are dependent on the type and in-place characteristics of backfill material, and are also a function of the wall movement. Consequently, the

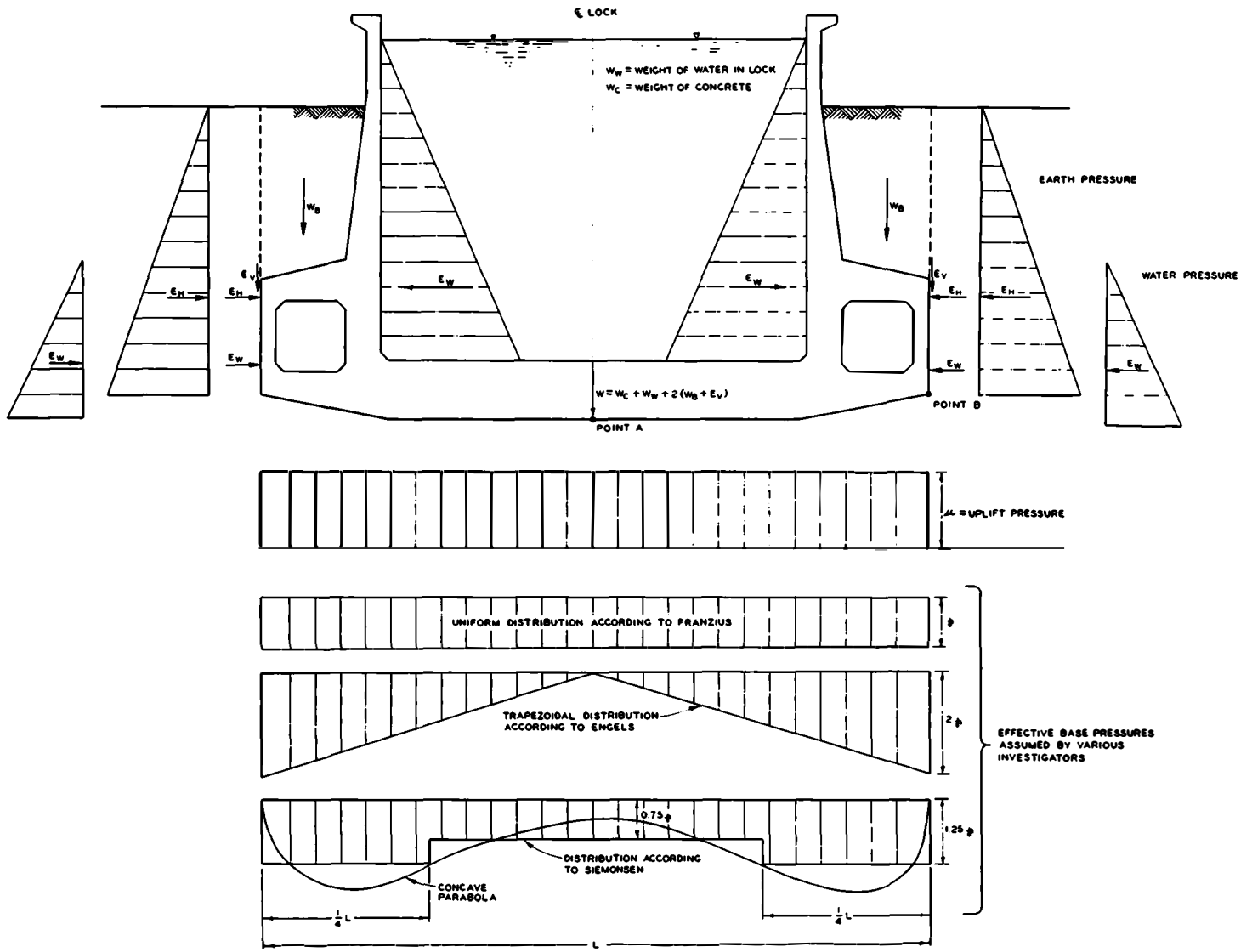

Fig. 4. Force system on lock and assumed base pressure distribution

principal elements of design for a U-frame section consist of ensuring the safety of the chamber sections against flotation, determining the stresses occurring at the center of the base slab and at its juncture with the chamber walls, analyzing the culvert frame, if used, and analyzing the stability of the sidewalls. The design is always based on two principal load conditions: (a) lock empty and (b) lock full. Other load conditions (i.e., lock complete with no backfill placed and lock partially filled) oftentimes as critical may develop during and after construction, and these must also be considered in design.

19. As indicated above, the most important elements in the design of a U-frame structure are the assumption regarding the pressure distribution at the base of the lock and the magnitude and distribution of lateral earth pressures, including vertical components. In the case of relatively rigid base slabs, it is common practice to assume a base pressure distribution, independent of the possible deformations, and to compute the resulting bending moments on the basis of the assumed base pressure distribution. Most early lock construction utilized relatively rigid base slabs, and the following three different assumptions regarding the distribution of base pressures have been commonly used for both the "lock full" and "lock empty" conditions: (a) a uniform pressure distribution, (b) a trapezoidal or double triangular pressure distribution, and (c) a concave parabolic pressure distribution. These distributions are shown in fig. 4. A uniformly distributed load assumption was advocated by Franzius.[7] On the basis of extensive studies, he concluded that for a uniform floor deformation, the stresses in the floor slab assume their highest value for a uniformly distributed pressure. Dehnert[8] attributes the assumption of a trapezoidal distribution to Engels, who assumed that the floor pressure must be at least equal to the maximum uplift for both empty and full chambers. Engels distributed the remainder of the structure load, consisting of deadweight less uplift, over each half of the width of the structure in a triangular fashion. Siemonsen[9] considered the distribution to be represented by a concave parabola and proposed approximating the concave parabola by rectangles for the sake of simplicity (see fig. 4). For the central half of the floor width, the pressure was taken as 0.75 times

the mean pressure, and for the outer quarters of the floor width, 1.25 times the mean pressure. In none of the above-cited design procedures were the relations between the structurally possible deflections of the floor slab and the possible deflections of the subsoil taken into consideration.

20. In the case of U-frame structures with relatively flexible base slabs, various assumptions have been introduced concerning the distribution of the base pressure; however, it has been generally accepted that the most satisfactory method for analyzing such structures is by the theory of elastic beams on a continuous elastic support. This theory is based on the fact that the vertical deformation of the base slab must at every point be equal to the settlement of the underlying foundation soils at the same point. The ratio between the intensity of load on the foundation and the corresponding settlement is designated the coefficient of subgrade reaction. Difficulties associated with the determination of reliable values of the coefficient of subgrade reaction have been discussed by Terzaghi.[10]

21. Examples of U-frame design using the theory of elastic beams on elastic supports have been presented by Benscoter,[11] Hetényi,[12] Ohde,[13] and Smith.[14] In these examples, consideration is given to the fact that the vertical deformation of the slab at a given point depends not only upon the intensity of load at this point but also upon the adjacent stresses and thus upon the entire base pressure distribution. The examples, however, were not considered applicable for the design of Port Allen Lock as they neglect foundation rebound and the effects of backfill placement; nevertheless, an example of a typical solution is presented in this report for comparison with observed base pressures and moments.

Design of base slab for Port Allen Lock

22. In determining the effective foundation base pressures for the design of Port Allen Lock, it was considered that available design procedures using the theory of beams on elastic foundations would not be a logical approach to the problem, as they neglected foundation rebound and the effects of backfill placement. Furthermore, the foundation conditions were relatively complex, and important time effects were anticipated. Therefore, a trial method was used in which the rebound of the foundation

due to excavation and the load imposed by the lock and backfill are taken into consideration, together with the attendant differential settlement between the lock walls and the center of the lock chamber. In this procedure, the distribution of the pressure was assumed to be defined by equating the deformations of the structural base slab and those of the foundation soils, and a distribution of the foundation pressure that satisfies the normal equation of equilibrium is assumed. The corresponding deformations of the soil are then computed on the basis of the consolidation characteristics of the foundation soils. The arbitrary assumption of a base pressure distribution will generally indicate deformations of the slab that differ from the corresponding deformations of the soil. Consequently, new base pressure distributions are chosen and analyzed until the desired degree of agreement between structure and soil deformations is obtained. Various distributions can be assumed. In the case of simple beams, it has been suggested[15] that parabolic distribution of either the second or fourth degree be used. For Port Allen Lock, a trapezoidal distribution was assumed (see fig. 5) that has the advantage that the distribution can be presented in terms of a single factor N for a wide variety of loadings. N is equal to the percentage of uniform base pressure acting beneath the center of the lock. The trapezoidal distribution also greatly facilitates the determination of vertical stresses within the foundation soils for purposes of estimating settlements. The assumption of a trapezoidal base pressure distribution was used for the design of the foundations of the gate bays at Bayou Boeuf Lock.[16] In regard to Port Allen Lock, preliminary assumptions were made with respect to lateral earth pressures against the walls and distribution of the foundation base pressures as expressed by different values of N. Moments and deflections of the base slab were then computed and compared with the deformation of the foundation obtained from a settlement analysis using the assumed base pressure distribution. In computing deflections, base slabs were treated as unreinforced concrete sections, and the elastic deflections were computed assuming that $E = 3{,}000{,}000$ psi. Elastic deflections thus determined were then increased 100 percent to allow for the effect of plastic flow. Results of the rebound and settlement analyses that were made to determine

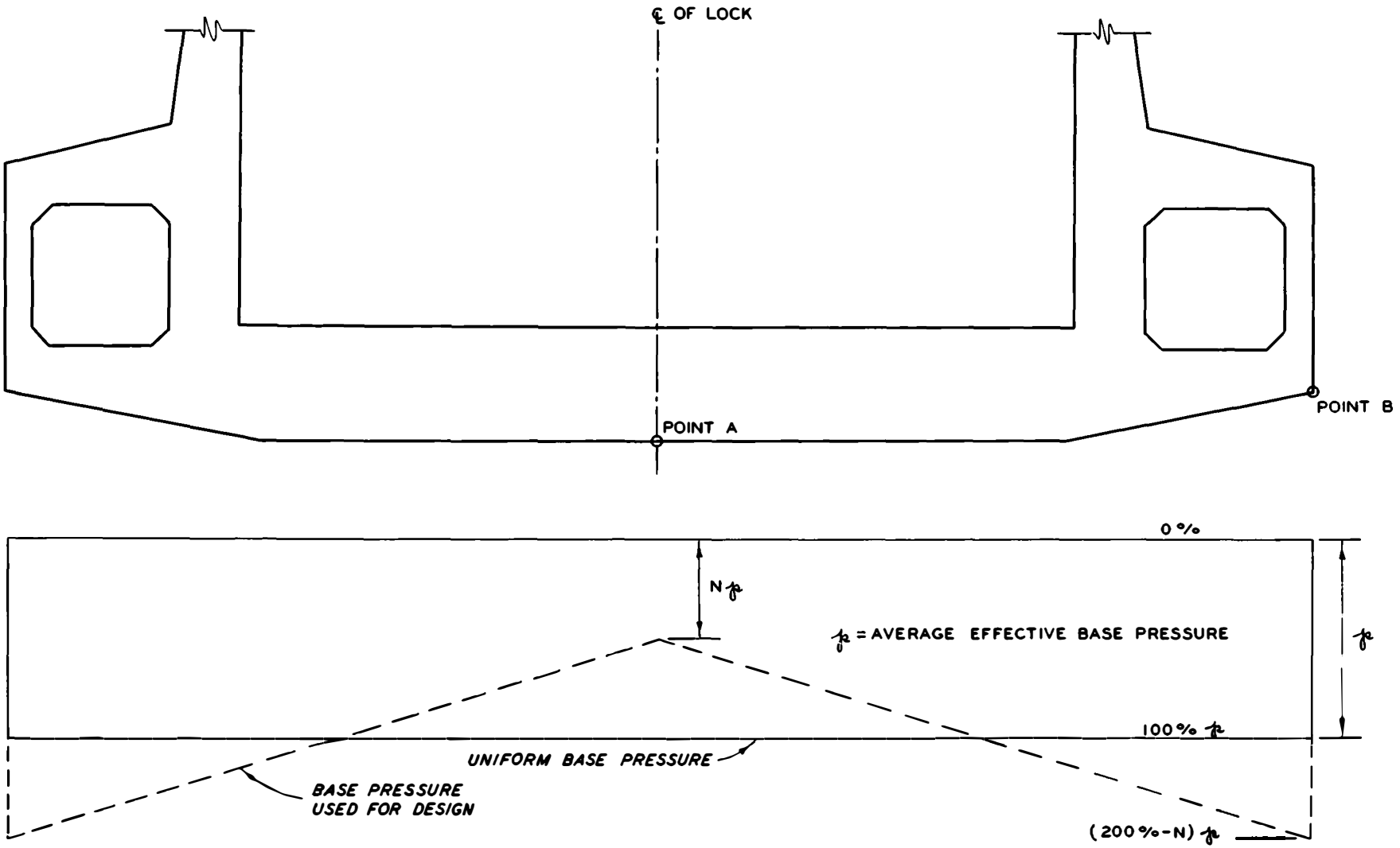

Fig. 5. Assumed base pressure distribution for design

the foundation base pressures for design loading conditions are described below. Analyses were made for each of the gate bays and the center monolith of the lock chamber; only the analysis made for the lock chamber is described.

Rebound and settlement analyses

23. Rebound analysis. It was assumed that the foundation was of an isotropic material to which elastic theory could be applied. All vertical stresses in the foundation were computed using charts and tables based on Boussinesq's equations. In computing the changes in stress due to excavation, it was assumed that the surface of the foundation was located at the level of the bottom of the excavation (el -26) and that the weight of the excavated material was applied as a negative stress at this level. At any depth, the negative stress resulting from excavation added algebraically to the original overburden pressure gave the excavation pressure. The overburden pressures and excavation pressures were computed for the midpoints of each of the design strata below points A and B (see fig. 5) under the lock chamber. Analyses were made for conditions at boring L-9U, which was considered typical of soil conditions beneath the riverward half of the lock chamber, and also for conditions at boring L-7U, which was considered typical of the more compressible materials located beneath the landward portion of the lock chamber (see plate 6 for boring logs).

24. The piezometric data shown in plate 5 were used in estimating the original overburden pressure; the average groundwater level in the silts was assumed to be at el 20, and the average hydrostatic head in the deep sands was assumed to be at el 10. The difference in head between the silts and deep sands was assumed dissipated in the clay stratum between el -72 and -108 in boring L-7U and between el -60 and -69 in boring L-9U (see fig. 3).

25. The foundation rebounds were computed using the rebound loops of the laboratory pressure-void ratio curves. The laboratory curves were adjusted, when necessary, to the computed overburden and excavation pressure for both points. The computed rebound was 3.2 and 2.4 in. at points A and B, respectively, at boring L-7U and 2.7 and 2.3 in. at points A and B, respectively, at boring L-9U.

26. Settlement analysis and determination of N . For design of the lock, settlement and effective base pressure beneath the lock chamber were computed assuming that all foundation rebound would occur before construction of the base slab was initiated. The assumption was considered reasonable, as the laboratory consolidation tests indicated that about 75 percent of the rebound would occur instantaneously. Ultimate settlements were computed for the following three cases:

a. Case I. Structure complete with no backfill in place. Hydrostatic pressures in deep sands and silts assumed lowered to 5 ft below bottom of excavation.

b. Case II. Structure complete with backfill in place, but no water in the lock. Uplift pressure beneath the base slab assumed equal to 33.5 ft (el 7.5). Hydrostatic pressure in deep sands assumed at el +10.

c. Case III. Structure in operation with water level in the lock at el 49. Uplift pressures beneath base slab assumed equal to 46 ft (el 20). Hydrostatic pressure in deep sands assumed at el 35.

27. At each point selected for analysis, ultimate settlements caused by the weight of the first lift of concrete for the base slab (assumed equal to 5.8 ft) were computed assuming this portion of the slab to act as a heavy fluid. All successive differential movement in the structure and foundation was referred to the elevations of the points after the first lift of concrete had set.

28. The ultimate settlement and foundation reaction for each case listed was computed for various assumed values of N (percentage of uniform base pressure at center of lock). The settlements at points A and B for each value of N , after the settlement caused by the first lift of the base slab had been deducted, were plotted as shown in fig. 6. The data in fig. 6 apply to conditions at boring L-9U. Similar plots were prepared for boring L-7U. It was found that the relation between N and settlement could be reasonably approximated by a straight line. On the same plots, the differential settlement between points A and B and the differential movement between points A and B resulting from elastic and plastic movement of the structure underload are shown as functions of N . The intersection of the line of differential movement of points A and B

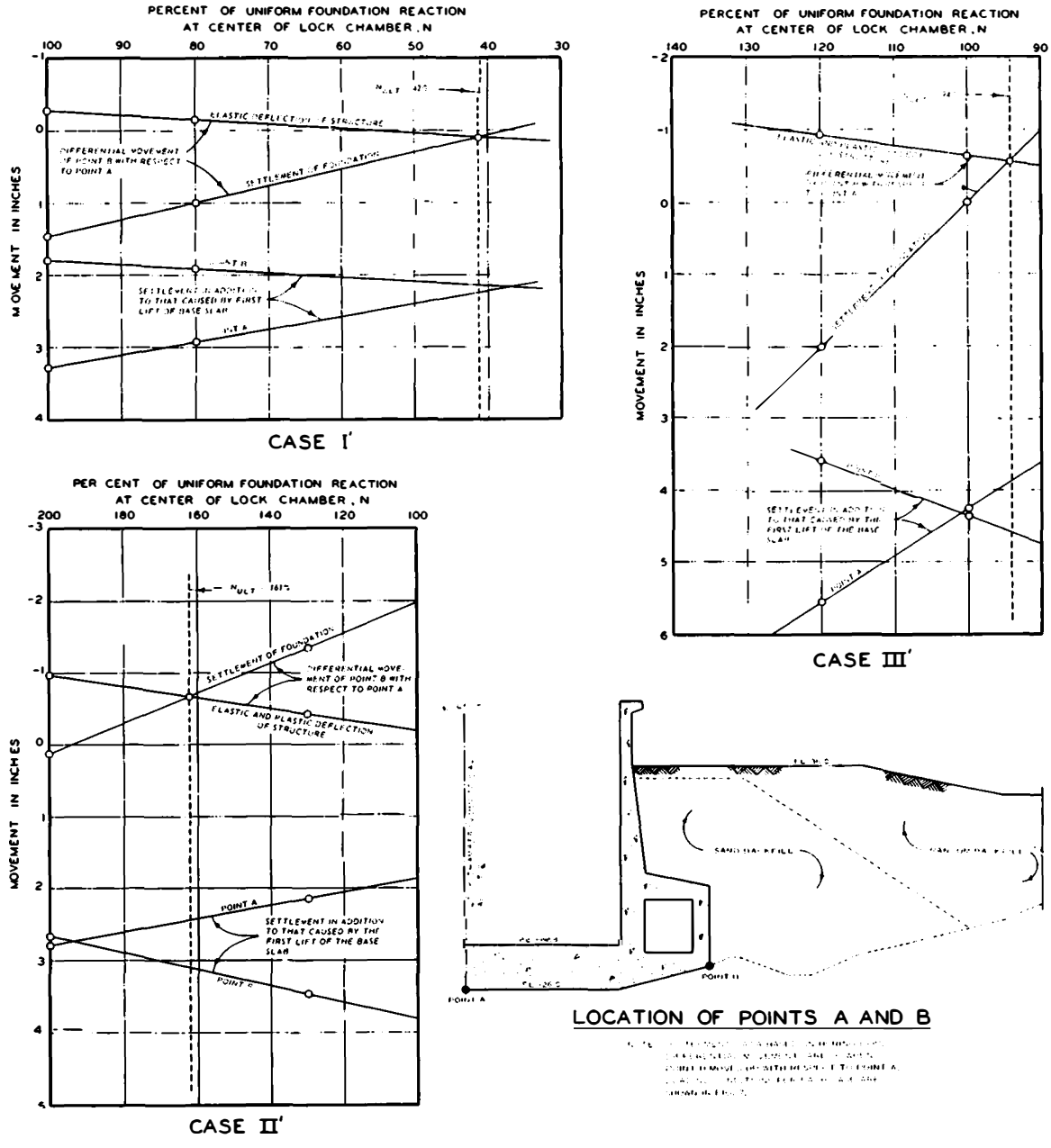

Fig. 6. Determination of base pressure distribution and settlement for design

due to foundation settlement and the line of differential movement of points A and B due to deflection of the structure gave the foundation base pressures in terms of N for each case. A summary of settlements and N values for each case is shown in fig. 6.

29. Design base pressures. A value of N = 200 percent was computed for the foundation base pressure distribution for case II on the basis of boring L-7U, and N = 161 percent on the basis of boring L-9U. Since, however, the base pressure distribution probably would not be exactly trapezoidal but would be somewhat curved, this would tend to reduce the differential settlement and thus give a lower base pressure at the center of the lock. It was also considered possible that the plastic flow of the concrete might in time increase beyond what was assumed, and the foundation might not consolidate fully under the weight of the first lift of concrete before additional load was applied. Both of the above-mentioned factors would tend to decrease the foundation reaction at the center of the lock; consequently, the lock chamber was designed for N = 150 percent for case II loading. This design was also checked for N = 175 percent, allowing an increase in stresses of 33 percent. For cases I and III, respectively, the lock chamber was designed for N = 80 and 100 percent. A summary of the foundation base pressures used for design is shown in fig. 7.

Design of lock chamber walls

30. As shown in fig. 7, the lock chamber walls were designed assuming an at-rest earth pressure for case II and a combination of passive earth pressure and at-rest pressure for case III. A coefficient of at-rest earth pressure equal to 0.5 was assumed. It was considered that maximum wall movements toward the backfill during case III loading would not be sufficient to develop a full passive earth pressure. On the basis of relations between wall movement and lateral earth pressure given by Terzaghi,[17] it was assumed that the mobilization of partial passive pressures could be represented by a coefficient of lateral earth pressure equal to 1. For case III, a coefficient of lateral earth pressure equal to 1 was assumed from the top of backfill to el 7.5, with the earth

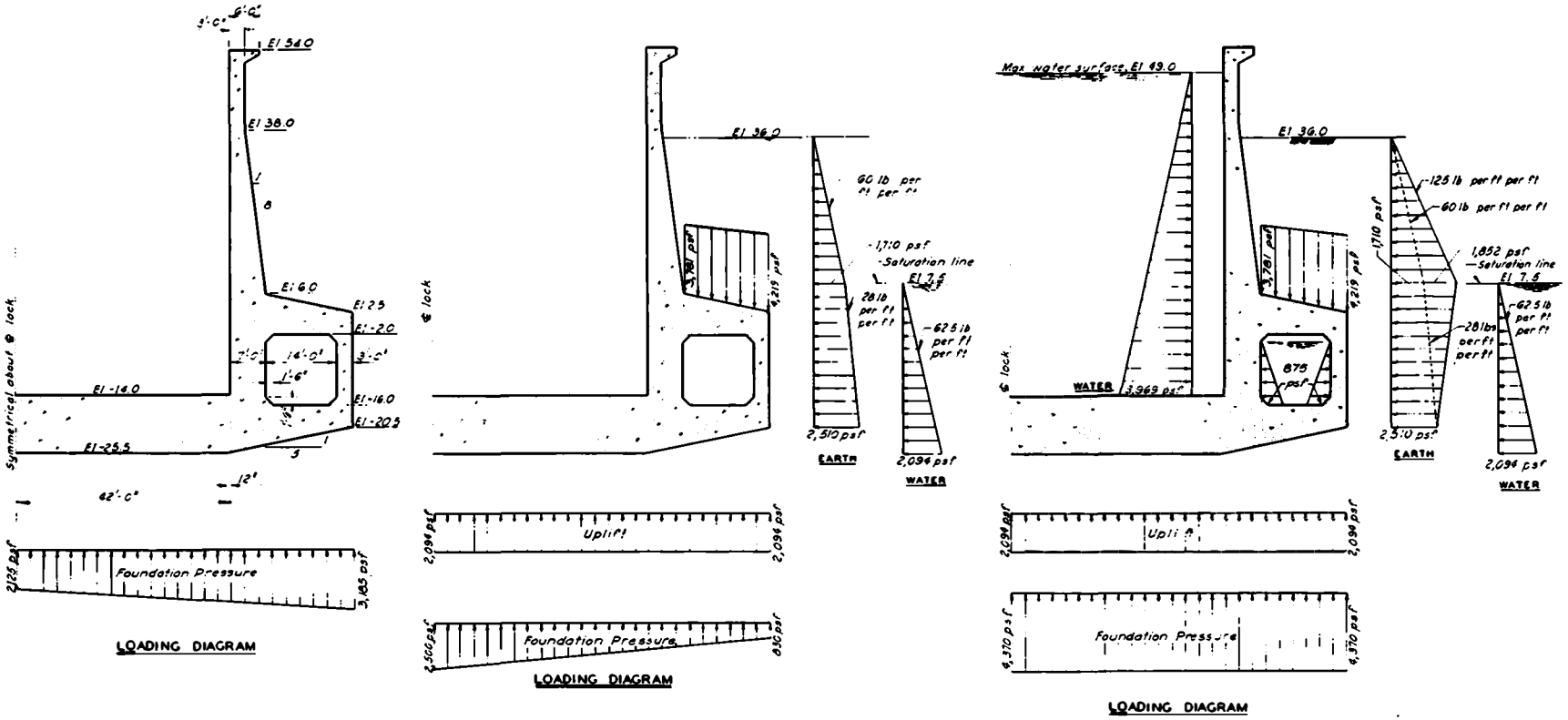

CASE I

LOADING CONDITIONS

STRUCTURE COMPLETE, NO BACKFILL IN PLACE. FOUNDATION PRESSURE DISTRIBUTION ASSUMED TO BE 80 PERCENT OF THE AVERAGE AT THE CENTER LINE AND 120 PERCENT OF THE AVERAGE AT THE HEEL. NO UPLIFT.

CASE II

LOADING CONDITIONS

DEWATERED CONDITION. FOUNDATION PRESSURE DISTRIBUTION ASSUMED TO BE 150 PERCENT OF THE AVERAGE AT THE CENTER LINE AND 50 PERCENT OF THE AVERAGE AT THE HEEL. UNIFORM UPLIFT FROM EL. 7.5. THIS CASE WAS CHECKED FOR A FOUNDATION PRESSURE DISTRIBUTION OF 175 PERCENT OF THE AVERAGE AT THE CENTER LINE ALLOWING AN INCREASE IN STRESSES OF 33 PERCENT. THIS CONDITION WAS NOT CRITICAL.

CASE III

LOADING CONDITIONS

MAXIMUM OPERATING CONDITION. FOUNDATION PRESSURE DISTRIBUTION ASSUMED TO BE UNIFORM. UNIFORM UPLIFT FROM EL. 7.5.

NOTE: LOADS, MOMENTS, AND REINFORCEMENT ARE FOR A ONE-FOOT STRIP.

Fig. 7. Summary of base pressures used for design

pressure decreasing linearly below el 7.5 to at-rest pressure at the base of the structure.

Design of joints

31. To allow for expansion and contraction, and to provide for settlement, the lock was constructed in monoliths ranging from 50 to 113 ft in length as shown in plate 2. Monolith joints were treated as expansion joints in the walls and as crack-control joints in the base slab. Details of the joints between the chamber monoliths are shown in fig. 8. The

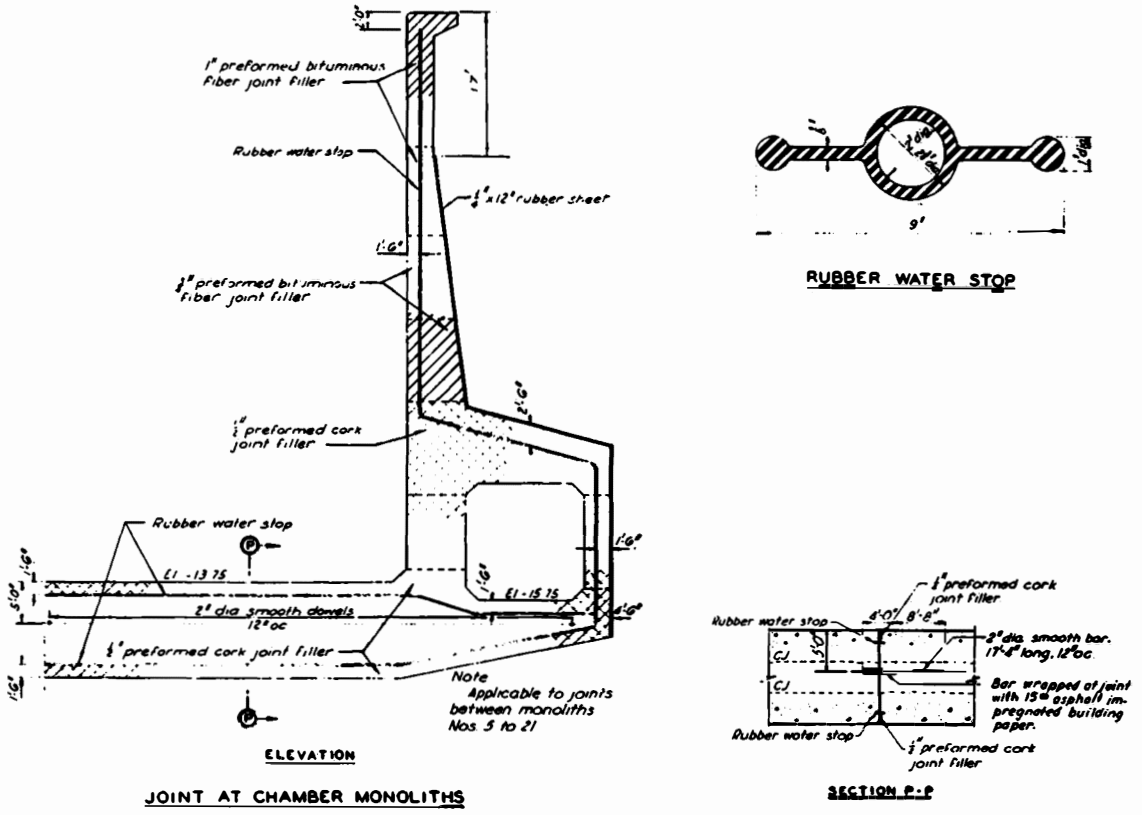

Fig. 8. Details of monolith joints

joints in the base slab contained a 1/2-in.-thick, expanding filler for a distance of about 1-1/2 ft from the top and bottom of the slab. Between these two points, the concrete was placed in contact with adjacent slabs. Three-bulb waterstops were installed near the top and bottom of the slabs. Steel dowels extended through the joints in the base slab and were wrapped about 2 ft on each side of the joint to prevent bonding with the concrete

if contraction should occur and cause the joint to open slightly. These dowels consist of smooth bars and are designed to tie the monoliths together but still allow opening of the joint due to contraction of the concrete. The dowels are also designed to prevent differential settlement between adjacent monoliths at the joint.

32. The thickness of the joint filler in wall joints was determined to allow for structure expansion and movement due to differential settlement of adjacent monoliths. Between lock chamber monoliths, where differential settlement would be minor, the thickness of joint material varies in steps from 1 in. at the top of the wall to 1/2 in. at the bottom. At the gate-bay monoliths, where greater movement was anticipated, the thickness of the joint material at the top of the walls was increased, the maximum being 2 in. between the river approach bay and the river gate bay, and between the canal approach bay and canal gate bay. Each joint was provided with a three-bulb waterstop and covered with a rubber strip to prevent backfill from infiltrating into the joint. To minimize differential settlement of the monoliths, it was specified that backfill be brought up concurrently on each side of the lock as soon as possible, and at as uniform a depth as possible.

PART III: INSTRUMENTATION

General Plan

33. The plan of instrumentation of Port Allen Lock included installation of the following engineering measuring devices:

a. A permanent bench mark.

b. Heave plugs to measure foundation rebound during excavation.

c. Settlement reference points, bolts, and plates to determine settlement at selected points in the lock during and after construction.

d. Sounding wells to determine the elevation of the water at various points in the lock chamber and gate bays.

e. Piezometers to measure hydrostatic pressures beneath the structure and in the backfill behind the walls of the lock.

f. Earth pressure cells to determine the magnitude and distribution of foundation and wall pressures.

g. Strain and stress meters and a pore pressure cell installed in concrete to measure stresses, strains, and pore pressures within the structure.

h. Resistance thermometers in concrete to determine the temperature near the top of the lock walls.

i. Wall deflection pipes to determine the deflection of the walls by means of a deflectometer.

34. The locations of engineering measuring devices are shown in plates 10 and 11. The primary installation of measuring devices, including all electrical measuring devices, was located near the center of the lock at monolith 15 where the lock is founded on about 60 ft of silt with some clay seams. As the canal-end portion of the lock was founded in an area where silty soils extend to a greater depth (about 80 to 100 ft) beneath the lock, some engineering devices were installed in the lock chamber in this area (monolith 6). Measuring devices, except for electrical instruments, were also installed in both of the gate bays.

Bench Mark and Level Observations

35. A permanent bench mark was installed on the north side of the

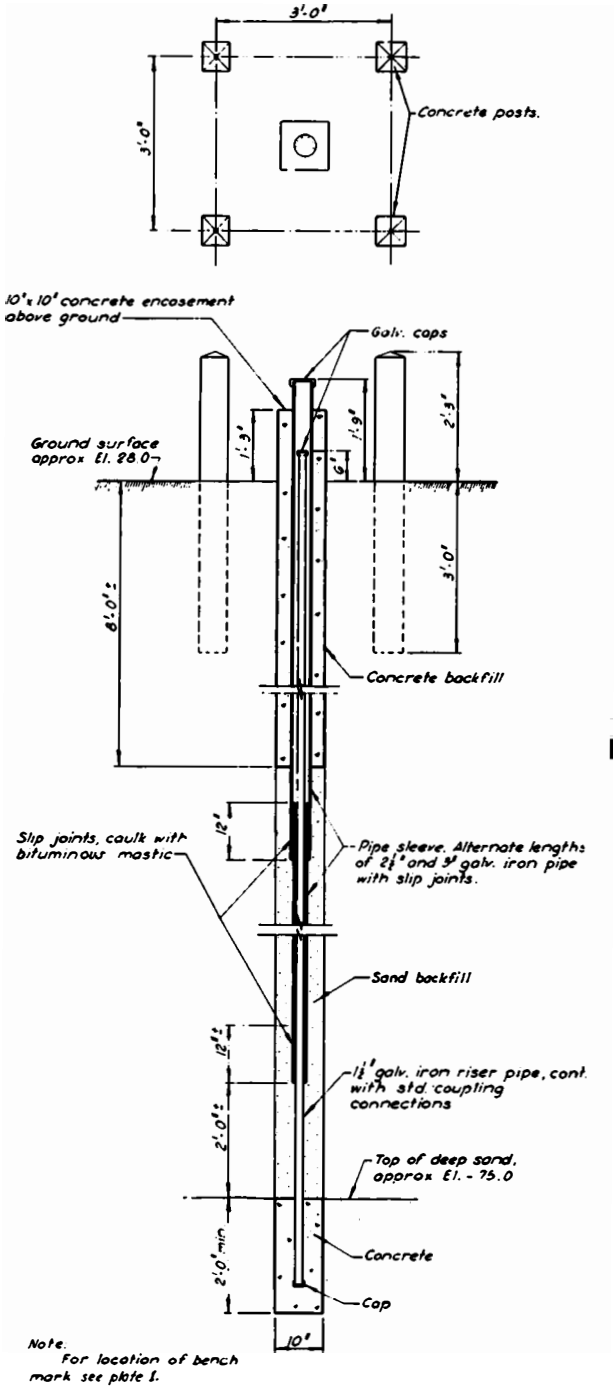

Fig. 9. Details of bench mark

excavation (see plate 1) a sufficient distance from the excavation so that it would not be affected by stress changes due to excavation and subsequent construction. The bench mark was founded in the deep sands, with the riser pipe protected by sleeves to eliminate the effects of drag resulting from movements of the overburden soils. Details of the bench mark are shown in fig. 9. In general, all level observations were referred directly to the permanent bench mark by means of precise leveling techniques.

Heave and Settlement Reference Points

Heave points

36. To determine the rebound of the foundation during and after excavation, seven heave points were installed in the foundation prior to construction. The heave points, each consisting of a 5-in.-diam steel pipe 2 ft long with a vented cap, were driven below the bottom of auger holes to elevations corresponding to about 2 ft below final excavation, and the exact elevation on the top of each heave point was determined at the time of installation. The locations and initial elevations of the heave points are given in table 1. As soon as the excavation

had been brought to grade, the soil above the top of the heave point was excavated carefully by hand, and the top of the heave point was uncovered enough that its elevation could be determined. The elevations were corrected for the lateral effect of the heave joints from the point of installation at ground surface. The lateral offsets are shown in table 1 with the corresponding corrections used to determine the exact elevations of the heave points.

37. The observed rebounds and subsequent settlements are shown in plates 12 through 16. Maximum observed rebound varied from 0.36 ft at monolith 2 to 0.26 ft at monolith 24. Analysis of the observed rebound and settlements is presented in Part IV of this report.

Temporary settlement reference points

38. Temporary settlement reference points were installed to determine settlement of the foundation during construction until permanent reference points were installed. Three of the points were installed in each gate bay (monoliths 2 and 24), five were installed in monolith 6, and five in monolith 15. Details of the reference points are shown in fig. 10. The reference points were driven about 3-1/2 ft into the foundation at the bottom of the final excavation just prior to placement of the stabilization slab. The elevations of the temporary reference points were obtained concurrently with those of adjacent heave points so that a continuous record of foundation movement was obtained. The temporary reference points were observed until the elevations were transferred to permanent reference points on the floor of the lock and on top of the culvert. The observed movements of the temporary reference points are shown in plates 12 through 15.

Type A reference points

39. Three type A reference points were installed at el -42.5, -69, and -90 in the foundation beneath the south edge of monolith 15 to obtain a comparison between the observed and estimated settlement of the foundation at these elevations. Two additional type A reference points were installed in the deep sands at el -90 and -120 at the river-side and landside gate bays, respectively. Details of the type A reference points and locations of the points are shown in fig. 11 and in plates 10 and 11.

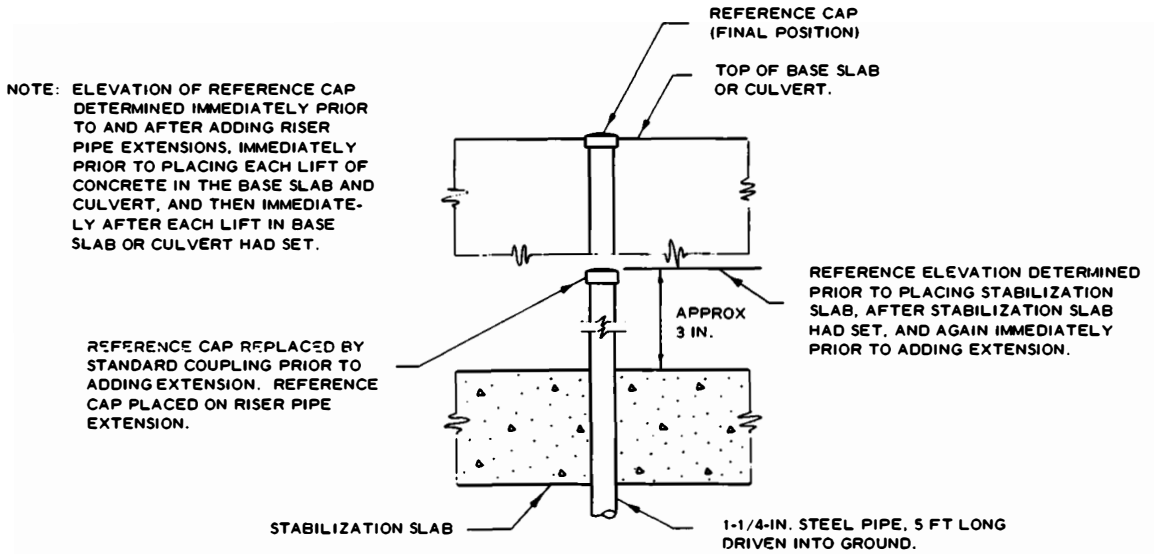

TEMPORARY SETTLEMENT REFERENCE POINT

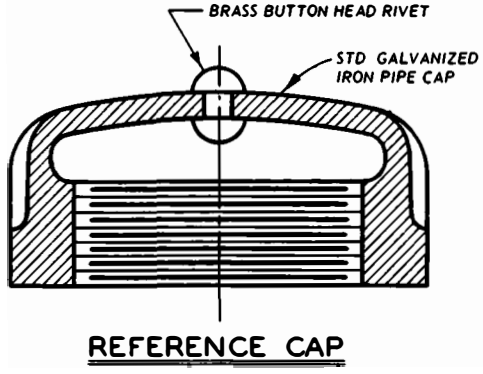

REFERENCE CAP

LOCATION OF TEMPORARY SETTLEMENT REFERENCE POINTS

POINT NO.	MONOLITH NO.	LOCK STATION	OFFSET FROM ℄ LOCK, FT	DATE INSTALLED
T-1	24	745+88	41 N	7 MAY 1958
T-2	24	745+88	℄	7 MAY 1958
T-3	24	745+88	41 S	7 MAY 1958
T-4	15	740+76	65 N	14 MAY 1958
T-5	15	740+76	41 N	14 MAY 1958
T-6	15	740+76	℄	14 MAY 1958
T-7	15	740+76	41 S	14 MAY 1958
T-8	15	740+76	65 S	14 MAY 1958
T-9	6	735+75	65 N	12 JUNE 1958
T-10	6	735+75	41 N	12 JUNE 1958
T-11	6	735+75	℄	12 JUNE 1958
T-12	6	735+75	41 S	12 JUNE 1958
T-13	6	735+75	65 S	12 JUNE 1958
T-14	2	733+38	41 N	6 JUNE 1958
T-15	2	733+38	℄	6 JUNE 1958
T-16	2	733+38	41 S	6 JUNE 1958

Fig. 10. Temporary settlement reference points

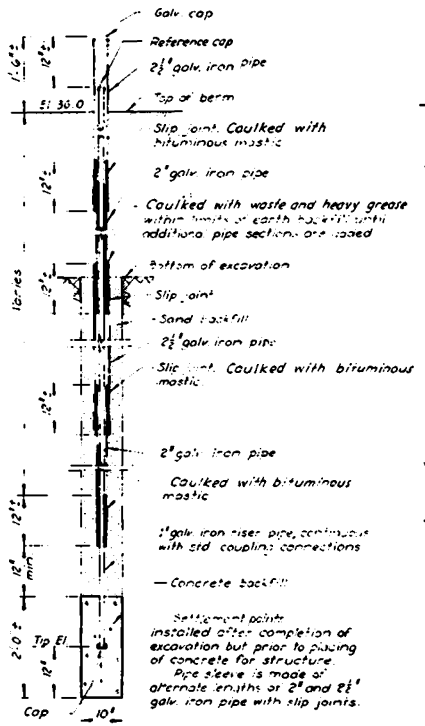

SETTLEMENT REFERENCE
POINT TYPE "A"

LOCATION OF SETTLEMENT REFERENCE POINTS, TYPE "A"

POINT NO	MONOLITH NO.	LOCK STATION	OFFSET FROM ℄ LOCK, FT	TIP EL	DATE INSTALLED
SP-1	15	740+76	71 S	-62.5	22 MAY 1958
SP-2	15	740+79	71 S	-70.0	22 MAY 1958
SP-3A	15	740+84	71 S	-80.0	22 MAY 1958
SP-3B	24	745+95	78 N	-80.0	29 JUNE 1958
SP-3C	2	739+45	80 N	-120.0	9 JUNE 1958

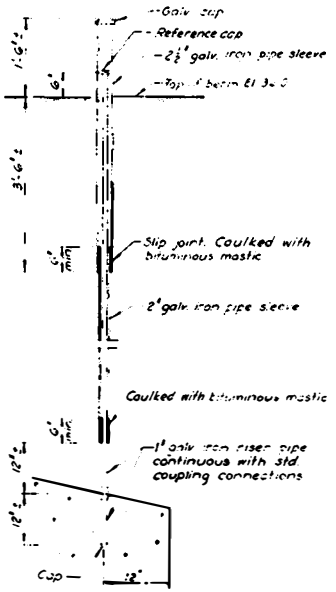

SETTLEMENT REFERENCE
POINT TYPE "B"

LOCATION OF SETTLEMENT REFERENCE POINTS, TYPE "B"

POINT NO	MONOLITH NO	LOCK STATION	OFFSET FROM ℄ LOCK, FT	DATE INSTALLED
SP-4	24	745+80.00	72 N	15 JAN 1959
SP-5	24	745+80.00	72 S	29 JAN 1959
SP-6	15	740+78.75	65 N	27 FEB 1959
SP-7	15	740+78.75	65 S	2 MAR 1959
SP-8	6	735+77.75	65 N	11 MAR 1959
SP-9	6	735+77.75	65 S	16 MAR 1959
SP-10	2	733+40.00	75 N	7 APR 1959
SP-11	2	733+40.00	75 S	16 APR 1959

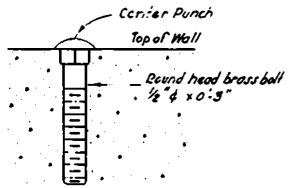

SETTLEMENT REFERENCE BOLT

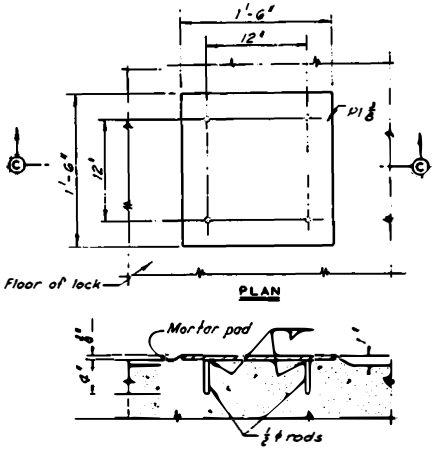

STEEL REFERENCE PLATE

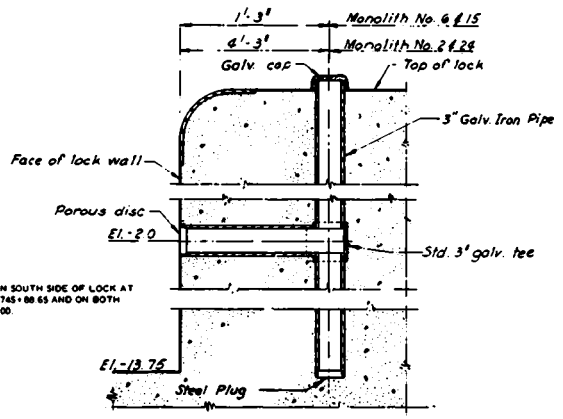

SOUNDING WELL

NOTE: SOUNDING WELLS INSTALLED ON SOUTH SIDE OF LOCK AT STA 739+38.57, 735+83.05, AND 745+88.65 AND ON BOTH SIDES OF LOCK AT STA 740+73.00.

Fig. 11. Settlement reference points, plates, and sounding wells

Each point consisted of a 10-in.-diam by 2-ft-long concrete plug with an embedded riser pipe that extended to ground surface. Additional sections of riser pipe were added as backfill was placed above the reference points. The observed movements of the type A reference points are shown in plate 17.

Type B reference points

40. The elevations of the top of the culverts at monoliths 2, 6, 15, and 24 were determined from type B settlement reference points. Details and locations of these points are shown in fig. 11. Each point is a riser pipe that has its lower end embedded in the concrete structure and its upper portion surrounded by an outer sleeve. The observed data are shown in plates 12 through 15.

Settlement reference plates

41. Description. Nine 18-in.-square stainless-clad steel settlement reference plates were installed near the center of each gate bay and in monoliths 6 and 15 to permit measurements of the deflection and settlement of the base slab during construction and after the lock had been placed in operation. Details and locations of the settlement reference plates are shown in fig. 11.

42. Initial elevations of the plates were determined using both the precise leveling method and a water-level measuring device described below. After the lock had been flooded, the elevations of the plates were determined using either the water-level device or a deepwater sounding device, also described below. The water-level device required the use of a boat and was generally used when the water level in the lock was less than 25 ft. Observations of the settlement plates are shown in plates 12 through 15. Deflections of the base slab computed from the settlement observations are shown in plates 18 through 21.

43. Water-level device. The water-level device, which is shown in fig. 12, consists of 100 ft of 1/2-in.-ID transparent plastic tubing, one end of which is attached to an aluminum sounding rod on which a point gage and vernier are mounted. The other end of the tubing is attached to the bottom of a 5-in.-diam and 2-ft 3-in.-high transparent plastic tank. The tank has two brackets that can be clamped to the rungs of a

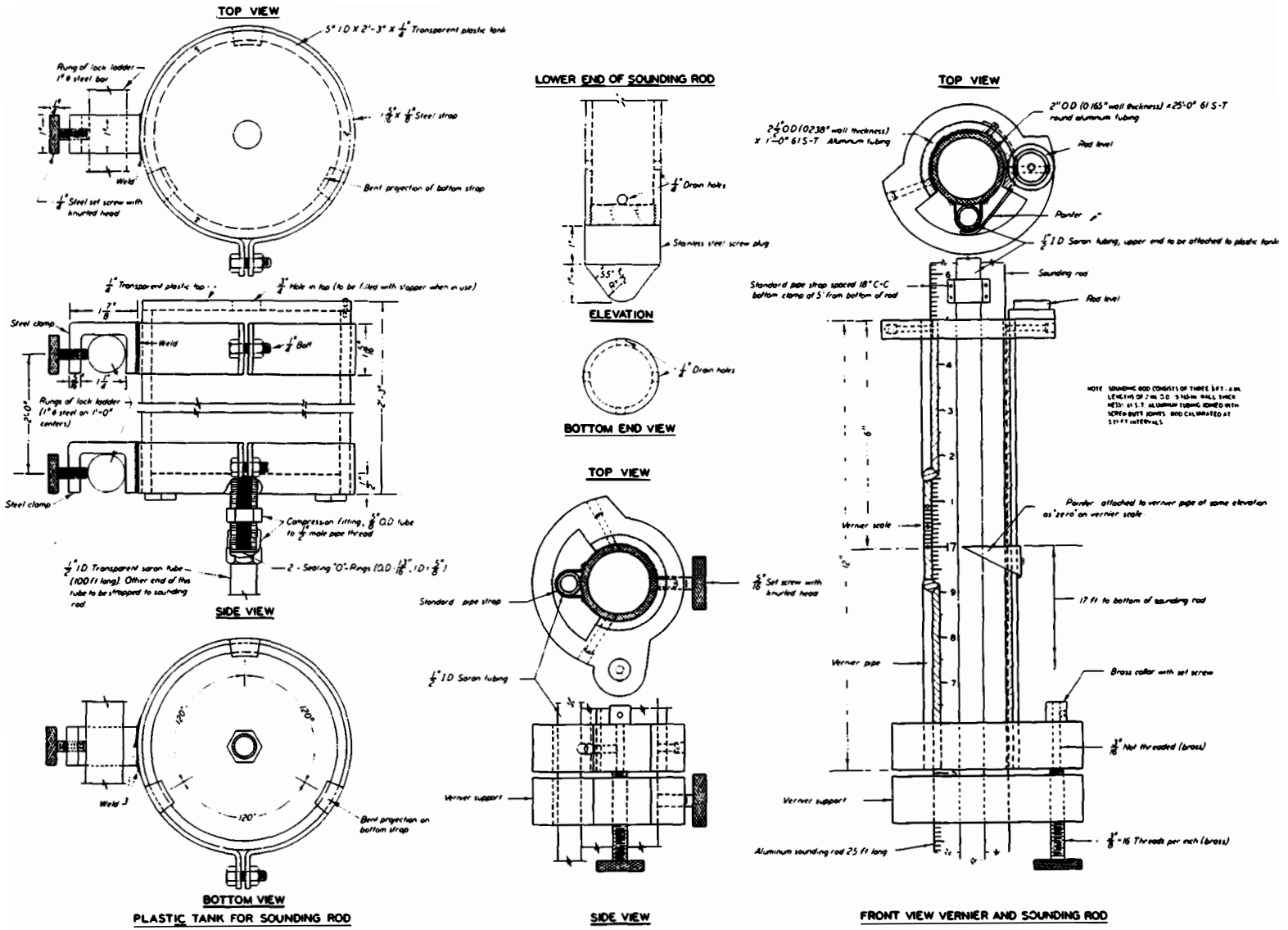

Fig. 12. Details of water-level device

nearby ladder on the lock wall. Water is added to the tank and tubing until the tank remains partially filled when the sounding rod is vertical and seated on a settlement reference plate. When level determinations are being made, the point gage on the sounding rod is set at the water level in the tubing. The length of the sounding rod as measured from the bottom of the rod is inscribed on the rod in 0.01-ft increments. The vernier is subdivided so that the distance from the point gage on the vernier to the bottom of the rod can be read to the nearest 0.001 ft. The sounding rod is maintained plumb during the observation with the aid of a spirit level attached to the rod. The elevation of each settlement plate is determined by subtracting the depth of the plate below the water surface in the plastic tube, as obtained from the sounding rod and vernier, from the elevation of the water in the plastic tank attached to the lock wall. The elevation of the water level in the plastic tank is determined by sounding with a calibrated steel tape from the reference point immediately above the tank on top of the wall. The air and water temperatures are recorded at the time of each observation, and the observed readings are corrected for changes in the length of rod due to temperature changes.

44. Deepwater sounding device. The deepwater sounding device is shown in fig. 13. The device consists of a weighted sounding rod that is suspended above the lock floor by means of a lightweight metal frame with two cables attached. The cables (A and B, fig. 13) are in turn attached to winches on top of the lock walls. The vertical movement of the rod can be controlled from the walls by means of cable C, which is attached to the rod and runs over a pulley attached to the frame for the rod. A 20-lb weight is attached to the bottom of the rod by means of a piano wire of such a length that the top of the rod extends about 5 ft above the top of the wall when the weight rests on the bottom of the lock. The horizontal movement of the rod is controlled by the two winches attached to the tops of the walls. Cables A and B are marked so that the rod can be placed exactly above each settlement plate. Just before the reading is taken, the rod is raised to its maximum height by means of cable C. The rod is then lowered so that the weight attached to the bottom of the rod rests

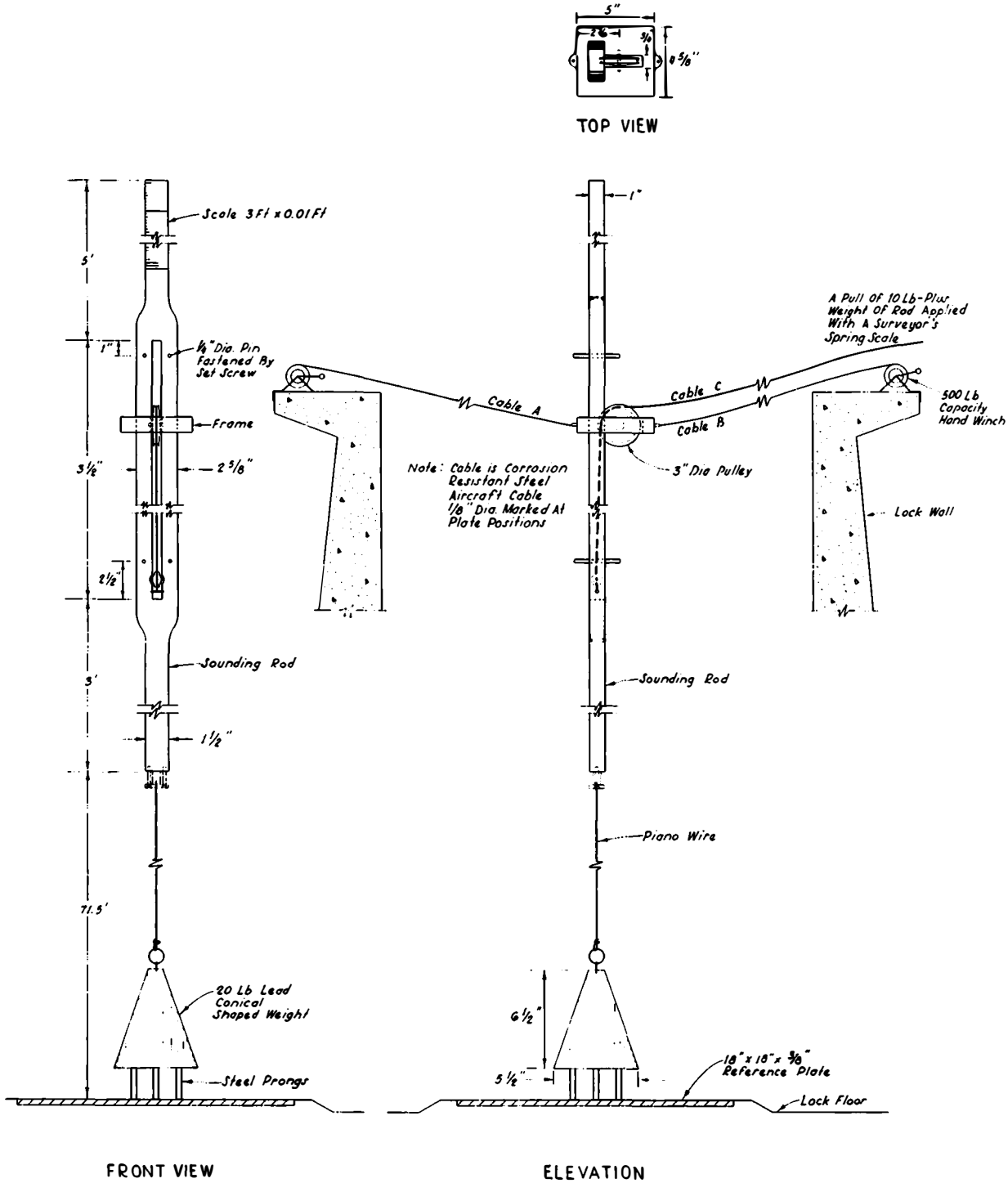

Fig. 13. Details of deepwater sounding device

on the settlement plate. A force of 10 lb plus the weight of the rod is applied to cable C by means of a surveyor's scale so that the wire and rod are vertical when the rod is read. As the exact distance from the top of the settlement plate to the top of the rod is known, the elevation of the settlement plate can be determined by taking a reading on the sounding rod with a leveling instrument. The temperature of the air and water is recorded at the time of each observation so that appropriate correction factors can be made for temperature variation between air and water.

Reference bolts on top of walls

45. Reference bolts (see fig. 11) for determining the settlement and movement of the walls of the lock were installed in the concrete at the top of the walls immediately after their completion at the locations shown in plate 10. Settlement surveys were made periodically, and the longitudinal distance between reference bolts on each side of a wall joint was determined at intervals to check on the amount of joint opening or closing occurring after construction. Profiles of settlement of the tops of the lock walls and movements at the joints are shown in plate 22.

Sounding Wells and Piezometers

Sounding wells

46. Five sounding wells consisting of 3-in.-ID pipe were installed in the walls of the lock chamber and gate bays at locations shown in plate 10 to permit accurate determinations of the water levels inside and outside the lock chamber. Details of the sounding wells are shown in fig. 11. The wells were sounded by means of electrical sounding devices used also for sounding piezometers.

Piezometers

47. Piezometers were installed beneath and adjacent to the lock structure at the locations shown in plate 10. The piezometers were designated as follows: "A" piezometers are those installed in the deep sands beneath the lock, "B" piezometers are those installed in the silty soils immediately beneath the lock, and "C" piezometers are those

installed in the sand wedge backfill along the lock. Details of the piezometers are shown in fig. 14. As the earth pressure cells and stress meters record total pressures, a sufficient number of piezometers were installed adjacent to these devices to determine the hydrostatic pressures and thus make possible the determination of the effective pressures acting on the devices.

48. The stage of the Mississippi River during and after construction is shown in plate 4 together with the average piezometric head in the deep sands and in the sand backfill at monolith 15. Time plots of the individual piezometers are shown in plates 23 through 27. Also included in these plates are piezometric data obtained during the 1962 high-water period when the lock was temporarily closed to navigation in order to permit observations under controlled equilibrium conditions. Piezometric profiles along the center line of the lock, indicating the piezometric head in the deep sands, and also directly beneath the base slab for selected dates corresponding approximately to water levels assumed for the design cases are shown in plate 28.

Electrical Measuring Devices

Description and location

49. Electrical measuring devices consisted of soil stress meters, concrete stress meters, strain meters, a pore pressure cell, and resistance thermometers obtained from Dr. R. W. Carlson, Berkeley, California, and pressure cells fabricated at WES. The devices are described in Appendix A. Additional details concerning the Carlson equipment are given in another report.[18] All electrical measuring devices were installed in the lock structure at monolith 15, a typical monolith near the center of the lock. The locations of these devices are shown in plate 11. All devices were carefully checked and calibrated in the laboratory prior to installation, and close control was maintained to ensure proper installation in the field. The results of the calibration tests and pertinent features of the installation of the devices are given in Appendix A.

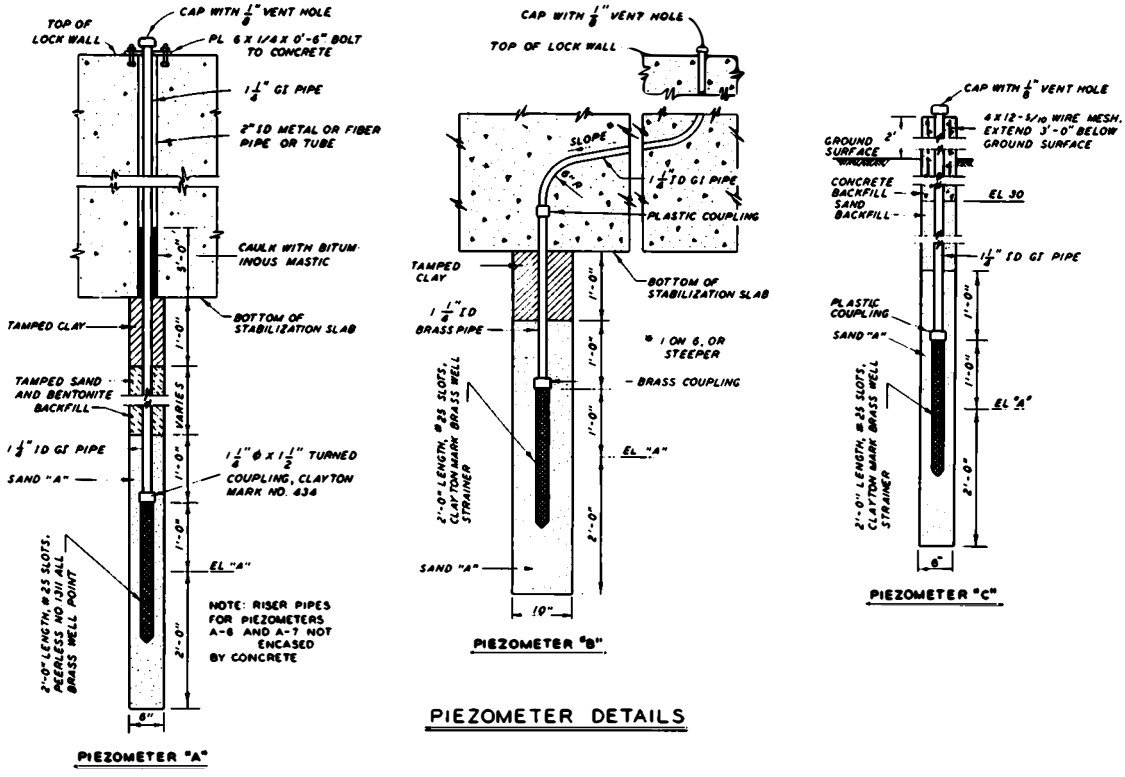

LOCATION OF PIEZOMETERS

PIEZ NO.	MONOLITH NO	LOCK STATION	OFFSET FROM ℄ LOCK, FT	EL "A"	DATE INSTALLED
A-1	24	745+85	44.0 S	-85.0	1 MAY 1958
A-2	15	740+85	44.0 S	-100.0	16 MAY 1958
A-3	6	735+78	44.0 S	-125.0	22 & 23 MAY 1958
A-4	2	733+40	44.0 S	-130.0	27 MAY 1958
A-5	--	732+00	0.0	-100.0	23 OCT 1958
A-6	--	730+45	0.0	-97.0	28 OCT 1958
A-7	--	727+70	0.0	-87.0	7 NOV 1958
B-1	24	745+90	0.0	-35.25	7 MAY 1958
B-2	15	740+80.75	44.0 N	-28.75	22 MAY 1958
B-3	15	740+80.75	0.0	-28.75	22 MAY 1958
B-4	15	740+80.75	21.0 S	-28.75	22 MAY 1958
B-5	15	740+80.75	44.0 S	-28.75	22 MAY 1958
B-6	15	740+80.75	65.0 S	-24.00	22 MAY 1958
B-7	6	735+78	0.0	-28.75	12 JUNE 1958
B-8	6	735+78	44.8 N	-28.75	12 JUNE 1958
B-9	6	735+80	44.0 S	-28.75	12 JUNE 1958
B-10	2	733+40	0.0	-35.25	6 JUNE 1958
C-1	25	746+72	73.5 N	-2.0	17 AUG 1959
C-2	25	746+75	73.5 S	-2.0	15 AUG 1959
C-3	24	745+90	75.0 N	-1.0	15 AUG 1959
C-4	24	745+90	75.0 S	-1.0	15 AUG 1959
C-5	15	740+74.75	50.0 N	+17.0	14 DEC 1959
C-6	15	740+74.75	68.0 N	-7.0	7 MAY 1959
C-7	15	740+74.75	50.0 S	+17.0	14 DEC 1959
C-8	15	740+74.75	52.0 S	+7.0	24 SEPT 1959
C-9	15	740+76.75	68.0 S	-1.0	22 JUNE 1959
C-10	15	740+74.75	68.0 S	-14.0	7 APR 1959
C-11	6	735+78	52.0 N	+7.0	24 SEPT 1959
C-12	6	735+78	68.0 N	-7.0	17 JUNE 1959
C-13	6	735+78	52.0 S	+7.0	24 SEPT 1959
C-14	6	735+78	68.0 S	-7.0	16 JUNE 1959
C-15	2	733+40	80.0 N	-1.0	12 AUG 1959
C-16	2	733+40	80.0 S	-1.0	12 AUG 1959

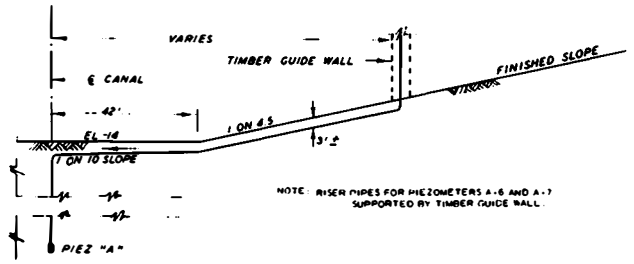

Fig. 14. Piezometer details

Observations

50. All devices were read immediately before and after concrete had been placed around them. The devices were also read the following day; subsequently until wall construction had been completed (31 December 1959), the devices were read once a week and before and after each lift of concrete had been placed in monolith 15. From January 1960 until the backfill had been completed (May 1960), the devices were read every two weeks, and from May 1960 to January 1961 the devices were read once a month.

51. As previously noted, provisions were made for closing Port Allen Lock to navigation for a period of 4 days during the peak of the 1962 high water to permit observation of the devices under equilibrium conditions. During the 4 days, all engineering measuring devices were read with (a) the water level in the lock at the same elevation as the Mississippi River, and (b) the water level in the lock at the same elevation as the canal.

Carlson soil stress meters and WES pressure cells

52. Twenty Carlson soil stress meters were installed beneath the base and along the walls of the lock to measure base pressures and lateral earth pressures. Five WES pressure cells were installed adjacent to the soil stress meters to provide an additional check on observed pressures. Both the Carlson soil stress meters and WES pressure cells indicated the total pressure acting on the devices. As the behavior and design of the base slab and walls are dependent on the distribution of effective pressures, all observed pressures were converted to effective pressures (total pressure minus uplift). Appropriate calibration constants, as discussed in Appendix A, were used for each device in computing the effect of uplift pressure determined from piezometers set beneath the lock and in the backfill. The resulting effective pressures at each device during and after construction are shown in plates 29 through 37. Also shown in these plates are the uplift pressures at the device, pertinent features of construction, and the special 1962 high-water observations. Computed pressures based on the weight of concrete in the base slab are also shown for the period prior to construction of the walls. For the devices located in the walls, a time plot of elevations of top of backfill is shown. In

those instances in which a WES pressure cell was installed adjacent to a Carlson soil stress meter, the data for the two devices are shown in the same plot.

53. In general, the devices beneath the base slab tended to reflect closely the weight of successive lifts of the base slab until construction of the walls and placement of backfill were initiated. Carlson soil stress meters S-6 and S-7 gave conspicuously lower readings than the other devices beneath the slab. The effective pressure-time plots shown in plates 28 through 36 served as a basis for construction of the effective base pressure diagrams discussed in Part IV of this report. Because of the effects of cell protrusion on the indicated readings of the WES pressure cells, subsequent data analyses are based solely on the Carlson stress meter observations.

Carlson strain meters

54. The length changes indicated by the strain meters were converted into elastic strains by making proper corrections for thermal expansion or contraction of the meter frame and surrounding concrete. The elastic strains are plotted versus time in plates 38 through 51. Data from strain meters M-19 and M-20 are not shown, as the observed readings were well outside the range of readings indicated by the other meters.

55. The main purpose of the strain meters was to permit computation of concrete stresses that, in the case of tensile stresses, cannot be measured by available devices such as concrete stress meters. Under rapid conditions of loading, the change in stress is determined by multiplying the change in strain by the modulus of elasticity of the concrete. However, for loads applied over a relatively long period of time, consideration must be given to the change in the modulus of elasticity with time and to deformations resulting from creep and other causes. The magnitude of deformations resulting from creep and other causes was estimated from the laboratory tests described in Appendix C. The computed stresses for each strain meter are shown with the measured strains in plates 38 through 51. Stresses were computed using a method suggested in another report.[19] The stress-time plots were used to determine the distribution of internal stresses as described in subsequent analyses.

Concrete stress meters

56. Time plots for stresses indicated by the three concrete stress meters are shown in plates 52 and 53. Also shown are the computed stresses for the nearest strain meters at approximately the same elevations (see detail A, plate 11). These strain meters are actually 10 ft south of the concrete stress meters that were installed along the center line of the base slab; however, no important differences in stress could be attributed to this difference in location. The observed stresses at stress meter C-1 agree reasonably well with those computed for strain meter M-6. In the case of stress meters C-2 and C-3, the stresses are relatively small and the agreement with stresses computed from adjacent strain meters is less favorable. Additional studies are required to establish the reason for the discrepancies between stresses measured by the concrete stress meters and those computed from strain meter data.

Concrete pore pressure cell

57. Data from the single pore pressure cell (PP-1) installed in the concrete slab are shown in plate 54 together with the pore pressure acting below the base slab as indicated by piezometer B-3. The estimated distribution of pore pressures within a vertical section of the base slab is also shown for selected dates. It is of interest to note that while the pore pressure in the concrete increased with increasing hydrostatic pressure on the bottom of the slab, the pore pressure tended to decrease after the early part of 1960 while the pressure beneath the base slab remained relatively constant. The reason for this anomaly is not known.

Resistance thermometers

58. No temperature-time plots were prepared for the resistance thermometers located near the top of the south wall in monolith 15; the data pertinent to particular case analyses are presented with the analyses.

Wall Deflection Pipes

59. During wall construction, deflection pipes were read after each lift of concrete had been placed in the monolith in which the pipes were located. The deflection pipes also were observed after the backfill behind

the lock walls had been completed (May 1960), and they were subsequently read at the same time that settlement reference plates were read. Data from wall deflection pipes in terms of horizontal movement of the top of the wall and angular rotation of the wall with respect to the base are shown in plates 55 through 58. Horizontal movements and deflections of the wall at various elevations are shown for selected dates in plates 18 through 21. As a check on the wall deflection pipe readings, the distances between reference points located on the top of each wall were measured with a steel tape at periodic time intervals after the walls had been completed. A plot showing the comparison of the change in distance between the lock walls as measured by the steel tape and the change in distance as computed from deflection pipe data is shown in plate 59. The differences between the two types of measurements may reflect errors inherent in the measuring techniques.

PART IV: REBOUND, SETTLEMENT, AND DEFLECTION

Rebound and Settlement

Observed and predicted rebound

60. The rebound of the foundation due to excavation at various sections perpendicular to the center line of the lock (at monoliths 2, 6, 15, and 24) is shown in plates 12 through 15; the rebound along the center line of the lock is shown in plate 16. A maximum rebound of 0.36 ft was observed at the canal-side gate bay (monolith 2). The rebound decreased along the length of the lock to a minimum of 0.26 ft at the river-side gate bay (monolith 24). At monolith 15, the rebound was slightly higher at the center (0.29 ft) than at the south side of the lock (about 0.26 ft). The higher rebound indicated on the north side appears questionable. Also shown in plates 13 through 16 are the rebounds predicted in design. The observed rebound at all monoliths was greater than that predicted for design. The predicted rebound varied from 0.27 ft near the canal gate bay to about 0.11 ft at the river-side gate bay. The predicted rebounds and settlements are shown in plate 16 at the locations of the borings where data were available for analysis. Predictions for the monoliths under study were assumed to be identical with those made at the nearest boring. In summary, the predicted rebounds were from 42 to 75 percent of the observed values. Close agreement between predicted and observed rebound was not realized because the groundwater level and the hydrostatic head in the deep sands after excavation had been completed differed appreciably from those assumed in design.

Observed and predicted settlement

61. Foundation settlements at monoliths 2, 6, 15, and 24 are shown in plates 12 through 15; settlements along the length of the lock are shown in plate 16. All settlements are referenced to the readings made just before the first lift of the base slab had been placed. With only the base slab in place, the settlement profile across the width of the lock followed the usual dish-shaped pattern, with more settlement occurring at the center than at the sides of the lock. At monolith 15, the observed

settlement just before wall construction was begun was 0.08 ft at the center of the lock and about 0.02 ft at the side. Placement of the walls and backfill resulted in a reversal of the shape of the settlement profile, with more settlement occurring at the sides than at the center of the lock.

62. In the schedule of observations of engineering measuring devices, readings of all engineering measuring devices were to be made when conditions were similar to those assumed in design. In August 1960, a condition existed that was similar to the case II loading conditions assumed in design and described in fig. 7 (lock and backfill complete, no water in the lock). The case I condition, which assumed the lock structure to be complete before placement of backfill, was not realized during construction since the backfill was brought up concurrently with the walls. During the peak of the 1961 high water (June 1961) before the lock was placed in operation, the river stage in the lock reached el 37, or 12 ft less than the project flood stage of el 49 assumed in the lock for case III design loading (see fig. 7). For simplicity in the following discussions, references to cases II and III will be used to designate loading conditions assumed in the design, and references to cases II' and III' will be used to designate corresponding cases, but with actual loading conditions existent when the observations were made. A comparison of conditions for cases II and II' and cases III and III' is shown below.

	Elevation in Feet MLG		
	Water Level in Lock	Water Level in Backfill	Piezometer Level Beneath Lock
Case II	Empty	7.5	7.5
Case II'	Empty	1.0	10.2
Case III	49.0	7.5	7.5
Case III'	36.3	13.6	19.6

63. Observed settlements for case II' and case III' conditions are shown in plates 12 through 16. Settlements at the gate bays (monoliths 2 and 24) were not observed at the crest of the 1961 high water but were observed during a minor river crest (el 34) that occurred in April 1961. These latter values of observed settlements are designated as case III'

for monoliths 2 and 24. The maximum observed settlement of the lock was measured at monolith 2 during the 1961 high water at which time the settlement was 0.37 ft at the side. The settlements predicted in design for case II and case III conditions are shown in plates 13 through 16. No predictions are shown for monolith 2, as no settlement analyses were made for this monolith. At monolith 24, the predicted settlement for case II conditions was in good agreement with the observed settlement. The predicted settlement was 0.19 ft at the center and 0.27 ft at the sides; the observed settlement was about 0.18 ft at the center and from 0.26 to 0.29 ft at the sides. However, the predicted settlement of monolith 24 for case III was lower than that observed for the case III' condition. At monoliths 6 and 15, the predicted settlements were considerably greater than observed settlements for both cases. For example, for the case II' condition at monolith 15, the observed settlement was about 0.19 ft at the center and from 0.22 to 0.28 ft near the sides; whereas, the predicted settlement for case II was 0.30 ft at the center and 0.33 ft at the sides.

Settlement and movement at wall joints

64. The settlement of the tops of the walls and longitudinal movement at the wall joints as of March 1962 are shown in plate 22. The observed settlement of the walls varied approximately from 0.05 to 0.18 ft. Settlements at the tops of the walls were relatively uniform along the length of the lock. Apparent differential settlements between monoliths reflect differences in completion time for individual monoliths. Very little movement at the wall joints has occurred since the walls were completed. The data indicate that some joints were opening while others were closing. The maximum observed joint opening was 0.12 in., and the maximum amount of closing observed was 0.18 in. The wall joints for the chamber monoliths were designed (see fig. 8) for a maximum closure of 0.50 in.; consequently, the observed movements are not considered excessive. Although the joints at the gate bays were designed for larger movements, the observed openings of joints were not so great as those observed for the chamber monoliths.

Time rate of settlement

65. As the foundation soils are comprised principally of silty

material, it was anticipated that settlement of the lock would be relatively rapid. As shown in plate 4, concrete placement and backfilling proceeded at a fairly uniform rate. Likewise, time-settlement plots in plates 12 through 15 indicate that settlement of the lock occurred at a fairly uniform rate during construction. At monolith 15, the lock settled about 0.01 ft per month. At the end of construction (May 1960), the rate of settlement decreased sharply until the lock was flooded (September 1960). Flooding of the lock caused additional settlement. Since the lock was flooded, it appears that the lock settles and rebounds with corresponding rising and falling river stages. When the river rises, the lock is subjected to a greater water load as well as higher uplift pressures. However, the increase in water load is greater than the corresponding increase in uplift pressure, and as a result, the lock settles. When the river stage falls, the lock is subjected to smaller water loads, and the lock rebounds. It appears from the time-settlement plots that the settlement of the lock as of 1962 was about completed, and very little additional settlement is expected.

Broken waterline incident

66. On 8 December 1959, the piezometer readings at monolith 15 (see plate 25) were unusually high. The piezometric level of the piezometer beneath the floor at the center of the monolith was at el +28 on 8 December as compared to el +11 on 3 December. An inspection of the area by project personnel revealed that a water supply line near the north wall of monolith 14 had broken and was discharging into the sand backfill. The waterline was quickly repaired, and the outlet for the drain in the sand backfill was opened to lower the water table in the backfill. The hydrostatic pressures beneath monolith 15 then decreased fairly rapidly, and by 10 December these pressures were about the same as before the broken waterline was discovered (about el +11). Only the hydrostatic pressure in the vicinity of monolith 15 was affected by the broken waterline.

67. Observed settlements of the reference plates on the floor of monolith 15 during November 1959-January 1960 are shown in fig. 15. The settlements shown in this figure are the observed settlements since 15 December 1958 (just prior to wall construction). As seen in fig. 15,

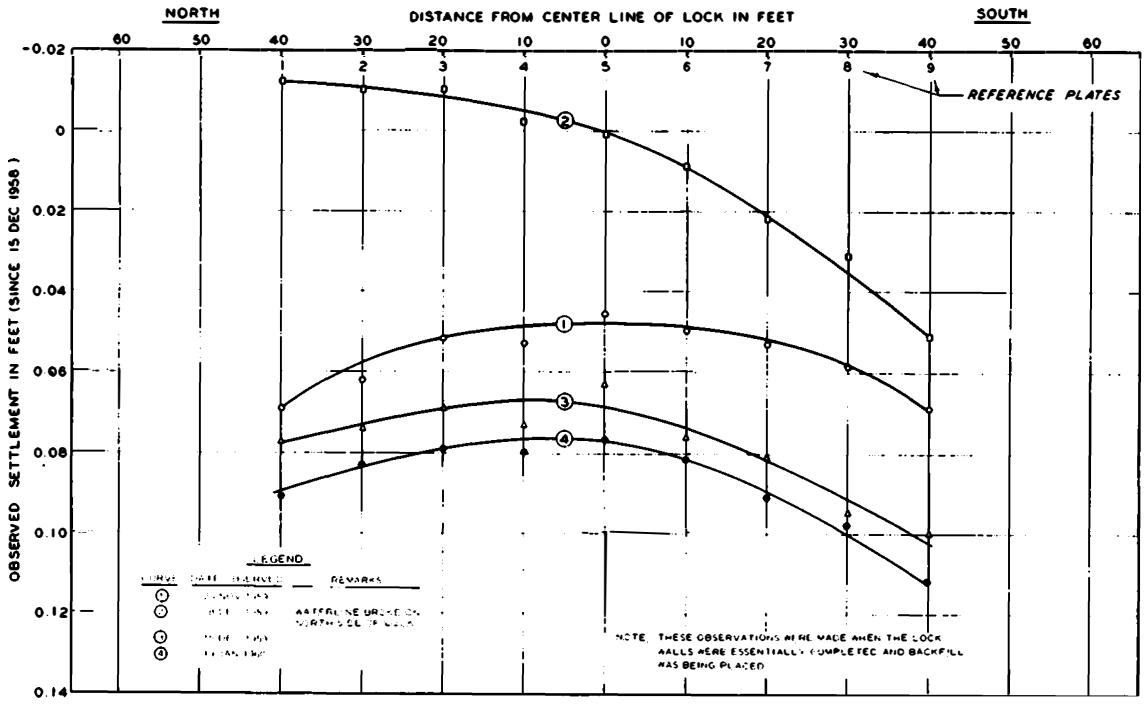

Fig. 15. Settlement observations at monolith 15, November 1959-January 1960

the observations made on 20 November 1958 indicated that settlements were nearly symmetrical about the center of the slab. Settlement observations made on 8 December 1958 (the day after the broken waterline was discovered) indicated that the slab had rebounded about 0.08 ft on the north side of the lock chamber and 0.02 ft on the south side of the chamber. After the high hydrostatic pressures beneath the lock had dissipated, the lock settled in a tilted position, as indicated by the observations made on 15 December 1958 and 10 January 1960, with the south side of the lock chamber being about 0.023 ft lower than the north side of the chamber. After January 1960, the settlement of the south side of monolith 15 tended to be greater than settlement of the north side.

Recomputed settlement and rebound

68. Purpose of computation. In order to evaluate the significance of the observed foundation movements, the rebound and settlement of the structure at monolith 15 were recomputed using actual loading conditions, which in some instances differed appreciably from those assumed for design. Comparisons were also made of rebound and settlements computed using

Boussinesq's and Westergaard's method of stress calculation to determine which of the two methods resulted in better agreement with the observed movements. The laboratory pressure-void ratio (p-e) curves, which were used in the settlement analyses for the design of the lock, were revised to represent more closely the actual loading conditions. The revised design p-e curves for point A (center of the lock) are shown in fig. 16 together with the original laboratory p-e curves. The conditions assumed for the revised computations and comparisons of observed and computed settlements are given in the following paragraphs.

69. Recomputed rebound. The initial overburden pressure existing at the time the heave points were installed was made practically identical with that assumed in the design computations (based on the water table in silt topstratum at el +20 and hydrostatic pressure in the deep sands at el +10); however, the foundation pressures after excavation differed substantially from those assumed for design. In the design computations, pressures after excavation were computed assuming that the piezometer level in both the silt stratum and deep sands would be at el -31 after the excavation had been completed. At monolith 15, the maximum rebound was observed on 22 May 1958, just before the stabilization slab was placed. Piezometer observations made about that time indicated that the hydrostatic pressures in the silt stratum and deep sands were at el -27 and el -35, respectively (see plate 25). These values were used in recomputing the rebound. In addition, it was assumed that the water table along the excavation slopes below el +20 was 2 ft lower than the slope surface instead of at ground surface as in design. In the revised computations, it was assumed (as in design) that the difference in hydrostatic pressure between the silt stratum and deep sand was lost in the clay stratum between el -60 and -69.

70. The stress influence at various depths in the foundation was computed using Boussinesq's equations. This stress influence, which would be produced by a loading configuration corresponding to the shape of the excavation, was subtracted from the original overburden pressure to give the foundation pressures after excavation. For the sake of comparison, stress influences were also computed using Westergaard's equations.

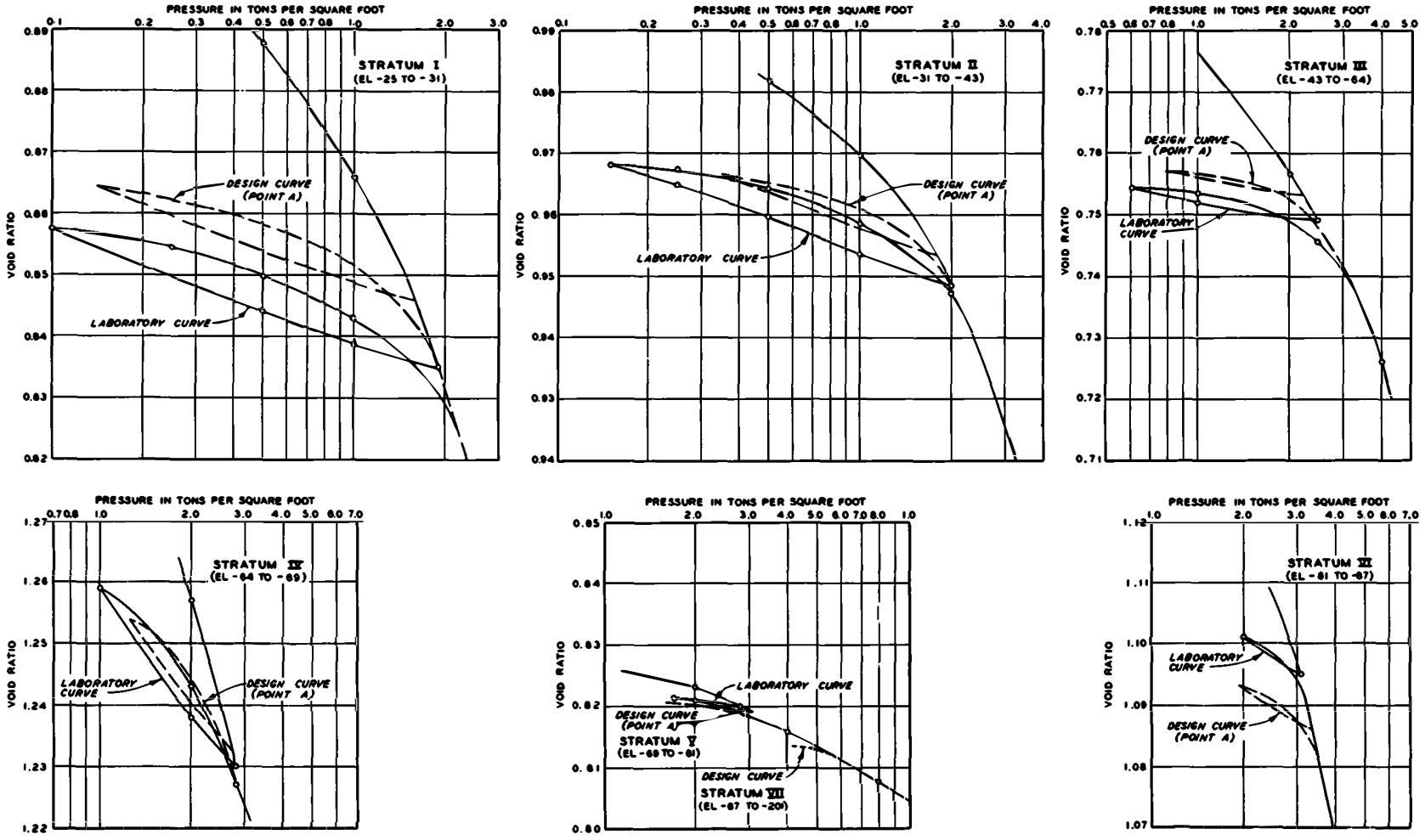

Fig. 16. Revised pressure-void ratio curves, boring L-9U

Boussinesq's equations are based on the assumption that the foundation is an isotropic homogeneous mass to which the elastic theory can be applied. Westergaard's equations represent a nonisotropic foundation condition in which the elastic foundation is laterally reinforced by numerous, closely spaced horizontal sheets of negligible thickness, but of infinite rigidity, which prevents the mass from undergoing lateral strain. As the foundation soils contain numerous silt lenses and partings, it was considered that Westergaard's solution might be more applicable to these conditions than Boussinesq's solution.

71. Results of the revised rebound computations for both the Westergaard and Boussinesq cases are shown in fig. 17 together with the observed rebound. Fig. 17 shows that the rebounds computed by both methods indicate an almost uniform rebound across the width of the lock. The rebound computed for Boussinesq's case is slightly larger and is in closer agreement with the observed rebound than the values computed for Westergaard's case, although for practical purposes the difference is negligible. The computed rebounds were about 0.24 and 0.28 ft for Westergaard's case and Boussinesq's case, respectively. The observed rebound was about 0.29 ft at the center and 0.26 ft at the sides of the lock.

72. Recomputed settlement. In recomputing the settlement for case II', foundation stresses were determined using both Boussinesq's and Westergaard's equations. The water table in the silt stratum was considered to be at el 10.3, the same as the observed piezometric head beneath the base slab at the center line of the lock. For case II', the piezometric head in the deep sands was at el 4.7 (see plate 28). Settlement for case III' was computed in the same manner as for case II'. The water table in the silt stratum and deep sands for this condition was considered to be at el 19.7 and el 31.3, respectively (see plate 28).

73. In the computation of foundation stresses due to structure load, the distribution of base pressures as indicated by observations on soil stress meters (see plate 60) was used. The observed base pressures (reaction) were greater than the actual structure load for the case II' conditions; apparently this was due to frictional forces acting on the

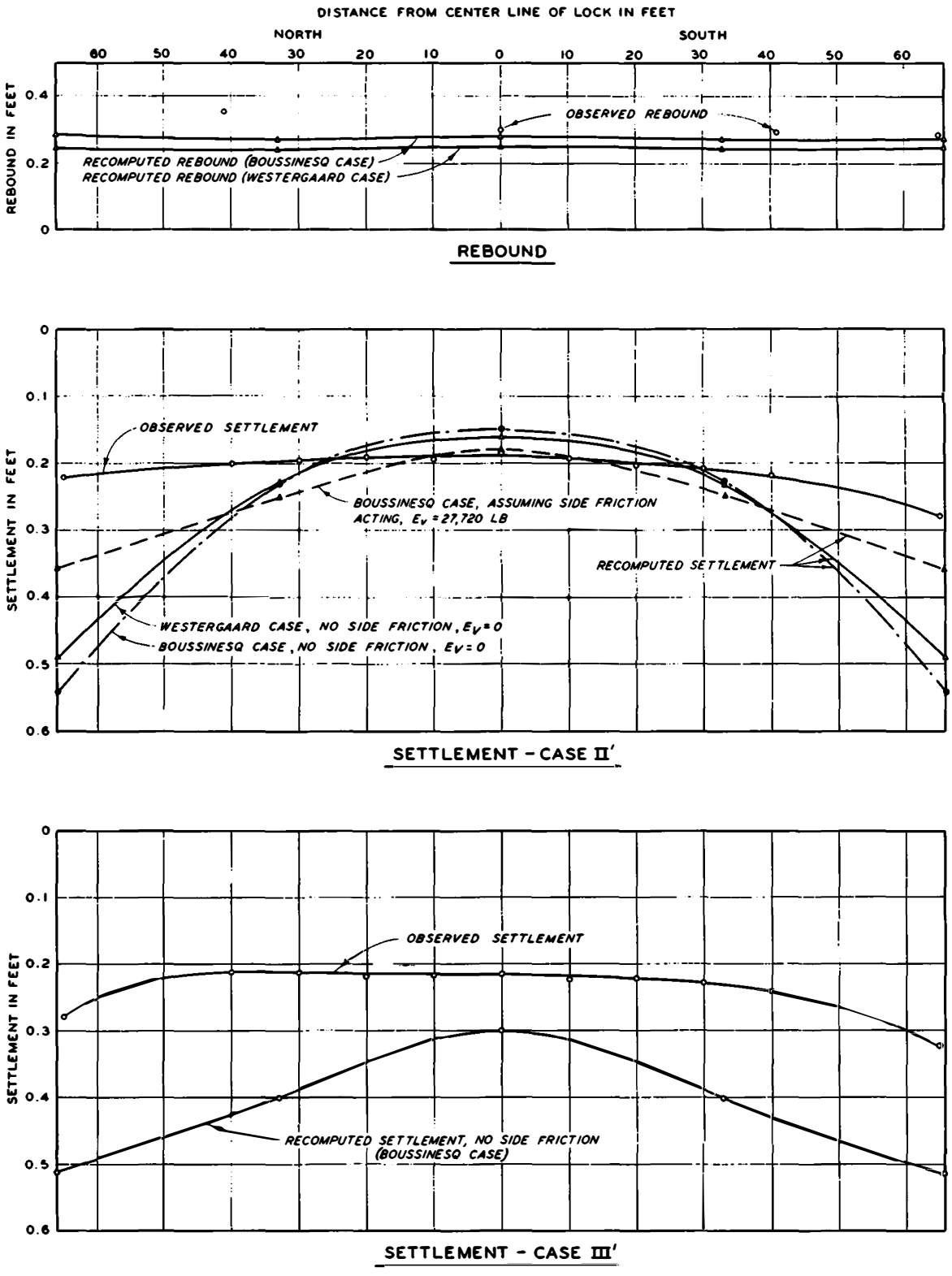

Fig. 17. Comparison of observed and recomputed rebound and settlement, monolith 15

sides of the lock due to settlement of the backfill relative to the lock. In the settlement analyses two different assumptions were made: (a) that there were no frictional forces acting on the sides of the lock and the observed pressures were higher than the actual computed structure loads (in this analysis, the observed effective base pressures, shown in plate 60, were proportionately reduced so that the total foundation reaction was equal to the actual structure load), and (b) that the observed pressures were correct and the difference between the reaction and actual structure load was due to frictional forces acting on the sides of the lock.

74. As shown in fig. 17, there was very little difference in the settlements for case II' computed using Boussinesq's and Westergaard's methods, with settlements computed by Westergaard's method giving slightly higher values at the center and slightly lower values at the sides of the lock than the values of settlement computed by Boussinesq's method. A comparison of the recomputed and observed settlements is shown in fig. 17, and the results are also tabulated below:

	Recomputed Settlement, ft		Observed Settlement, ft	
Procedure Used	Center	Sides	Center	Sides
Westergaard's method without frictional force	0.16	0.49	0.19	0.22-0.28
Boussinesq's method without frictional force	0.15	0.54		
Boussinesq's method with frictional force	0.18	0.36		

It can be noted that computed settlements assuming frictional forces along the outer edges of the wall were in closer agreement with observed settlements than computed settlements assuming no frictional forces. Computed settlements at the center of the lock generally were in good agreement with observed settlement; however, computed settlements at the sides of the lock were considerably greater than those observed. It is concluded that for such structures founded on alluvial deposits similar to that found at Port Allen Lock, the computed settlement will give the general magnitude of the

settlement to be expected but not a sufficiently accurate estimate of the transverse settlement profile.

75. Settlements were computed for case III' conditions using Boussinesq's equations for computing stresses and observed base pressures for the structure load, and assuming no frictional force at the sides of the lock. For case III' conditions, the observed base pressures were approximately the same as the actual structure load. Therefore, it was assumed that there were no frictional forces acting on the sides of the lock. As shown in fig. 17, the computed settlements were greater than observed settlements both at the center and sides of the lock. Recomputed settlements were 0.30 ft at the center of the lock and 0.52 ft at the sides. Observed settlements were 0.21 ft at the center and from 0.28 to 0.33 ft at the sides. As the high-water condition for case III' was effective for only a relatively short period of time, it is possible that complete consolidation under these loading conditions was not realized. This may account for the fact that observed settlements were less than the recomputed values for case III'.

Settlement of type A reference points

76. The observed settlements of deep reference points (type A) installed at various elevations in the foundation along the side of the lock are shown in plate 17 together with the observed settlements at the center and side of monolith 15. Practically no settlement occurred below el -42 (elevation of SP-1) before the backfill was placed. After backfilling operations had been begun, the deep points settled at a fairly uniform rate of about 0.02 ft per month. This would indicate that before the backfill was placed, settlement of the structure resulted primarily from consolidation of foundation soils above el -42. However, during placement of backfill, settlement resulted primarily from consolidation of the soils below el -42. After the lock had been flooded, the movements of the deep reference points in the foundation varied with rising and falling river stages as did the reference points at the base of the structure.

77. A comparison of observed and computed foundation settlements at various depths below the side of monolith 15 for cases II' and III' are shown in fig. 18. The deep reference points indicate that over half of

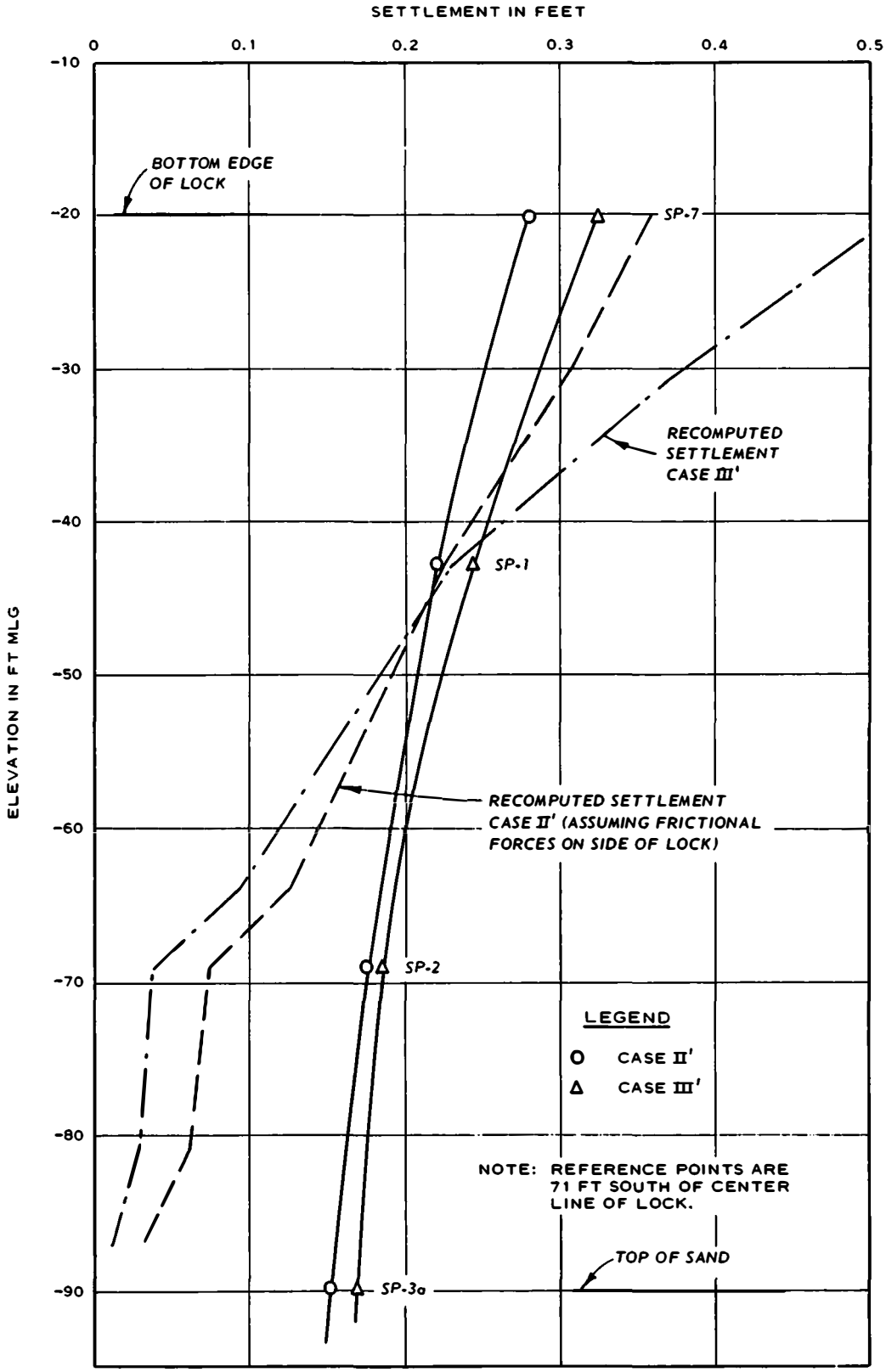

Fig. 18. Observed settlement versus depth

the foundation settlement occurred in the sand stratum below el -90, whereas computation indicates that most of the settlement should have resulted from the consolidation of the silts above el -90. The reason for this discrepancy is not known; however, one possible explanation is that the deep reference points may not be indicating the settlement of the tip of the reference points. During backfilling operations when the risers for the type A reference points were brought up through the backfill, it was very difficult to maintain the riser in a vertical position. On numerous occasions hauling equipment working in the sand backfill passed so close to the risers for the settlement points that the risers were bent slightly. It is quite possible that the risers of the reference points may be binding to the outer sleeves and thus not indicating true settlement of the tips of settlement points. On the other hand, the settlement of the deep sands as indicated by deep reference points beneath the gate bays (see plate 17) tend to corroborate the validity of the deep sand settlement at monolith 15.

Deflection of Base Slab

Deflections computed from settlement observations

78. The deflected shapes of the base slab were determined from the settlement profiles. Deflected shapes for the base slabs of monoliths 2, 6, 15, and 24 are shown in plates 18 through 21 for (a) the condition existing after the second lift of concrete had been placed, and (b) an initial condition that existed after the slab had been completed and just prior to wall construction. The deflections of the slab from this initial condition to case II' condition and from the initial condition to case III' condition are also shown in these plates. The deflection curves were drawn with respect to: (a) a straight line through the two points representing the settlement at the sides of the lock for the case of greater settlement at the center with respect to the sides, and (b) a horizontal line through the point of minimum settlement for the case of greater settlement at the sides with respect to the center.

79. For all monoliths, before wall construction was begun, the

center of the slab deflected downward with respect to the side. At monoliths 6 and 15, the maximum deflections at the center of the slab were 0.046 and 0.034 ft, respectively. At monoliths 2 and 24, there were no temporary settlement reference points at the sides of the lock. Therefore, the deflection prior to wall construction was estimated by extrapolating data from the reference points. At monoliths 2 and 24, the estimated deflections at the center of the slab were 0.027 and 0.010 ft, respectively.

80. In determining deflections of the base slab at monolith 15 for cases II' and III', corrections were made for tilting of the base slab. As previously explained, during the broken waterline incident in December 1959, the lock at monolith 15 rebounded and then settled in a tilted position, with the south side of the lock being slightly lower than the north side. Consequently, in determining deflections from settlement observations made subsequent to January 1960, a correction was made for tilting of the base slab by taking the deflections with respect to a reference plane drawn through the settlements at plates 1 and 9. For case III', elevations of plates 1 and 2 were unusually high as compared to elevations previous to and subsequent to case III'. The plates were probably covered with sediment, and the deflection was determined from the assumed settlement profile shown in plate 14.

81. As shown in plates 18 through 21, construction of the wall and placement of backfill resulted in the sides of the lock deflecting downward with respect to the center (see case II' conditions). Also, there was very little difference in deflection from case II' to case III' conditions. For both cases II' and III' conditions, deflections in the base slab of monolith 6 were about the same as deflections in the base slab of monolith 15, and deflections at the gate bay monoliths (2 and 24) were less than the deflections in the lock chamber (monoliths 6 and 15). Deflections of the side of the lock with respect to the center at monoliths 6 and 15 were of the general magnitude of about 0.15 ft, whereas deflections at the gate bay monoliths were about 0.10 ft.

Deflection computed
from observed strains

82. The deflections of the base slab in monolith 15 were also

computed from observed strains indicated by the Carlson concrete strain meters in the base slab at various distances from the center line of the lock. By assuming that the actual length change per unit length at a given meter (meter reading corrected only for temperature effects on the meter itself) is the average unit length change over the half distances to the adjacent meters, a corresponding total length change for the distance may be computed. Assuming further that a plane section remains plane after deflection of the slab has taken place, the average angular change at the meter can be determined and the deflection computed by integrating the angular change versus distance relation (see fig. 19). In a graphical analysis, the area under the curve of angle change plotted against the distance from the center line was taken as the deflection of the base slab with respect to the center line. The deflection computed in this manner is independent of the modulus of elasticity and the moment of inertia of the base slab. The computed deflections for cases II' and III' are compared with deflections determined from the settlement profiles for the same conditions in fig. 20. The computed deflections are about 60 percent less than those determined directly from the settlement observations. Noting the trend of unit length changes for the meter array located 10 ft south of the center line, it appears that the unit length changes at the top of the slab are too low, suggesting the existence of tensile cracks in the top of the slab.

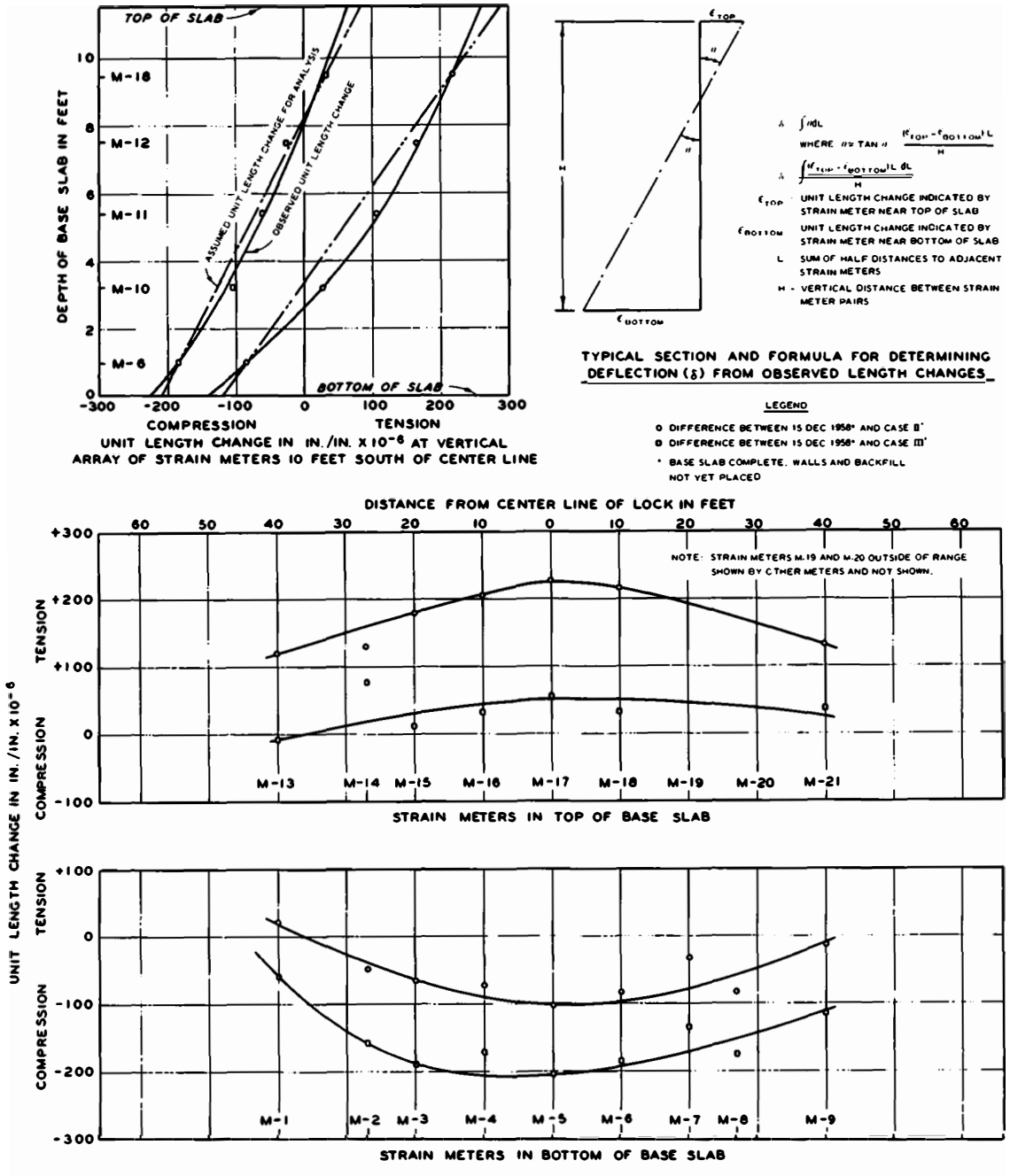

Fig. 19. Base slab deflections computed from strain meter data

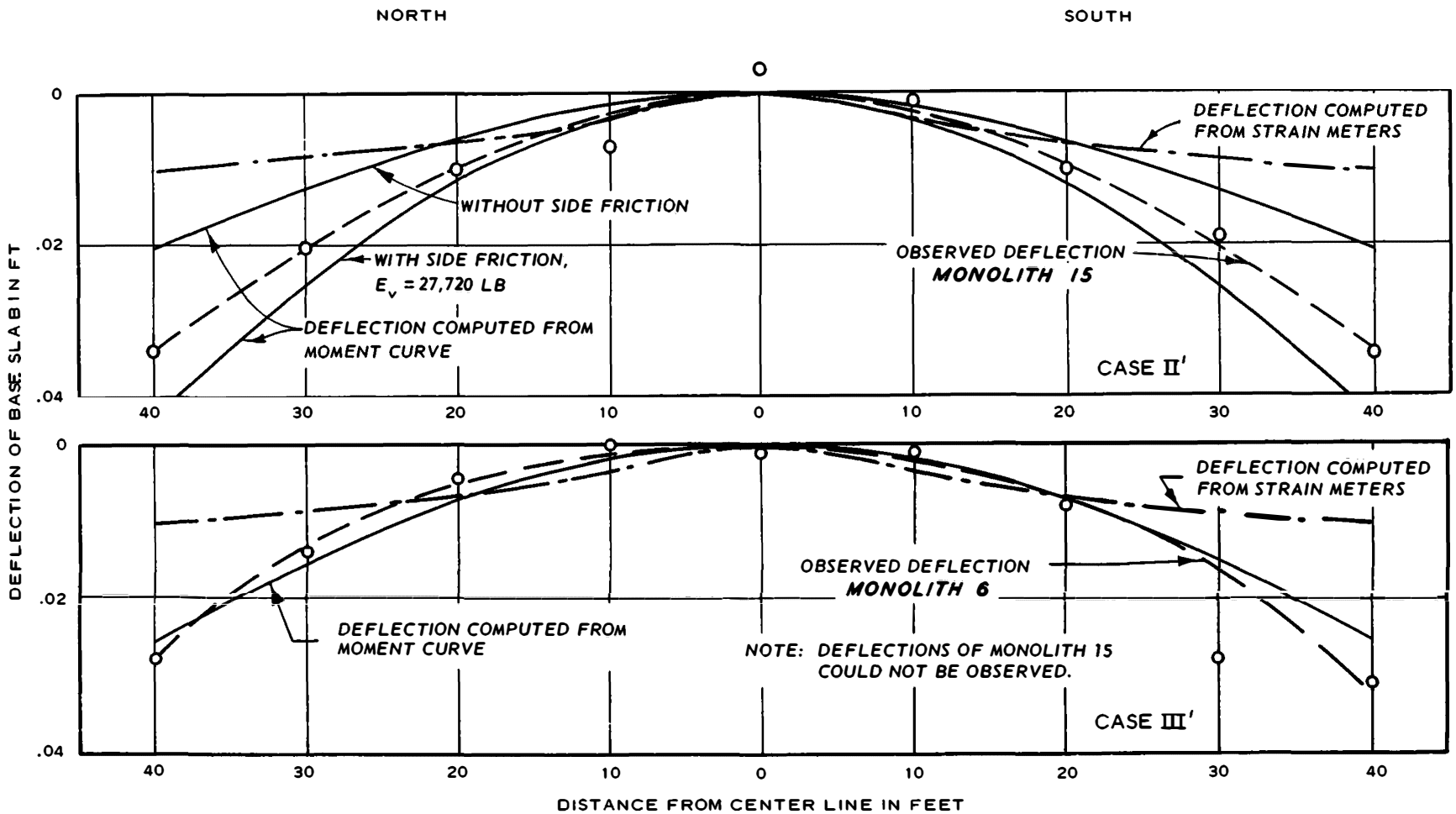

Fig. 20. Observed and computed deflections of base slab, monolith 15

PART V: EARTH PRESSURES AND WALL MOVEMENTS

Sand Backfill

83. A description of the sand backfill material behind the lock walls, of placement procedures, and of the results of laboratory tests on representative samples of the sand backfill are presented in Appendix C. Laboratory tests indicated that the backfill behind monolith 15 was placed at an average dry density of 100 pcf, corresponding to a relative density of 71 percent. Because of errors inherent in the drive sample method of sampling, the actual density and thus the relative density may be somewhat higher than indicated above; this is discussed in Appendix C. The angle of internal friction for the material at a density of 100 pcf was estimated to be 40 deg, based on shear strength test data.

Observed Earth Pressures

Earth pressures versus time

84. The variations of the earth pressure between the backfill and the lock wall for monolith 15 with respect to time, as measured by soil stress meters S-12 through S-20 and WES pressure cells W-4 and W-5 are shown in plates 34 through 37. The locations of these measuring devices are shown in plate 11. In general, an increase in the soil pressure was noted at all the pressure measuring devices as the backfill was placed. Significant is the increase in the effective pressure at meters S-12 and S-13 associated with the decrease in the hydrostatic pressure after December 1959 when the backfill was subjected to sprinkling, rather than inundation, during placement. The low reading of S-12 during backfilling operations is attributed to arching effects that resulted from consolidation of the underlying foundation soils beneath the weight of the backfill. After backfilling operations had been completed, meter S-12 indicated an increase in pressure. All meters showed a decrease in pressure after operation of the lock was begun.

Distribution of
lateral earth pressure

85. Case II'. The observed effective earth pressures on the lock walls for case II' conditions are shown in plate 60. Pressures measured at the two stress meters on the north wall were generally similar to those at the same elevation on the south wall. The observed effective earth pressures were in fair agreement with the effective earth pressures assumed in design, particularly for the upper part of the wall. The design effective earth pressures, as previously explained, were based on an at-rest earth pressure coefficient of 0.5.

86. The coefficient of lateral earth pressure k was computed directly from the observed pressure measurements according to the expression:

$$k = \frac{p_h}{p_v}$$

It is assumed that p_h, the effective pressure in a horizontal direction, is represented by the effective earth pressure indicated by the stress meter; p_v is the effective overburden pressure at the elevation of the meter. The coefficient of lateral earth pressure along the wall for case II' conditions is shown in fig. 21. The actual earth pressure coefficients varied from 0.33 along the culvert wall to approximately 0.62 at the topmost stress meter near the top of the backfill.

87. Case III'. The observed effective earth pressures along the walls of the lock for case III' conditions are shown in plate 61 together with the effective earth pressures assumed in design. For design purposes, a coefficient of lateral earth pressure of 1.0 was assumed acting from ground surface to the top of the culvert below which the coefficient was assumed to decrease linearly to a value of 0.5 (assumed earth pressure at rest) at the base of the wall. The assumed coefficient of lateral earth pressure of 1.0 was considered to be a conservative value since it would not require mobilization of shearing stresses in the backfill and thus would be developed without excessive wall deflection. The observed earth pressures for case III' differed considerably from those assumed for design, being higher along the upper half of the wall stem and lower along

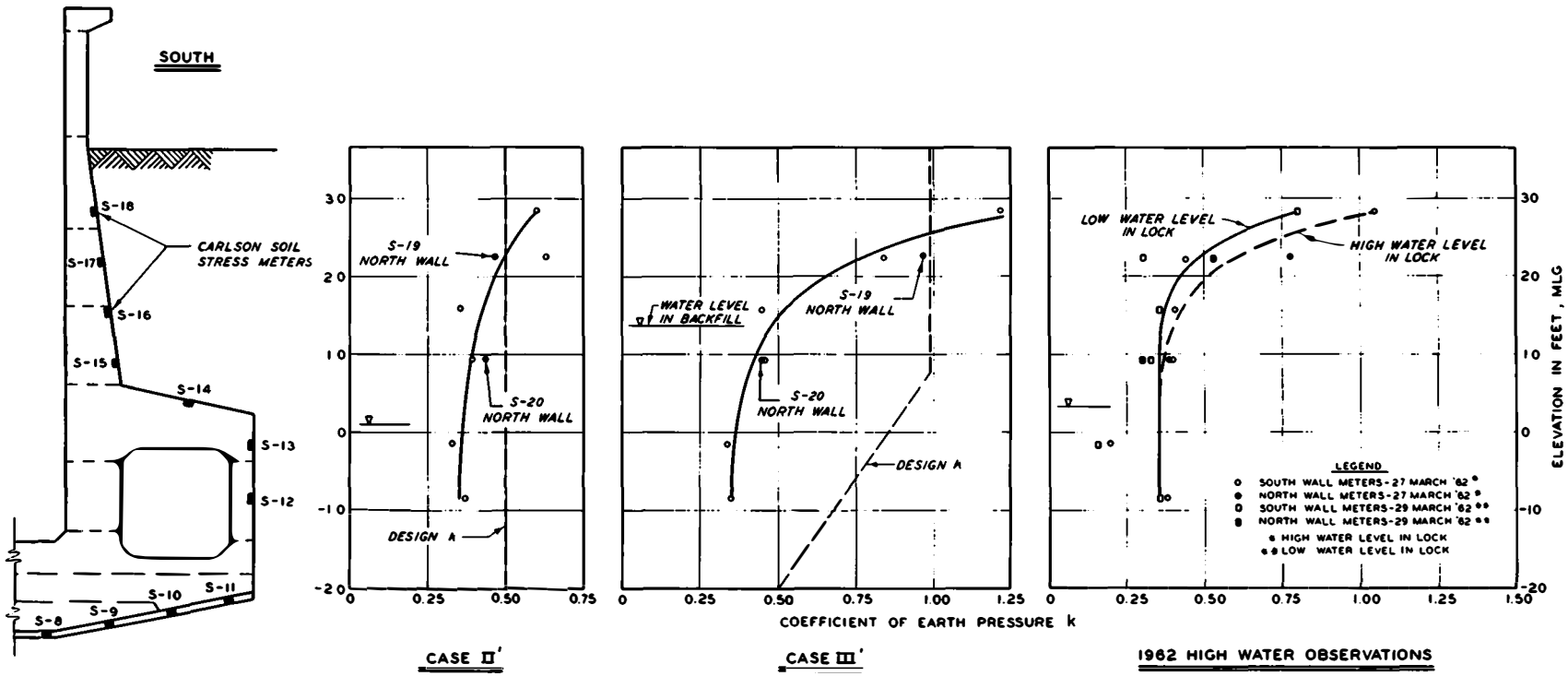

Fig. 21. Distribution of coefficients of lateral earth pressure k

the lower portion of the wall. The distribution of coefficients of lateral earth pressure shown in fig. 21 for case III' conditions indicates a range from about 0.33 along the culvert wall to 1.22 at the topmost stress meter.

88. 1962 high-water period. The observed effective earth pressures on the lock walls during the 1962 high-water period are shown in plate 62. The distribution of effective earth pressures changed only slightly after the water level in the lock was lowered. The distribution of coefficients of lateral earth pressure for this condition is shown in fig. 21. After lowering of the water level in the lock, the coefficients of lateral pressure decreased along the upper portion of the walls.

Wall Movements

89. Published data on field and laboratory investigations have demonstrated that the magnitude of the coefficient of lateral earth pressure is intimately related to the movement of the wall supporting the backfill. As shown in plates 55 through 58, considerable variations in the movement of the lock walls occurred during and after construction. During placement of backfill, the walls rotated toward the backfill as shown by the time plots of angular rotation α in plates 55 through 58. After the backfill had been completed, the tops of the walls tended to move toward the center line of the lock. At monolith 15 (plate 56), the maximum displacement was in the order of 0.7 to 0.8 in. Using the wall deflection pipe measurements, time plots were prepared of wall displacement versus time at the level of each meter. The zero position of the wall was taken as the position of the wall at the time the backfill reached the elevation of the particular pressure meter. Wall displacement data are shown in plates 63 and 64. Also shown is the coefficient of earth pressure computed at the location of each meter. The wall movement versus time relation more or or less reflects the inverse of the coefficient of earth pressure-time relation. In other words, as the wall moves toward the lock center line, the coefficients decrease, but as the wall moves toward the backfill, the coefficients increase. The wall movements are related to the position at an arbitrary time, as the wall was continuously in

movement during construction. In order to relate the measured coefficients of lateral pressure to the imaginary zero movement position, it is necessary to introduce the concept of earth pressure at rest.

Earth Pressure Coefficients

90. The coefficient of earth pressure at rest k_o is that value of the coefficient of lateral earth pressure acting on a wall prior to any movement of the wall. Several different approaches have been used to determine the coefficient of earth pressure at rest. Tschebotarioff,[20] assuming an elastic, isotropic medium, established the theoretical relation:

$$k_o = \left(\frac{1}{m - 1}\right)$$

where m is the reciprocal of Poisson's ratio μ. Using a value of 0.25 for Poisson's ratio, the resulting at-rest earth pressure coefficient is 0.33. Jáky[21] and Bishop[22] have proposed, through experimental efforts, the relation:

$$k_o = (1 - \sin \phi)$$

where ϕ is the angle of internal friction. Using an average value of $\phi = 40$ deg, this relation indicates a value of 0.36 for the coefficient of at-rest earth pressure. Assuming that ϕ may be as high as 43 deg, the resulting coefficient of at-rest earth pressure becomes 0.32. Bjerrum,[23] in conducting triaxial tests on sand in which a principal stress ratio was so employed that there were no changes in the diameter of the specimens during consolidation, determined a relation between the coefficient of earth pressure at rest and the initial porosity. For a dry density of 100 pcf, this relation indicates a k_o value of 0.43. Assuming the actual density is 5 pcf higher (105 pcf), the resulting value of k_o is 0.30. Based on laboratory and field tests conducted by Terzaghi,[17] k_o for a compacted sand may range anywhere from 0.35 to 0.70. In preliminary tests at WES in 1962, earth pressures at rest were determined using triaxial

testing equipment on a saturated clean sand. The resulting ratio of lateral to vertical pressure was 0.37 at a relative density of 74 percent.

91. At the locations of meters S-12 and S-13, no significant wall displacements are possible because of the structural geometry. At these locations, the computed coefficients of earth pressure average about 0.31. This average value is somewhat lower than that commonly used for the coefficient of earth pressure at rest; however it was chosen as a basis for interpreting the observed measurements for meters located above the culvert. The value of 0.31 may not truly represent an at-rest condition, as the settlement of the backfill may have induced arching around the culvert walls. In fig. 22, the coefficients of lateral earth pressures are plotted versus "adjusted" wall movement. In constructing fig. 22, the wall movements shown in plates 63 and 64 were adjusted as described below. For those meters that indicated any values of k equal to k_o (0.31), the wall movements shown in plates 63 and 64 were referenced with respect to the position of the wall at k equals k_o. For those meters that always exhibited a k greater than k_o, the position of the wall for the lowest value of k was used as the reference, and the curves were shifted to correspond to the curves with a defined k_o. In fig. 22, the curves have been drawn through the plotted points to indicate the chronological sequence of wall movement. All of the movements toward the backfill represent partial mobilization of passive pressures. The curves show a rather sharp increase in the value of k with initial small movements of the wall into the backfill. After a small relaxation in pressure caused by a reversal in the direction of wall movement, the rate of increase of k was less with continued movement toward the backfill. The manner in which the value of k varied with the wall movement at this first unloading cycle appears to be different from the behavior depicted in the latter portion of the curves; no reason is known for this variance. After reaching a maximum value, k decreases at a decreasing rate of change with wall movement away from the backfill.

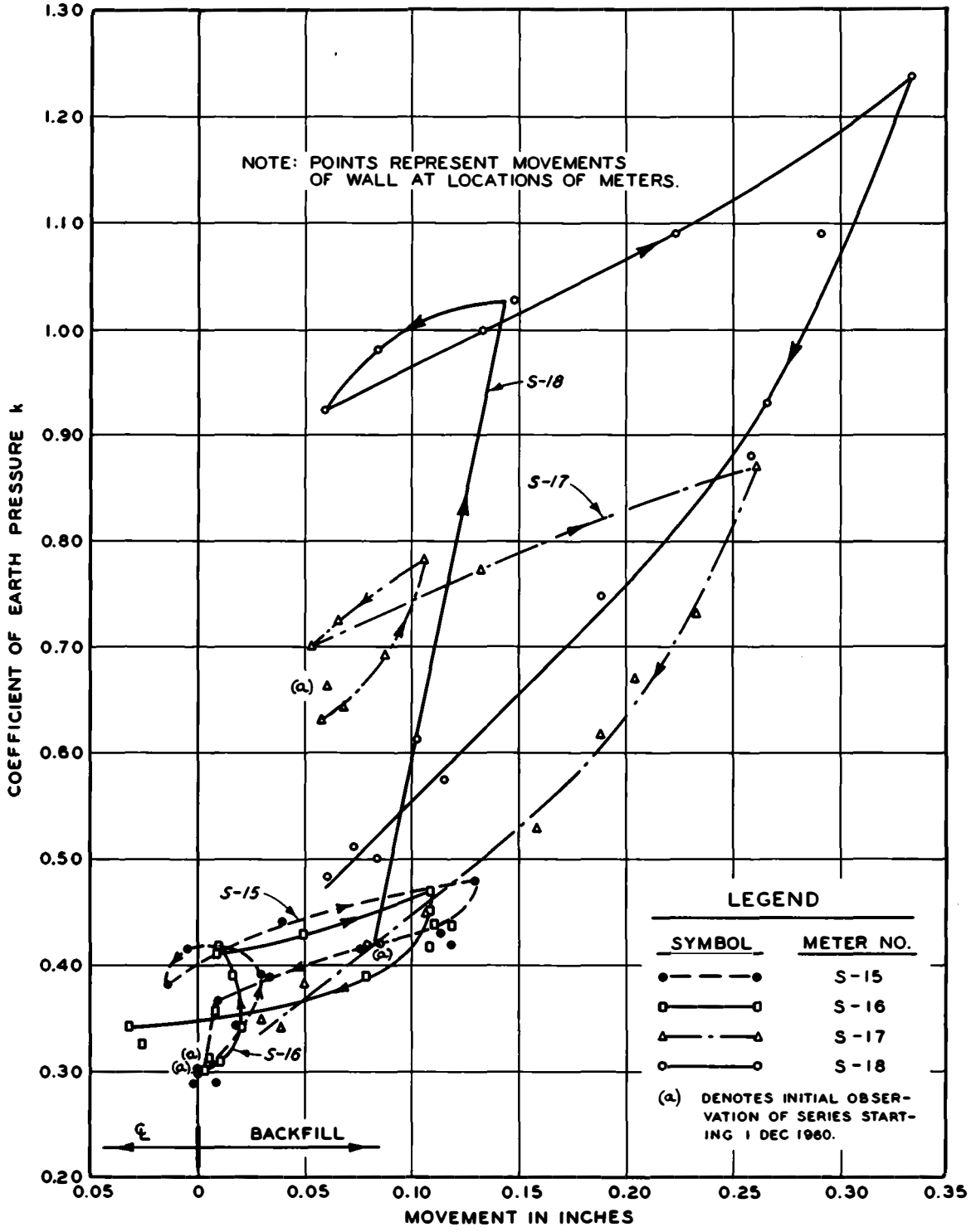

Fig. 22. Coefficient of earth pressure versus movement of walls

PART VI: FOUNDATION BASE PRESSURES AND UPLIFT

Foundation Base Pressures

Effective base pressures

92. From the time plots of observed base pressures shown in plates 29 through 33, profiles were constructed of effective base pressures and uplift pressures beneath the lock for (a) a condition that existed just before wall construction was begun, (b) case II' condition, (c) case III' condition, and (d) 1962 high-water period. These profiles are shown in plates 60, 61, and 62. The profiles, and time plots in plates 31 and 32 show that soil stress meters S-7 and, to a lesser extent, S-6 indicated consistently low pressure values. It is believed that these meters were probably functioning properly and that the low readings indicated the presence of a soft area in the foundation in the vicinity of the two meters. The excess soil pressures apparently were taken up by adjacent portions of the slab, since the reading of soil stress meters S-5 and S-8 for each condition shown in plates 60 and 61 indicated relatively high values of stress adjacent to meters S-6 and S-7.

93. A time plot showing the actual weight of the structure (including the weight of backfill above the culverts and water in the lock and culvert) and the measured effective base pressures, uplift pressures, and measured total base pressures are shown in plate 65. In computing the weight of the structure, the average density of concrete adjusted for the presence of steel was taken as 150 pcf. The density (saturated unit weight) of the sand backfill above the culvert was taken as 125 pcf. The measured effective base pressure is equal to the area under the effective base pressure diagram. (See plates 60 through 62 for examples of base pressure diagrams.) The measured total base pressure corresponds to the foundation reaction and is equal to the measured effective base pressure plus the uplift pressure (area under the uplift diagram).

94. At the beginning of construction, the effective base pressures increased with increasing amounts of concrete placed in the structure. The pressures increased to a maximum of about 250 kips in January 1959.

After January 1959, the effective base pressures decreased as the uplift pressures beneath the base slab increased due to decreased pumping of the dewatering system. At the beginning of December 1959, the uplift reached about 305 kips, and the effective base pressure decreased to about 145 kips. Just after the broken waterline incident in December 1959, the uplift pressures dropped to about 255 kips, resulting in an increase in effective base pressures. The effective base pressures continued to increase as the remainder of the backfill was placed, whereas the uplift pressures remained fairly constant. After the lock was flooded (September 1960), uplift pressures remained about the same as they had been for some time before the lock was flooded, and the increase of load on the lock was immediately reflected in higher effective base pressures. The maximum total base pressure or reaction was 800 kips during the 1961 high water.

Difference between weight of structure and measured reaction

95. The time plot in plate 65 shows a difference between the actual weight of the structure and the measured reaction. This difference, expressed both in kips and in percent of actual weight, is also plotted versus time. The measured reaction varies between 10 percent greater and 5 percent less than the actual weight. This plot also shows that the base pressures beneath the north half of monolith 15 were usually greater than those beneath the south half.

96. The discrepancies between measured total base pressure and actual weight of the structure could be due to the following:

a. Limitations in constructing accurate soil pressure diagrams.

b. Under- or overregistration of the soil stress meters and time effects.

c. Frictional forces generated by settlement of adjacent backfill acting along the sides of the lock.

The effect of errors in drawing the soil pressure diagram was minimized by drawing all soil pressure diagrams with respect to the plotted points in as similar a manner as possible so that the resulting error, if any, would be a constant percentage of the reaction. For comparison, the difference in the actual load and the reaction computed using the effective base

pressures measured beneath the north half of the lock and beneath the south half of the lock are shown in plate 65. A relatively substantial difference between the two differences is noted, although the basic trends are similar.

97. Time effects on meter readings can be demonstrated by the reading taken during placement of the three lifts of the base slab (see plates 29 through 34). In some cases, the meters reacted relatively slowly and did not register a stable pressure until a week after placement of concrete. Measured reactions for these analyses were generally selected in periods of construction inactivity because of this lag; however, any errors due to possible over- or underregistration are still included in the measured values.

98. Probably, the difference between the measured base pressures and the actual weight of the structure is primarily the result of frictional forces acting along the sides of the lock. For instance, from January to August 1960 placement of sand backfill behind the lock walls resulted in a greater load existing under the backfill than under the lock. The increased settlement of the backfill with respect to the lock presumably was effective in creating a downward drag on the sides of the lock that in turn resulted in the measured reaction being progressively greater than the actual structure load. During the 1961 high water, the actual load increased but the measured reaction was less than structure load. This can be explained as the result of frictional forces acting upward on the sides of the lock due to settlement of the lock with respect to the backfill. Likewise during the 1961 low water, the structure load decreased, with the reaction tending to be larger than the structure load. This may have been caused by frictional forces increasing in a downward direction. The same phenomenon was also noted during the 1962 high-water observation. These observations indicate that the development of frictional forces along the walls of the structure might have been possible; however, it cannot be established conclusively. Indirect evidence lends strong support to the possible presence of varying frictional forces along the sides of the lock.

Comparison of Observed and Predicted Base Pressures

99. The effective base pressures and uplift pressures observed at monolith 15 for case II' conditions are shown in plate 60 together with the base pressures assumed in design for the case II condition. The uplift pressures for case II' (plate 60) are somewhat greater than those assumed for design case II. The average observed uplift pressure was about 15.7 psi for case II', whereas an uplift pressure of 14.5 psi was assumed in design for case II. The observed effective base pressure distributions are considerably different from those predicted in design. The observed pressures for case II' indicated that maximum pressures occurred from about 40 to 50 ft on either side of the center of the lock, with a lesser amount of pressure occurring at the center. For design case II, it was assumed that 150 percent of the uniform foundation pressure would act at the center line of the lock and 50 percent at the sides of the lock. For case II', the observed effective base pressure at the center of the lock was about 66 percent of the uniform foundation pressure, and the pressure from about 40 to 50 ft from the center line was about 136 percent of the uniform pressure. The observed base pressures and uplift pressure for case III' are shown in plate 61. A comparison between base pressures for case III' and case III would not be exactly valid because the latter case is for the design high water, which is 12.7 ft higher than case III' high water. To obtain a more realistic comparison, the distribution of foundation pressure was recomputed for case III' uplift pressures and water loads using the same procedure used in design. The recomputed distribution (see plate 61) indicates 125 percent of the uniform foundation pressure at the center line of the lock and 75 percent at the sides of the lock. This is in poor agreement with the observed pressures, which show about 88 percent of the uniform foundation pressure at the center line of the lock and 124 percent about 40 ft from the center line.

100. When moments were computed from external load and when foundation stresses were computed for the settlement analysis, the effective base pressure observed for the north half of the lock was assumed to apply also to the south half of the lock. As previously mentioned, the

development of the frictional force could not be definitely established from the observed data. Therefore, in the computations of moments, the observed effective base pressures were proportionately reduced so that the reaction was equal to the actual structure load. For case II' analyses, computations were also made assuming that the difference between the observed reaction and actual structure load was caused entirely by frictional forces acting at the sides of the lock. In the latter case, the frictional force F_f acting on each side of the lock was 27,700 lb. The lateral force F_h, as determined from observations of soil stress meters along the walls, was 72,460 lb. Considering the angle of wall friction equal to arc tan F_f/F_h, the computed angle of wall friction for case II' was 21 deg, or about one half the angle of internal friction of the sand backfill.

PART VII: BENDING MOMENTS IN BASE SLAB AND WALLS

101. In order to determine the actual bending moments imposed on the structure, moments in the base slab and walls were recomputed on the basis of data from the instrumentation program, and a comparison was made between the recomputed moments and those computed for design. Moments were recomputed only for monolith 15 and were based on the following:

a. Externally applied loads on the structure, as measured by soil stress meters and piezometers.

b. Deflections.

c. Internal stresses, as measured by concrete stress meters and computed from concrete strain meters.

Moments Based on Applied Loads

Moments in the base slab

102. Observed base pressures. Observed external loads acting on monolith 15 are shown in plates 60 and 61 for cases II' and III', respectively. In computing moments in the base slab, the effective base pressures observed for the north side of the lock were assumed to apply also to the south side of the lock. Moments for case II' condition were computed for the two following assumptions: (a) no frictional forces on the sides of the lock (here the observed effective base pressure was reduced so that the total measured reaction was equal to the actual weight of the structure), and (b) the total difference between observed base pressures and structure load was considered to have been caused by friction acting on the sides of the lock. Moments computed on the basis of these assumptions are shown in fig. 23. Considerable difference will be noted in the moments computed, with the maximum moment computed for assumption (b) being about 80 percent greater than the maximum moment computed for assumption (a). Moments computed for assumption (a) were in good agreement with moments computed for design case II. The maximum computed moment (at the center of base slab) was 1077 ft-kips (tension at the top of the slab) as compared to a moment of 1329 ft-kips computed in design case II. The

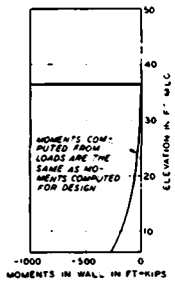

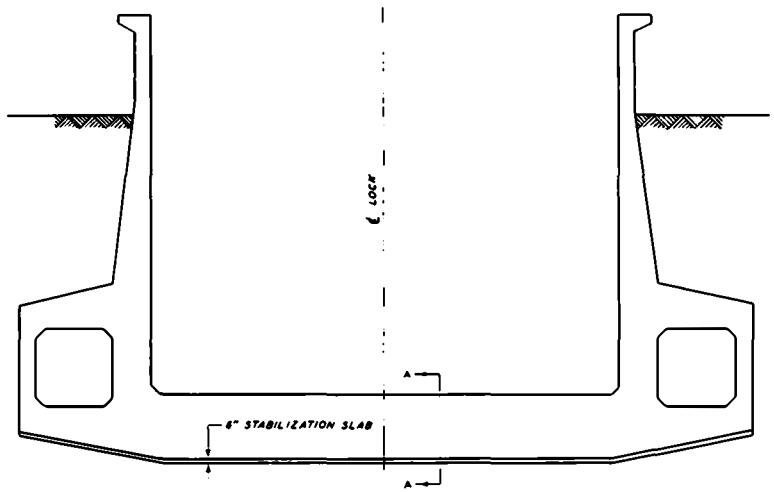

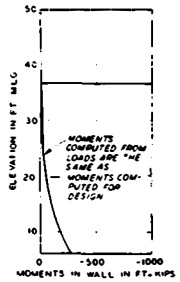

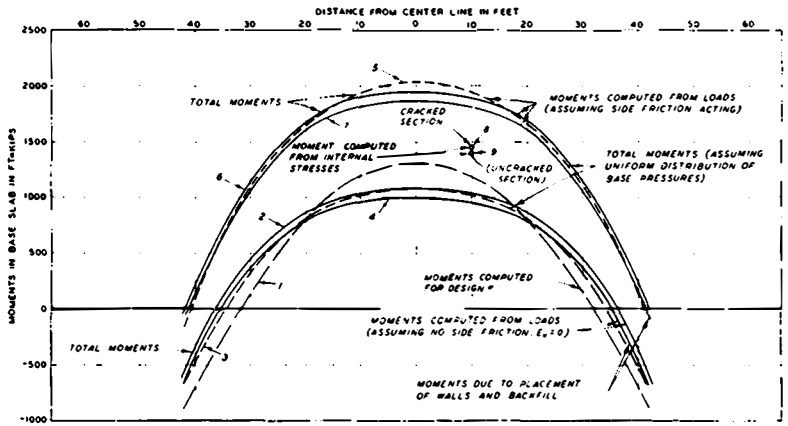

* VALUES FOR CASE II' LOADING SHOWN IN FIG. 7

SUMMARY OF MOMENTS COMPUTED 10 FT FROM CENTER LINE IN FT-KIPS

LOADING CONDITION	BASED ON EXTERNAL LOADS: WITH SIDE FRICTION	BASED ON EXTERNAL LOADS: WITHOUT SIDE FRICTION	BASED ON INTERNAL STRESSES: UNCRACKED SECTION	BASED ON INTERNAL STRESSES: CRACKED SECTION
1. CASE II' LOADINGS FROM THE TIME BASE SLAB WAS COMPLETED	1810(7)	950(4)	1391(9)	1437(8)
2. CASE II' LOADINGS TOTAL				
(a) OBSERVED BASE PRESSURE	1890(6)	1040(2)	..	..
(b) UNIFORM BASE PRESSURE	1950(5)	1020(3)	..	..
3. CASE II LOADINGS TOTAL	–	1190(1)	–	..

NOTE: NUMBERS IN PARENTHESES REFER TO MOMENT DIAGRAM. SEE PLOT AT LEFT.
CLOCKWISE MOMENTS DESIGNATED POSITIVE.

Fig. 23. Summary of moments computed for case II' loading condition, monolith 15

moment at the side of the wall for assumption (a) was computed to be -564 ft-kips as compared to a value of -887 ft-kips computed for design. The maximum moment computed for assumption (b) was 1940 ft-kips at the center line or about 46 percent greater than the maximum moment computed for design case II. The moment at the side of the walls for assumption (b) was computed to be -9 ft-kips. As shown in fig. 23, the moments resulting from construction of the walls and backfill for case II' were also computed for subsequent comparisons.

103. Moments computed from loads for case III' condition are shown in fig. 24. As the measured base pressures were within one percent of the actual structure load, it was assumed that there was no side friction, and the actual measured base pressures were used in the moment computations. If frictional forces had been acting along the outer sides of the structure for the case III' condition, the forces would have been in an upward direction and would have decreased the moments in the base slab. The maximum computed moment at the center of the base slab was 1110 ft-kips; the computed moment at the edge of the wall for case III' was 155 ft-kips. Although the loading conditions assumed for design case III differed substantially from the loading conditions observed for case III', moments computed for case III' were in the same order of magnitude as those computed for design case III (fig. 24). Water levels in the lock higher than those observed for case III' will tend to induce higher moments in the base slab. However, these higher moments will be counteracted to some extent by moments caused by an increase in lateral soil pressure against the walls.

104. Uniform base pressures. Inasmuch as the observed base pressure distributions cannot be conveniently defined mathematically or geometrically, it was considered desirable to formulate an approximate distribution that could be used with reasonable accuracy for design purposes. It appeared that the actual base pressure distribution could be simulated reasonably closely by a uniformly distributed load. Moments in the base slab computed using a uniform distribution of base pressure instead of the observed distribution of pressure for cases II' and III' are shown in figs. 23 and 24. In these computations it was assumed that total effective vertical pressure, as indicated by the areas under the observed stress

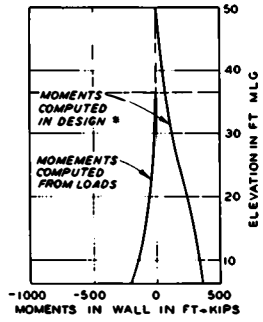

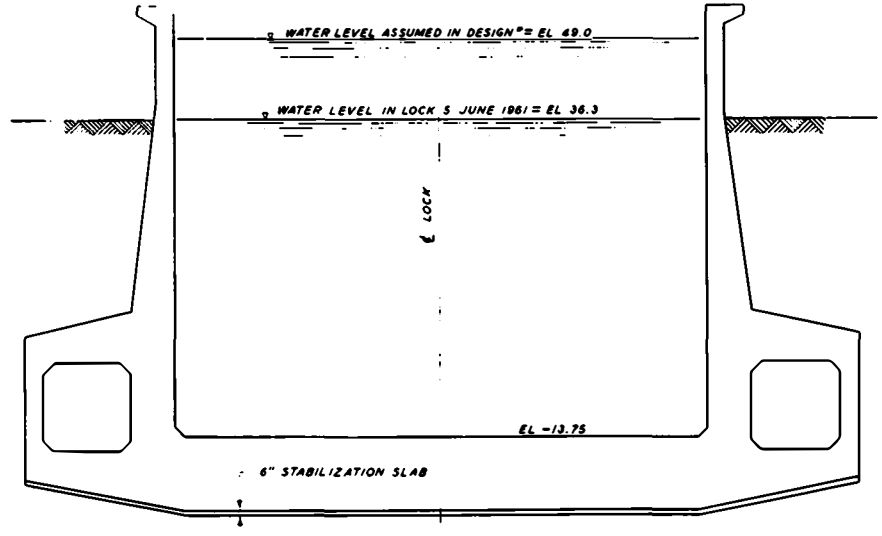

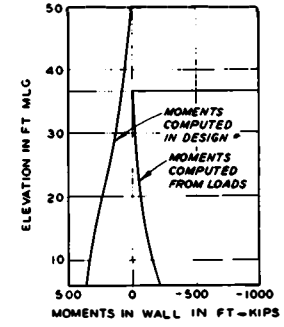

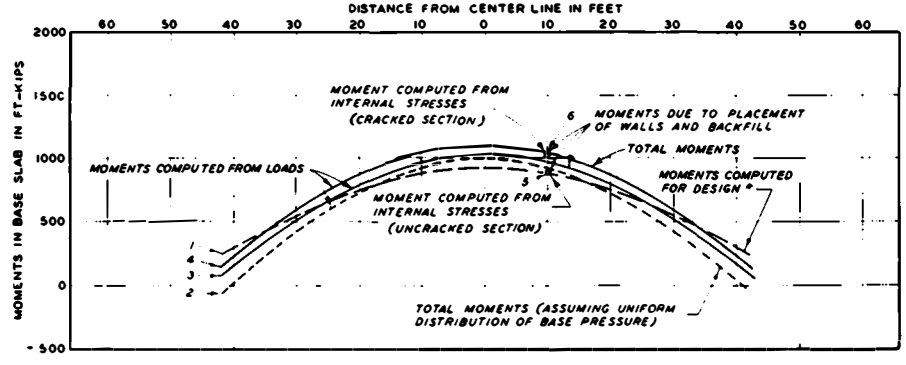

* VALUES FOR CASE III'LOADING SHOWN IN FIG. 7

SUMMARY OF MOMENTS COMPUTED 10 FT FROM CENTER LINE IN FT-KIPS

LOADING CONDITION	BASED ON EXTERNAL LOADS	BASED ON INTERNAL STRESSES	
		UNCRACKED SECTION	CRACKED SECTION
1. CASE III' LOADINGS FROM THE TIME BASE SLAB WAS COMPLETED	970[3]	881[5]	1396[6]
2. CASE III' LOADINGS TOTAL			
(a) OBSERVED BASE PRESSURE	1030[4]	..	..
(b) UNIFORM BASE PRESSURE	920[2]	..	..
3. CASE III LOADINGS TOTAL	880[1]	..	..

NOTE: NUMBERS IN PARENTHESES REFER TO MOMENT DIAGRAM. SEE PLOT AT LEFT.

NO FRICTIONAL FORCES ON SIDES OF LOCK WERE OBSERVED FOR CASE III'.

CLOCKWISE MOMENTS DESIGNATED POSITIVE.

Fig. 24. Summary of moments computed for case III' loading condition, monolith 15

diagrams, was distributed uniformly over the entire width of the base. The moments computed at the center of the base slab are given below:

	Computed Moments, ft-kips	
	Observed Distribution of Base Pressures	Uniform Distribution of Base Pressures
Case II' (with side friction)	1940	2035
Case II' (without side friction)	1077	1121
Case III'	1110	1014

105. It is concluded that fairly good agreement exists between moments computed using a uniform distribution of base pressures and moments computed using observed base pressures. It appears, therefore, that realistic moments in the center of the base slab could have been computed in the design of Port Allen Lock by assuming that the base pressure was uniform.

Moments in the walls

106. Moments in the walls computed from observed lateral pressures for cases II' and III' are shown in figs. 23 and 24. The observed lateral pressures on the wall for case II' condition were about the same as the lateral pressures assumed for design case II (see plate 60). Consequently, the moments computed from observed loads are about the same as moments computed in design. The maximum computed moment in the walls (just above the culvert) for case II' was 275 ft-kips (tension on the backfill side of the wall). The maximum moment in the wall computed for design case II was 284 ft-kips.

107. The loading condition on the wall for case III' was considerably different from the condition assumed in design case III, as the water level in the lock was 12.7 ft lower than the water level assumed in design. For that reason, the moments computed for case III' were considerably different from the moments computed in design. The maximum moment computed in the walls for case III' (shown in fig. 24) was about 200 ft-kips (tension on the backfill side of the wall). The maximum moment computed for design case III was 360 ft-kips (tension on the inside of the wall).

Analysis of culvert frame

108. Design assumptions. The magnitude and distribution of earth and water pressures assumed acting on the culvert frame for design cases II and III are shown in fig. 7. In determining the moments and shears around the culvert, moments and relative deflections were computed neglecting the strut action of the back wall of the culvert. The strut load and resulting moments were then computed assuming that the strut would restore the distance between top and bottom slabs of the culvert to the original distance. Final moments were then obtained by combining the original moments with the moments of the strut load. Axial thrusts were neglected in computing required areas of reinforcement.

109. Observed pressures. Plates 60 and 61 show a comparison of observed pressures on the sides of the culvert frame for cases II' and III' conditions and the pressures assumed for design cases II and III. For case II', the observed base pressures beneath the culvert exceed the pressures assumed for design case II, and for case III', the observed uplift and observed lateral water pressures exceed those values assumed for design case III. For the most part, however, observed pressures were equal to or less than those assumed for design. The maximum deviation of the observed pressure from the assumed pressure around the culvert frame was a 40 percent increase for the lateral water pressure, a 20 percent increase for the uplift, a 3 percent increase in the foundation reaction, and a 40 percent decrease in the lateral earth pressure. The assumed overburden pressure agrees closely with the pressure recorded by stress meter S-14, located on top of the culvert (see plate 35).

110. Observed deflections. Observations at settlement plate 9 and reference point SP-7 (see locations in plate 14) indicate rotations of the culvert floor. Observations of the wall deflections indicate rotations of the lock-side culvert wall. The angular rotation of the bottom of the floor (or top) β and the angular rotation of the lock-side wall α and the differences in these two angles are plotted versus time in fig. 25. The distortion of the culvert frame is also shown schematically in the same figure. In design, the assumption of no frame distortion was only an expedient used in computing wall deflections for estimating earth pressures

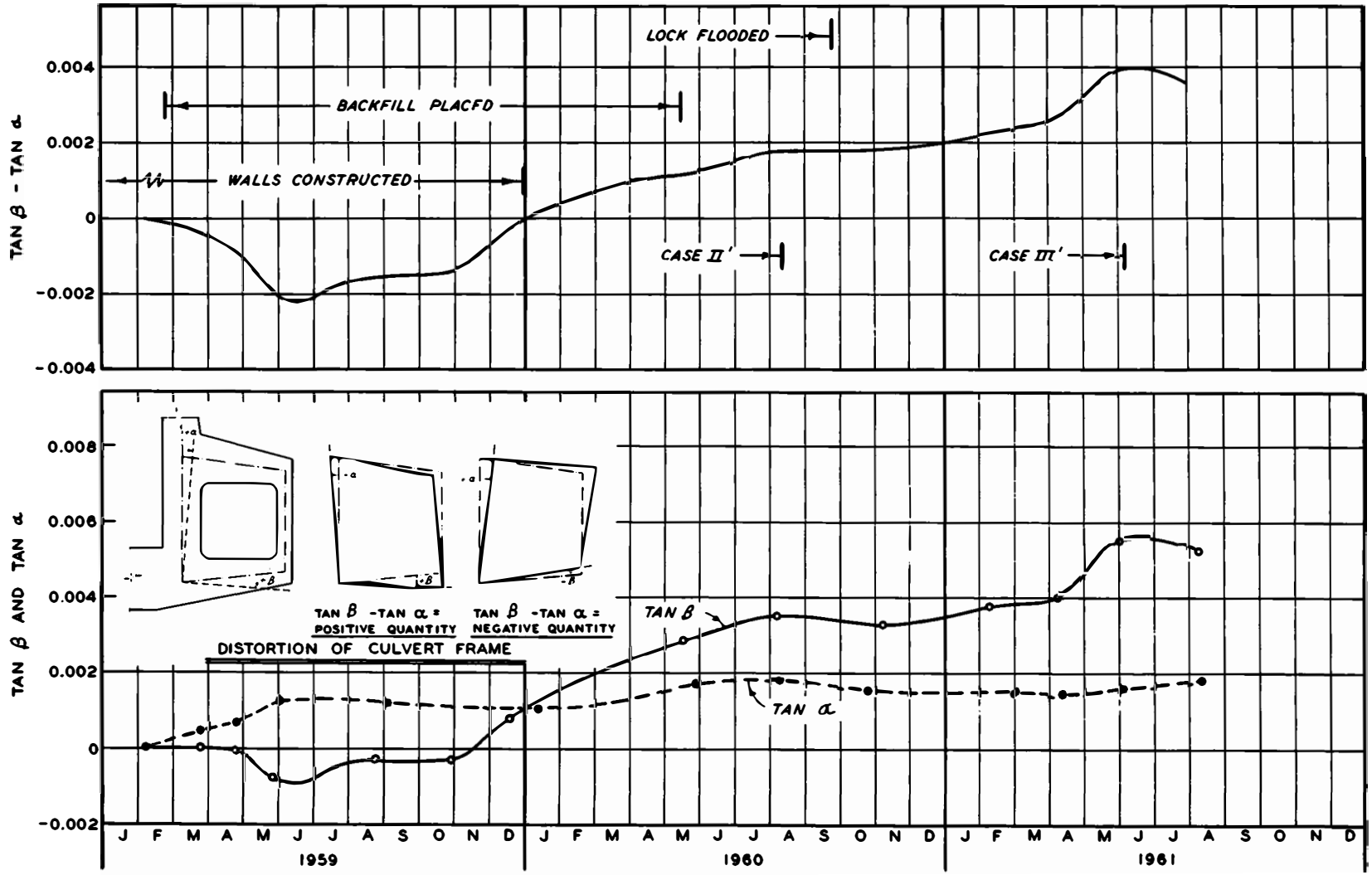

Fig. 25. Angular distortion of culvert frame

for case III loading. The observed data show that the assumption of no frame distortion was not realistic but on the safe side.

111. Bending moments. As observed pressures are generally equal to or less than design loadings, no computations were made of bending moments resulting from applied loads. A rigorous solution to determine the moments caused by the superimposed effects of the observed pressures and deflections was not justified, as the deflections were not measured to a sufficient degree of accuracy. However, the type of moment indicated by the direction of the distortion indicates that actual moments in the culvert frame generally were less than those estimated for design.

Computation of Moments from Deflection

112. In order to verify the values of base slab bending moments computed from observed loads at monolith 15, an attempt was made to compute moments in the base slab on the basis of observed deflection of the slab. In order to simplify the analysis, the net deflection of the base slab for case II' that was caused by placement of the walls and backfill was selected for computing a net moment. That part of the deflection resulting from thermal gradients in the base slab was found to be insignificant. A curve of best fit, determined by the method of least squares, was fitted to the observed deflection data. The second derivative was taken of the equation of best fit, and the moments were computed by multiplying the results by the product EI (modulus of elasticity of the concrete $\times$ moment of inertia). The value of E is the sustained modulus of elasticity (instantaneous modulus corrected for deformation due to creep) and was determined from values obtained in creep tests reported in Appendix C. A value of E of 5.3×10^{-6} psi was selected as the average E for the age of concrete at the time that case II' measurements were made. The value of I (moment of inertia of the base slab) was computed for a cracked section.

113. It was immediately apparent that a very small change in the deflection data (about 0.003 ft between two adjacent points) would result in widely different values of computed moments. Consequently, it was

concluded that the deflection of the base slab was not determined with sufficient accuracy to enable computation of reasonable moment values.

114. In order to provide a better correlation, the net deflection of the slab was computed directly from the moment curve resulting from case II' conditions after completion of the base slab and was compared with the observed deflection. For case II', assuming no frictional force, the equation of best fit for the moment curve was:

$$M = 1196 - 0.986x^2$$

where

M = moment in ft-kips

x = horizontal distance from center line of slab in ft

The deflection was computed from the equation:

$$y = \frac{1}{EI}\int_0^x \int_0^x (1196 - 0.986x^2)\, dx^2$$

In the computations, it was assumed that zero deflection occurred at the center of the lock.

115. A comparison of the observed deflection of monolith 15 and deflections computed from moments is shown in fig. 20. For case II', deflections were computed for two moment curves; one moment curve was computed assuming friction along sides of the lock, and the other curve was computed assuming no side friction. A good comparison between the observed deflection and deflection computed from moments is obtained if frictional forces are assumed acting at the outer sides of the wall. For the assumption of no side friction, the computed deflection is about half the observed deflection. For case III', the deflection of monolith 15 could not be determined accurately because of sediment on the settlement plates. Consequently, a comparison of computed deflections for monolith 15 was made with the observed deflections for monolith 6. As shown in fig. 20, the deflections computed from the moment curve are somewhat less than but generally in fair agreement with the observed deflection for monolith 6.

Moments from Internal Stresses

Internal strains and stresses

116. A summary of the internal strains as measured by the strain meters for cases II' and III' conditions are shown in plates 66 and 67, respectively. The changes in internal strains resulting from lowering the water level in the lock during the 1962 high-water observations are shown in plate 68. The internal stresses computed from the strain meter data as previously described are shown for cases II' and III' conditions in plates 69 and 70, respectively. The change in internal stresses for the 1962 high-water case is shown in plate 68. The internal stress distribution in the base slab was used as a basis for computing bending moments and thus provides a comparison with moments computed by other methods. The moment in the base slab was computed at a section 10 ft south of the center line using the distribution of internal stresses computed from the array of strain meters at this location. Plate 66 shows that the stress distribution in the base slab prior to placement of the walls and backfill was very complex; therefore, no attempt was made to compute moments in the base slab for conditions existing prior to this time. Instead, the internal stresses just prior to placement of the walls (15 December 1958) were considered as a zero reference, and moments caused by subsequent loads were computed. As previously noted, it appears that observed strains in the upper (tension part of the slab for cases II' and III') do not reflect true strains because of cracking that has developed. Consequently, moments were computed assuming both an uncracked and cracked section.

Analysis of uncracked section

117. The analysis of moments based on an uncracked section is shown in fig. 26. Assuming complete bond between the concrete and the steel reinforcing bars, the strains in the steel bars were estimated from strain meter data and the resulting stresses in the steel were computed using a value of E of 29.3×10^6 psi (see Appendix C). Adding the computed internal forces in the concrete and steel provided a means to check the static equilibrium of horizontal forces. Since there was a net deficiency of tensile forces (excess of compressive forces), the vertical axis of the

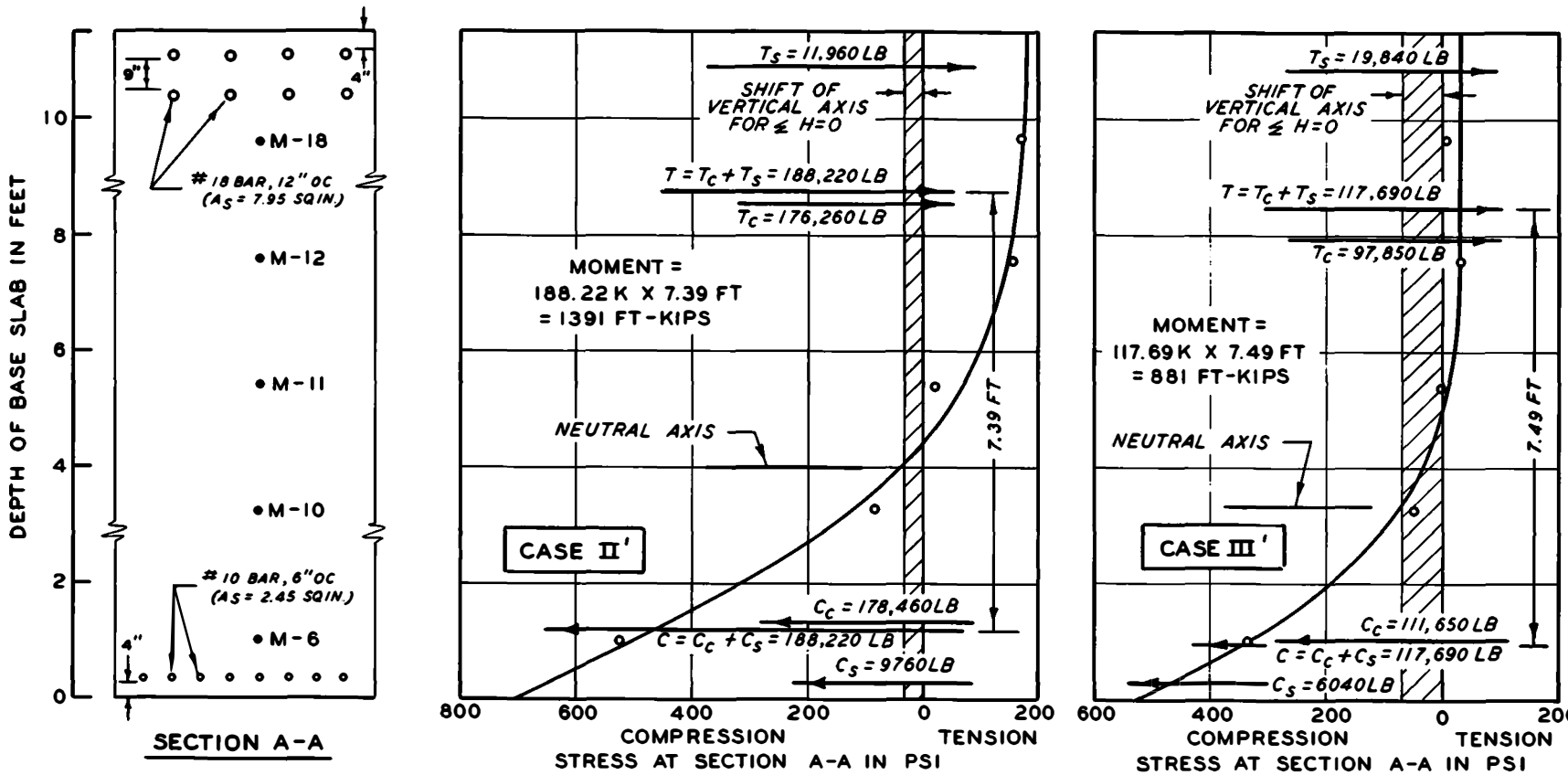

NOTE: SEE FIG 23 FOR LOCATION OF SECTION A-A.

Fig. 26. Moments computed from internal stresses in base slab at uncracked section A-A

stress plot was shifted to a new position, as indicated by the shaded area in fig. 26, so that the summation of horizontal forces would be equal to zero. It should be noted that the section under consideration is also subject to a compressive force equal to the lateral thrust on the sides of the lock. However, part of this thrust may have been taken up by friction along the base of the lock. Further, the distribution of the resultant stress across the section is unknown. Consequently, it was not considered necessary that the force represented by the shift of the vertical axis be equal to the force resulting from the lateral thrust. In shifting the vertical axis of the stress plot, the steel strain and resulting computed steel loads were also revised accordingly. By shifting the vertical axis 30 psi for case II, the condition of static equilibrium of the section was satisfied, although only part of the full lateral thrust of 56.8 psi for case II' is thus accounted for. For case II', the neutral axis of the cross section was taken as the location of zero stress, 4.0 ft from the bottom of the slab. The summation of moments about this point indicates a moment of 1391 ft-kips. For case III', it was necessary to shift the vertical axis 68 psi, or actually more than the full lateral thrust of 27.5 psi for this condition. For case III', the neutral axis was taken as 3.3 ft from the bottom of the slab, and the computed moment was 881 ft-kips.

118. Moments computed from internal stresses and from observed external loads are shown in figs. 23 and 24. As previously mentioned, moments computed from external loads for case II' condition were computed assuming (a) frictional forces along the sides of the lock and (b) no frictional forces. As shown in fig. 23, the moment computed from internal stress is about midway between the values computed for the assumptions above. This would indicate that frictional forces did exist during the case II' conditions, but the forces were less than those considered in assumption (a). As seen in fig. 24, the moment computed from internal stresses for the case III' condition is in good agreement with moments computed from external loads, although in view of the relatively large discrepancy between the lateral thrust and the force represented by the shift of the vertical axis, it appears that the agreement is fortuitous.

Analysis of cracked section

119. The nonlinearity of strains across the depth of the base slab and trends noted with time for the strain meters that registered tension indicate that cracking extended to a sufficient depth to prevent the development of a full tensile stress block in the concrete. Visual indications of cracking were noted on the surface of the slab prior to filling of the lock. The large tensile strains indicated by strain meters M-19 and M-20 in the upper part of the slab also constitute reliable evidence concerning the existence of cracks. In the analysis, it was assumed that cracks developed so that all of the tensile force in the slab was carried by the tensile steel, and the difference between the observed concrete compression block and the tensile force in the steel was equal to the lateral thrust. The effect of the lateral thrust was considered by reducing the concrete compression block and increasing the tensile force in the steel so that (a) the remaining compressive force was equal to the remaining tensile force, and (b) the moment about the center of the slab that was caused by the decrease in compression force was equal to moments caused by increase of tensile force (see fig. 27). Under this assumption, the computed moment for case II' is 1437 ft-kips and for case III' is 1095 ft-kips. Although the computed moments for case II' are somewhat larger than those estimated for design, it is not considered that the safety of the structure was endangered. The computed maximum stress in the reinforcing steel for case II' was 13,600 psi, which is well below the average yield point of approximately 40,000 psi. The computed maximum compressive stress in the concrete was 700 psi for case II', which value is well below the maximum compressive stress of approximately 4600 psi indicated by compression tests on concrete.

1962 high-water observations

120. The measurement of external load changes and of changes in strain resulting from lowering the water level in the lock during the 1962 high-water observations provided an opportunity for comparing the change in moment based on (a) the change in external load, and (b) the change in internal stress computed from the change in observed strain. Because of the rapid change in load, the change in internal stress can be computed

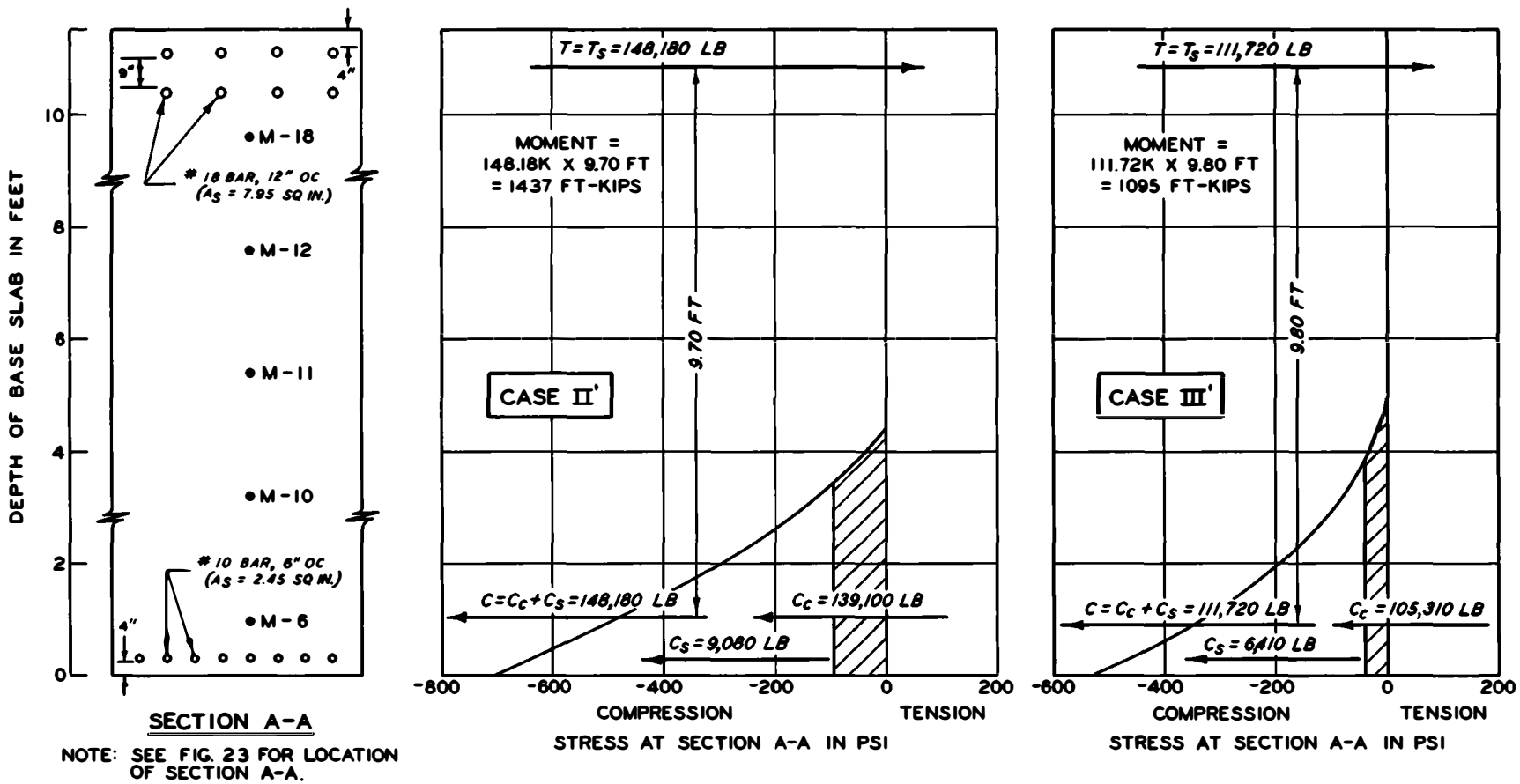

Fig. 27. Moments computed from internal stresses in base slab at section A-A, cracked section

directly by multiplying the change in strain by the instantaneous modulus of elasticity. The effects of creep and other time-dependent strain effects can be disregarded. Thus, the change in internal stress due to changes in external load can be accurately determined on the basis of the strain distribution across the base slab as shown in plate 68.

121. It was concluded that bending moments for the rapid change in loading should be computed only for a cracked section, disregarding the observed tensile stresses in the base slab. The change in bending moment at a point 10 ft south of the center line of the base slab was 668 ft-kips, and the corresponding change in bending moment computed on the basis of the change in external loading (see plate 65) was 729 ft-kips, or a difference of only 8.4 percent. Included in the external loadings was a downward frictional force of 31.8 kips. Disregarding the side friction would have resulted in still larger discrepancy between moment computed from changes in internal stresses and moment computed from changes in external load. Consequently, these computations lend further support to the existence of frictional forces acting on the sides of the lock.

Moments Computed Using Theory of Beams On Elastic Foundations

Theoretical assumptions

122. As previously noted, the classic problem of computing the pressure developed under a loaded area has been the subject of many investigations. The problem is of considerable practical significance and, consequently, has attracted a variety of solutions ranging from simple and sometimes crude approximations to highly refined mathematical treatments. Basically, two approaches have been utilized. In the first approach it is assumed that the contact pressure is proportional to the deflection at the same point. The ratio between the intensity of load under the foundation and the corresponding settlement is assumed to be a constant k called the coefficient of subgrade reaction. The assumption corresponds to a physical model of the foundation equivalent to a set of elastic, uniformly spaced springs. In the second approach, it is assumed that the subgrade

behaves as a homogeneous, isotropic, elastic solid whose elastic properties can be defined in terms of a modulus of deformation E_s and a Poisson's ratio μ. Vesić[24] and Terzaghi[10] have shown that these two approaches yield different results, the difference being due primarily to the effects of the ends of the beam; that is, the two approaches will furnish practically the same results if the beam is sufficiently long.

123. Using the second approach, a number of theoretical solutions have been suggested for a U-frame structure founded on a semi-infinite elastic medium. Using a simple U-frame section, Hetényi[12] equated the elastic deflection curve of the base slab to the deformation curve of the foundation with great mathematical precision. For this reason, the solution is long and laborious. Benscoter[11] offered a similar solution for a U-frame cross section in which slope deflection equations were used as a basis for the analysis. Simplified solutions to the U-frame problem have been presented by Ohde[13] and Smith,[14] using finite difference methods. Ohde utilized Boussinesq's solution for displacements (deflections) under a concentrated load by integrating over a uniformly loaded area (see fig. 28). In the Smith method, displacements are computed for triangular elements of load instead of the rectangular elements used by Ohde. The deflection at the center of an arbitrarily chosen element is the summation of the deflections caused by all other elements. The condition of continuity of the slope at elastic line is satisfied by writing a system of equations containing deflections and moments in terms of the unknown pressures. The simplification of these equations yields a system of simultaneous linear equations that can be solved for the unknown pressures.

Elastic beam theory applied to Port Allen Lock

124. In applying the theoretical solution for a beam on an elastic foundation to the Port Allen Lock structure, the finite difference methods suggested by Ohde and Smith were used due to their simplicity in application. A value of E equal to 5.3×10^6 psi was used, this value being the sustained modulus of elasticity. The moment of inertia of the base slab ($I = 126.7$ ft^4) was based on the full uncracked section. Since the value of the sustained modulus is smaller than that of the instantaneous

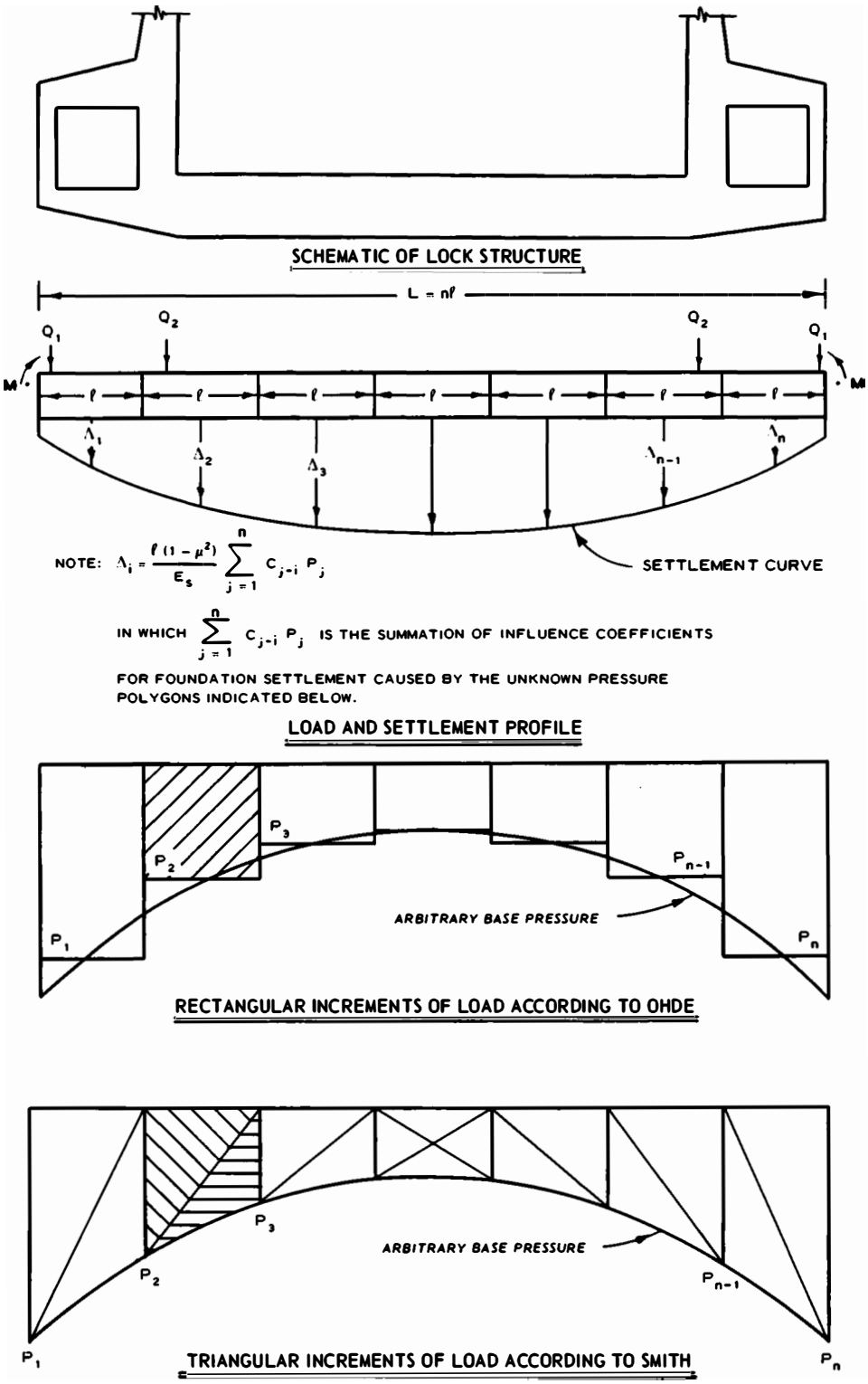

Fig. 28. Schematic diagrams of Ohde's and Smith's methods for computing base pressures

or elastic modulus, and since the moment of inertia for the full section is larger than that for the cracked section, the values selected result in an average value of the product EI . Two values of I were assumed to apply to the culvert section: 26.1 ft^4 and 1391.6 ft^4. The smaller value was the average of the culvert floor, and the larger value was the gross I of the culvert section. Two values of E_s (520 and 133 ksf) were assumed to apply. The larger value was based on the stress produced in the triaxial tests on foundation soils at a strain of 2.5 percent, and the smaller value was based on the strain produced in triaxial tests on representative samples at a stress equal to the average total stress under the structure. The vertical load caused by the weight of the wall stem was assumed to be carried totally by the inside wall of the culvert. The weight of the backfill, including frictional forces for case II', and the top of the culvert were assumed to be carried by the outside wall of the culvert. The average weight of the floor of the culvert was assumed to be uniformly distributed, as was the weight of the base slab. The moment caused by the horizontal thrust of the backfill was replaced by a coupling between the wall stem and the back face of the culvert. A schematic view of the simplified structure and net loading diagram is shown in fig. 29.

125. Analyses by Smith's and Odhe's methods give essentially the same magnitude and distribution of pressure, and consequently only Smith's solution is presented. Fig. 29 indicates the result of Smith's solution using the smaller I of the culvert section and the larger E_s . The solution is practically unaffected by using the larger I or the smaller E_s . The computed base pressures and resulting bending moment differ markedly from the observed pressures and corresponding bending moments.

126. As the largest difference in observed and computed pressure is at the sides of the lock, an attempt was made to incorporate into Smith's solution the effect of the backfill. Considering the backfill as a flexible load projected on the plane of the base slab, the computed elastic deformations were superimposed on the deformations that had been caused by structural loads. The resulting deflection diagram (not shown) indicated a large deflection near the sides that theoretically would necessitate a tensile base pressure at the side of the lock. The occurrence

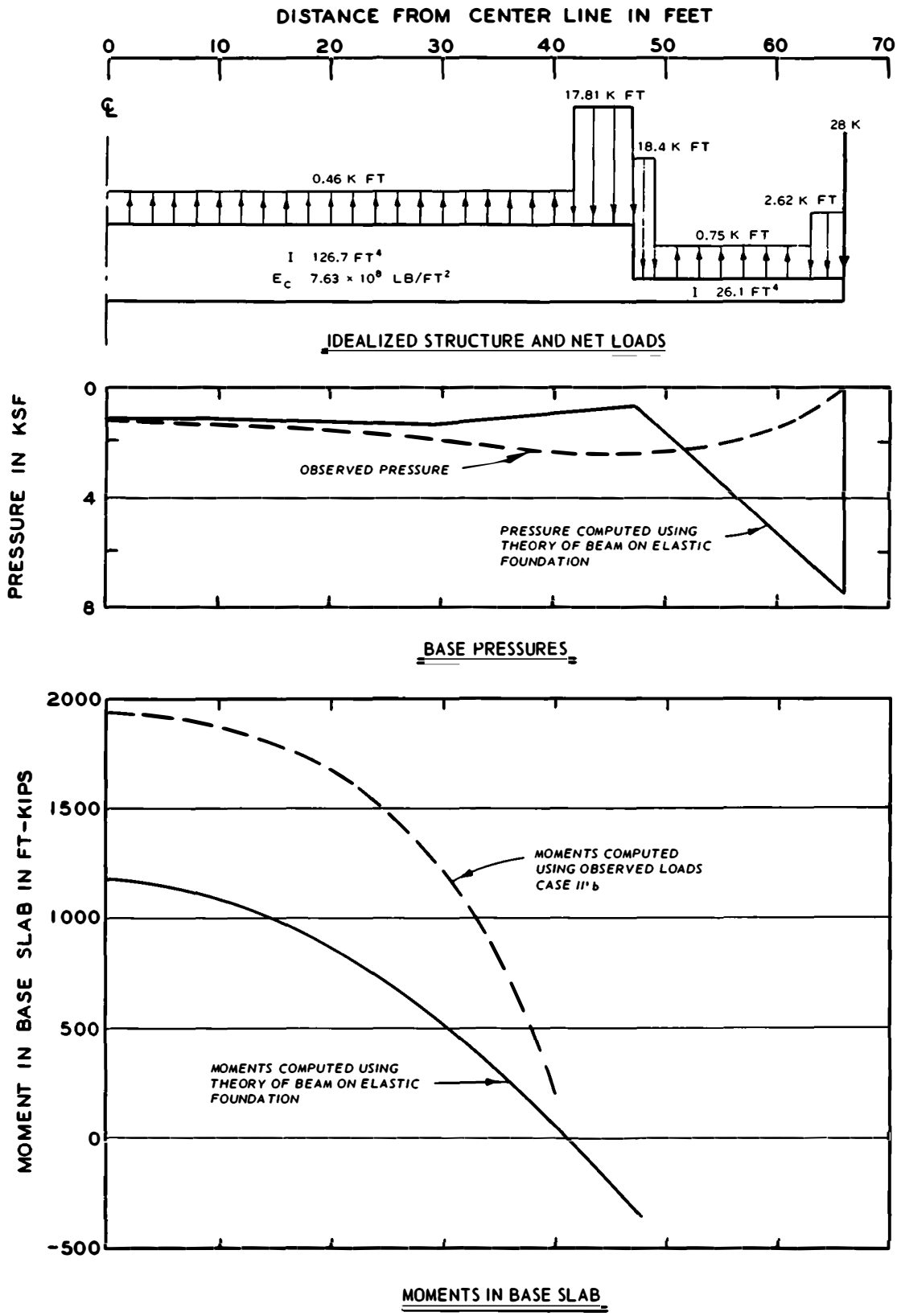

Fig. 29. Base pressures and moments based on theory of beam on elastic foundation

of tensile base pressures is, of course, impossible. The computed deflection of the structure according to Smith's method resulted in a smaller deflection in the central portion and much greater deflection at the sides than those observed. This suggests that the soil is not accurately described as being elastic, with consolidation and compression effects being too important to neglect.

Comparison with design procedure

127. The use of theory of beams on elastic foundations for U-frame structures leads to base pressure distributions and bending moments that are significantly different from the observed pressures at Port Allen Lock. In contrast, the procedure used for determining the bending moments for design, utilizing trapezoidal base pressure distributions, results in bending moments that agree closely with those computed from actual stress and load observations, providing cognizance is taken of frictional forces acting on the sides of the lock. The trapezoidal base pressure distributions assumed for design differed in form from the observed base pressure distributions. As previously noted, the assumption of a uniform base pressure distribution will also provide a realistic indication of the true moment in the base slab. The important fact is that the distribution of the foundation base pressure, within certain limits, has a relatively small effect on the resulting moments. The magnitude of the frictional forces along the sides of the lock has a relatively greater effect on the resulting moments than the base pressure distribution itself. For future U-frame structures with similar width-to-depth ratios and similar soil condition as those for Port Allen Lock, it is recommended that uniform base pressure distributions be assumed for design purposes and that cognizance be taken of the frictional forces that might develop along the sides of the lock during various stages of construction.

PART VIII: CONCLUSIONS AND RECOMMENDATIONS

Conclusions

128. Based on the analysis and observations of engineering measurement devices at Port Allen Lock, the following conclusions are believed warranted.

Instrumentation

129. The Carlson soil stress meters and other electrical devices performed in a satisfactory manner and constitute an accurate and reliable means of obtaining field measurements provided they are thoroughly checked and tested prior to installation. With the exception of one WES pressure cell, all of the electrical measurement devices were operating as intended after approximately five years of service.

130. The engineering measurement devices generally functioned as intended, and the number and types of devices employed were adequate. In retrospect, the direct measurement of strains in the reinforcing steel in the base slab, utilizing bonded electrical strain gages, would have facilitated the computation of bending moments. It is also believed that settlement plates within the backfill along the lock chamber walls would have contributed to a better understanding of the development of negative skin friction on the walls. Utilization of a pressure cell capable of measuring both shear and normal stresses would be of considerable benefit in similar future installations.

131. The wall deflection pipes provided a simple means of determining accurate measurements of the rotation and deflection of the lock walls.

132. Both the water level device and deepwater sounding device operated satisfactorily for measuring settlements of the lock floor; however, these methods are not sufficiently precise for measuring deformations of the floor slabs.

Observations and analysis

133. The predicted rebound was from 42 to 75 percent of the observed rebound, which ranged between 0.26 and 0.36 ft. A close agreement between predicted and observed rebound should not be expected, as the groundwater

level and the hydrostatic head in the deep sands after excavation had been completed differed appreciably from those assumed in design. A close agreement between the observed and computed rebound was obtained using revised rebound computations based on actual load conditions.

134. Rebound and settlement computations using Boussinesq's and Westergaard's equations indicated very little difference in the results for the two methods of determining stresses in the foundation.

135. In general, observed settlements were less than the predicted settlements. Settlements computed using actual load conditions were in generally good agreement with observed settlements for case II', but were significantly greater than observed settlements for case III'. The difference between computed and observed settlements for case III' was due in part to difference in load and probably to inadequate time for the foundation to consolidate. For structures founded on alluvial deposits, the computed settlements will give the general magnitude of settlement to be expected, but not an accurate estimate of the transverse settlement profile.

136. The lock settled at a relatively uniform rate during construction, and as of 1963 settlement appeared to be essentially complete. However, the lock still tends to settle and rebound a minor amount with rising and falling river stages.

137. The observed base pressure distribution curve differed in shape from that of the distribution curve assumed for design. The distribution curve of effective base pressures beneath the lock is in the general shape of a concave parabola, with maximum pressures occurring about 40 to 50 ft from the center line of the lock.

138. Differences in magnitude between the measured total base pressures and the actual structural load for case II' are attributed to frictional forces acting at the sides of the lock that are probably caused by greater settlement beneath the backfill than beneath the lock itself. For case III', with the high-water level in the lock, the lock settled more than the backfill, thus tending to produce upward frictional force on the side of the lock.

139. The observed lateral earth pressures for case II' were in

fairly close agreement with lateral earth pressures assumed for design case II. The observed lateral earth pressures for case III' differed considerably from those assumed for design case III', being greater than the latter along the upper half of the wall stem and smaller along the lower portions of the wall. In all cases, the wall moved toward the backfill. The lateral earth pressure in all cases varied from approximately at-rest pressure near the base of the walls to partially passive pressures along the upper part of the wall. The average computed coefficient of earth pressure near the base of the walls was 0.31.

140. The moment in the base slab at the center line of the lock computed from observed external loads for case II' was approximately one and a half times the value computed for design case II. The difference is attributed to the neglect of frictional forces acting along the sides of the lock for case II. The higher computed moments in the base slab for case II' are not considered detrimental with respect to the safety of the structure.

141. The observed stresses at one of the three concrete stress meters agree reasonably well with those computed for the adjacent strain meter. In the case of the other two stress meters, the agreement with stresses computed from adjacent strain meters was less favorable. No reasons are known for these discrepancies.

142. The moments in the base slab can be computed with reasonable accuracy by using an assumed uniform distribution of base pressures. Computations of base pressures and moments using theories for a beam on an elastic foundation were in poor agreement with actual base pressures and moments.

Recommendations

Recommendations regarding Port Allen Lock

143. It is recommended for Port Allen Lock that:

a. All electrical measuring devices, settlement reference points and plates, and wall deflection pipes be

read once yearly during the low-water season when the river and canal stages are approximately equal. Measurements should be made on all devices whenever the lock is dewatered.

b. Additional studies be made to evaluate the significance of internal stresses and strains measured shortly after placement of each lift of concrete in the base slab. Studies should be made to establish the reasons for the discrepancies between stresses computed from strain meter data and those measured by the concrete stress meters.

Recommendations regarding similar structures

144. On the basis of data obtained from the instrumentation program at Port Allen Lock, the following recommendations are made with regard to similar structures having the same height-depth ratio and having similar foundation soils and backfill materials:

a. The lateral earth pressures acting on the lock walls should be assumed to vary from at-rest pressures near the base of the walls to partially passive pressures along the upper part of the wall. The magnitude of the lateral earth pressures will depend on the sequence of construction, particularly the relation of the sequence of wall construction to backfill placement. Inasmuch as the coefficient of lateral earth pressure k varies along the height of the wall, values of k selected for future design should be based on observed k values contained in this report (see fig. 27).

b. For practical purposes, the distribution of base pressures beneath a lock founded on similar soils can be simulated by a uniformly distributed base pressure. Use of the methods based on theory of beams on an elastic foundation does not result in base pressures that are in reasonable agreement with observed base pressures. The method of predicting distribution of foundation base pressures at Port Allen Lock may be reasonably reliable for other soil conditions. However, consideration should be given to the relative settlement of the lock and adjacent backfill and to the resulting frictional forces that may develop between these two elements. Such frictional forces may act either upward or downward with respect to the walls. For estimating purposes where settlement of the backfill will exceed that of the lock, it is recommended that a value of angle of wall friction equal to about one-half the angle of internal friction of the backfill material be used in computing a downward drag on the lock.

c. It is essential in U-frame lock construction that the backfill be brought up concurrently on both sides of the lock. Slight differences in loading, such as unequal water levels in the backfill, may cause tilting of the lock and undesirable stresses in the lock frame.

LITERATURE CITED

1. U. S. Army Engineer Division, Lower Mississippi Valley, Vicksburg, CE, "Gulf Intracoastal Waterway, Plaquemine-Morgan City Route, Port Allen Lock; Lock Masonry," Design Memorandum No. 5, Feb 1956, Vicksburg, Miss.

2. _____, "Gulf Intracoastal Waterway, Plaquemine-Morgan City Route, Port Allen Lock; Instrumentation," Design Memorandum No. 5B, July 1956 (revised Mar 1957), prepared by U. S. Army Engineer Waterways Experiment Station, CE, Vicksburg, Miss.

3. Sherman, W. C., "Instructions for Installation and Observations of Engineering Measurement Devices, Port Allen Lock; Gulf Intracoastal Waterway, Plaquemine-Morgan City Route," Instruction Report No. 3, Dec 1957, U. S. Army Engineer Waterways Experiment Station, CE, Vicksburg, Miss.

4. _____, "Calibration and Installation of Electrical Measuring Devices and Wall Deflection Pipes - Port Allen Lock," Miscellaneous Paper No. 3-432, June 1961, U. S. Army Engineer Waterways Experiment Station, CE, Vicksburg, Miss.

5. Sherman, W. C. and Trahan, C. C., "Results of Tests on Concrete Cylinders and Sand Backfill, Port Allen Lock," Miscellaneous Paper No. 3-437, June 1961, U. S. Army Engineer Waterways Experiment Station, CE, Vicksburg, Miss.

6. Mansur, C. I. and Kaufman, R. I., "Dewatering the Port Allen Lock Excavation," Transactions American Societ of Civil En ineers Vol 126, Part I, Paper No. 3215, 19 1, pp 1037-1057.

7. Franzius, O., "Uber die Berechnung von Trockendocks (The Design of Dry Docks)," Zeitschrift für Bauwsen, 1908.

8. Dehnert, H., "Schleusen und Hebewerke (Locks and Ship Lifts)," Springer-Verlag, Berlin-Gottingen-Heidelberg, 1954.

9. Siemonsen, F., "Die Lastaufnahmekrafte in Baugrund und die dadurch hervorgerufenen Spermurgen in linen Grundkorper (The Forces in Foundation Soils Caused by Applied Loads and the Resulting Stresses in Foundation)," Bautechnik, 1942.

10. Terzaghi, K., "Evaluation of Coefficients of Subgrade Reaction," Geotechnique, Vol 5, No. 4, 1955, pp 297-326.

11. Benscoter, S. U., "A Symmetrically Loaded Base Slab on an Elastic Foundation," Transactions, American Society of Civil Engineers, Vol 109, Paper 2220, 1944, pp 763-776.

12. Hetényi, M., Beams on Elastic Foundation, University of Michigan Press, Ann Arbor, 1946.

13. Ohde, J., "Einfache Berechnung biegefester Schleusensohlen (Simple Design of Moment Resisting Lock Floors)," Die Bautechnik, Vol 30, No. 5, May 1953, pp 140-146.

14. U. S. Army Engineer District, Omaha, CE, "Appendix B: Portion of Analysis of Design - Outlet Works" in "Interim Report on Powerhouse and Stilling Basin Pressure Cell Observations, Garrison Dam," Dec 1961 (revised May 1962).

15. De Beer, E. E., "Computation of Beams Resting on Soil," Proceedings, Second International Conference on Soil Mechanics and Foundation Engineering, Rotterdam, Vol 1, 1948, pp 119-122.

16. Kaufman, R. I. and Webb, R. R., "Review of Soils Design, Construction, and Performance Observations, Bayou Boeuf Lock," Technical Report No. 3-458, June 1957, U. S. Army Engineer Waterways Experiment Station, CE, Vicksburg, Miss.

17. Terzaghi, K., "Large Retaining-Wall Tests," Engineering News-Record, Vol 112, Nos. 5, 8, 10, 13, 16, and 23, 1934.

18. Carlson, R. W., "Manual for the Use of Stress Meters, Strain Meters, and Joint Meters in Mass Concrete," 1954, Gillick and Company, Berkeley, Calif.

19. Raphael, J. M. and Carlson, R. W., "Measurement of Structural Action in Dams," 1956, Gillick and Company, Berkeley, Calif.

20. Tschebotarioff, G. P., Soil Mechanics, Foundations, and Earth Structures, McGraw-Hill, New York, 1951.

21. Jáky, J., "Die Klassische Erddrucktheorie mit Besonderer Rucksicht auf die Stutzwandbewegung," Memoires, Association Internationale des Ponts et Charpentes, Vol 5, 1957.

22. Bishop, A. W., "Test Requirements for Measuring the Coefficient of Earth Pressure at Rest," Brussels Conference 58, Earth Pressure Problems, Proceedings, Vol 1, 1950, pp 2-14.

23. Bjerrum, L., Kringstad, S., and Kummeneje, O., "The Shear Strength of a Fine Sand," Publication No. 45, 1961, Norwegian Geotechnical Institute, Oslo.

24. Vesić, A. B. and Johnson, W. N., "Model Studies of Beams Resting on a Silt Subgrade," ASCE, Soil Mechanics and Foundations Division, Journal, Vol 89, SM1, Feb 1963, pp 1-31.

25. Woodman, E. H., "Pressure Cells for Field Use," Bulletin No. 40, Jan 1955, U. S. Army Engineer Waterways Experiment Station, CE, Vicksburg, Miss.

26. U. S. Army Engineer Waterways Experiment Station, CE, "Handbook for Concrete and Cement," Aug 1949 (with quarterly supplements), Vicksburg, Miss.

Table 1

Heave Point Installation Data

Heave Point No.	As Installed (3 January 1957) Station	Offset from Center Line ft	Elevation ft mlg	Offset in Plan of As-Installed Position from True Position ft	Corrected Initial Elevation ft mlg
H-1	745+85.00	0	-32.193	0.65	-32.189
H-2	740+80.00	41.00 N	-27.599	0.62	-27.596
H-3	740+80.00	0	-27.700	0.57	-27.697
H-4	740+80.00	41.00 S	-27.703	1.00	-27.694
H-5	740+80.00	65.00 S	-22.977	0.57	-22.974
H-6	735+80.00	0	-27.713	1.25	-27.699
H-7	733+35.00	0	-32.213	0.66	-32.209

Note: As-installed positions of heave points were measured at ground surface assuming that the heave points were set directly below the point of installation at ground surface. True positions of heave points were determined at the time of recovery.

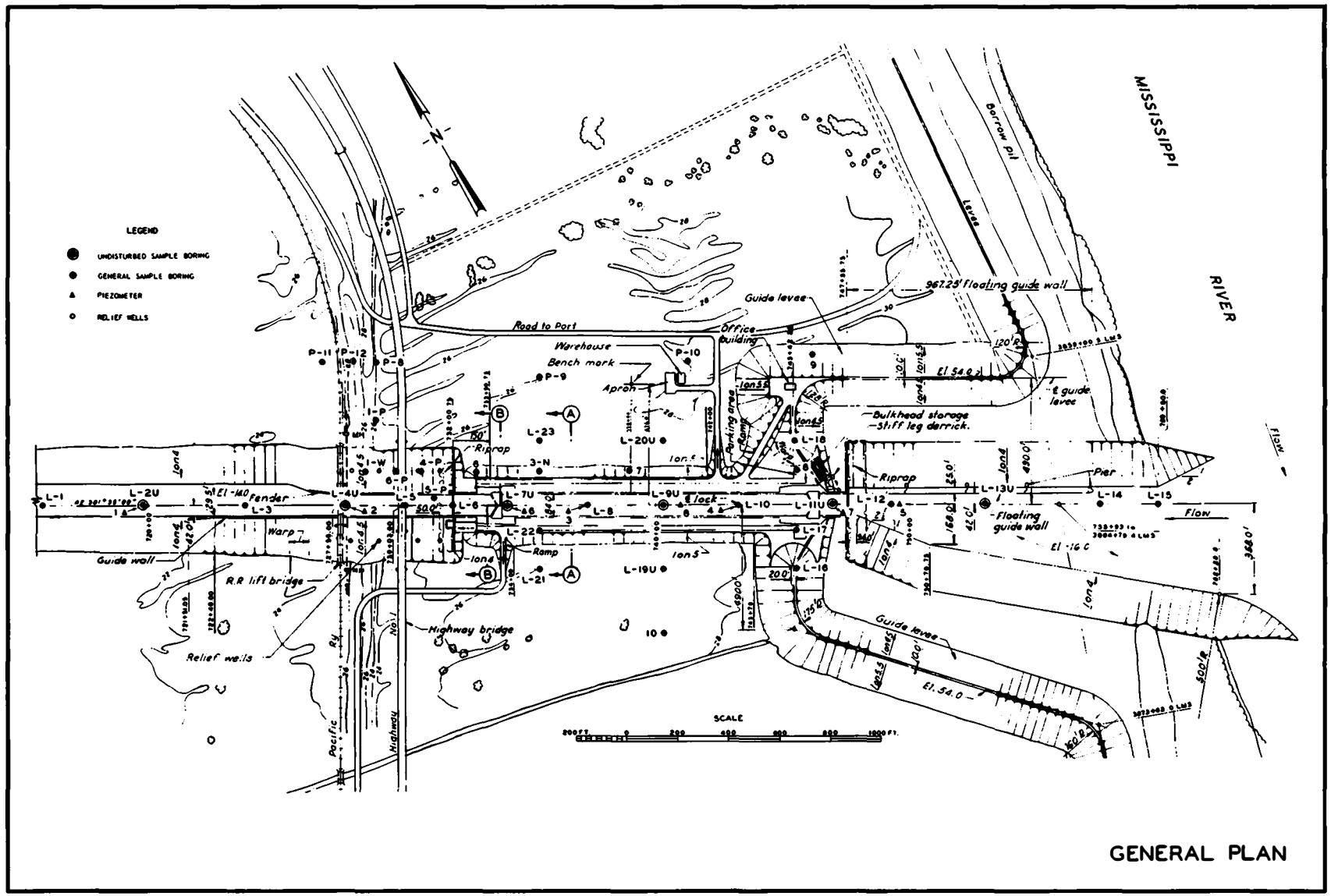

GENERAL PLAN

PLATE 2

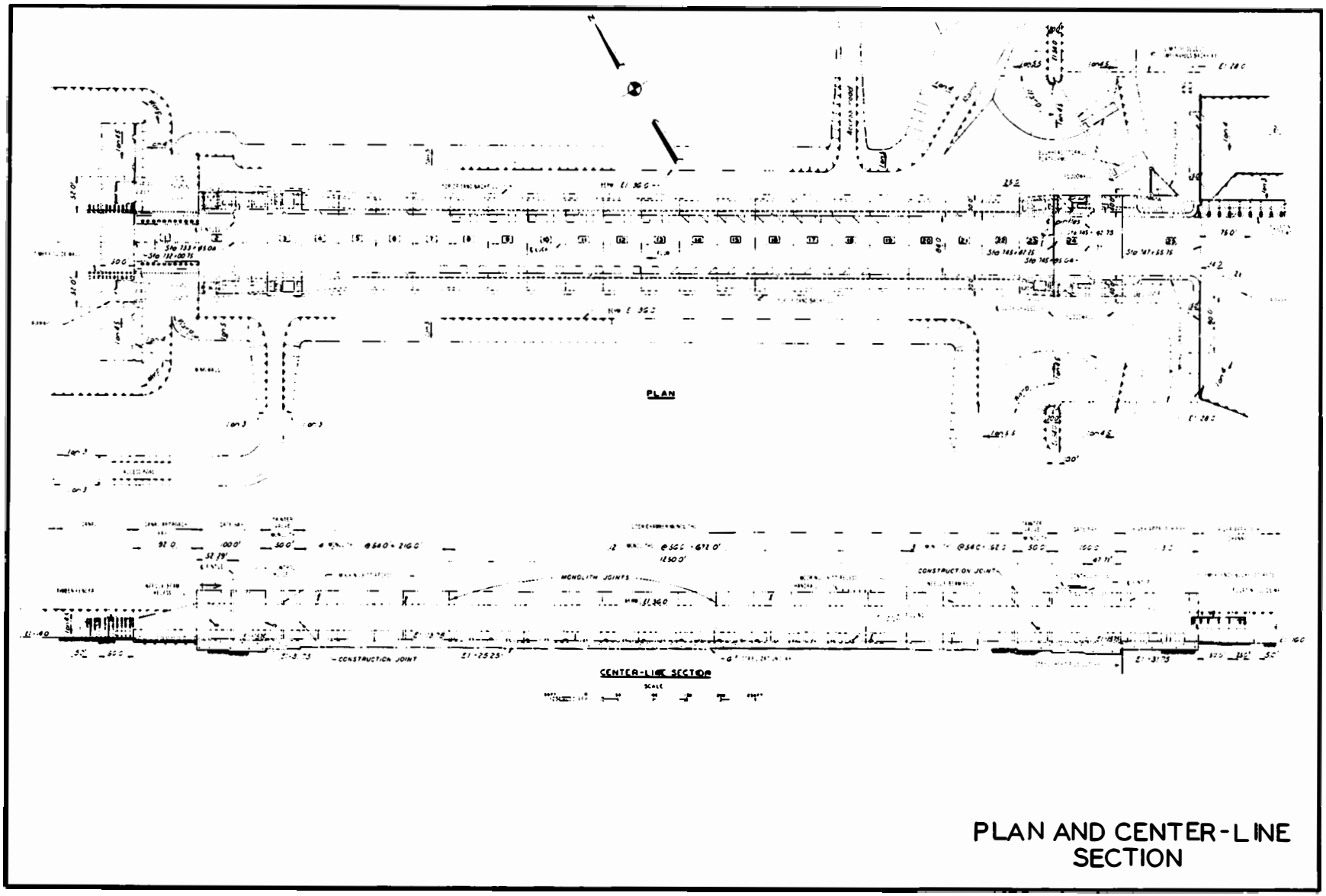

PLAN AND CENTER-LINE SECTION

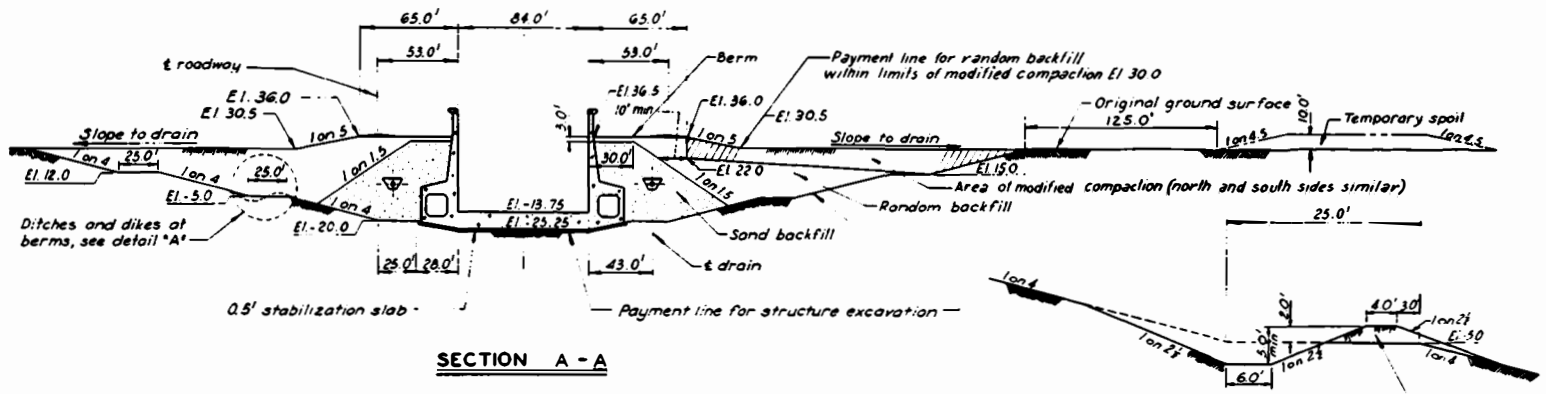

NOTE SEE PLATE 1 FOR LOCATIONS OF SECTIONS.

TYPICAL SECTIONS

PLATE 3

PLATE 4

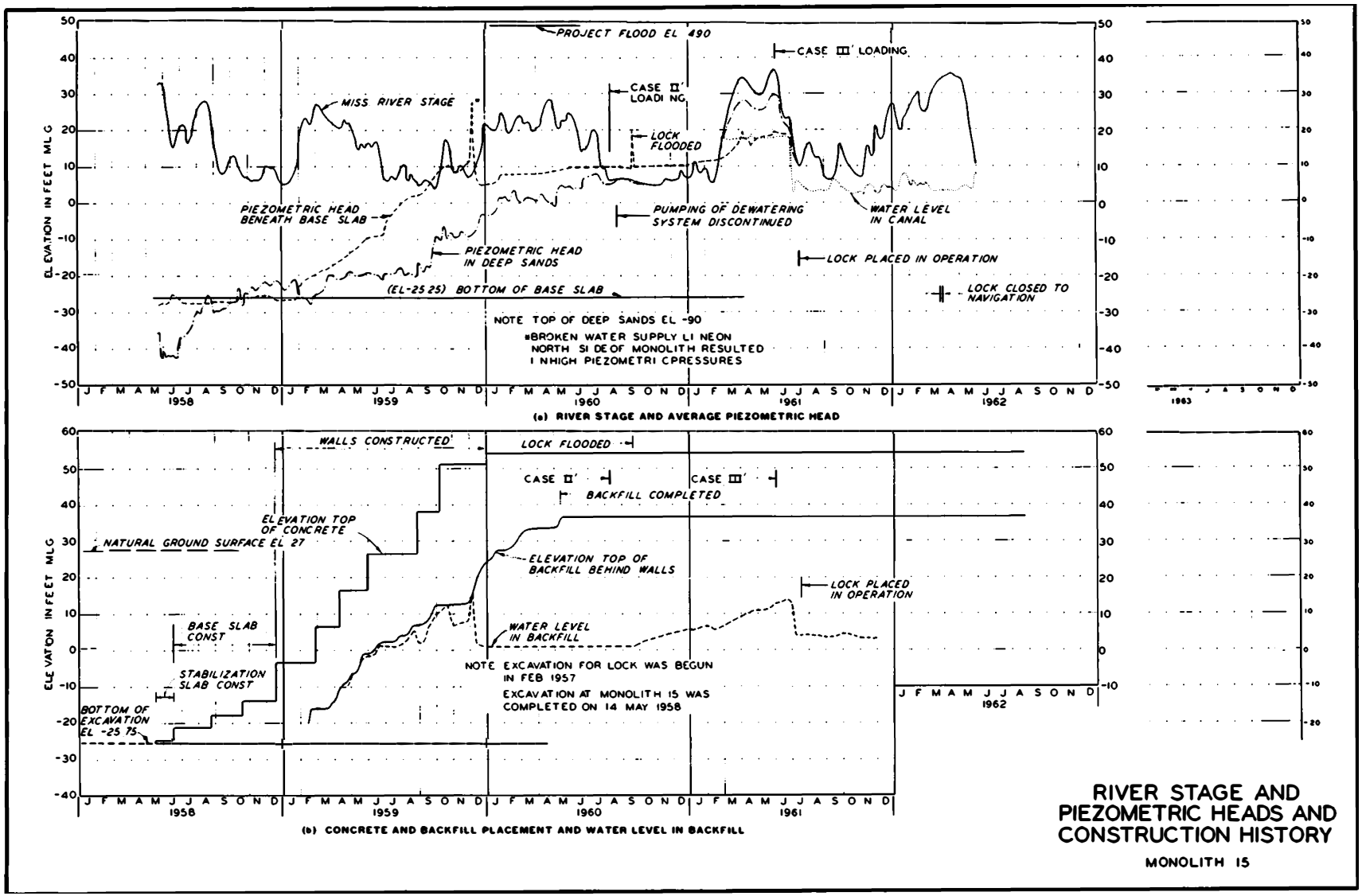

RIVER STAGE AND PIEZOMETRIC HEADS AND CONSTRUCTION HISTORY

MONOLITH 15

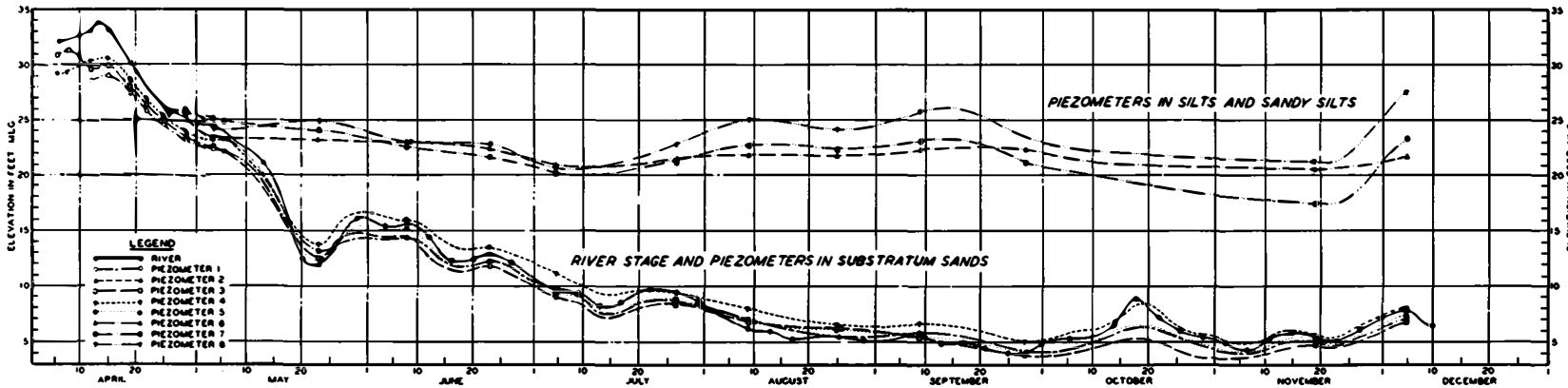

1955 PIEZOMETRIC DATA

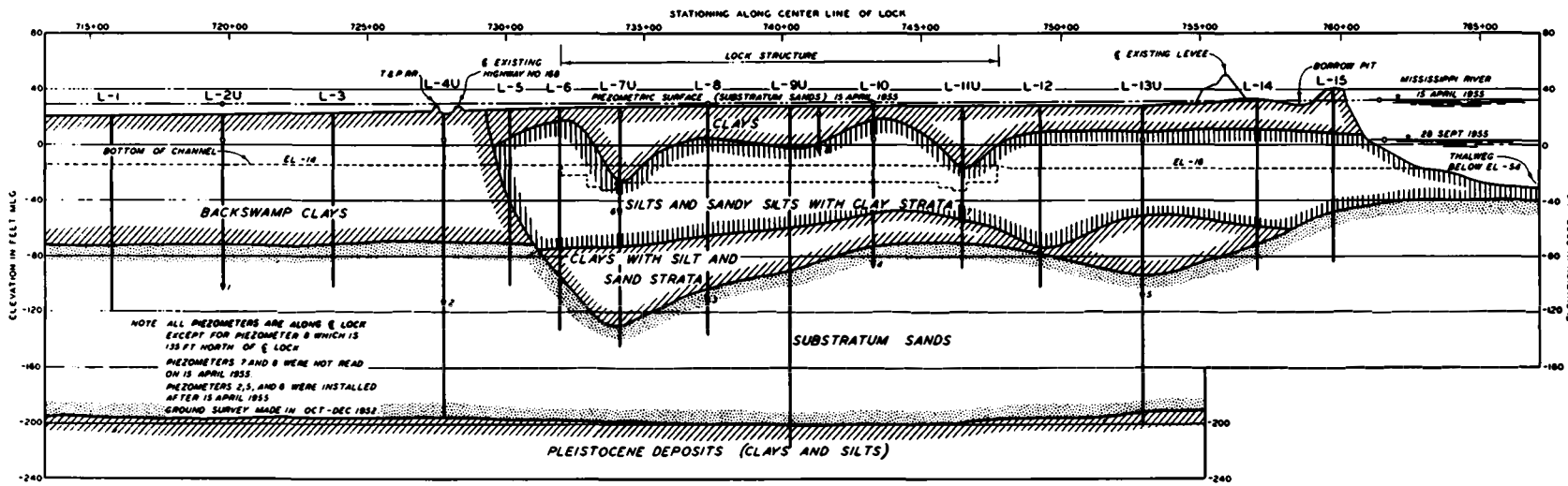

GENERALIZED SOIL PROFILE AND PIEZOMETER DATA

PLATE 5

PLATE 6

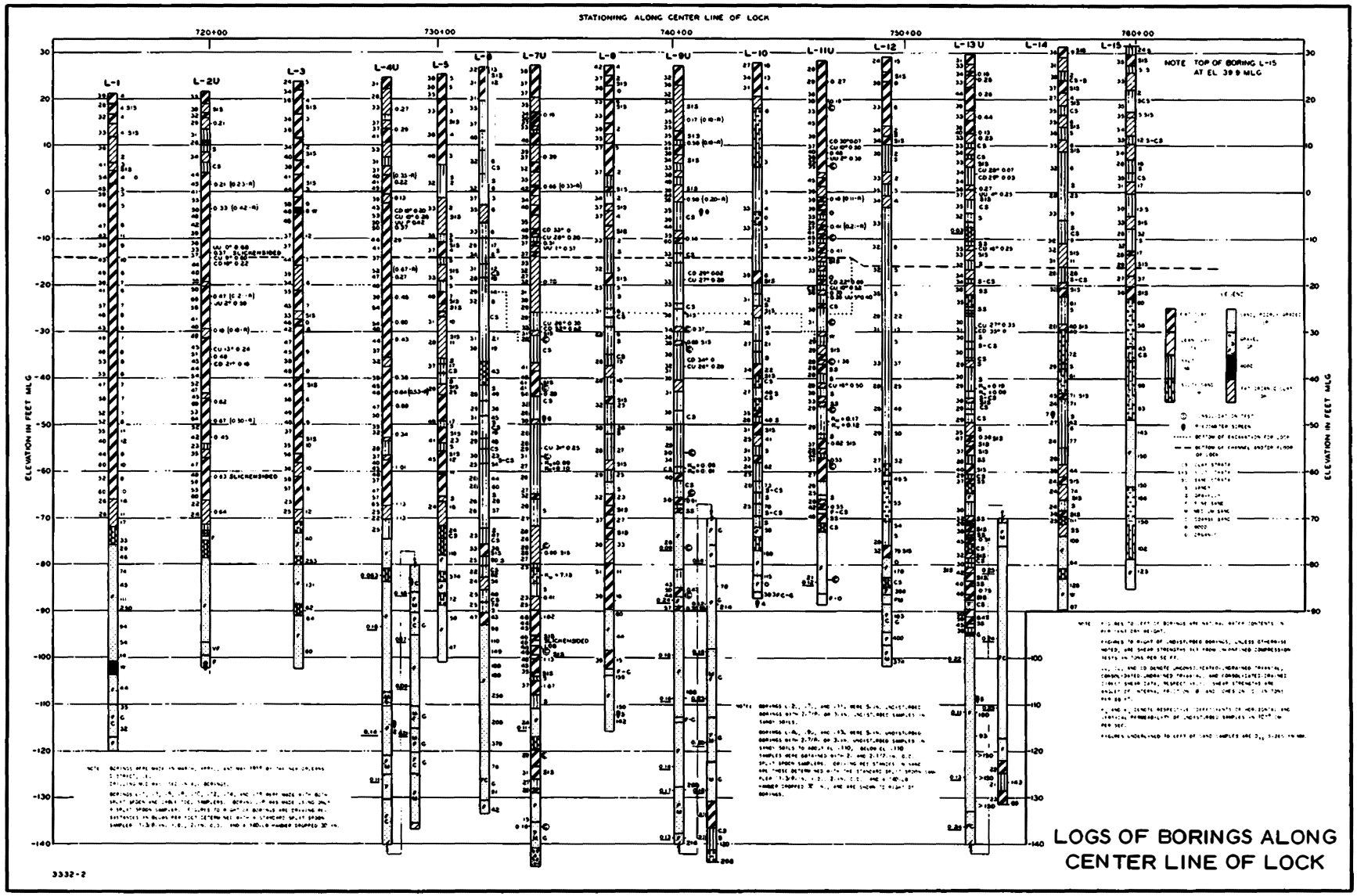

LOGS OF BORINGS ALONG CENTER LINE OF LOCK

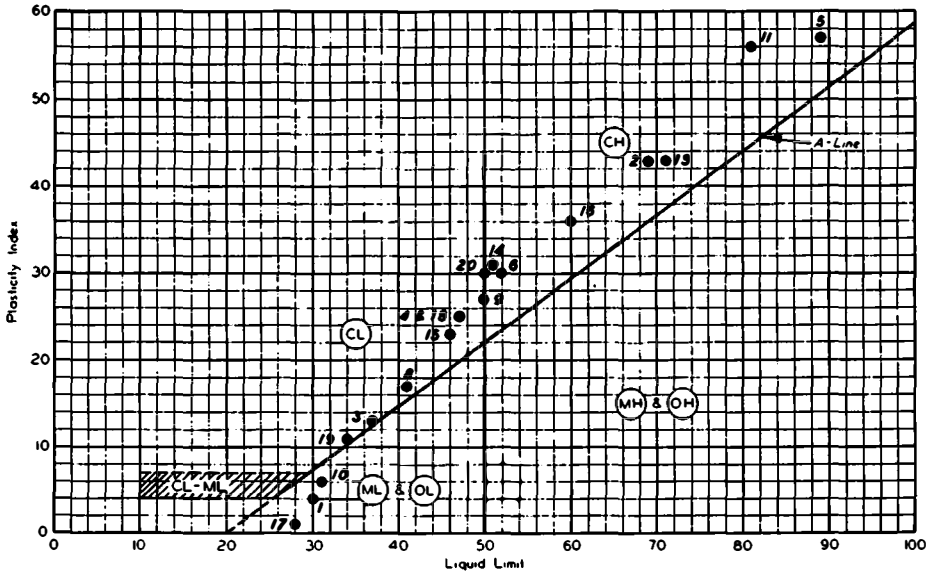

PLASTICITY CHART

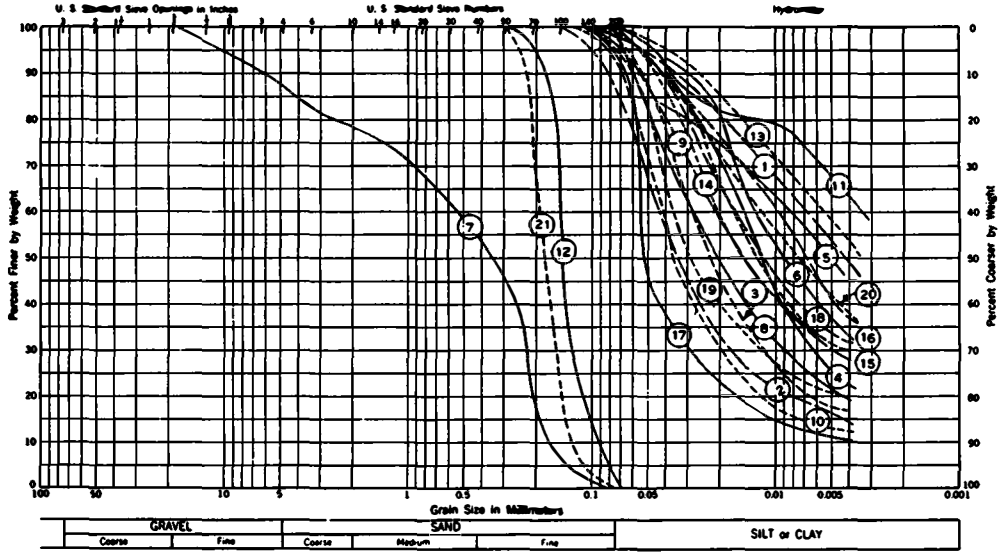

GRAIN-SIZE CURVES

NOTE: SEE PLATE 8 FOR IDENTIFICATION OF SAMPLES.

CLASSIFICATION DATA FOR
SOILS BENEATH LOCK

PLATE 7

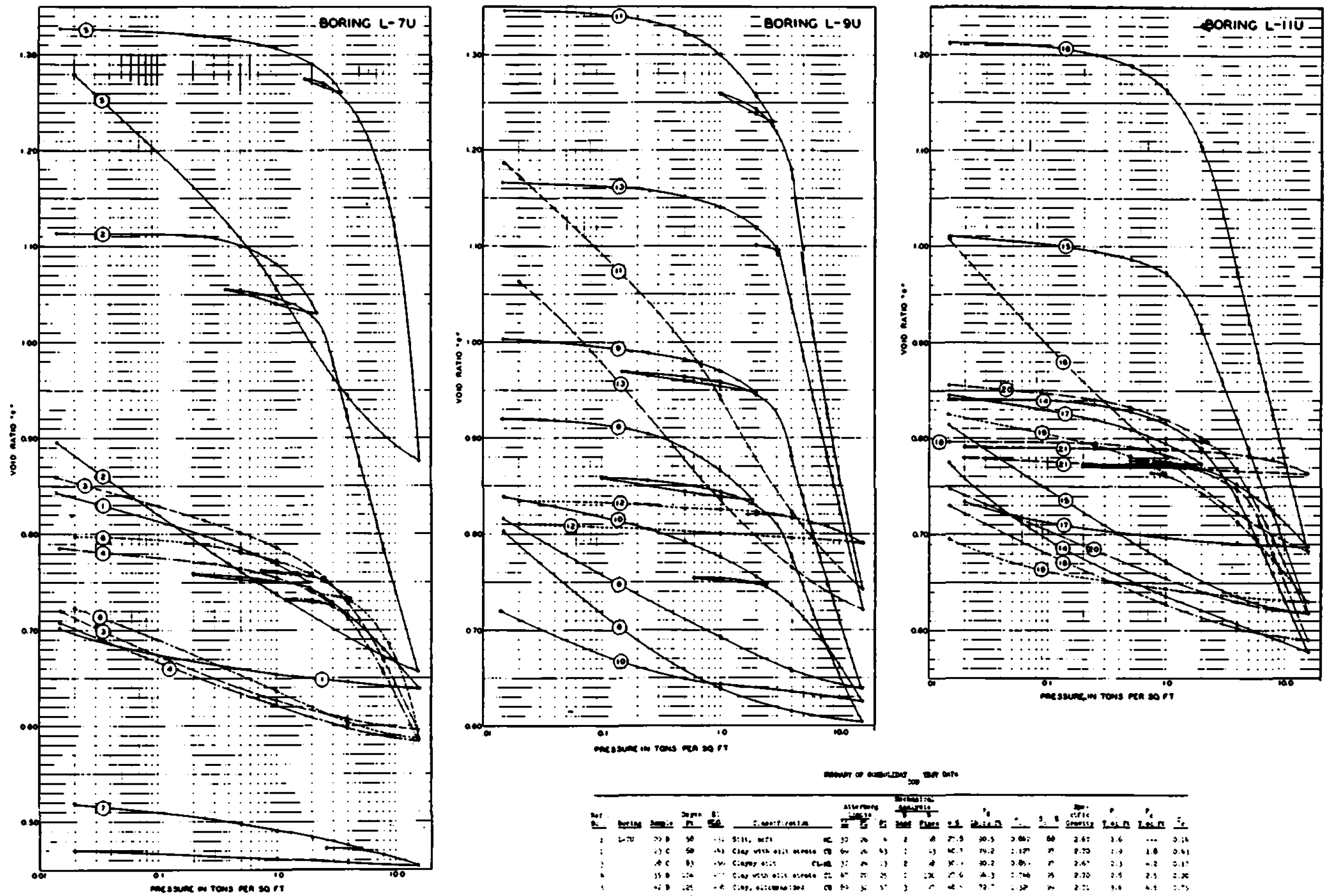

SUMMARY OF CONSOLIDATION TEST DATA

Ref No.	Boring	Sample	Depth Ft	El. MSL	Classification		Atterberg Limits LL	PL	PI	Mechanical Analysis % Sand	% Fines	w %	γ_d lb/cu ft	e_0	S_0 %	Specific Gravity	P T/sq ft	P_c T/sq ft	C_c
1	L-7U	23 B	50	[illegible]	Silt, soft	ML	30	26	4	2	98	27.9	90.5	0.867	88	2.67	1.6	---	0.14
2		43 C	50	-45	Clay with silt strata	CH	64	26	[illegible]	1	[illegible]	40.7	79.2	1.127	[illegible]	2.70	1.9	1.8	0.41
3		48 C	83	[illegible]	Clayey silt	CL-ML	32	26	[illegible]	2	98	30.[illegible]	90.2	0.85[illegible]	[illegible]	2.67	2.3	4.2	0.17
4		55 B	104	[illegible]	Clay with silt strata	CL	47	[illegible]	25	1	100	27.6	[illegible]	[illegible]	95	2.70	2.5	2.5	[illegible]
5		62 B	125	[illegible]	Clay, slickensided	CH	85	36	5[illegible]	3	[illegible]	4[illegible]	72.[illegible]	[illegible]	[illegible]	2.7[illegible]	5.6	4.5	[illegible]
6		62-3'	148	[illegible]	Clay	CH	[illegible]	2[illegible]	[illegible]	3	[illegible]	29.5	94.3	[illegible]	98	2.73	4.3	4.9	0.36
7		15-3'	153	[illegible]	Sand	SP	Nonplastic			96	2	14.5	106.[illegible]	0.530	75	2.63	4.7	---	----
8	L-9U	14 C	36	-29	Clay, soft	CL	4[illegible]	24	[illegible]	2	98	34.0	86.6	0.940	[illegible]	2.69	1.6	2.3	0.34
9		20 C	54	-32	Clay, firm	CL	50	23	27	0	100	36.4	84.3	1.000	98	2.70	1.7	2.5	0.44
10		30 B	83	-76	Sandy silt	ML	3[illegible]	2[illegible]	6	12	88	29.2	9[illegible]	0.858	[illegible]	2.6[illegible]	[illegible]	3.5	0.15
11		37 B	35	[illegible]	Clay, soft	CH	8[illegible]	2[illegible]	56	0	100	50.0	71.3	1.340	100	2.68	2.5	3.5	0.56
12		15-3'	103	-75	Sand	SP	Nonplastic			[illegible]	3	27.5	90.5	0.9[illegible]	8[illegible]	2.66	1.2	---	----
13		36 C	113	-86	Clay with silt strata	CH	7[illegible]	30	43	1	[illegible]	[illegible]	76.3	[illegible]	96	2.7[illegible]	2.4	2.5	0.31
14	L-11U	3 C	8	-0	Clay	CH	52	1[illegible]	3[illegible]	2	98	30.2	9[illegible].5	0.96[illegible]	87	2.70	0.6	2.6	0.27
15		9 B	23	-5	Clay	CL	46	23	23	0	100	3[illegible]	83.9	1.010	93	2.70	0.8	2.0	0.42
16		13 B	30	-10	Clay, medium, with organic matter	CH	56	26	30	0	100	4[illegible]	75.8	1.223	100	2.70	1.2	1.7	0.50
17		1[illegible] B	4[illegible]	-26	Sandy silt	ML	28	2[illegible]	[illegible]	[illegible]	[illegible]	[illegible]	10[illegible]	0.9[illegible]	[illegible]	2.6[illegible]	[illegible]	2.5	0.10
18		22 B	65	-37	Clay, firm	CL	4[illegible]	[illegible]	2[illegible]	2	98	2[illegible].2	93.2	0.792	96	2.70	[illegible]	3.5	0.30
19		2[illegible] C	7[illegible]	-46	Sandy silt	ML	34	23	[illegible]	[illegible]	3[illegible]	2[illegible]	9[illegible]	0.[illegible]	[illegible]	2.68	2.[illegible]	2.5	0.15
20		2[illegible] B	56	-50	Clay	CH	54	24	30	0	100	32.9	91.5	0.846	98	2.72	2.5	2.6	0.26
21		15-3'	121	-83	Sand	SP	Nonplastic			98	2	21.1	98.6	0.730	73	2.65	3.3	---	----

RESULTS OF LABORATORY
CONSOLIDATION TESTS

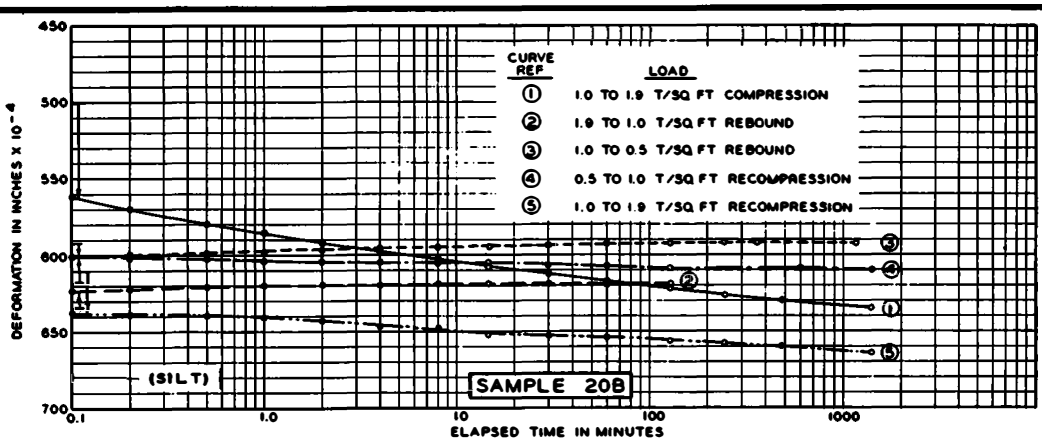

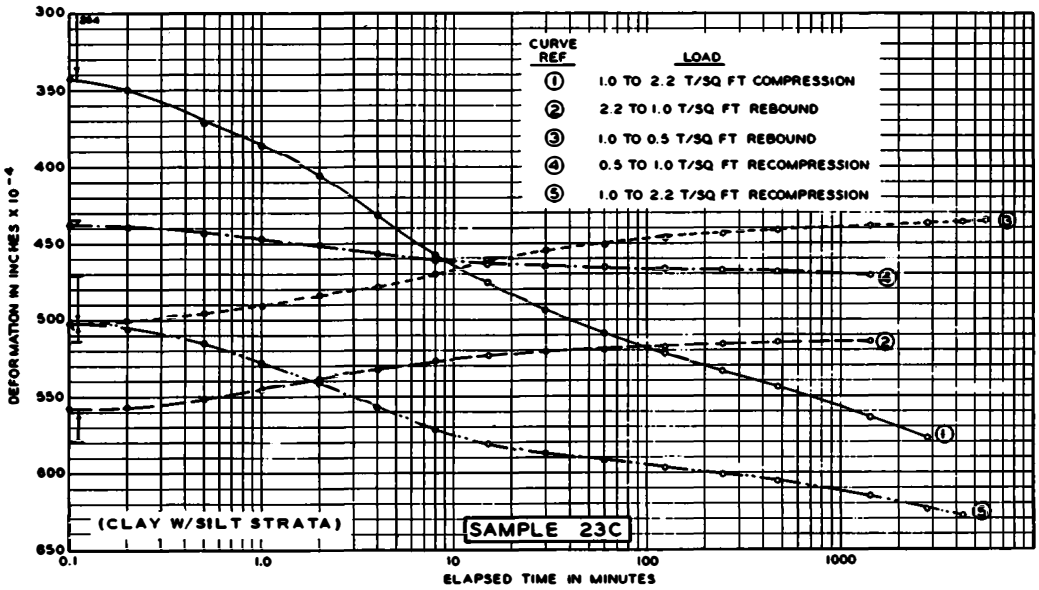

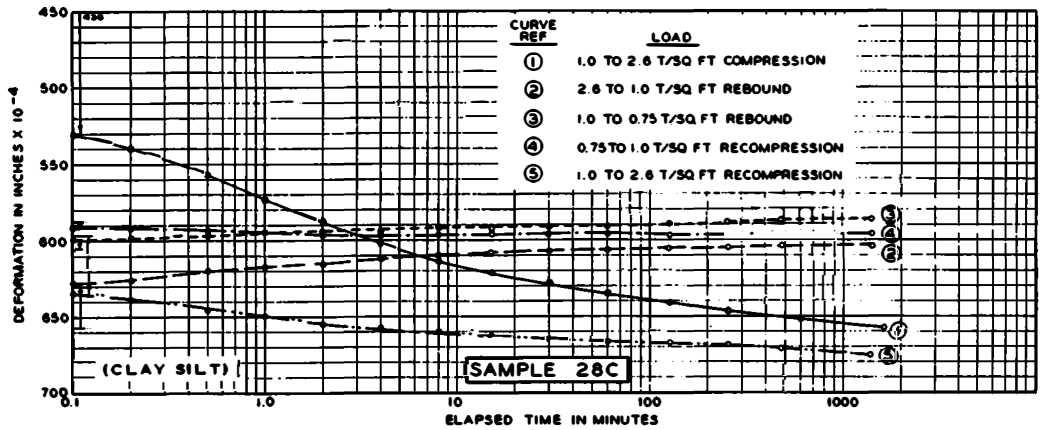

TYPICAL CONSOLIDATION TIME CURVES
BORING L-7U

PLATE 9

PLATE 10

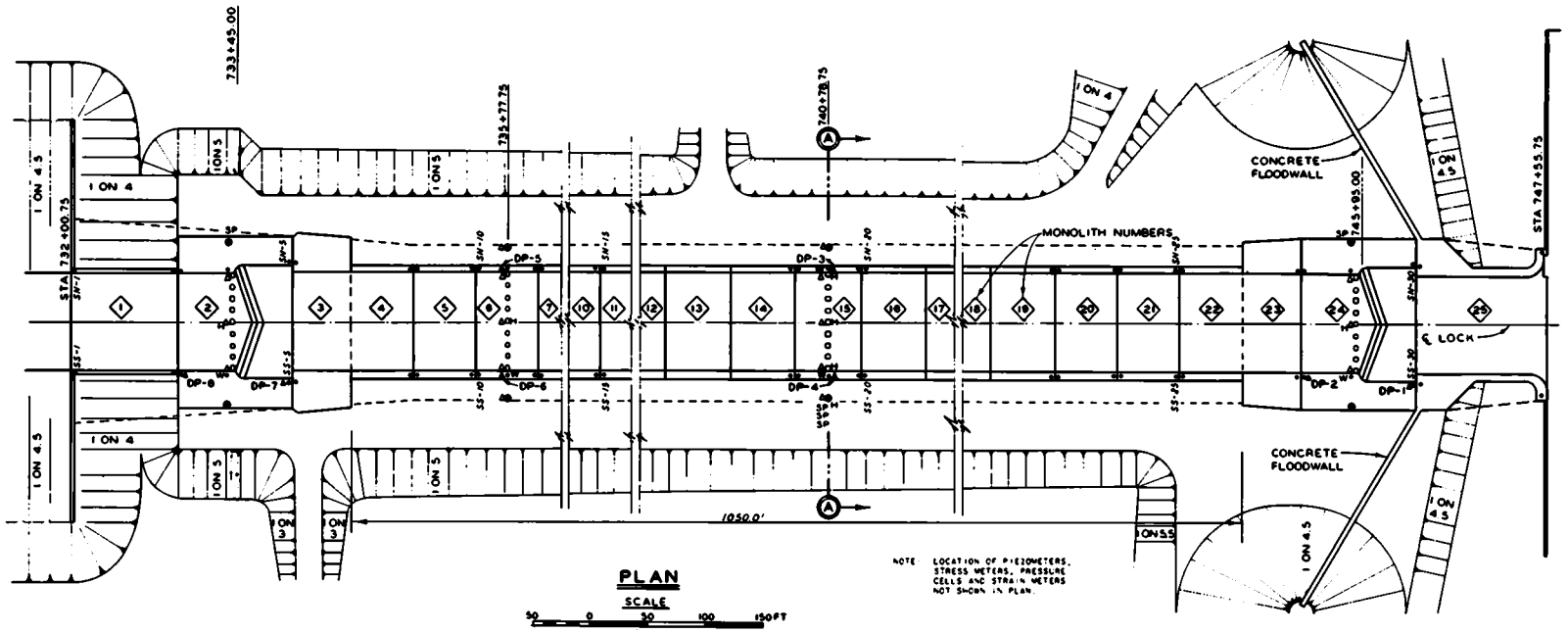

SUMMARY OF ENGINEERING MEASUREMENT DEVICES

SYMBOL SEC	SYMBOL PLAN	SYMBOL EL	DEVICE	NUMBER INSTALLED MON 2	MON 8	MON 15	MON 24	TOTAL
			TYPE A	1	-	-	1	2[2]
●		●	PIEZOMETER[1] TYPE B	3[3]	3[3]	4	0[4]	10
			TYPE C	2	4	6	2	14[5]
P			CARLSON HOPE PRESSURE CELL	---	---	1	---	1
o		o	AES PRESSURE CELL	---	---	9	---	9
■		■	CARLSON SOIL STRESS METER	---	---	20	---	20
C			CARLSON CONCRETE STRESS METER	---	---	3	---	3
I			CARLSON STRAIN METER	---	---	33	---	33
	▲		WALL DEFLECTION PIPE	2	2	2	2	8
H	H		HEAVE POINT	1[6]	1[6]	4	1[6]	7
△	△		TEMPORARY SETTLEMENT REFERENCE POINT	3	4	5	3	15
•	•	•	SETTLEMENT REFERENCE BOLT	8	8	8	8	64[7]
T			RESISTANCE THERMOMETER	---	---	2	---	2
	W		SOUNDING WELL	1	1	2	1	5
SP	SP		SETTLEMENT REFERENCE POINT (TYPE "A")	1	---	2	1	5
	●		SETTLEMENT REFERENCE POINT (TYPE B)	2	2	2	2	8
●	○	○	18" x 18" x 2.0" REFERENCE PLATE	9	9	9	9	36

[1] FOR DESIGNATION OF PIEZOMETER TYPE, SEE FIG 14.
[2] INCLUDES "A" PIEZOMETERS AT STA 732+00, 730+45, AND 727+70.
[3] AT ℄ LOCK ONLY.
[4] ONE AT ℄, ONE 44 FT ON EACH SIDE OF ℄.
[5] INCLUDES TWO AT MONOLITH 25.
[6] INCLUDES BOLTS ON MONOLITHS 1-25, INCLUSIVE.

PLAN OF INSTRUMENTATION

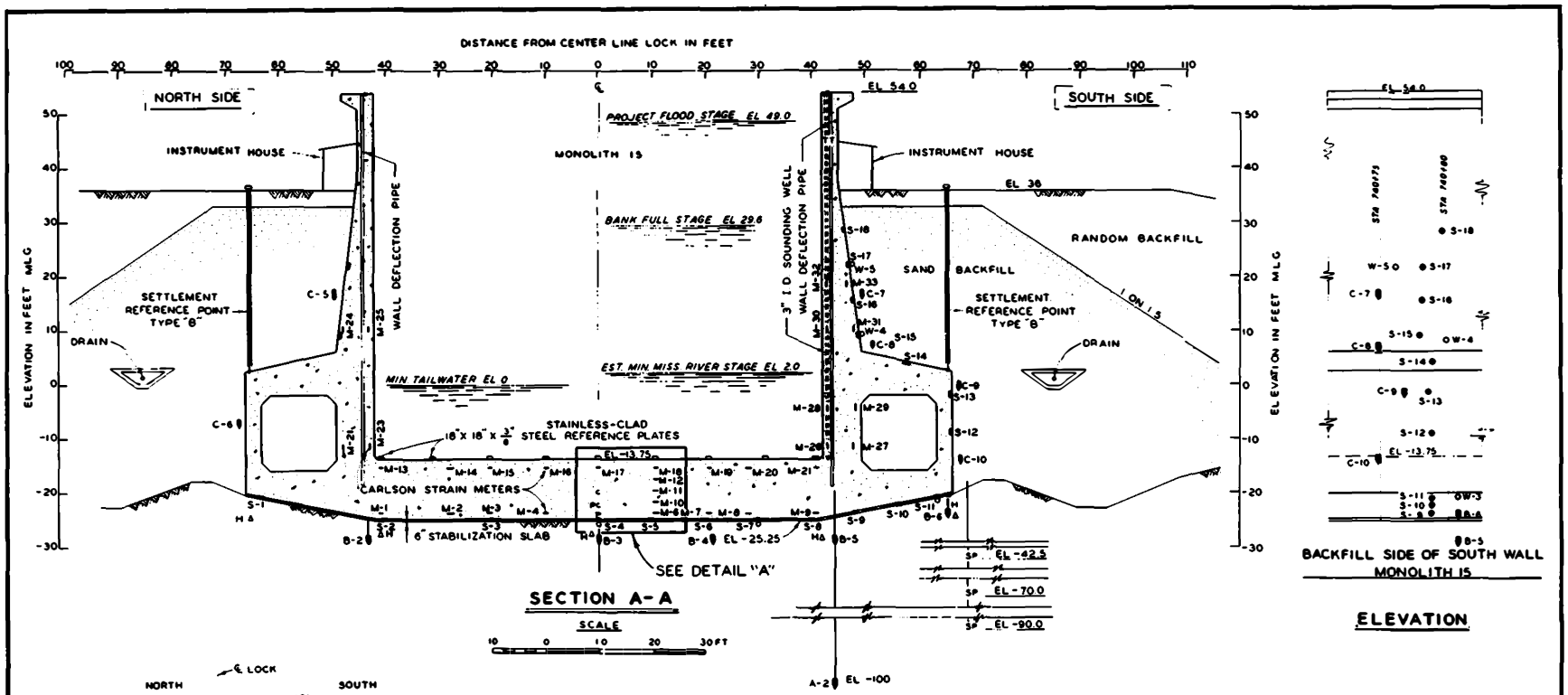

SECTION A-A

SCALE

10 0 10 20 30 FT

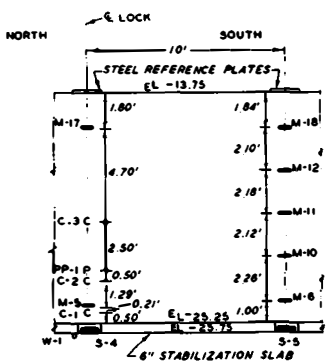

DETAIL A

NOTE 18" - 18" - 3/8 IN REFERENCE PLATES INSTALLED ON TEN FOOT CENTERS AT LOCK STA 733 + 41.75, 735 + 77.75, 740 + 78.75, AND 745 + 93.

SEE PLATE 10 FOR LEGEND

BACKFILL SIDE OF SOUTH WALL MONOLITH 15

ELEVATION

INSTRUMENTATION AT MONOLITH 15

PLATE 11

PLATE 12

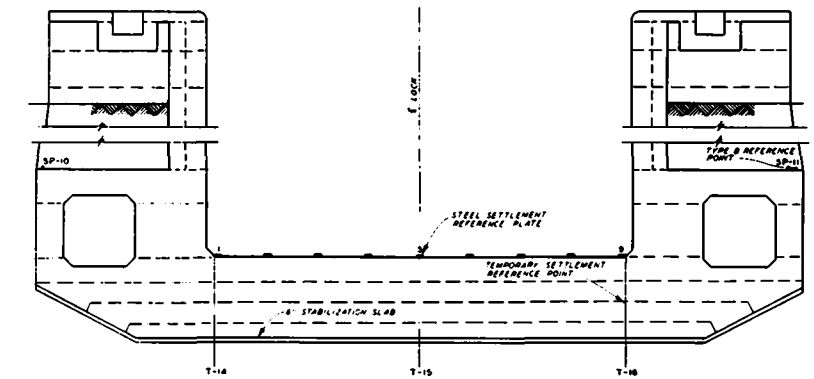

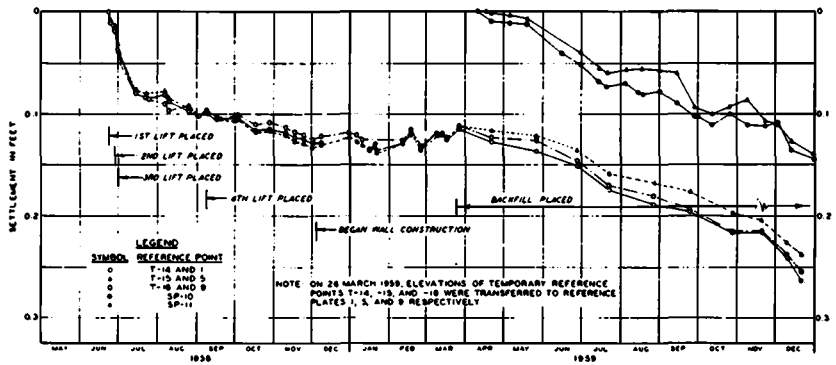

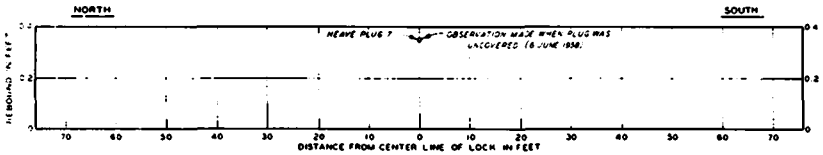

FOUNDATION REBOUND

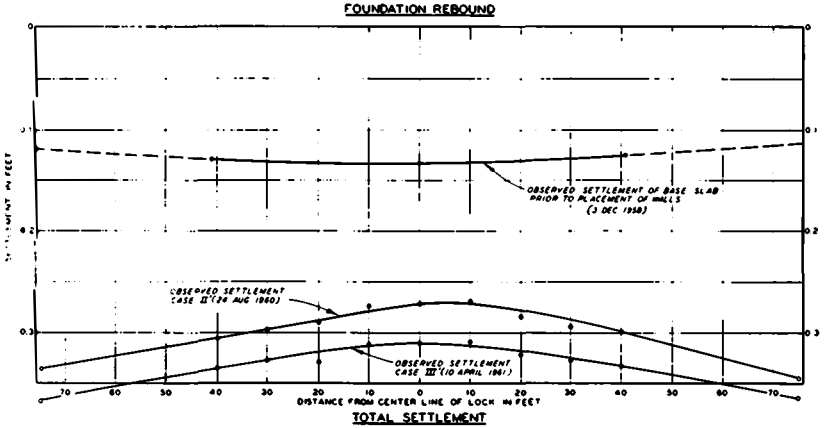

TOTAL SETTLEMENT

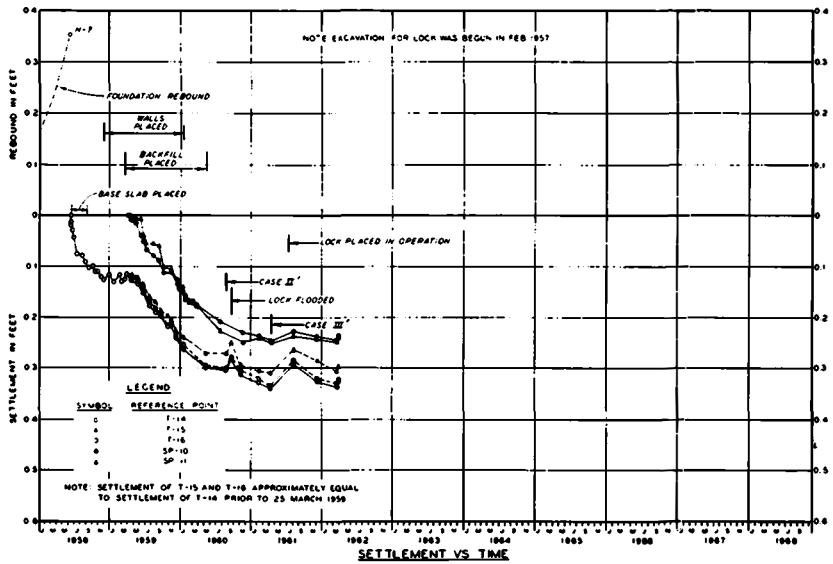

SETTLEMENT VS TIME

OBSERVED REBOUND AND SETTLEMENT
MONOLITH 2

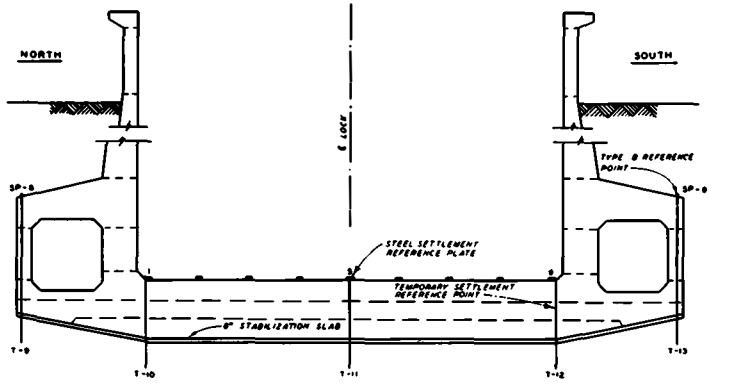

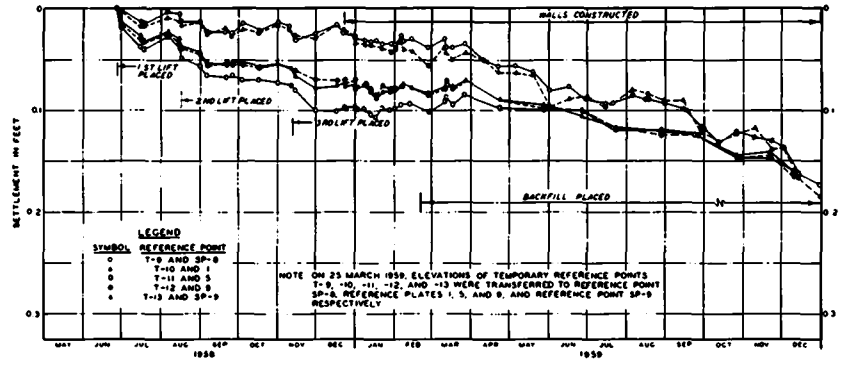

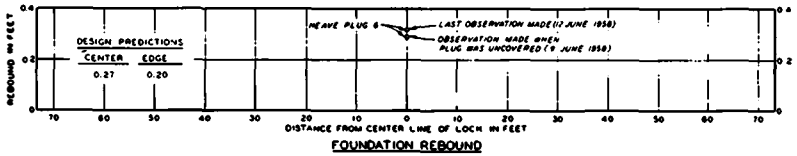

FOUNDATION REBOUND

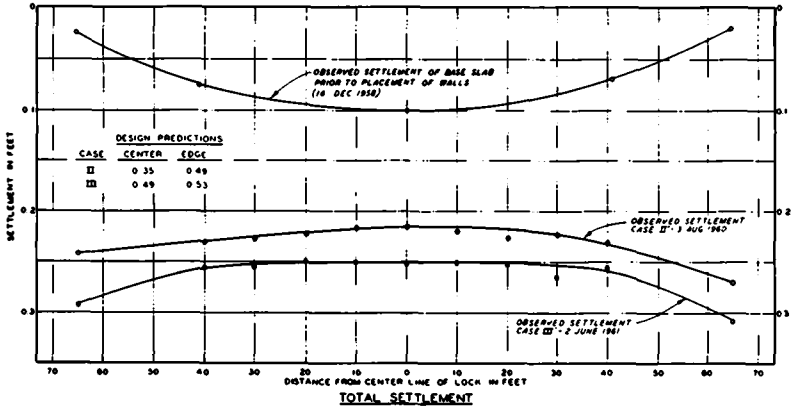

TOTAL SETTLEMENT

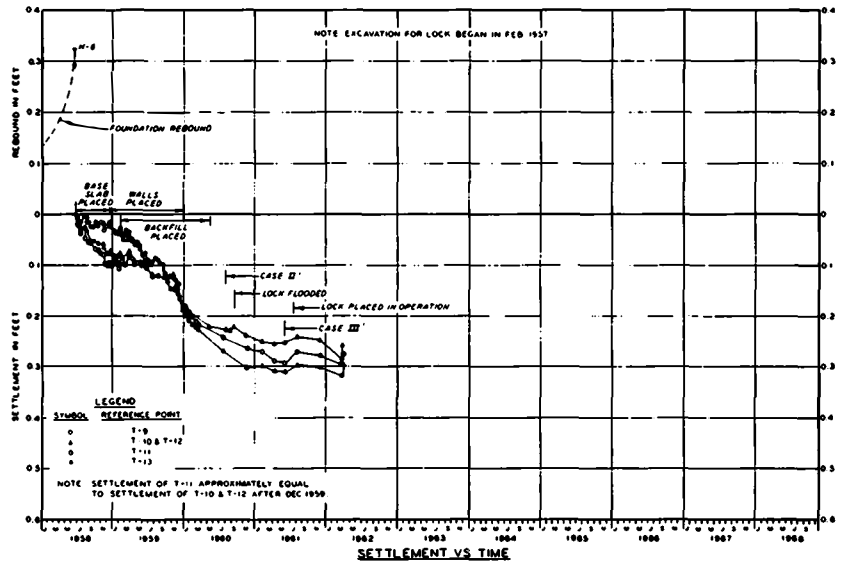

SETTLEMENT VS TIME

OBSERVED REBOUND AND SETTLEMENT
MONOLITH 6

PLATE 13

PLATE 14

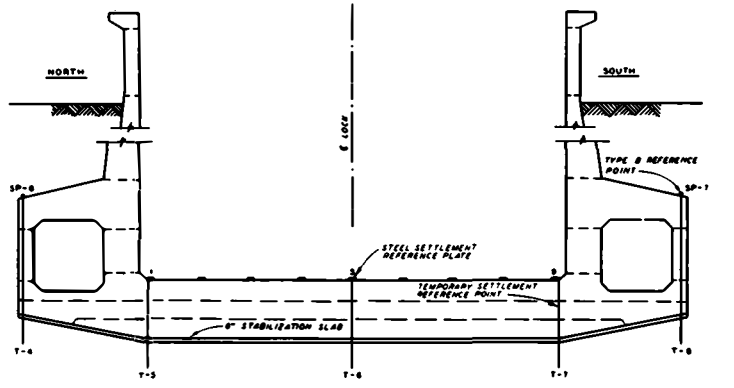

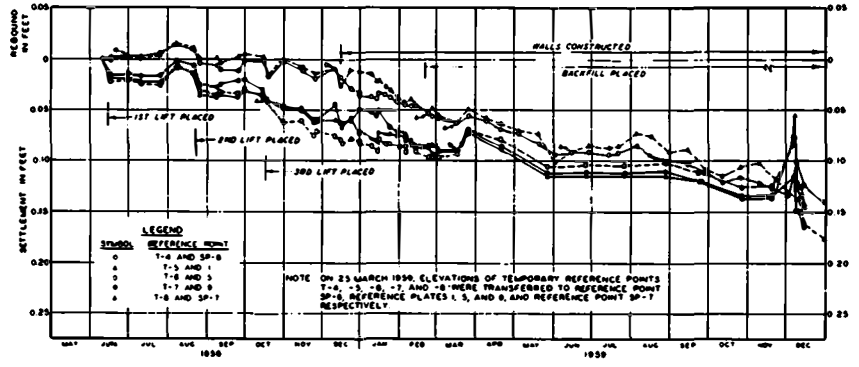

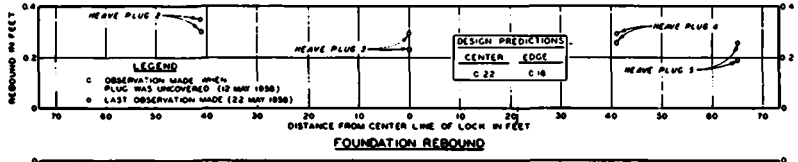

FOUNDATION REBOUND

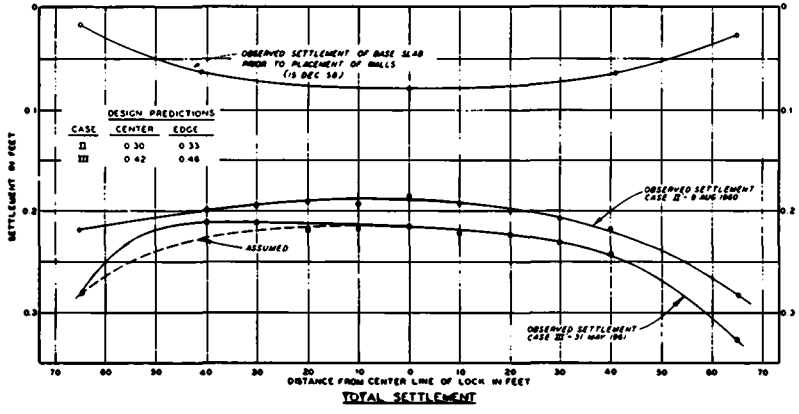

TOTAL SETTLEMENT

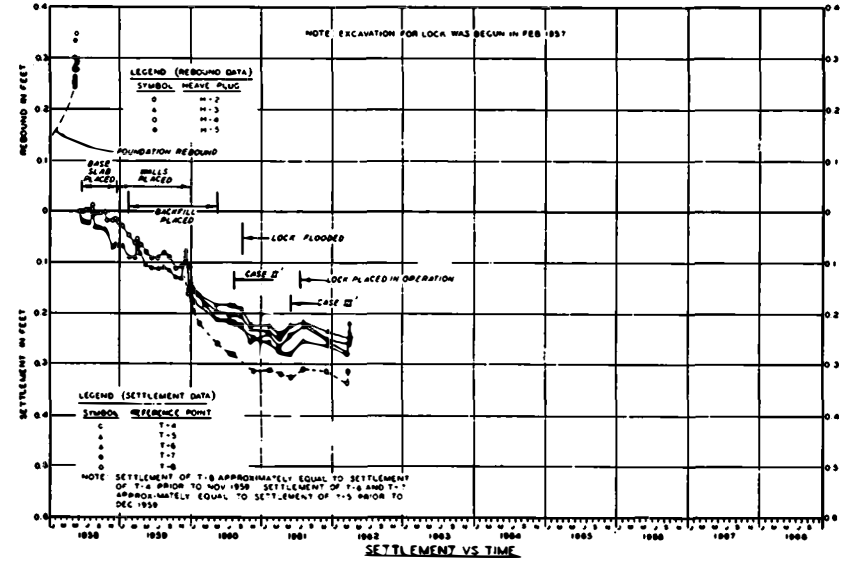

SETTLEMENT VS TIME

OBSERVED REBOUND AND SETTLEMENT
MONOLITH 15

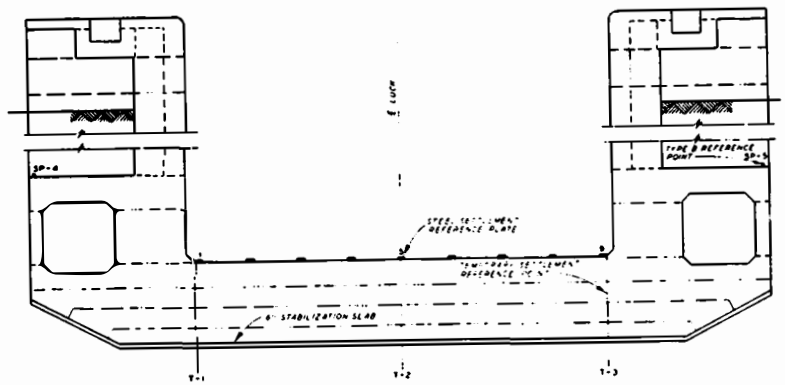

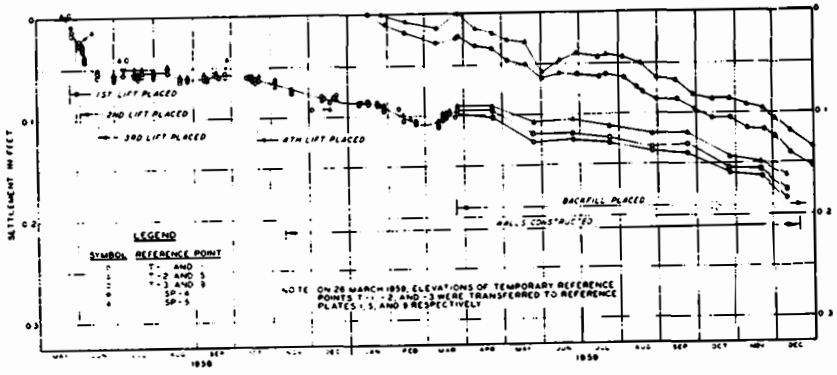

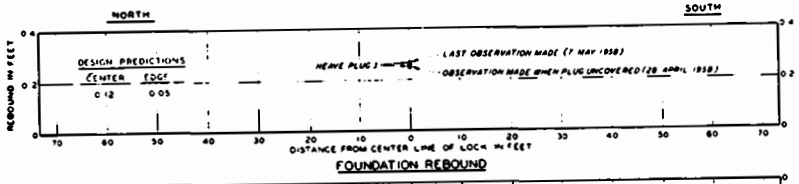

FOUNDATION REBOUND

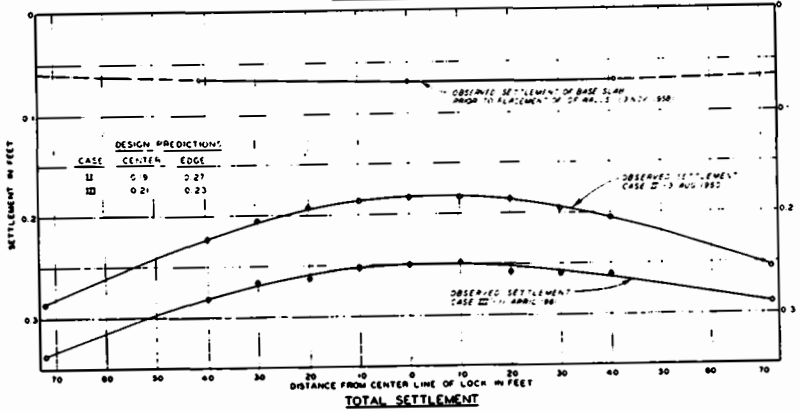

TOTAL SETTLEMENT

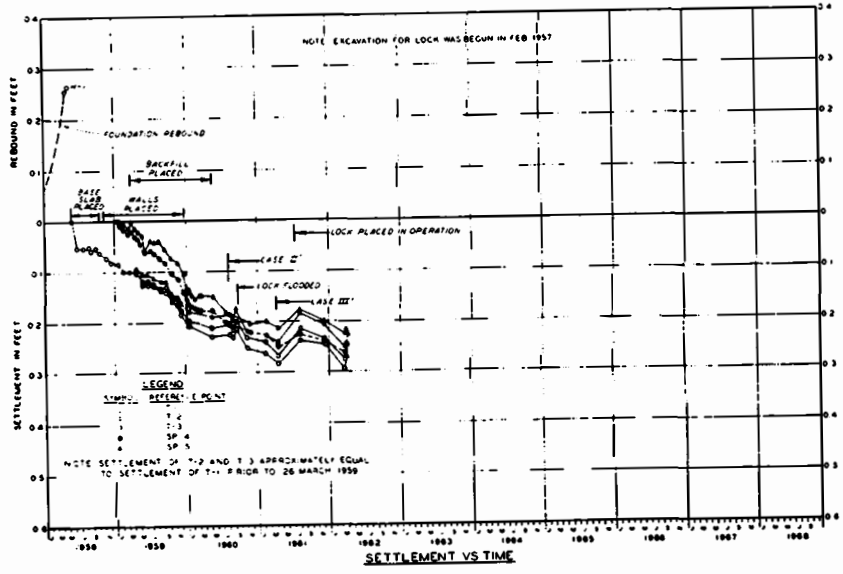

SETTLEMENT VS TIME

OBSERVED REBOUND AND SETTLEMENT
MONOLITH 24

PLATE 15

PLATE 16

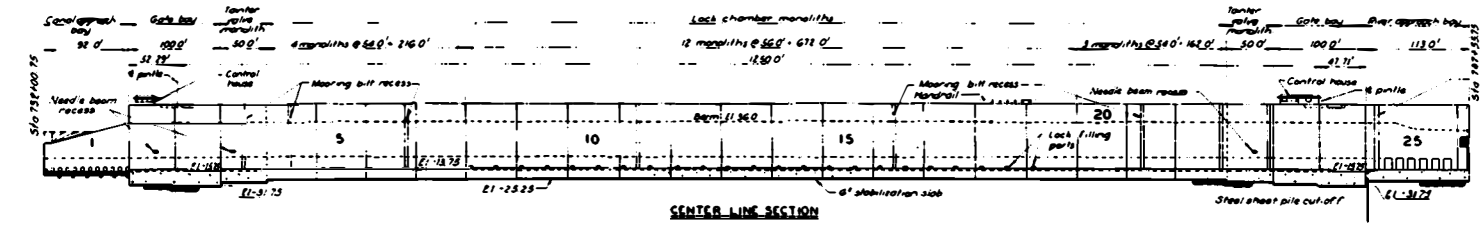

CENTER LINE SECTION

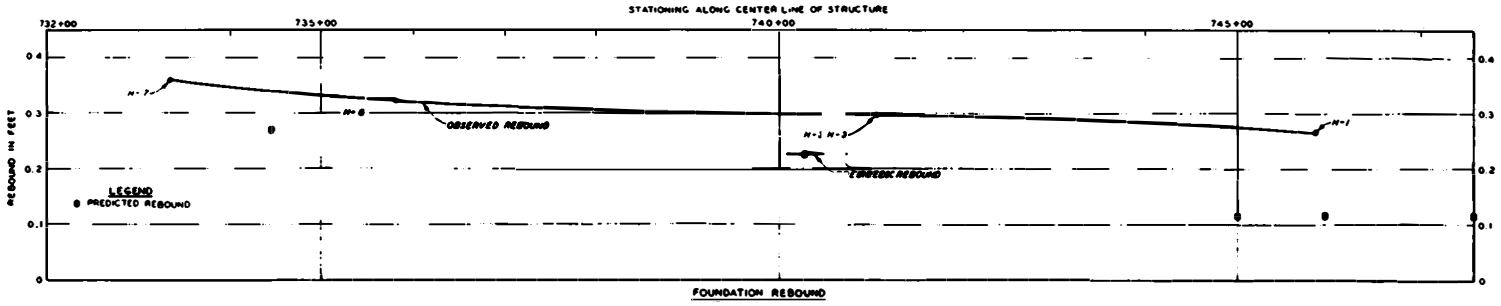

FOUNDATION REBOUND

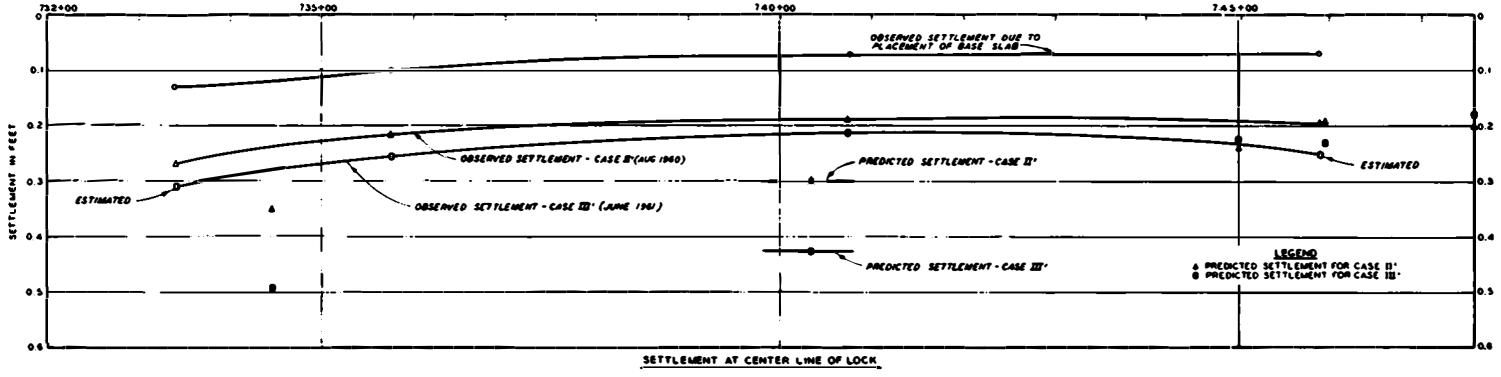

SETTLEMENT AT CENTER LINE OF LOCK

OBSERVED REBOUND AND SETTLEMENT ALONG CENTER LINE OF LOCK

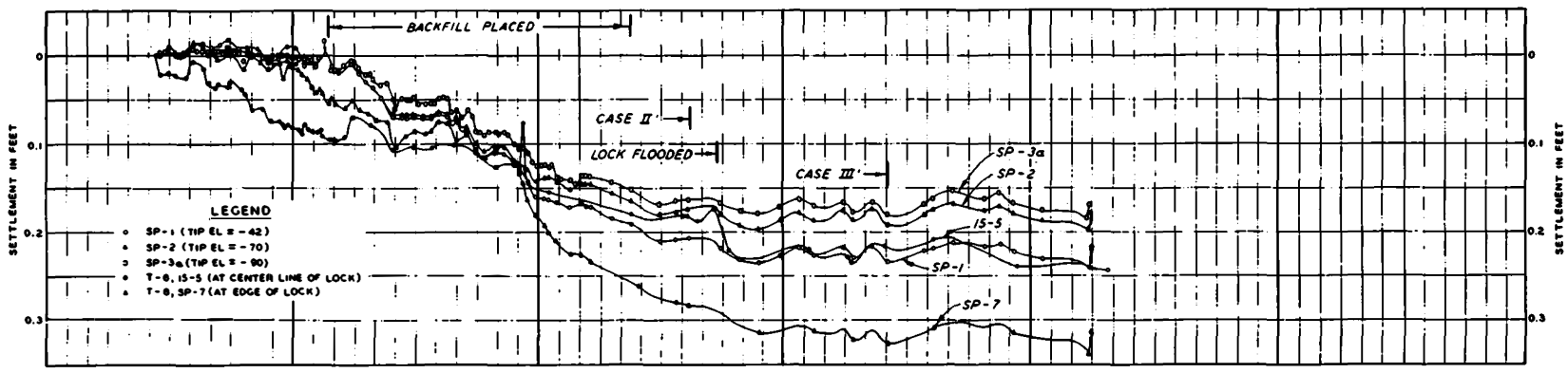

OBSERVED SETTLEMENT AT MONOLITH 15

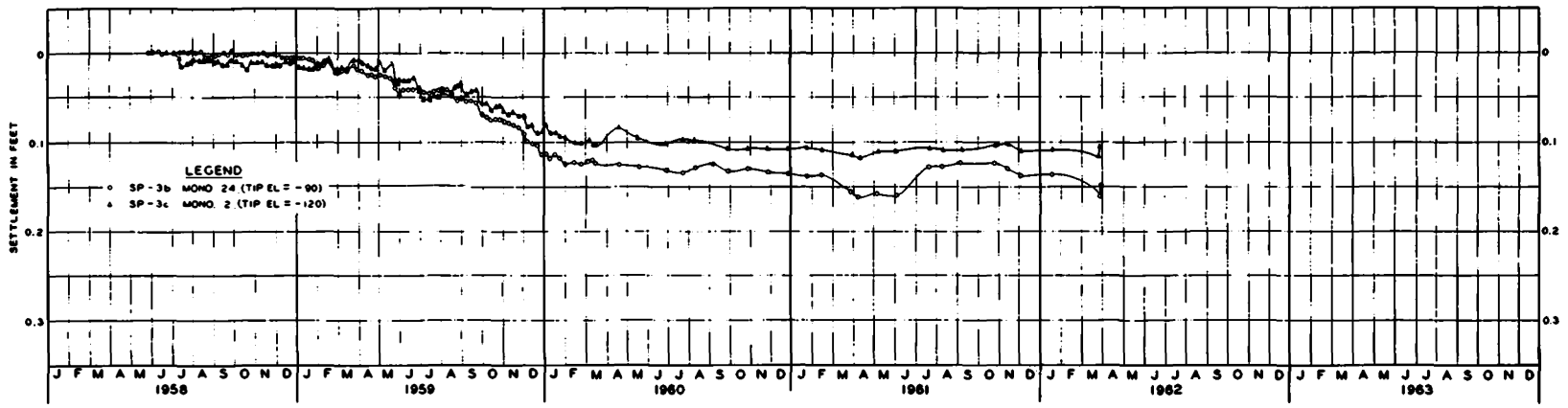

OBSERVED SETTLEMENT AT GATE BAYS

SETTLEMENT OF TYPE A REFERENCE POINTS

PLATE 17

PLATE 18

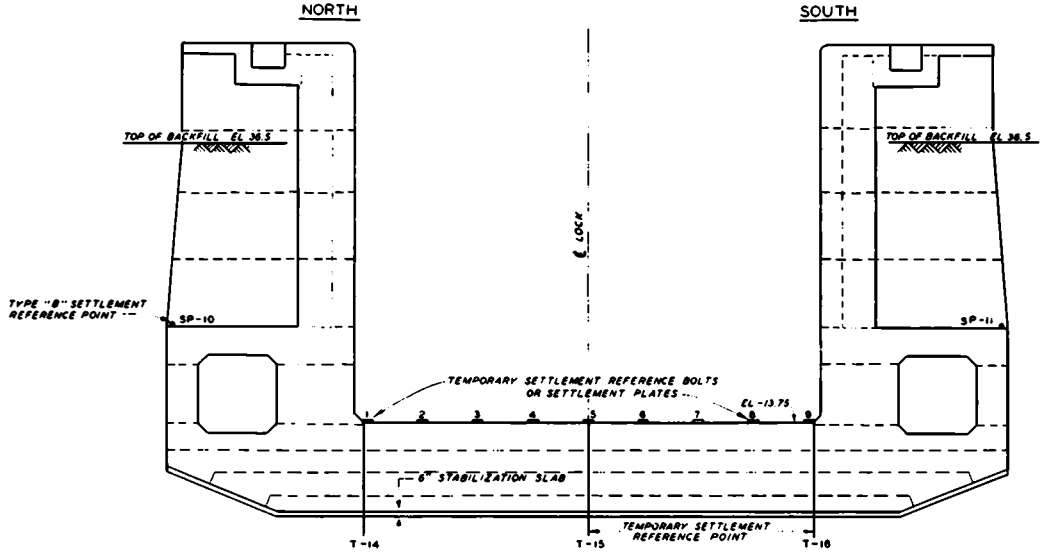

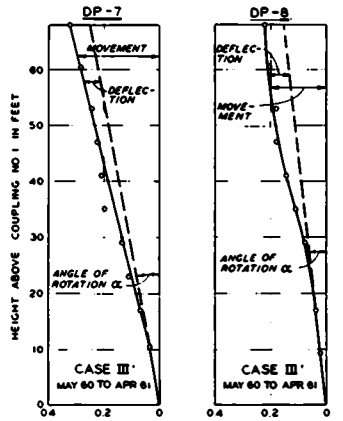

HORIZONTAL MOVEMENT IN INCHES WITH RESPECT TO COUPLING NO 1 SINCE BACKFILL COMPLETED

NOTE COUPLING NO 1 INSTALLED AT SAME ELEVATION AS TOP OF BASE SLAB.
NO CASE II MEASUREMENTS WERE MADE

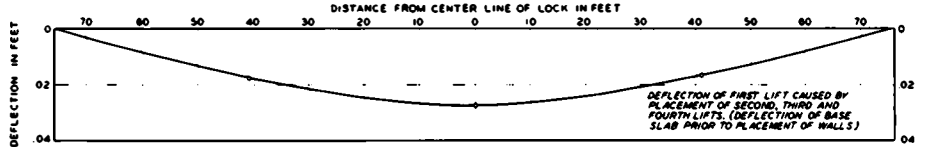

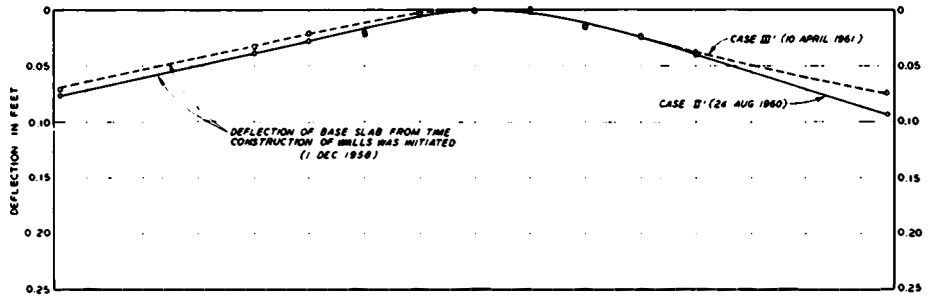

DEFLECTION OF BASE SLAB AND WALLS

MONOLITH 2

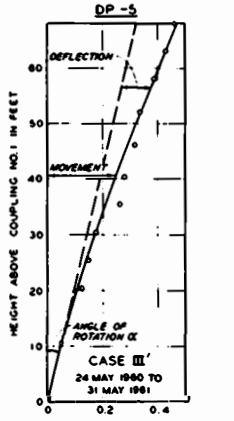

HORIZONTAL MOVEMENT IN INCHES WITH RESPECT TO COUPLING NO. 1 SINCE BACKFILL WAS COMPLETED

NOTE: NO CASE II' MEASUREMENTS WERE MADE.

COUPLING NO. 1 INSTALLED AT SAME ELEVATION AS TOP OF BASE SLAB

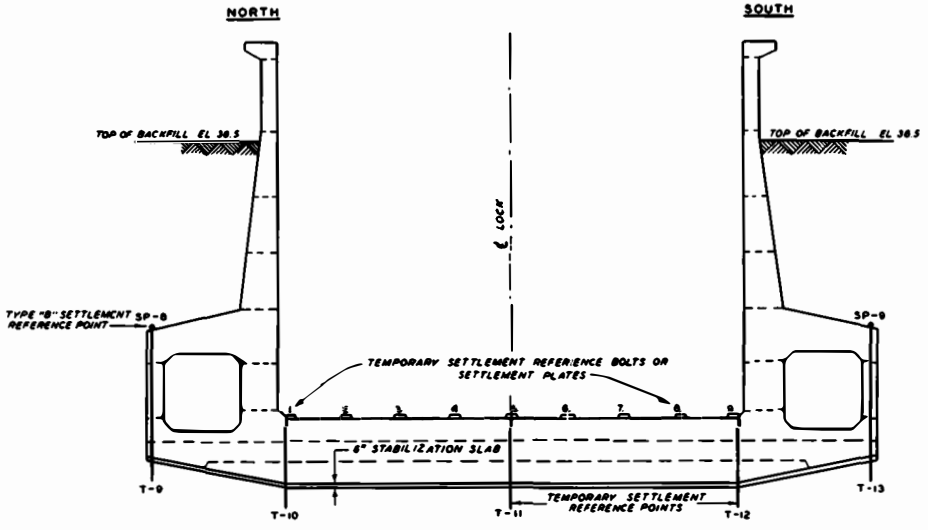

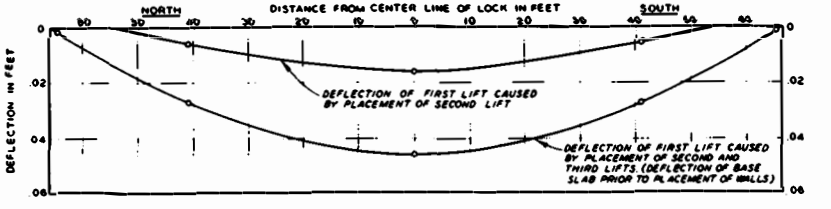

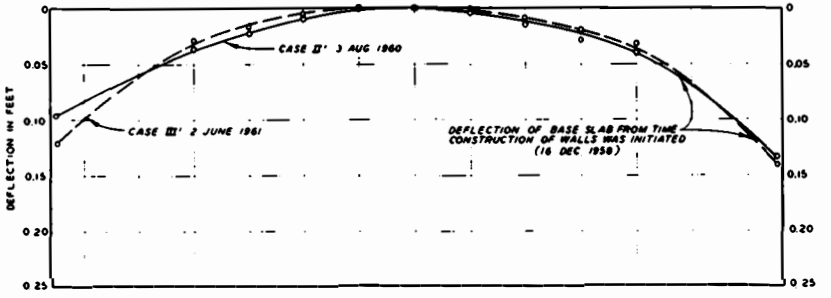

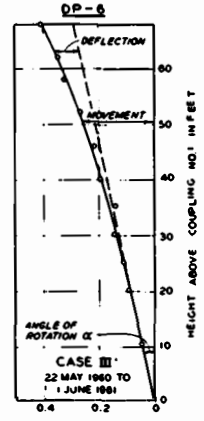

HORIZONTAL MOVEMENT IN INCHES WITH RESPECT TO COUPLING NO. 1 SINCE BACKFILL WAS COMPLETED

NOTE: NO CASE II' MEASUREMENTS WERE MADE.

DEFLECTION OF BASE SLAB AND WALLS
MONOLITH 6

PLATE 9

PLATE 20

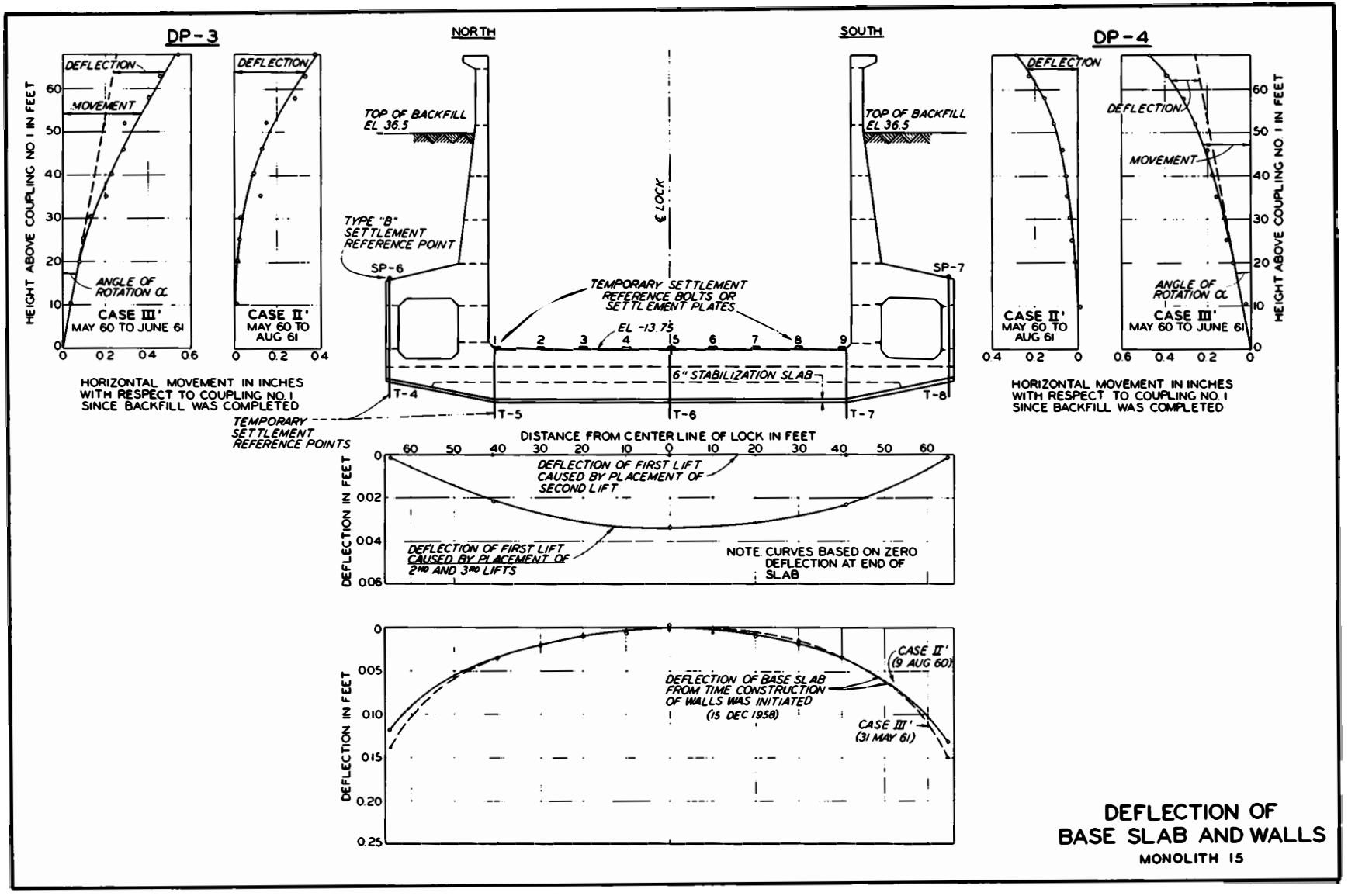

DEFLECTION OF BASE SLAB AND WALLS

MONOLITH 15

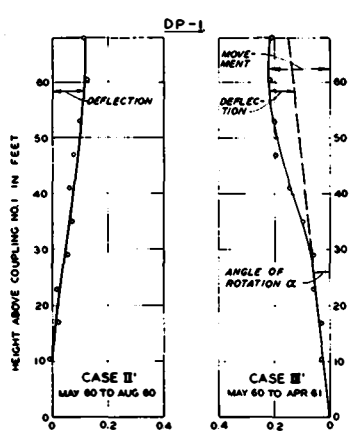

HORIZONTAL MOVEMENT IN INCHES WITH RESPECT TO COUPLING NO. 1 SINCE BACKFILL WAS COMPLETED.

NOTE: COUPLING NO. 1 WAS INSTALLED AT SAME ELEVATION AS TOP OF BASE SLAB.
BOTH DEFLECTION PIPES DP-1 AND DP-2 ARE LOCATED IN SOUTH WALL OF MONOLITH 24.

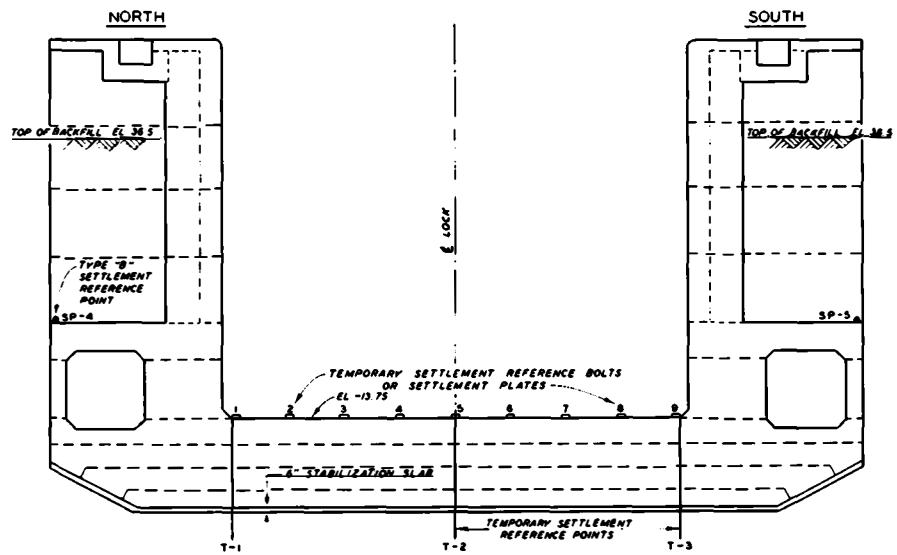

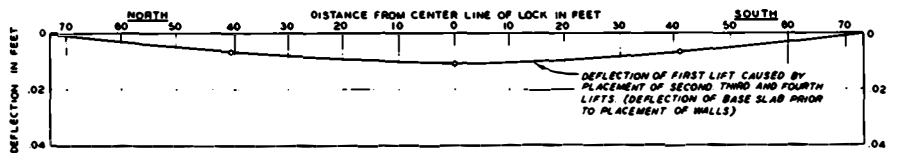

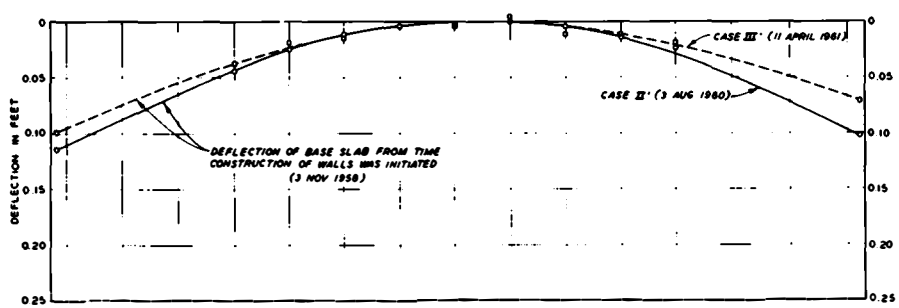

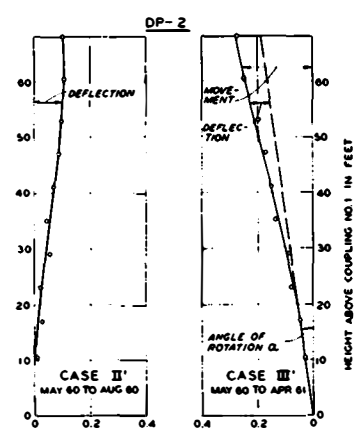

HORIZONTAL MOVEMENT IN INCHES WITH RESPECT TO COUPLING NO. 1 SINCE BACKFILL WAS COMPLETED.

DEFLECTION OF BASE SLAB AND WALLS

MONOLITH 24

PLATE 21

PLATE 22

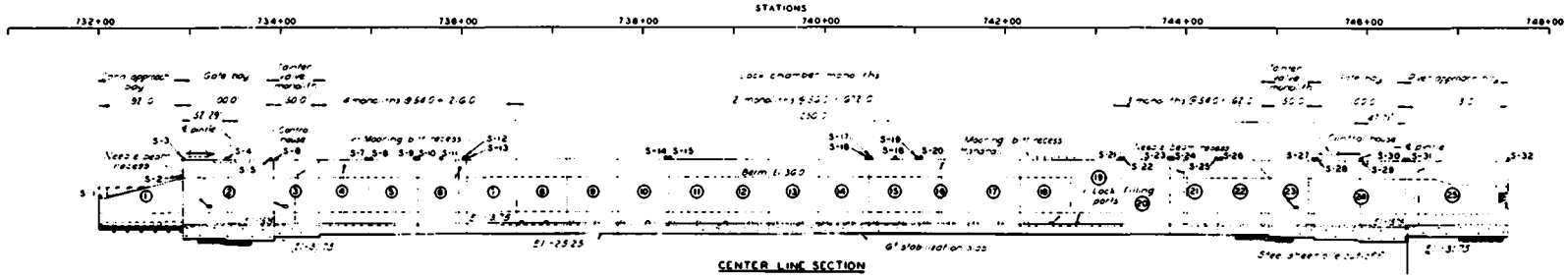

CENTER LINE SECTION

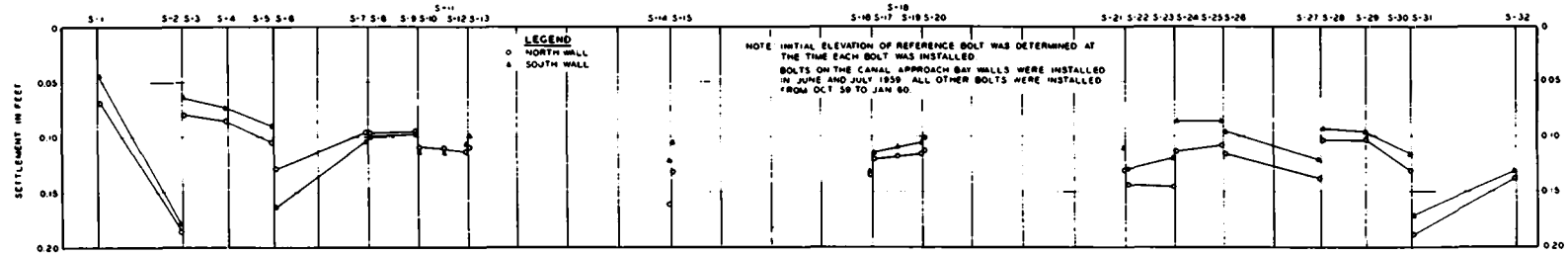

SETTLEMENT OF WALLS (26,27 MARCH 1962)

LONGITUDINAL MOVEMENT AT WALL JOINTS (26,27 MARCH 1962)

SETTLEMENT OF TOPS OF LOCK WALLS AND MOVEMENT AT JOINTS

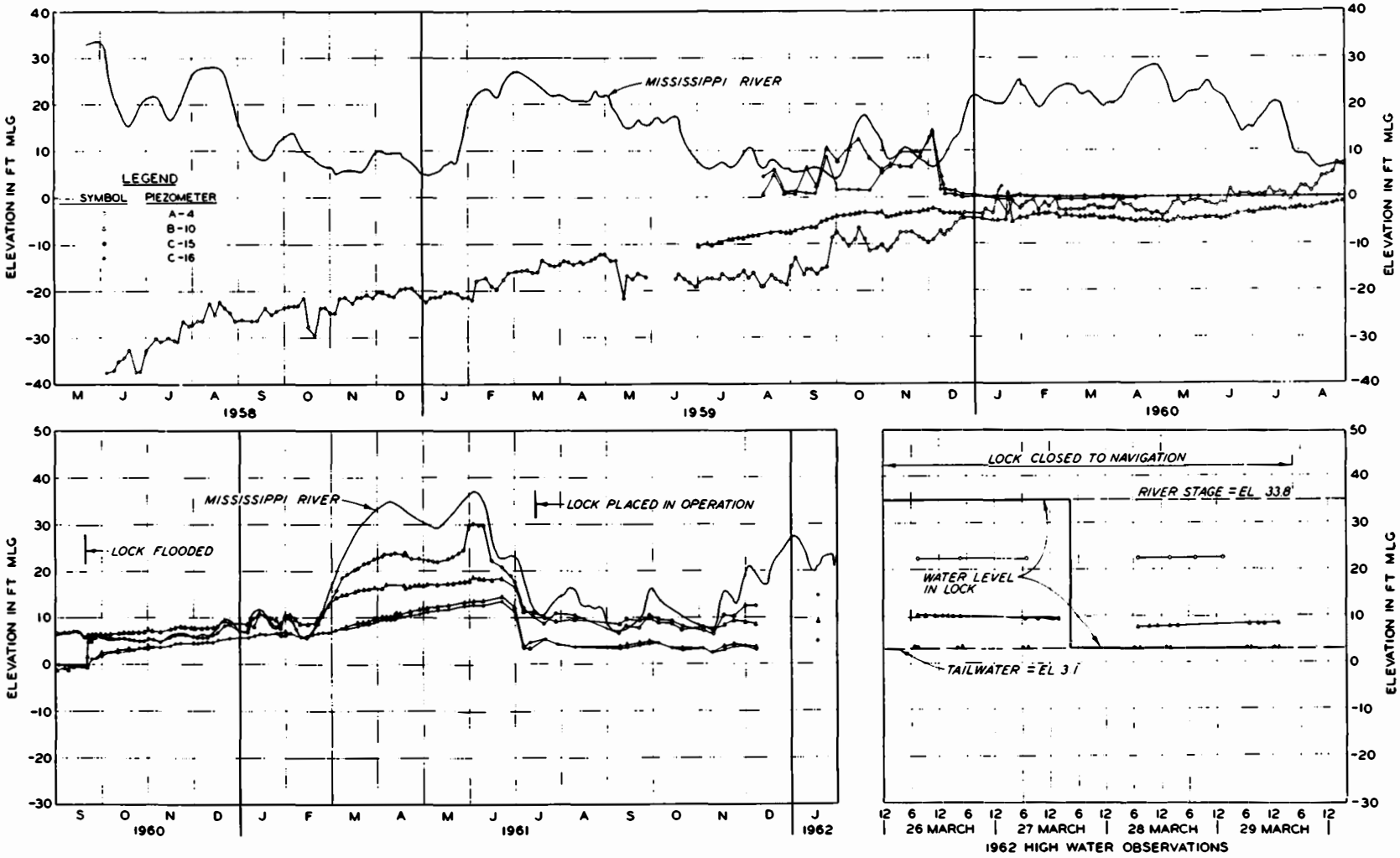

NOTE: LOCATIONS OF PIEZOMETERS SHOWN IN FIG 14

DATA FROM PIEZOMETERS LOCATED BENEATH AND ADJACENT TO MONOLITH 2

PLATE 23

PLATE 24

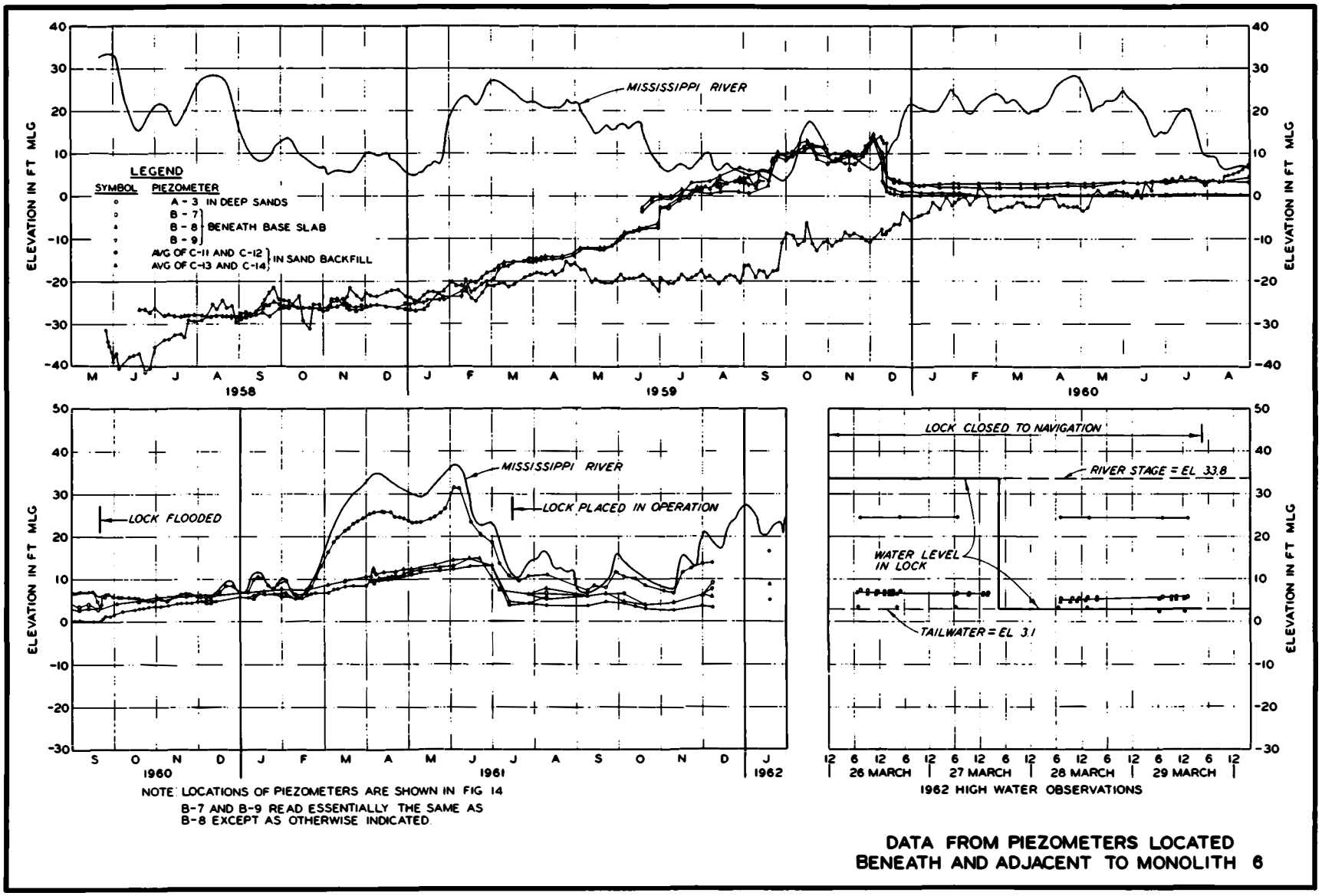

NOTE: LOCATIONS OF PIEZOMETERS ARE SHOWN IN FIG 14
B-7 AND B-9 READ ESSENTIALLY THE SAME AS B-8 EXCEPT AS OTHERWISE INDICATED

DATA FROM PIEZOMETERS LOCATED BENEATH AND ADJACENT TO MONOLITH 6

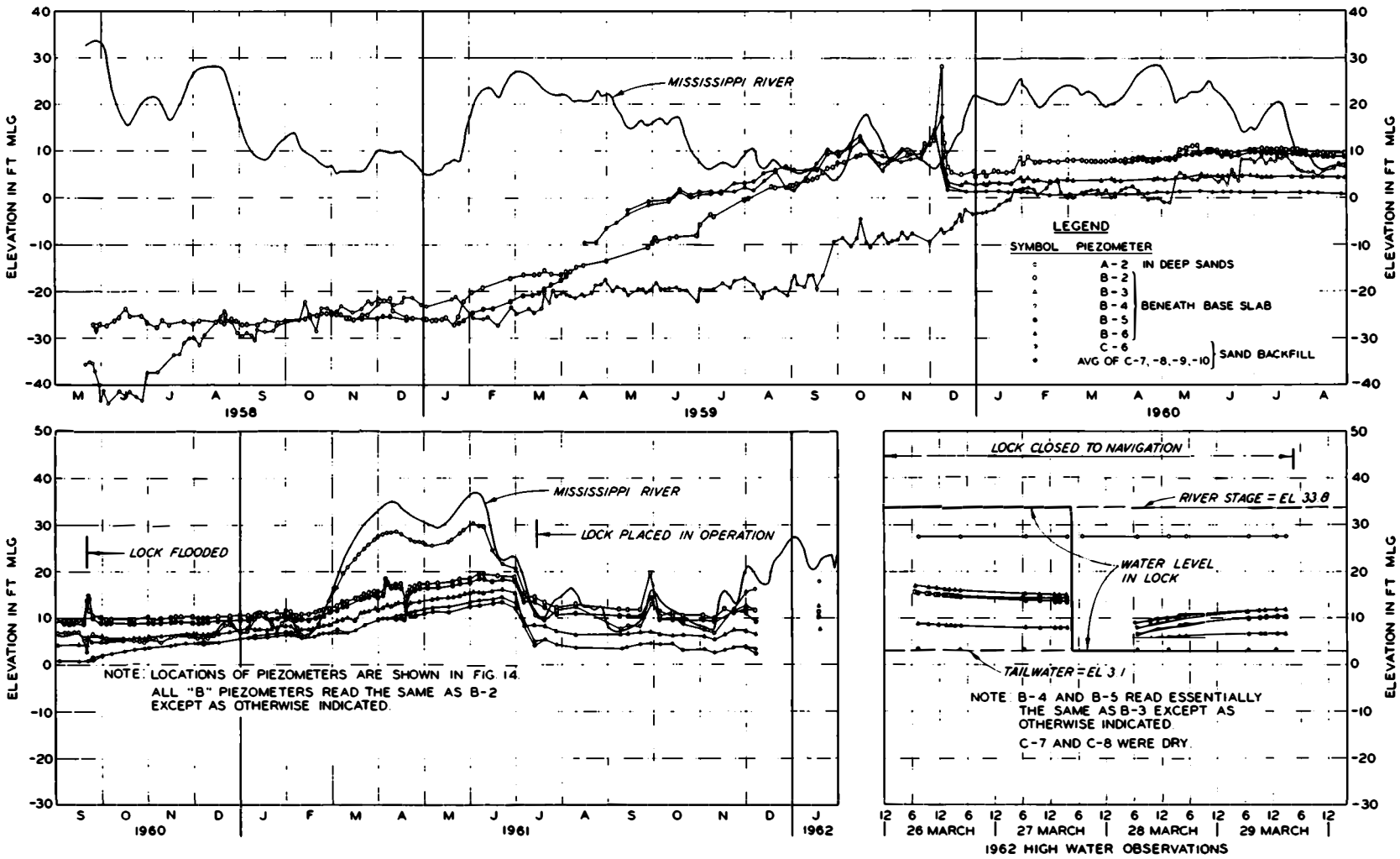

DATA FROM PIEZOMETERS LOCATED BENEATH AND ADJACENT TO MONOLITH 15

PLATE 25

PLATE 26

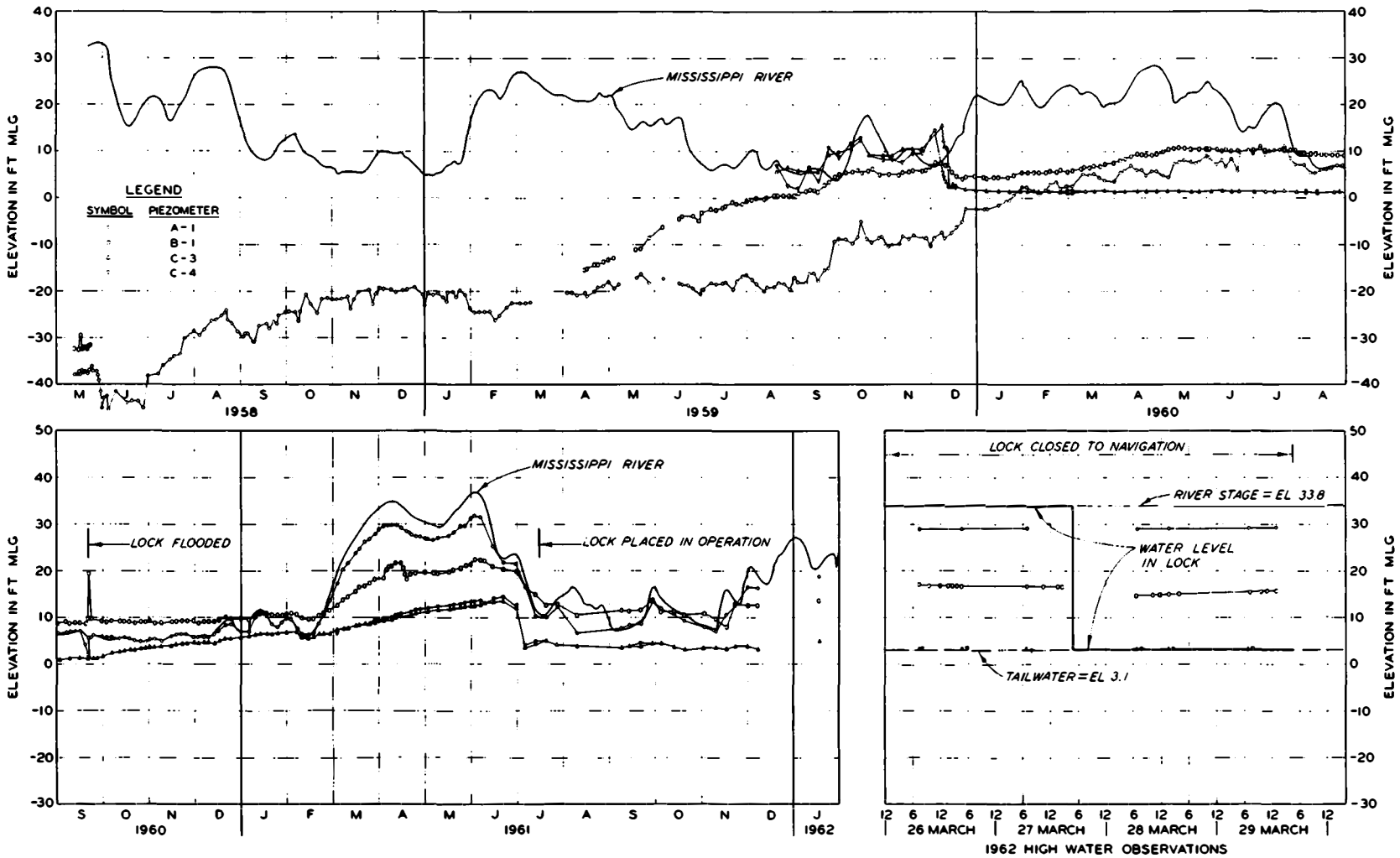

NOTE: LOCATIONS OF PIEZOMETERS SHOWN IN FIG. 14.
B-4 READ THE SAME AS B-3 EXCEPT AS OTHERWISE INDICATED.

DATA FROM PIEZOMETERS LOCATED BENEATH AND ADJACENT TO MONOLITH 24

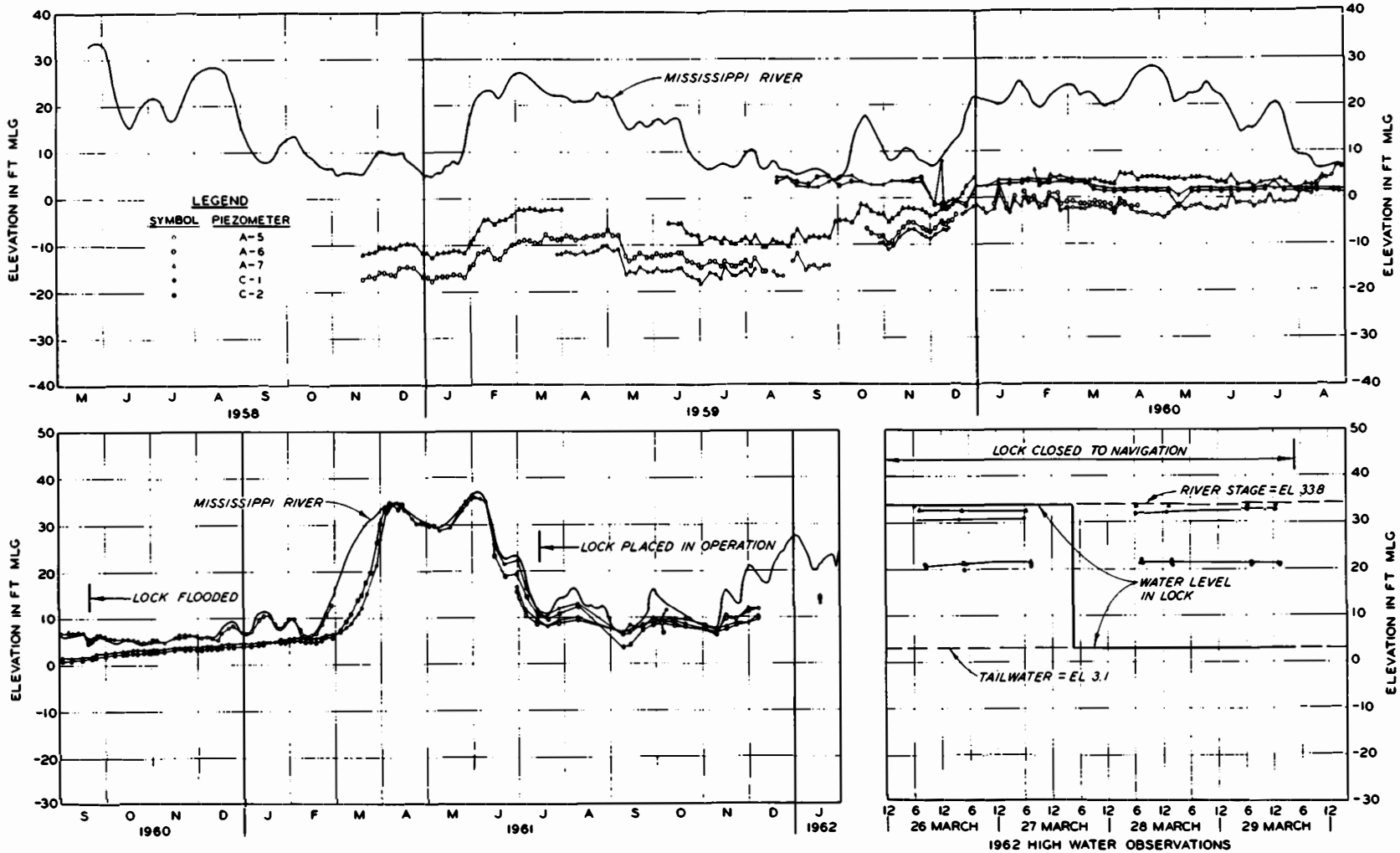

NOTE: LOCATIONS OF PIEZOMETERS ARE SHOWN IN FIG 14
AFTER 11 AUG 1960 A-6 AND A-7 READ THE SAME AS A-5 EXCEPT AS OTHERWI SE INDICATED

DATA FROM PIEZOMETERS LOCATED BENEATH MONOLITH 25 AND APPROACH CHANNEL

PLATE 27

PLATE 28

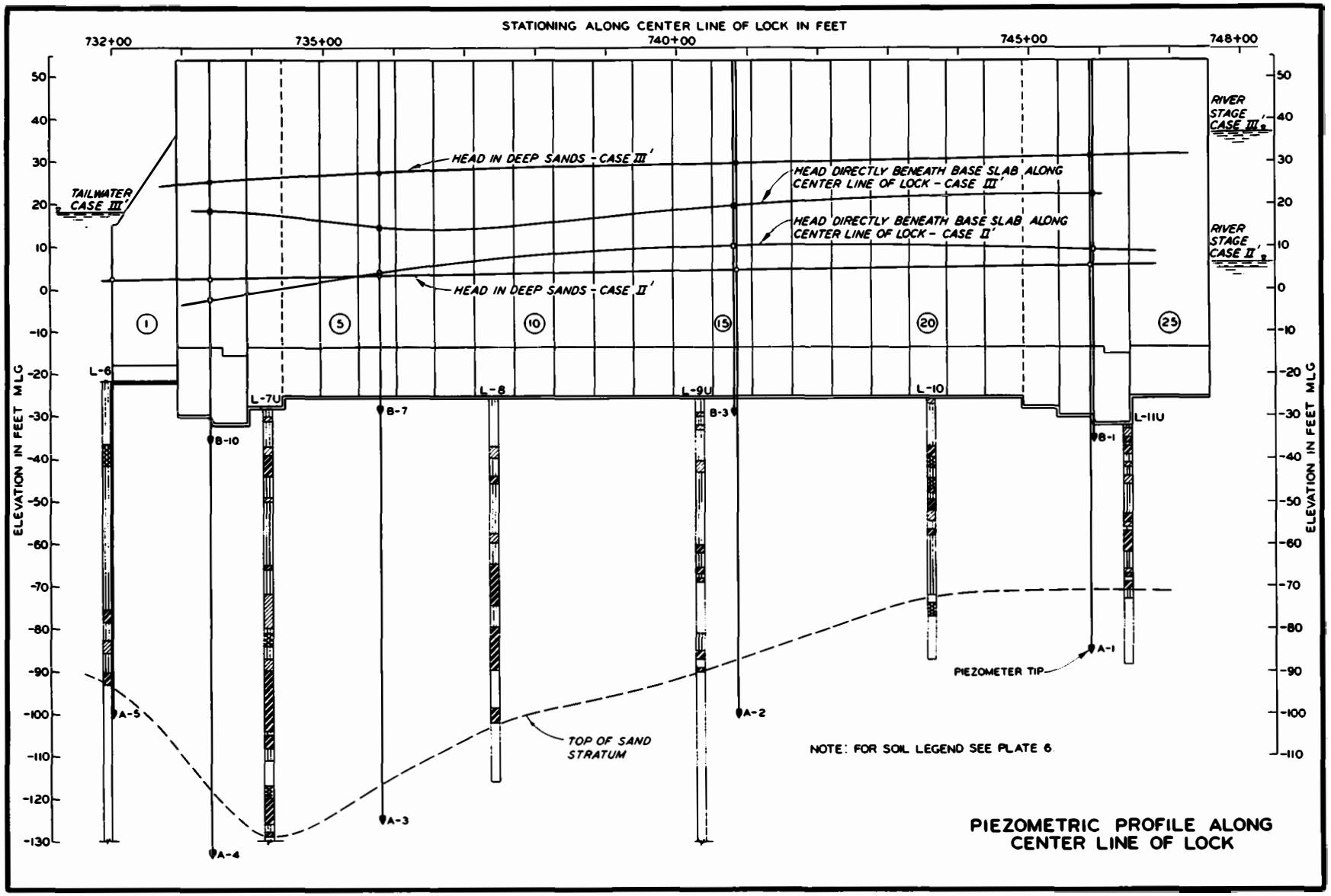

PIEZOMETRIC PROFILE ALONG CENTER LINE OF LOCK

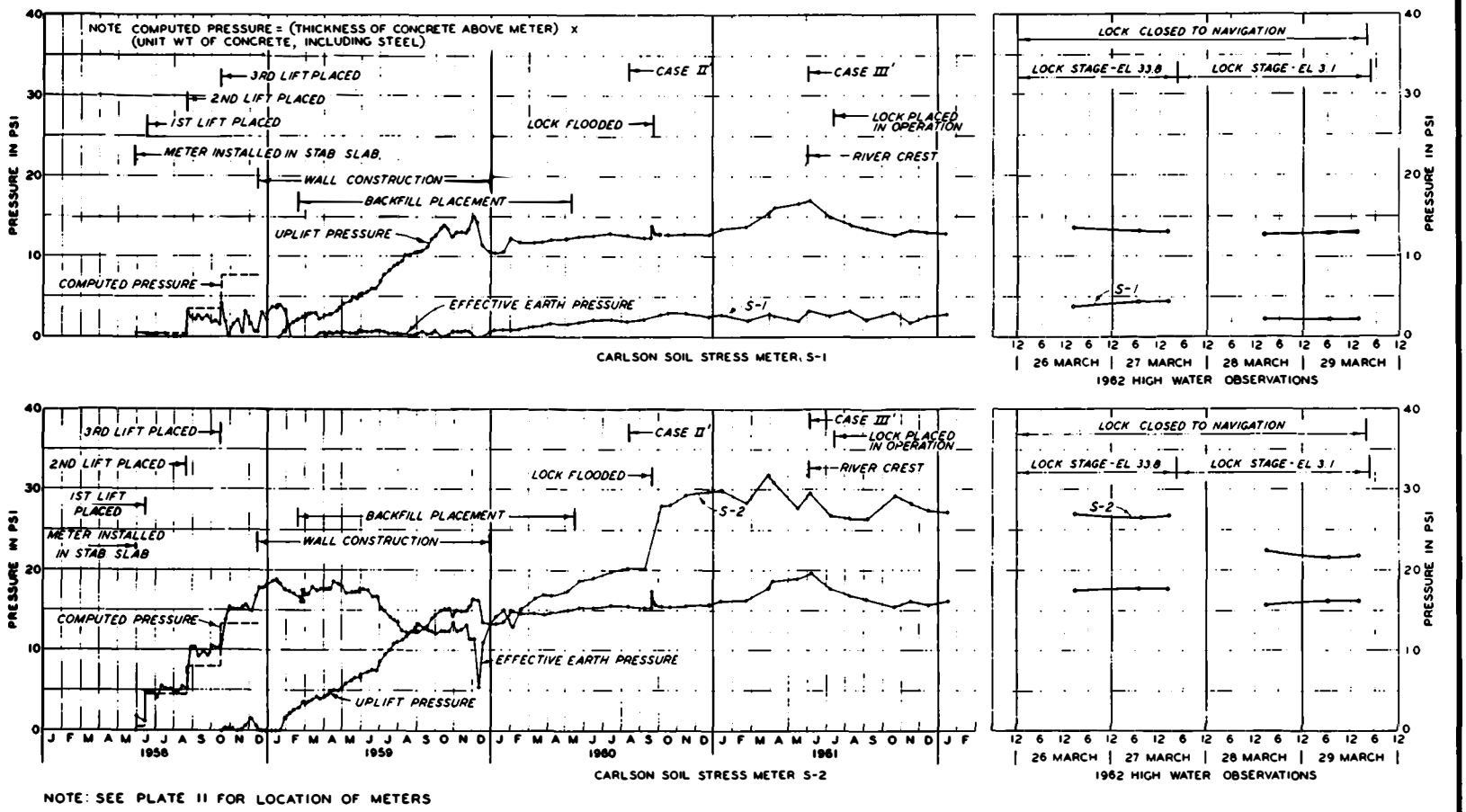

DATA FROM
SOIL STRESS METERS S-1 AND S-2

PLATE 29

PLATE 30

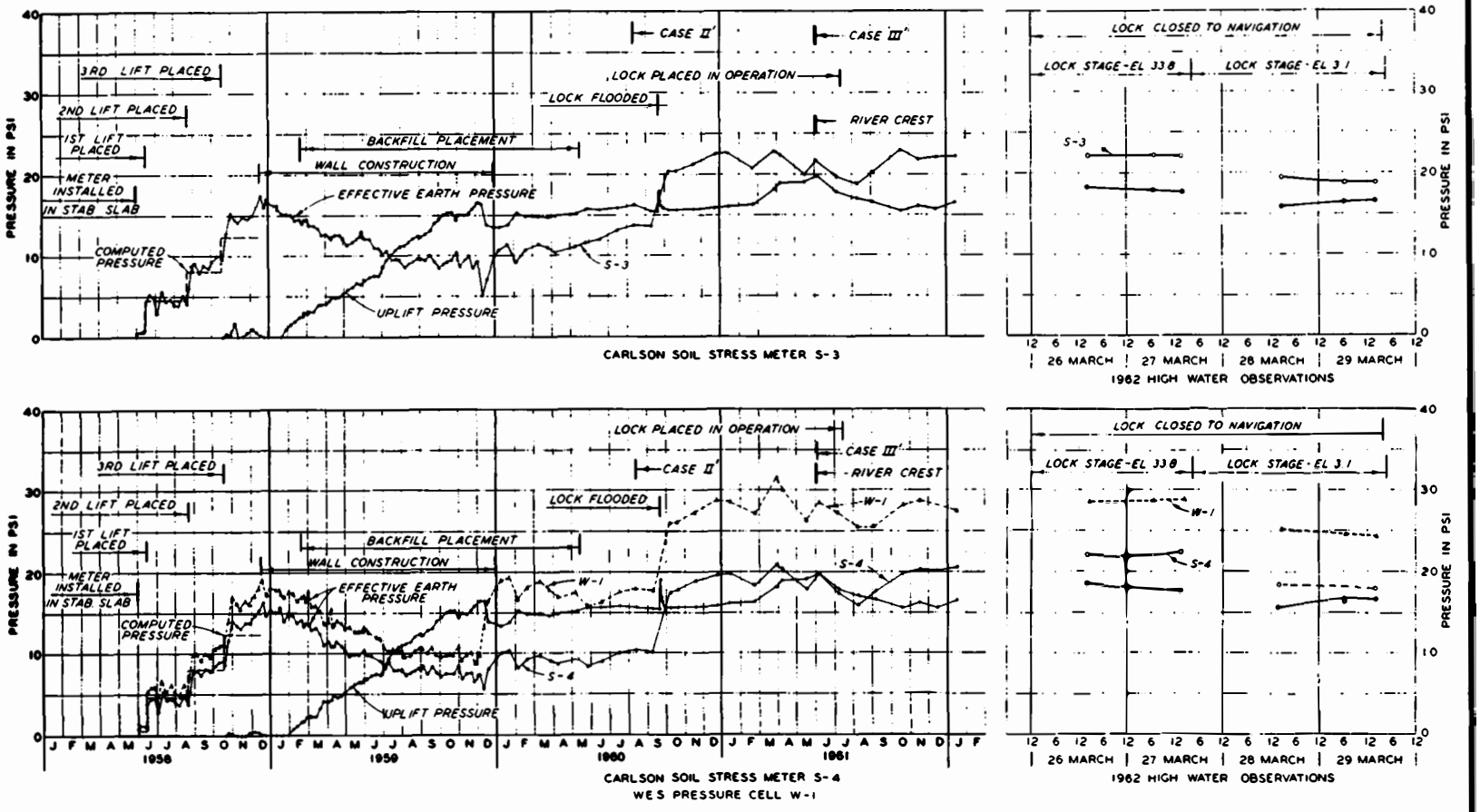

DATA FROM
SOIL STRESS METERS S-3 AND S-4

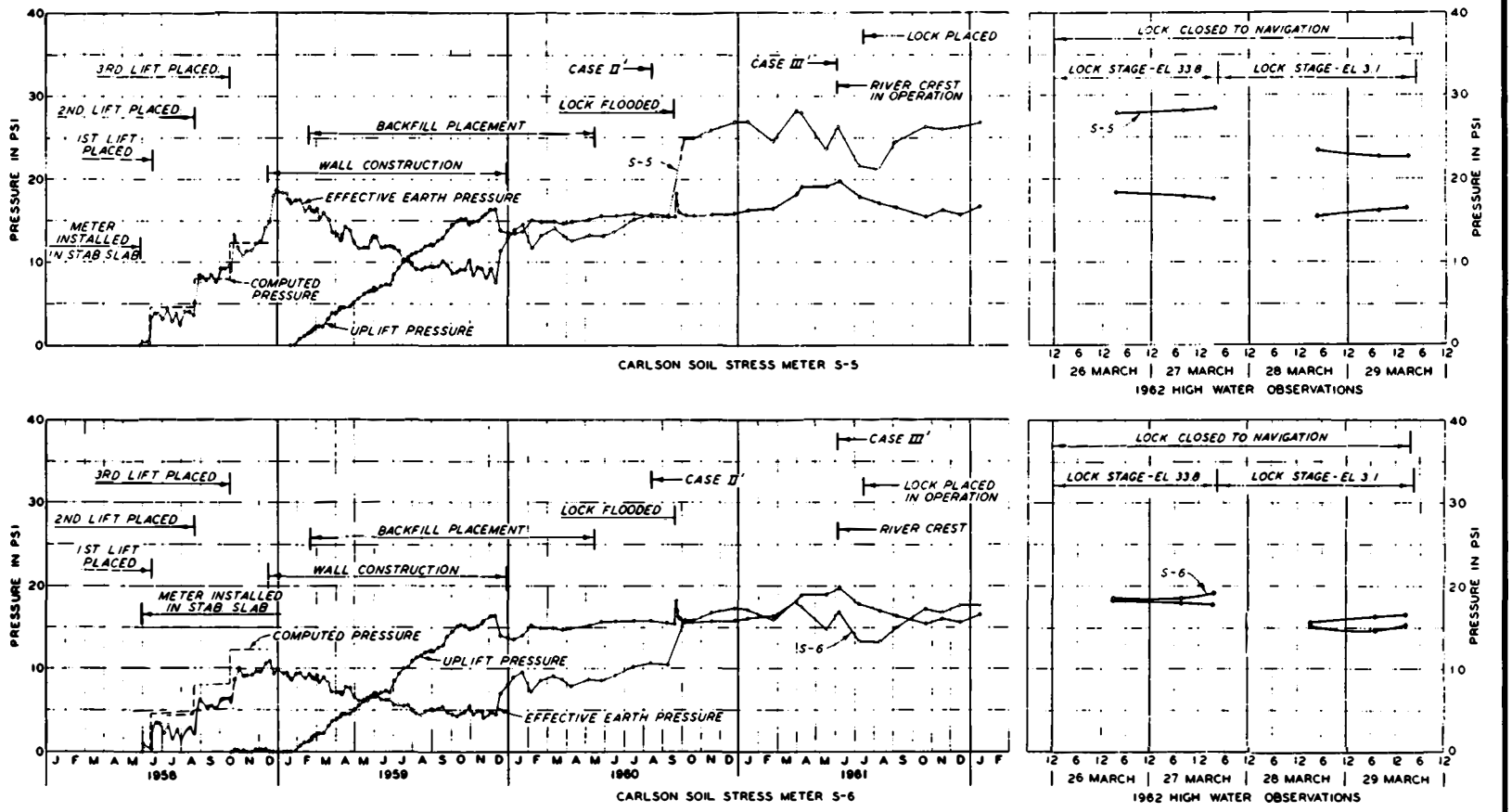

DATA FROM
SOIL STRESS METERS S-5 AND S-6

PLATE 31

PLATE 32

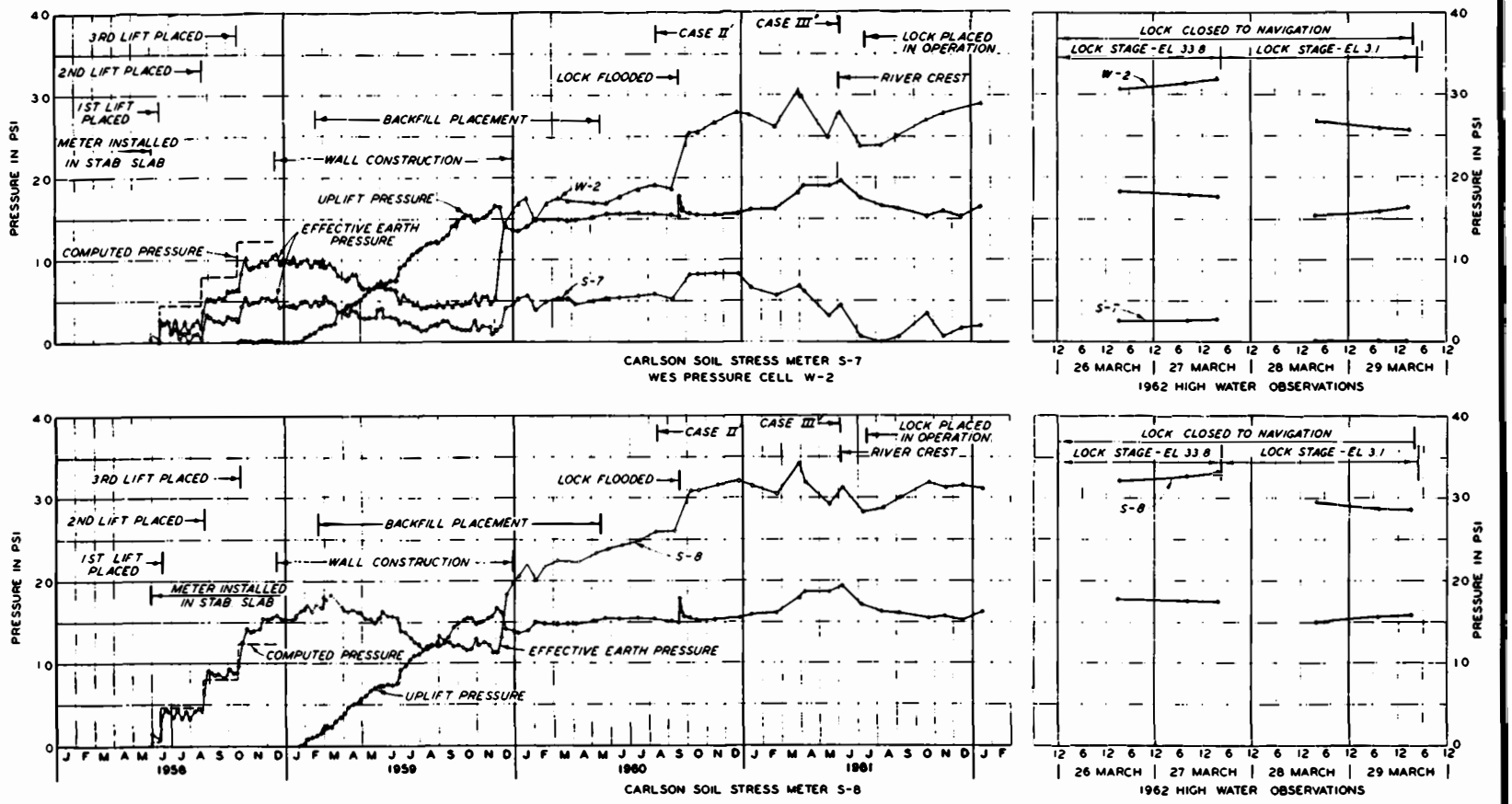

DATA FROM
SOIL STRESS METERS S-7, S-8, AND
PRESSURE CELL W-2

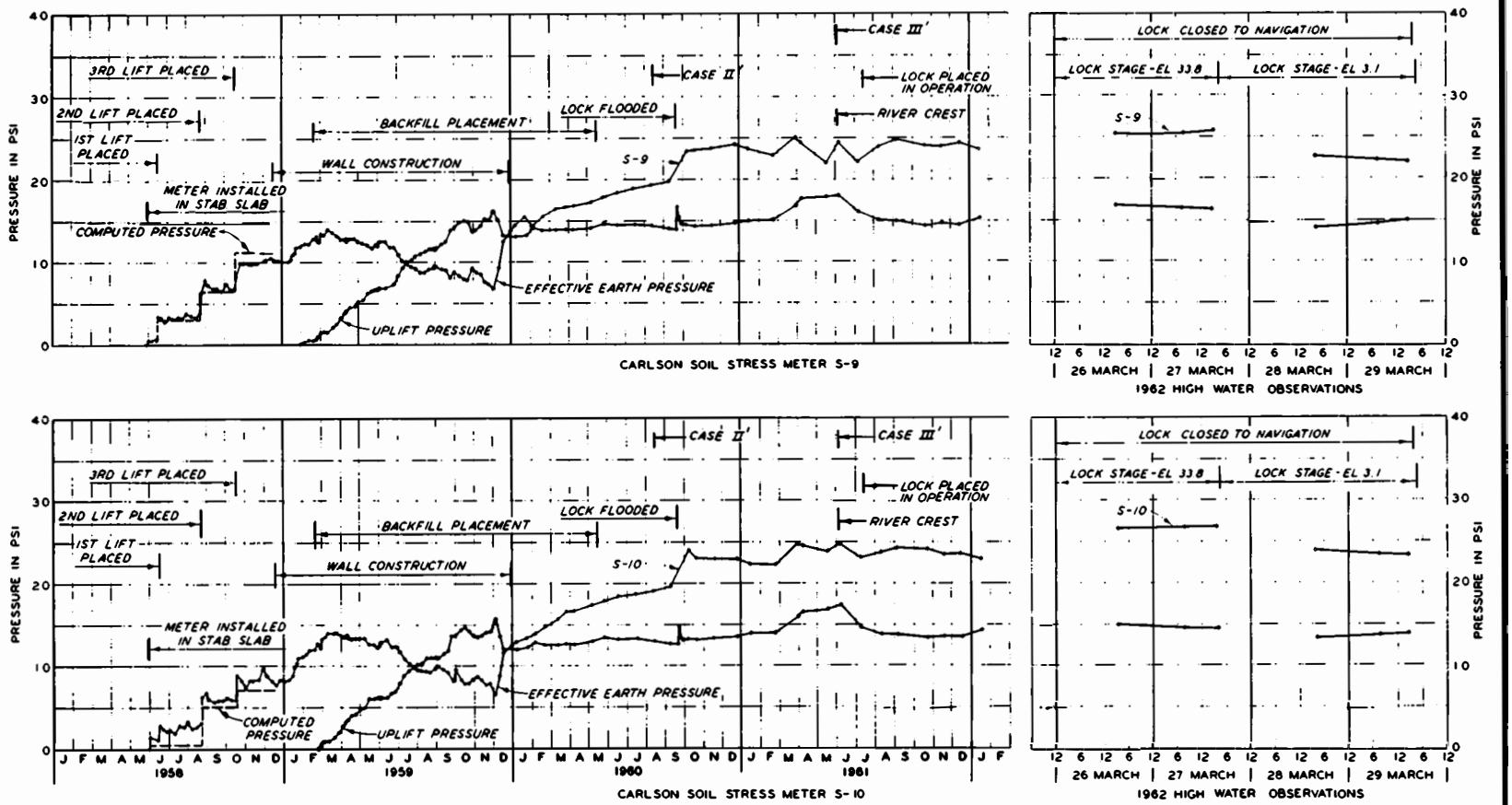

DATA FROM
SOIL STRESS METERS S-9 AND S-10

PLATE 33

PLATE 34

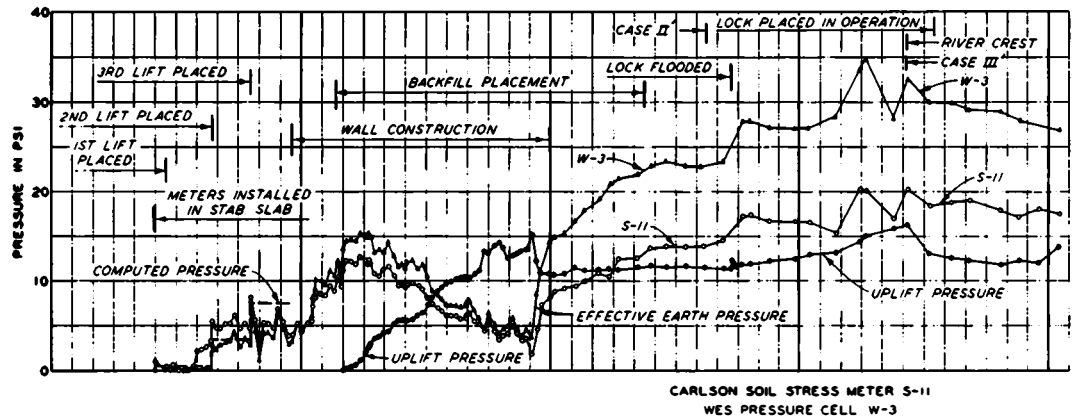

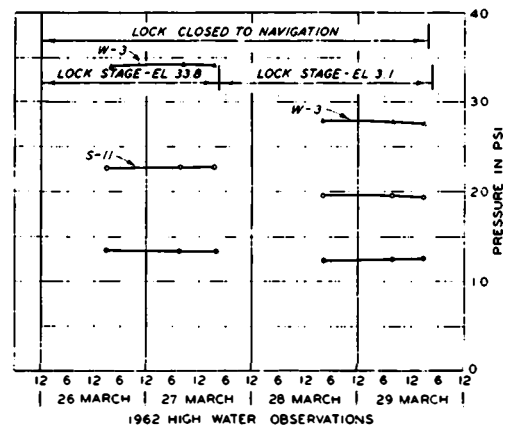

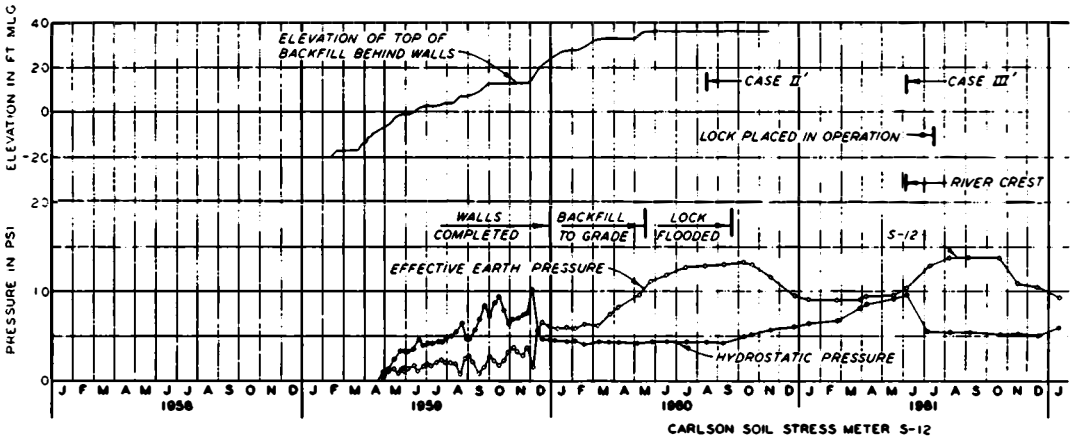

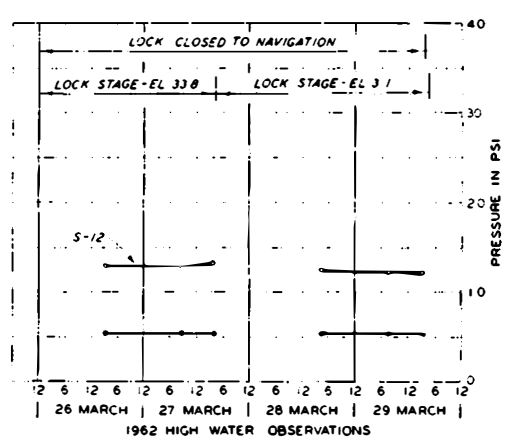

DATA FROM
SOIL STRESS METERS S-11, S-12, AND
PRESSURE CELL W-3

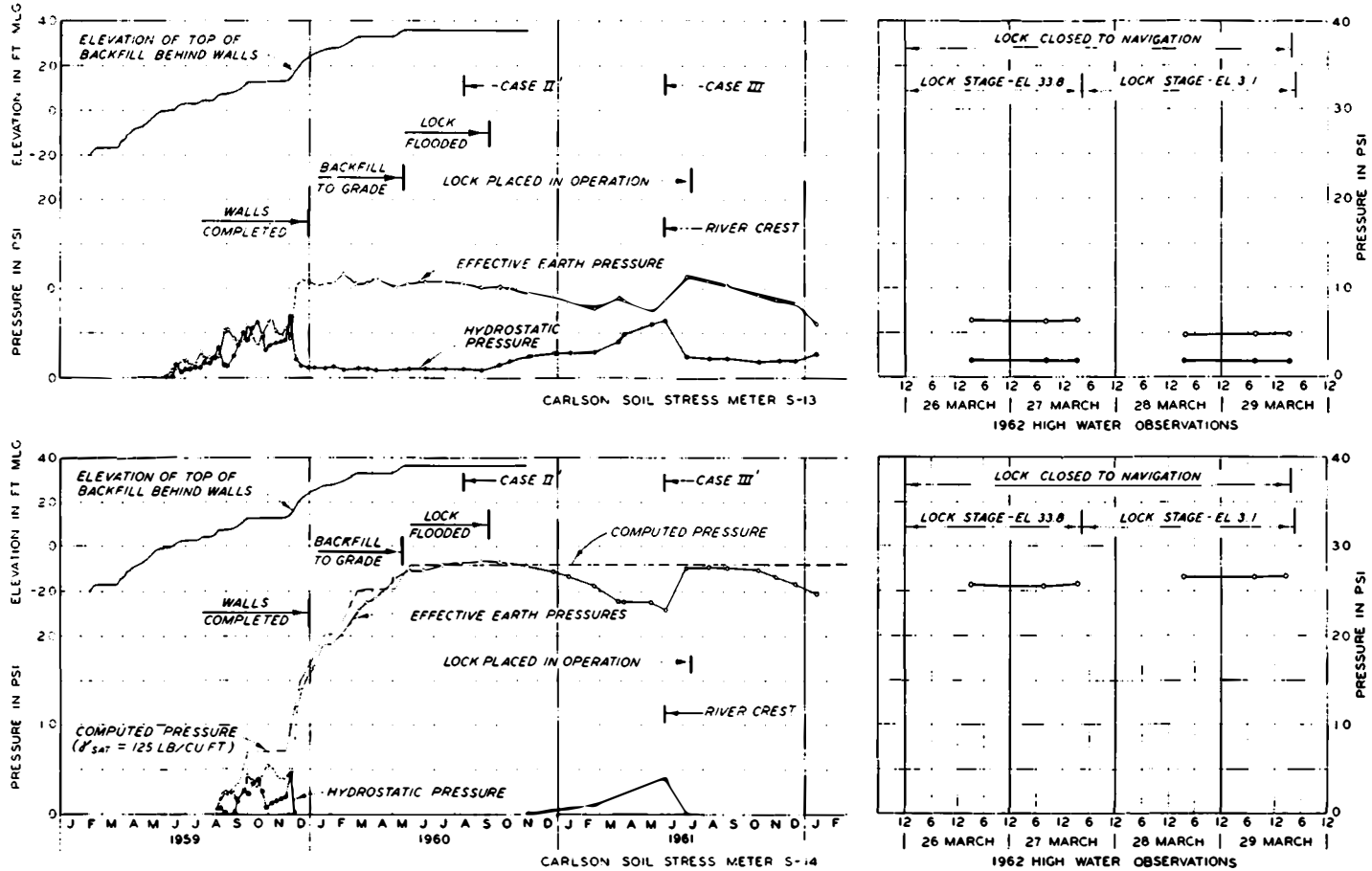

DATA FROM SOIL STRESS METERS S-13 AND S-14

PLATE 35

PLATE 36

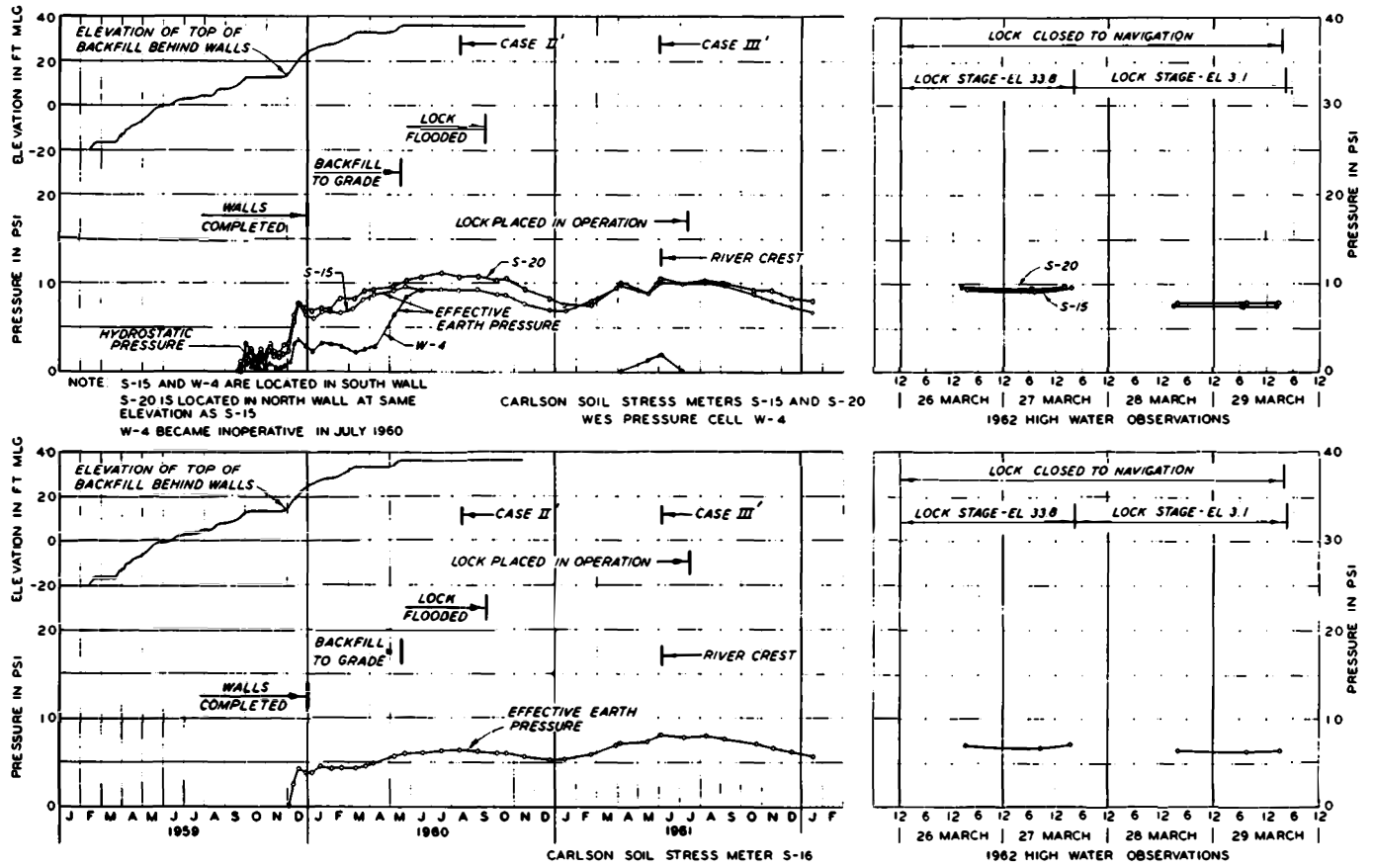

DATA FROM
SOIL STRESS METERS S-15, S-16, S-20, AND
PRESSURE CELL W-4

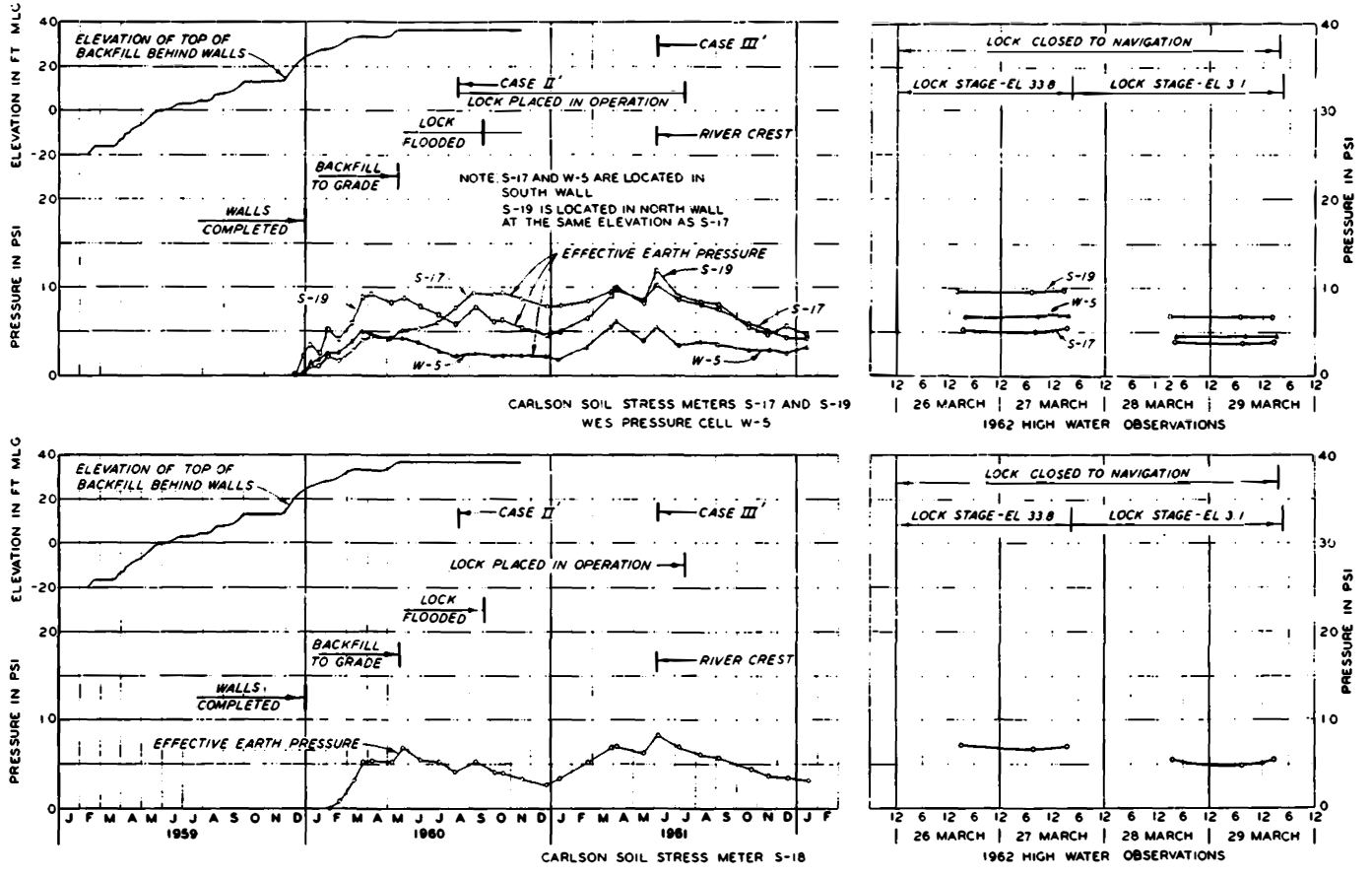

DATA FROM
SOIL STRESS METERS S-17, S-18, S-19, AND
PRESSURE CELL W-5

PLATE 37

PLATE 38

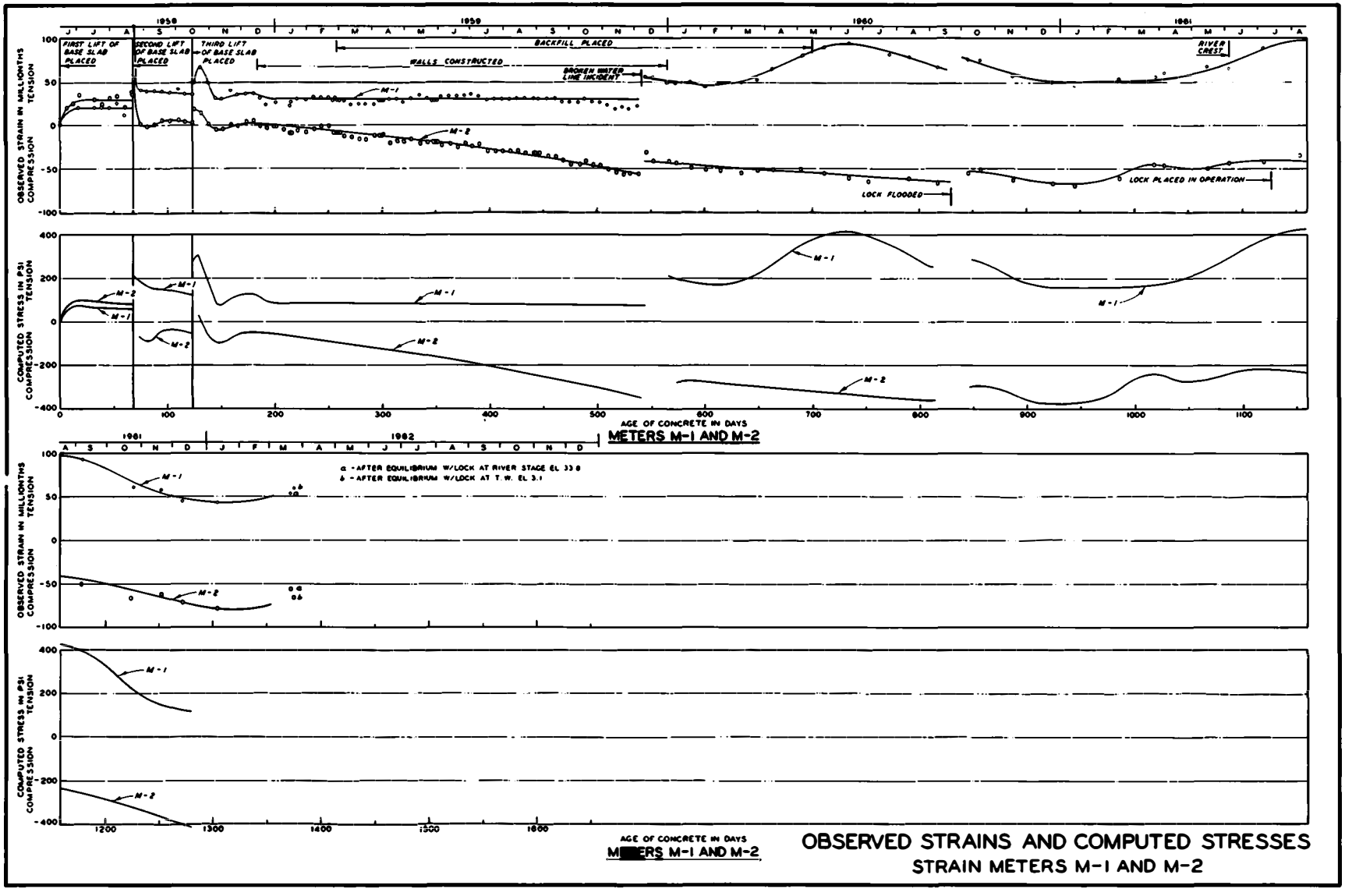

OBSERVED STRAINS AND COMPUTED STRESSES
STRAIN METERS M-1 AND M-2

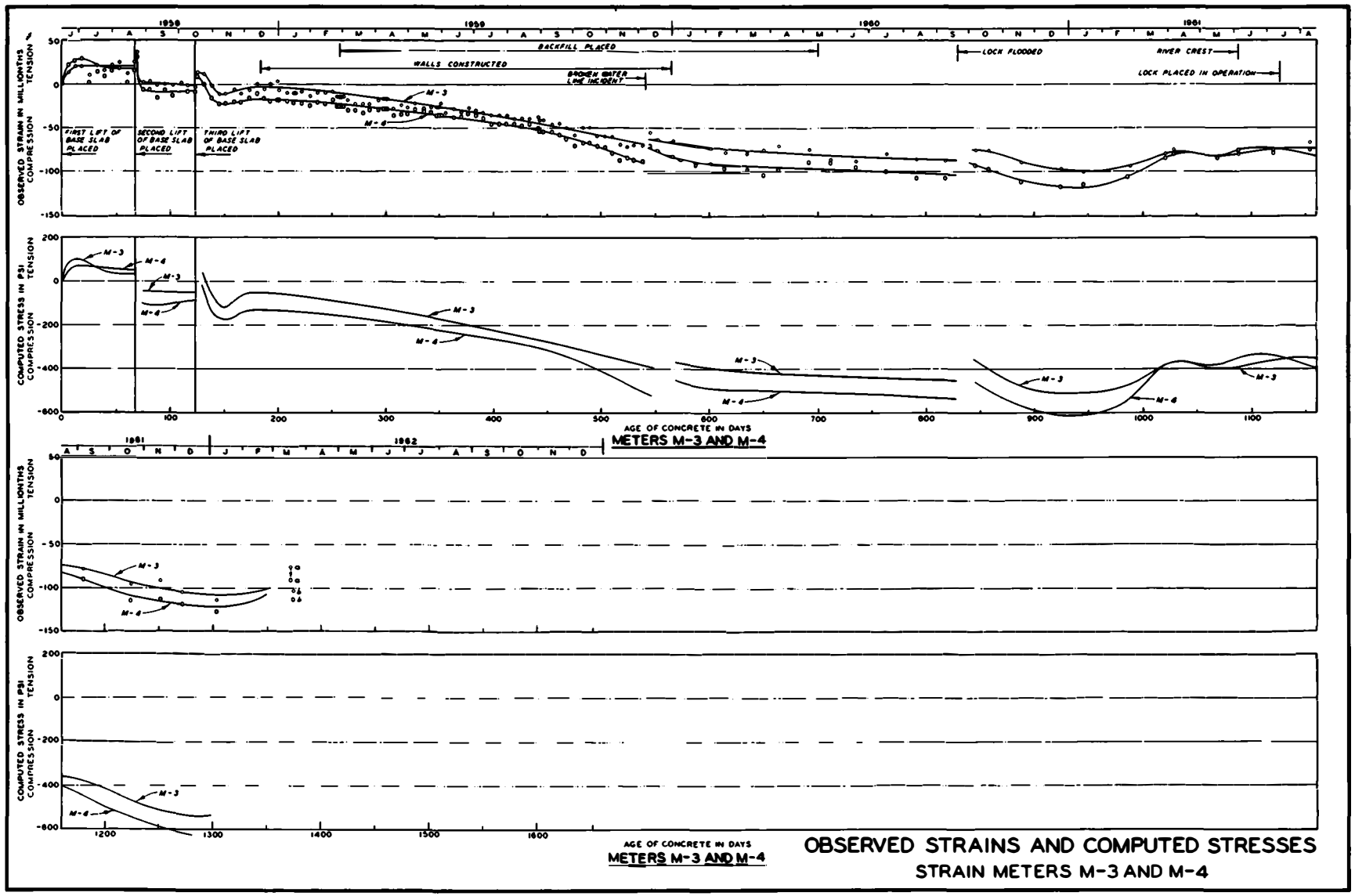

OBSERVED STRAINS AND COMPUTED STRESSES

STRAIN METERS M-3 AND M-4

PLATE 39

PLATE 40

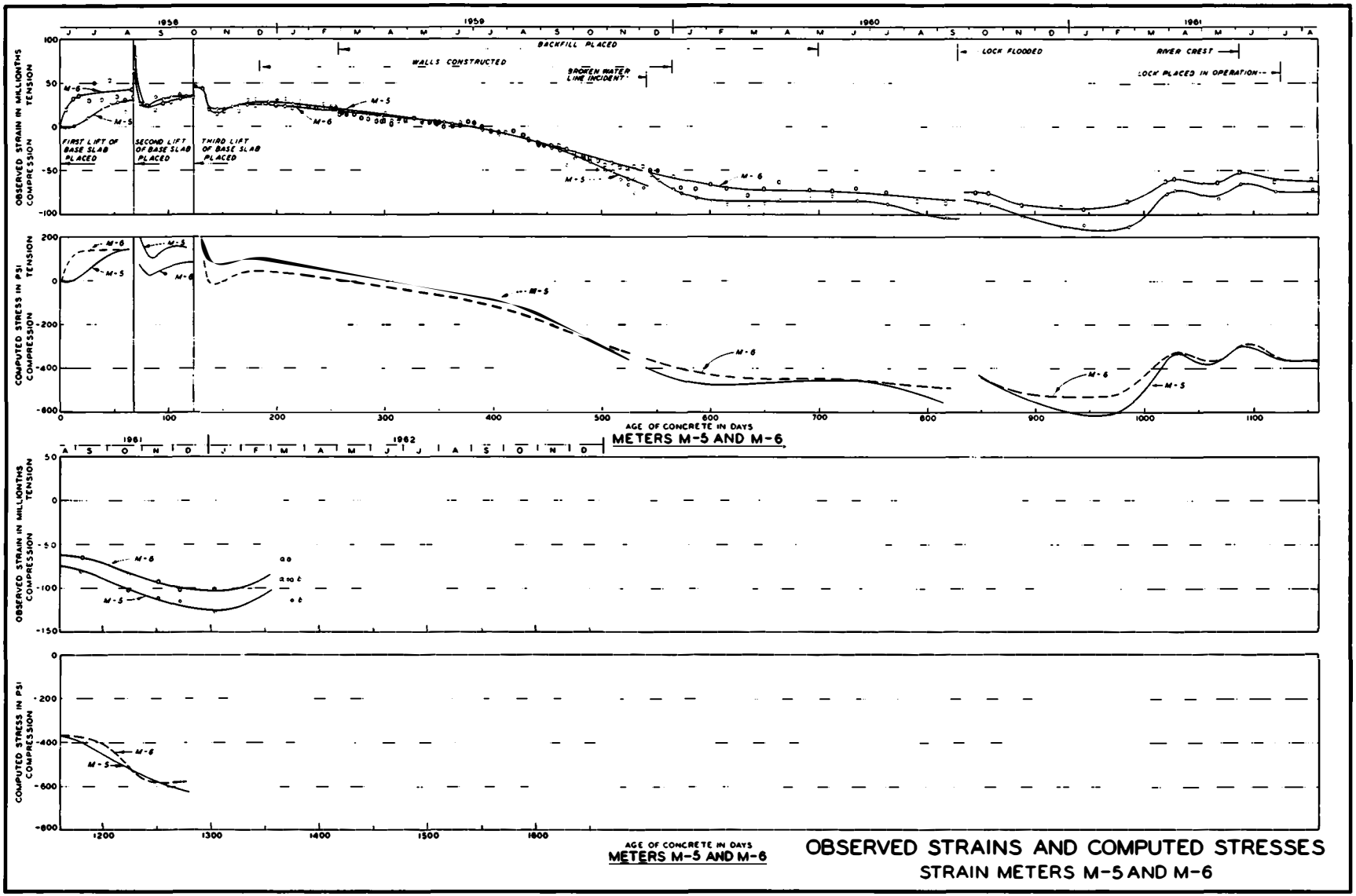

OBSERVED STRAINS AND COMPUTED STRESSES

STRAIN METERS M-5 AND M-6

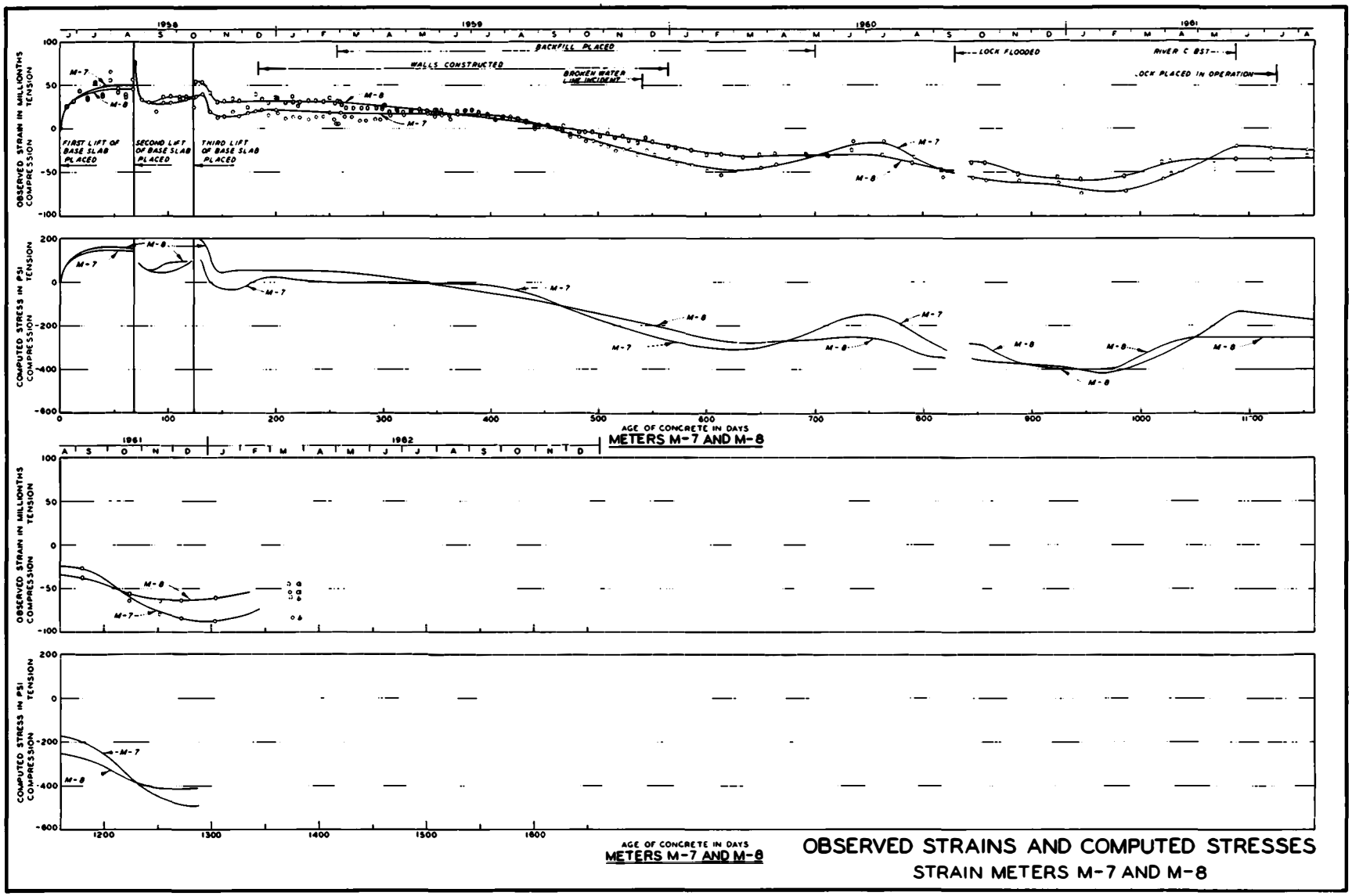

PLATE 41

OBSERVED STRAINS AND COMPUTED STRESSES

STRAIN METERS M-7 AND M-8

PLATE 42

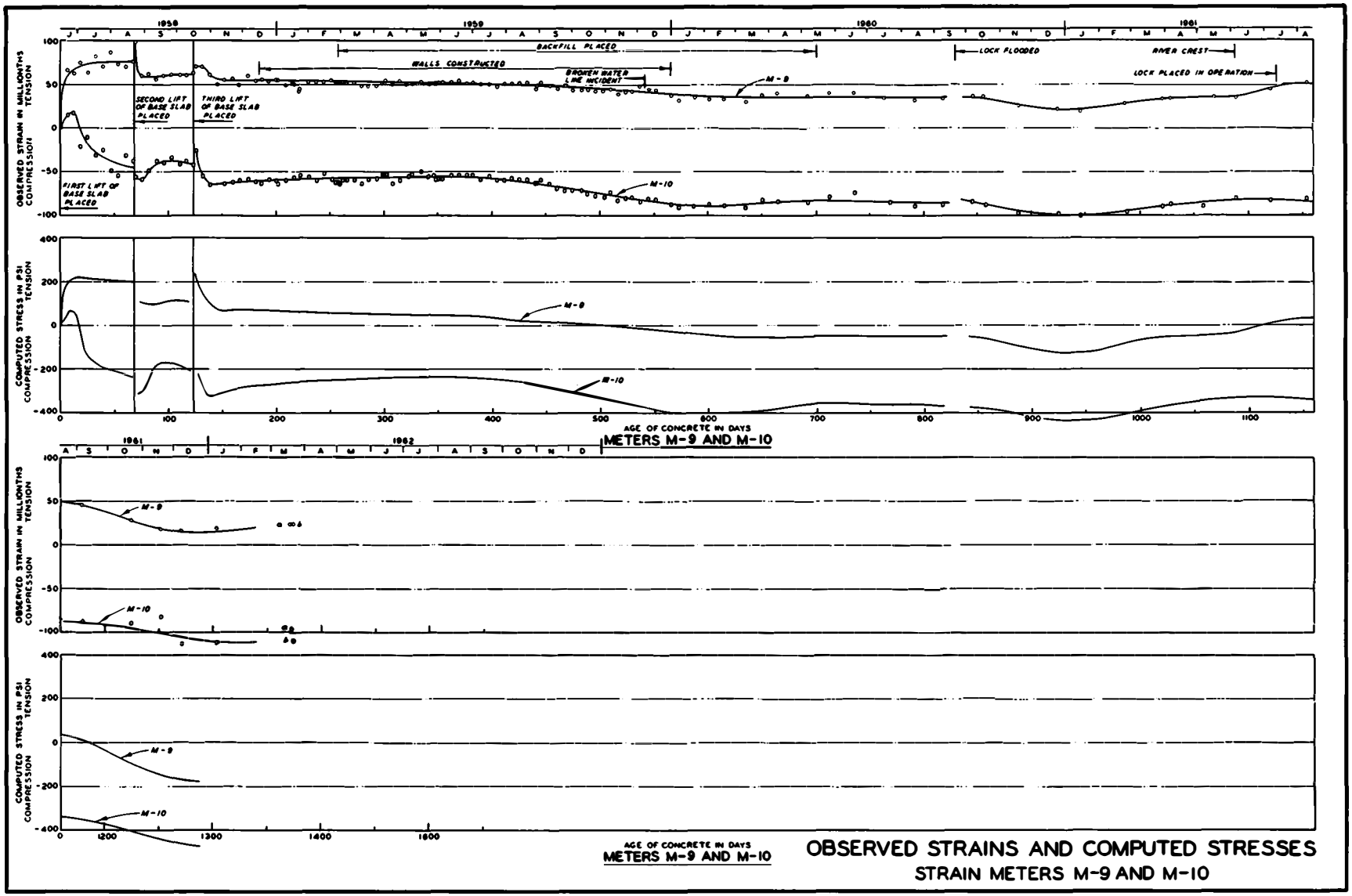

OBSERVED STRAINS AND COMPUTED STRESSES

STRAIN METERS M-9 AND M-10

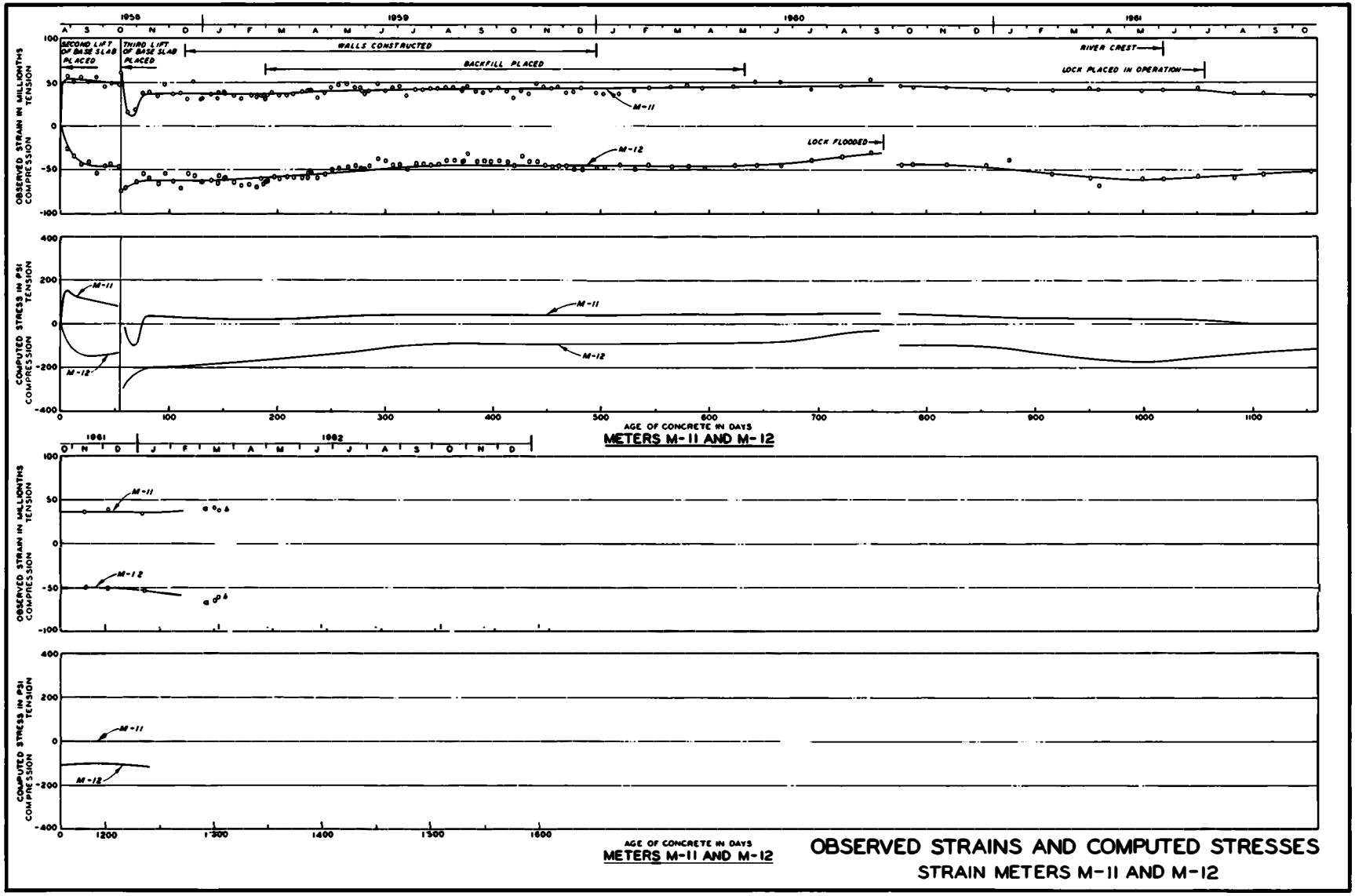

PLATE 43

OBSERVED STRAINS AND COMPUTED STRESSES

STRAIN METERS M-11 AND M-12

PLATE 44

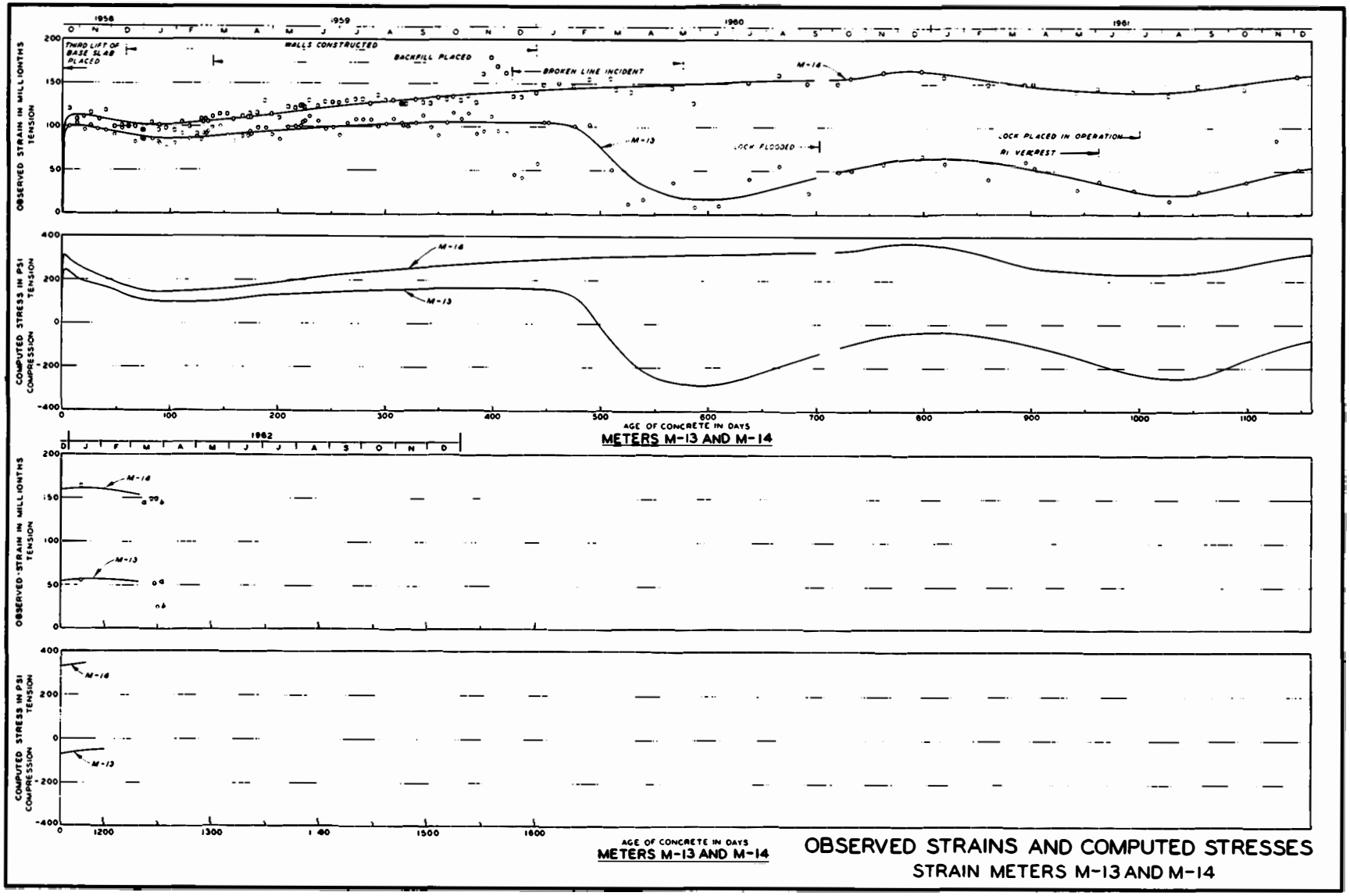

OBSERVED STRAINS AND COMPUTED STRESSES
STRAIN METERS M-13 AND M-14

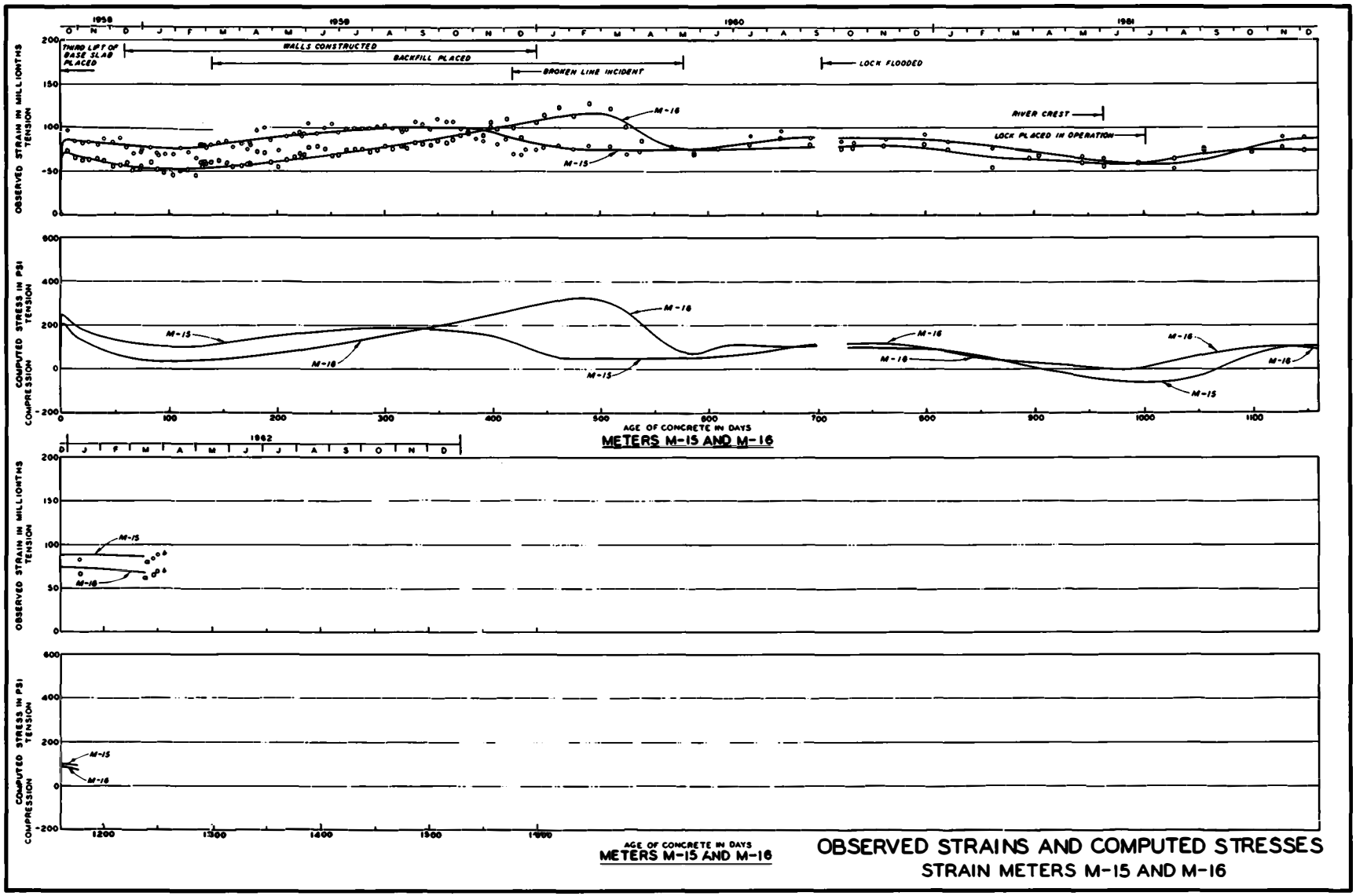

PLATE 45

OBSERVED STRAINS AND COMPUTED STRESSES
STRAIN METERS M-15 AND M-16

PLATE 46

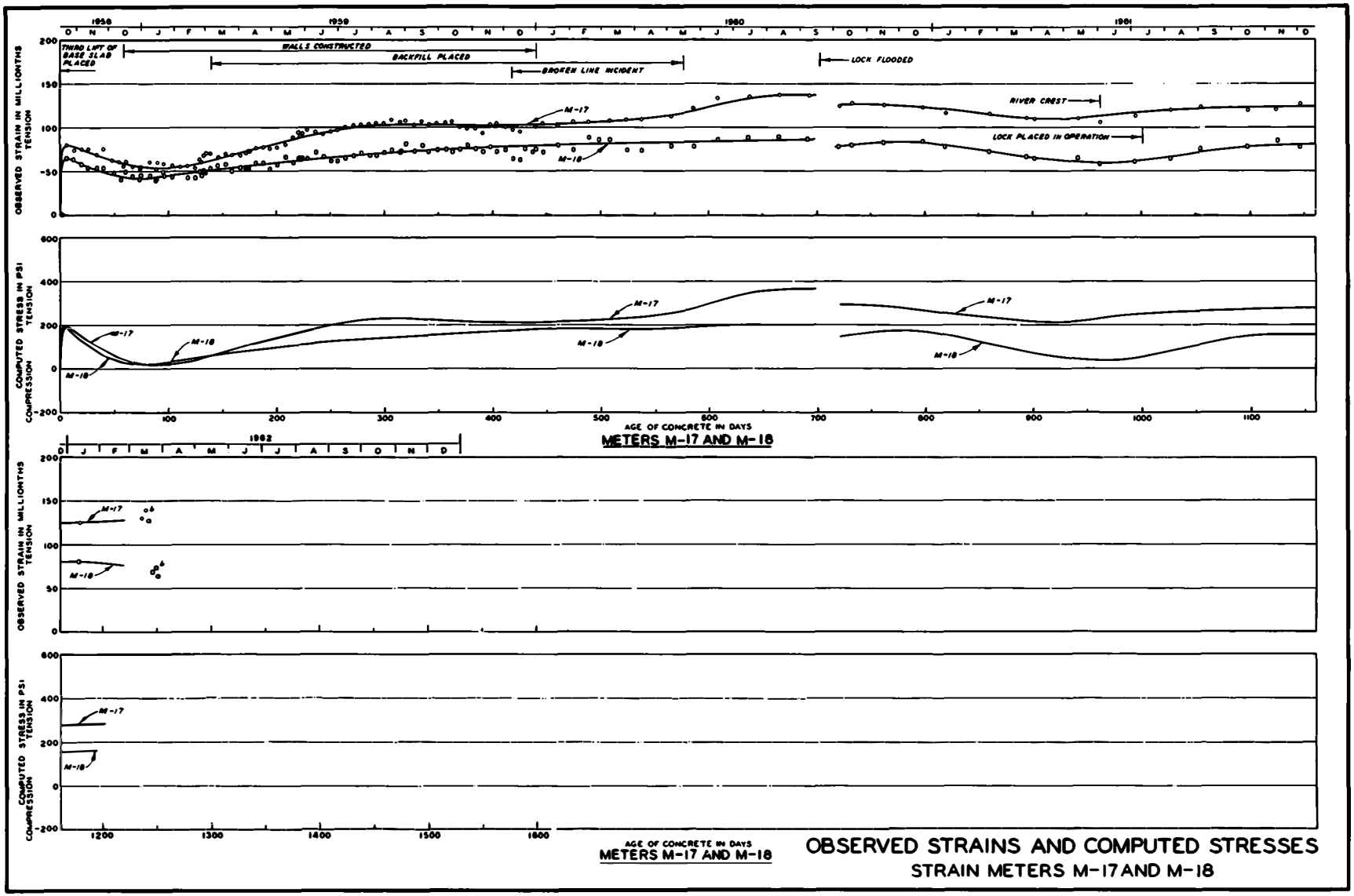

OBSERVED STRAINS AND COMPUTED STRESSES

STRAIN METERS M-17 AND M-18

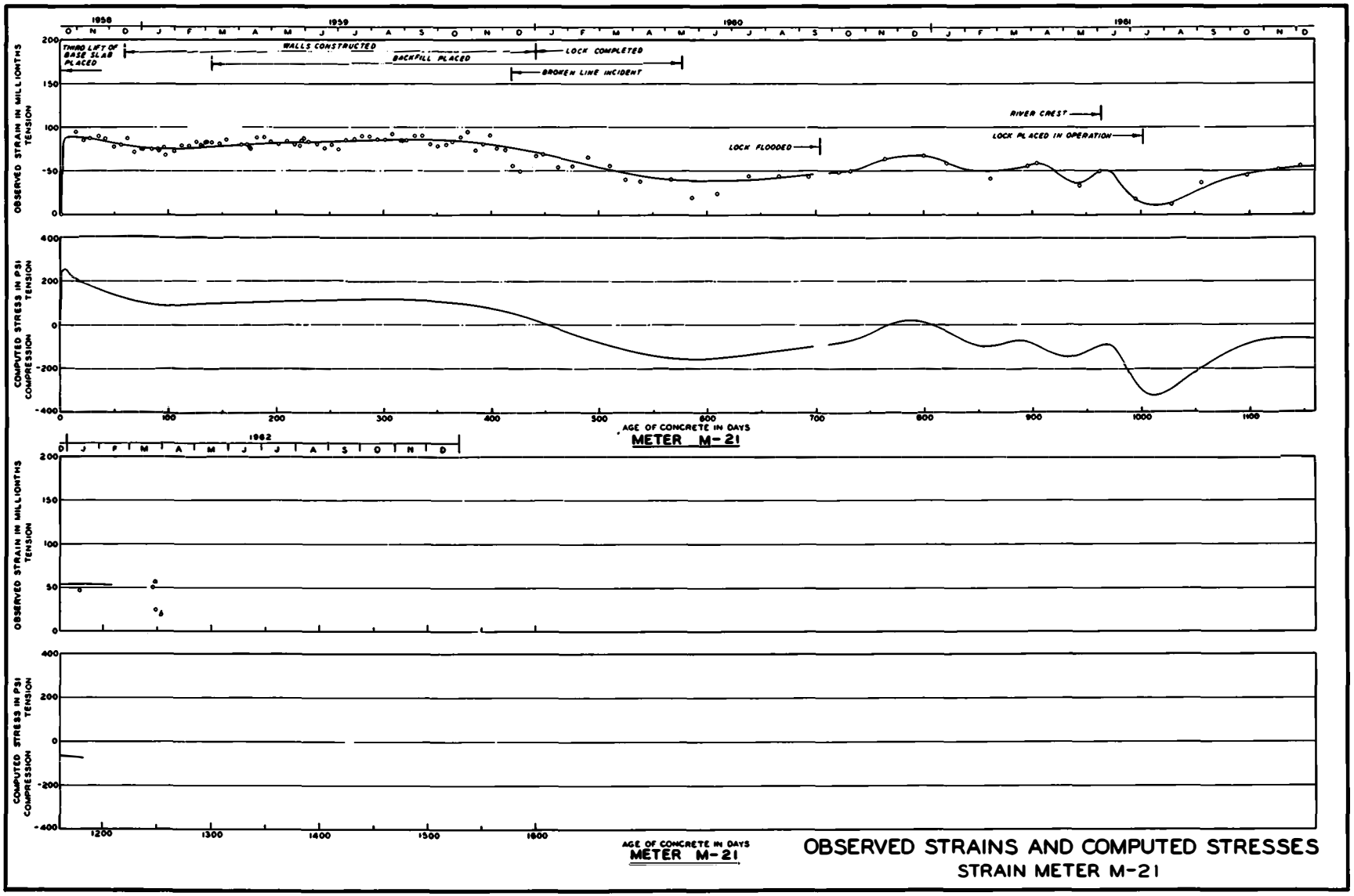

OBSERVED STRAINS AND COMPUTED STRESSES
STRAIN METER M-21

PLATE 47

PLATE 48

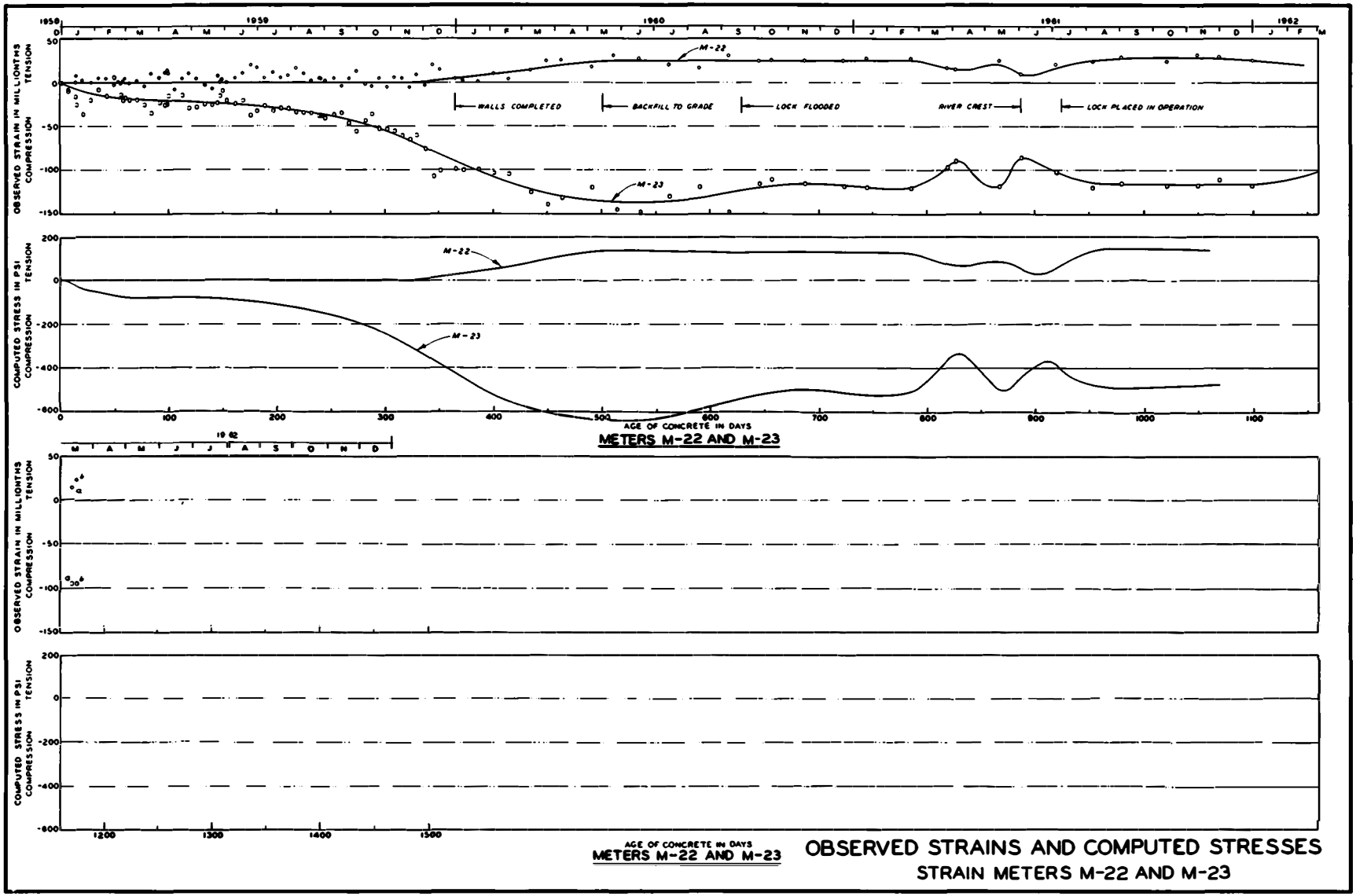

OBSERVED STRAINS AND COMPUTED STRESSES

STRAIN METERS M-22 AND M-23

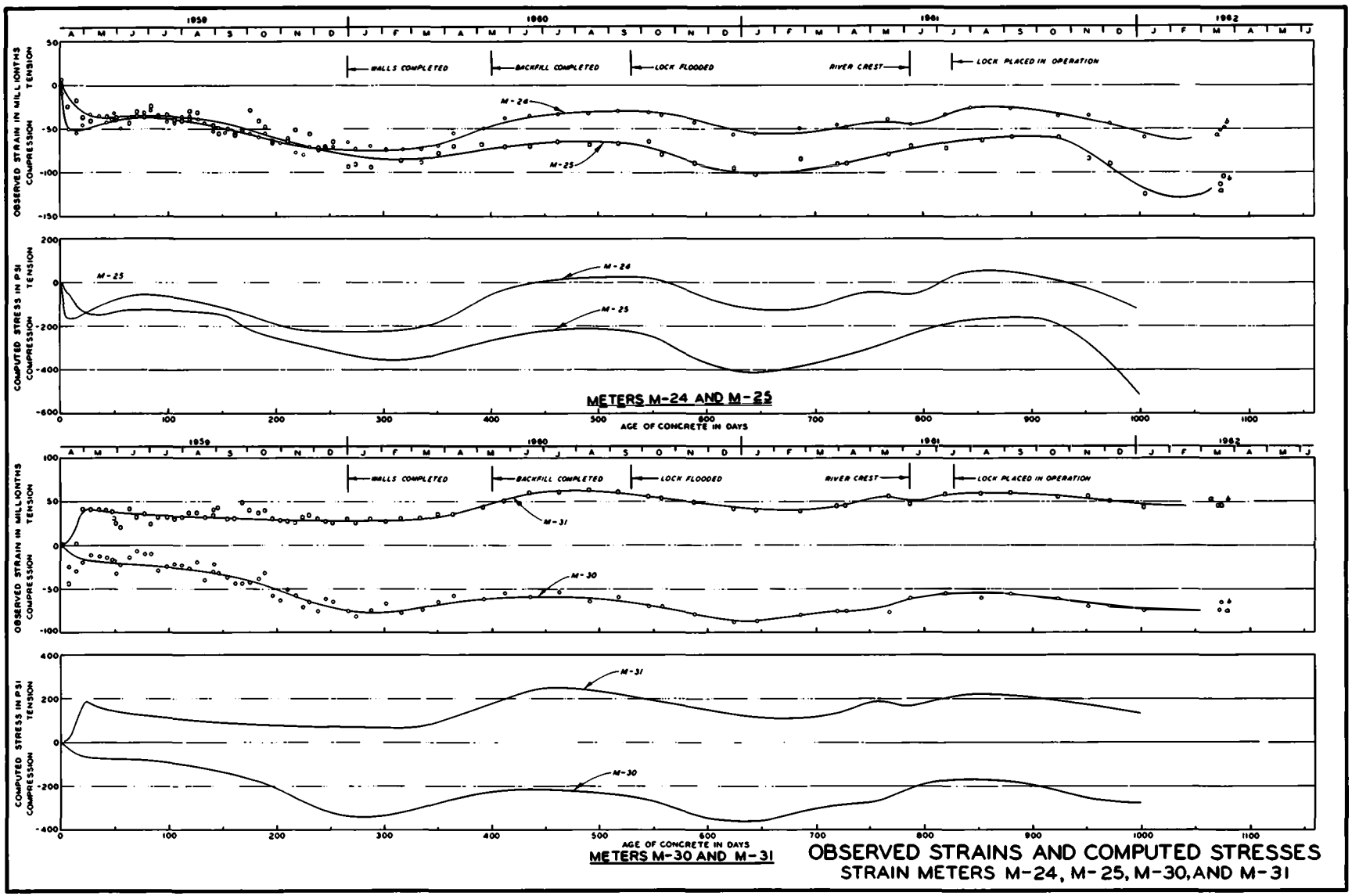

OBSERVED STRAINS AND COMPUTED STRESSES
STRAIN METERS M-24, M-25, M-30, AND M-31

PLATE 49

PLATE 50

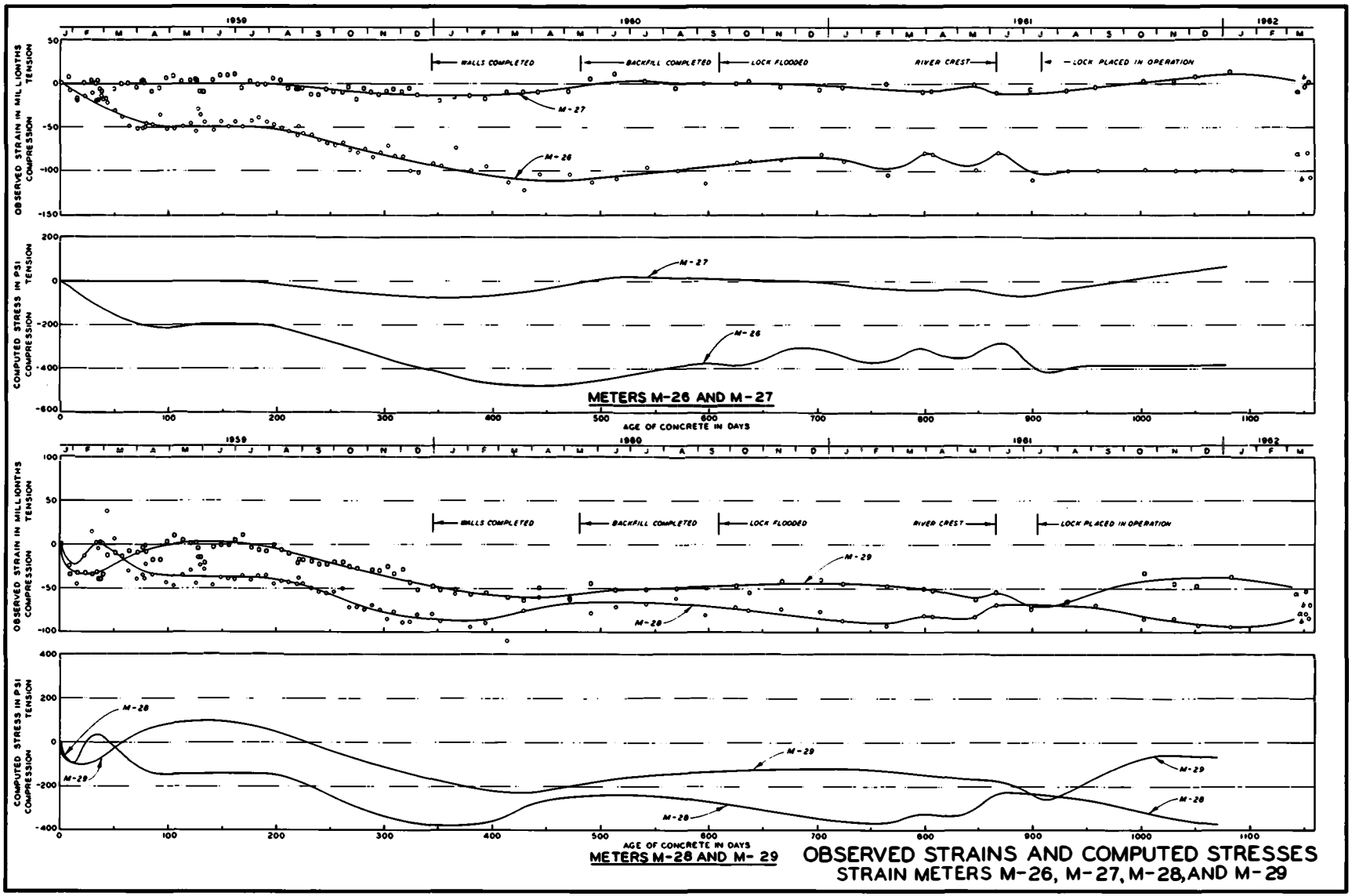

OBSERVED STRAINS AND COMPUTED STRESSES
STRAIN METERS M-26, M-27, M-28, AND M-29

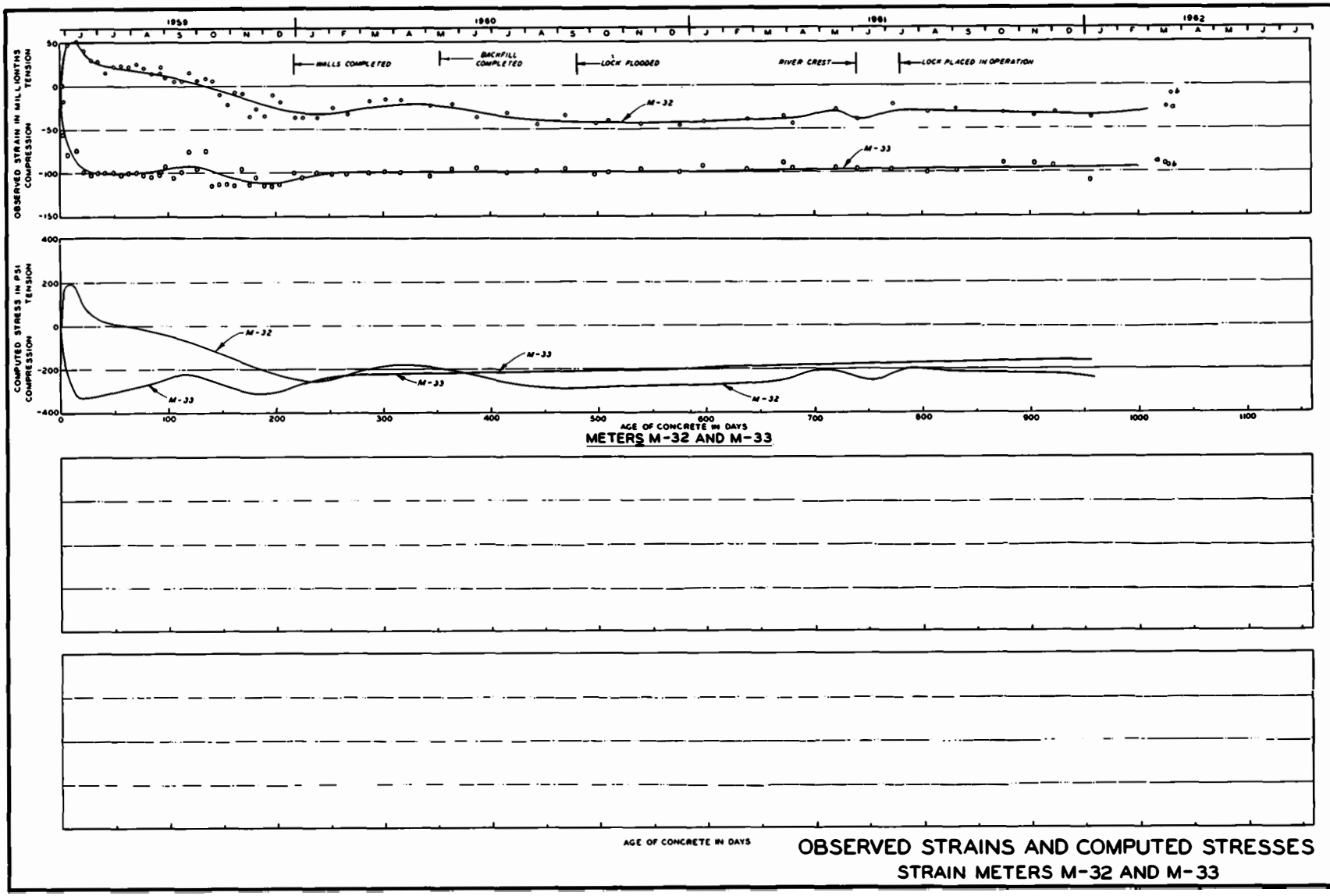

OBSERVED STRAINS AND COMPUTED STRESSES
STRAIN METERS M-32 AND M-33

PLATE 51

PLATE 52

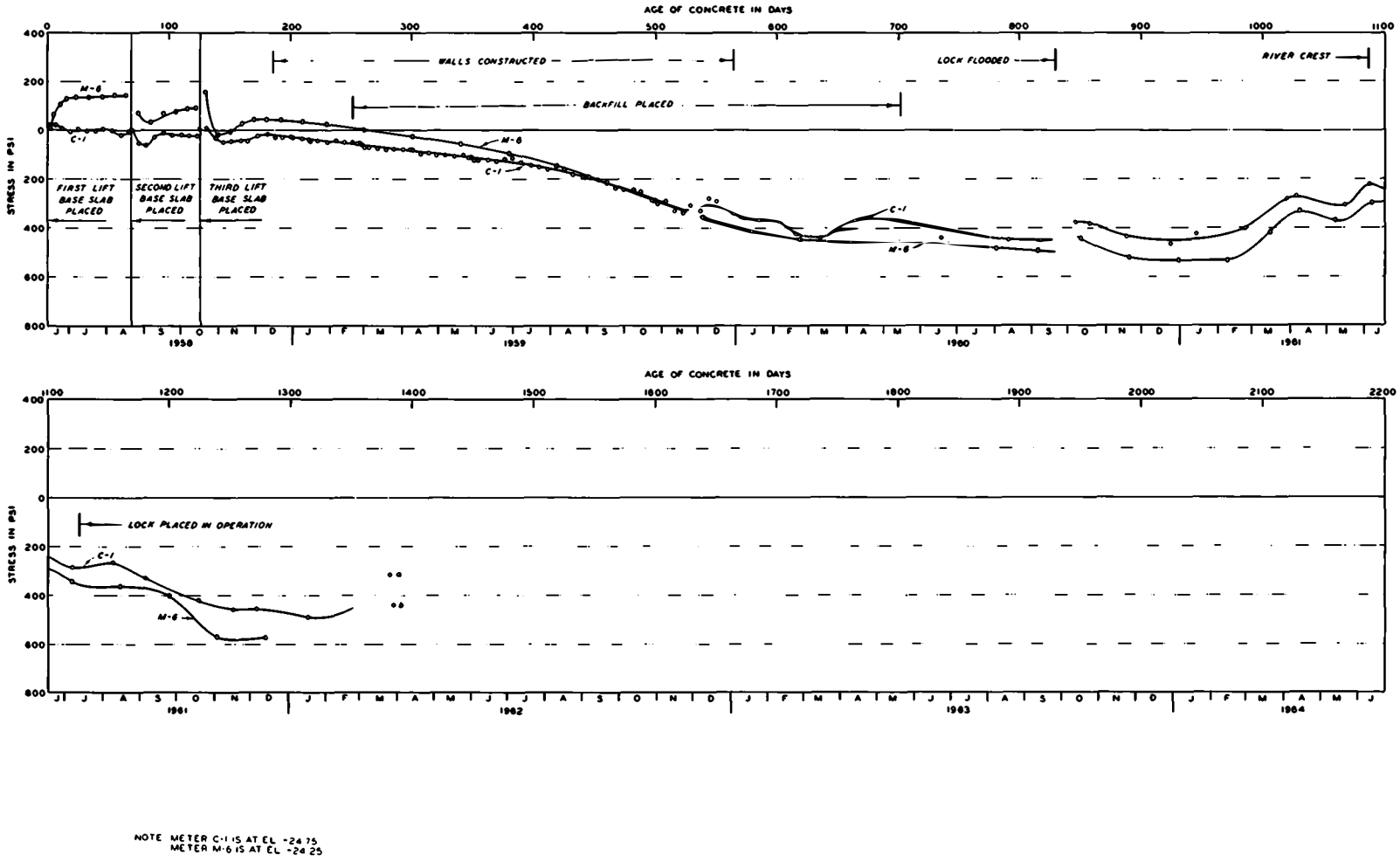

NOTE METER C-1 IS AT EL -24.75
METER M-6 IS AT EL -24.25

OBSERVED STRESSES
CONCRETE STRESS METER C-1,
AND COMPUTED STRESSES

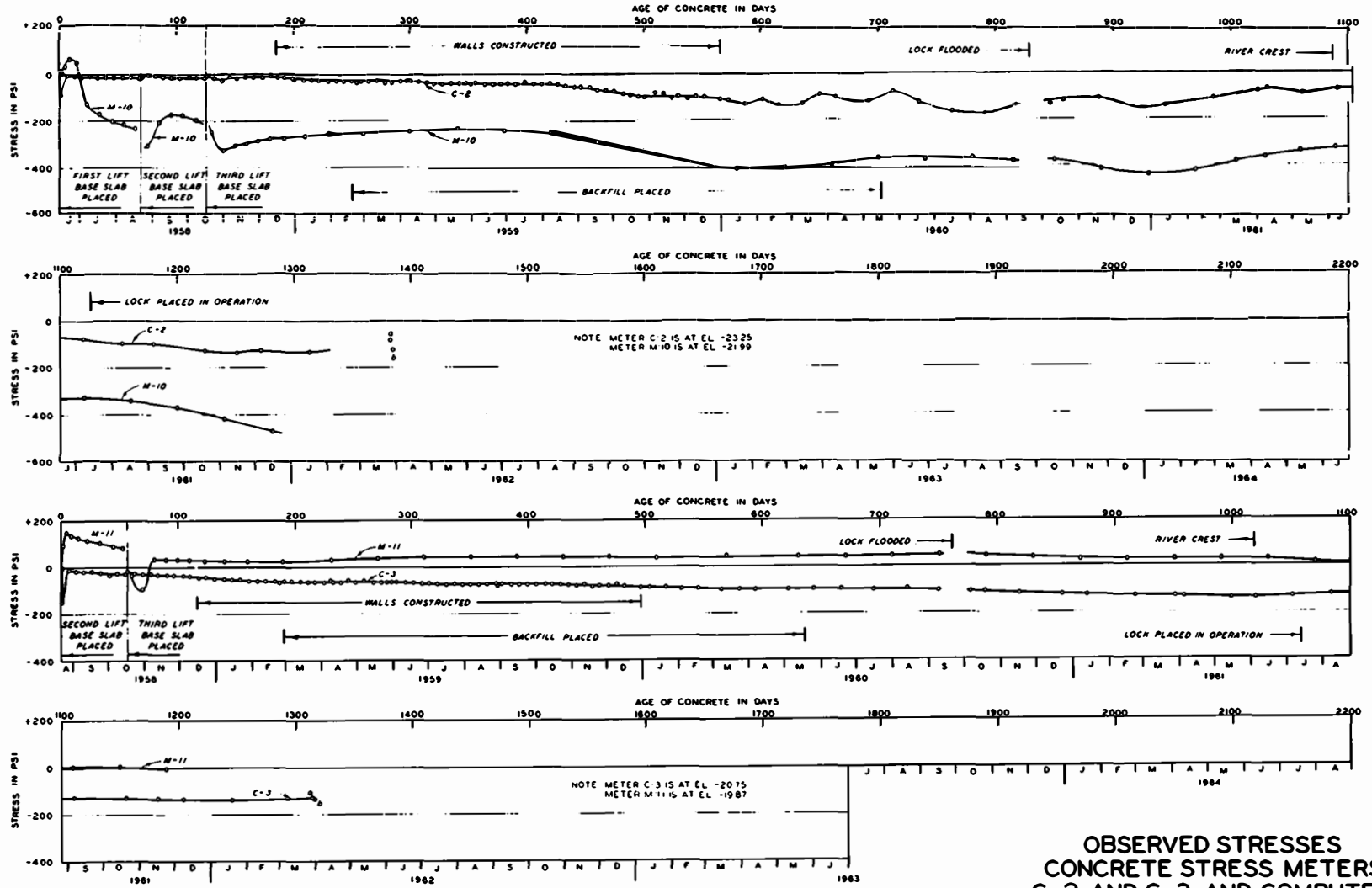

OBSERVED STRESSES CONCRETE STRESS METERS C-2 AND C-3, AND COMPUTED STRESSES

PLATE 53

PLATE 54

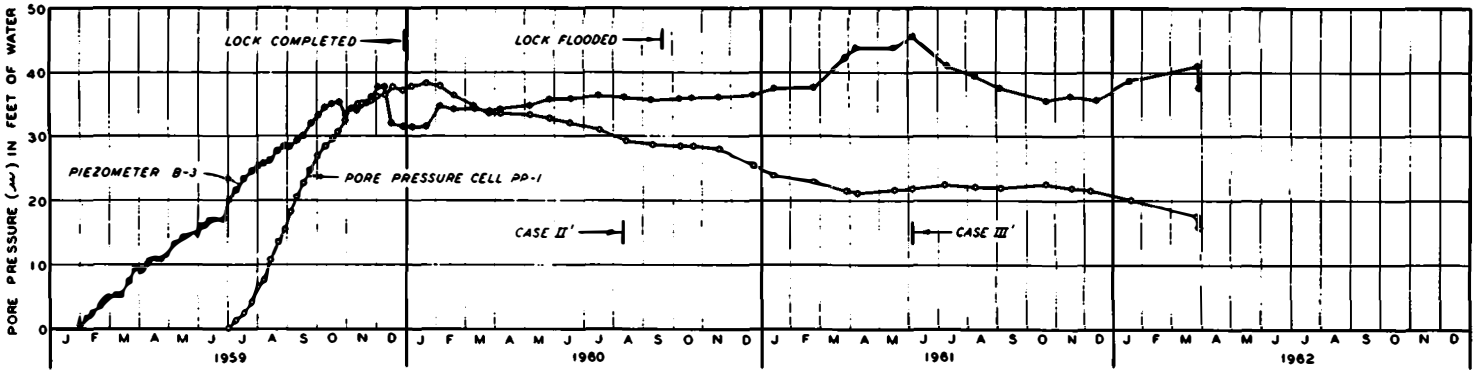

PORE PRESSURES IN AND BENEATH BASE SLAB VS TIME

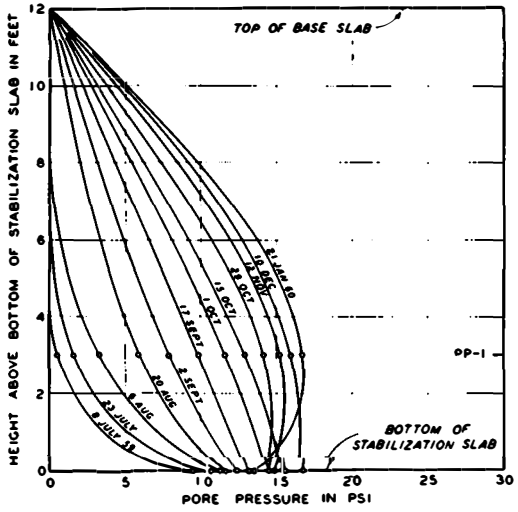

ESTIMATED DISTRIBUTION OF PORE PRESSURES WITHIN BASE SLAB FROM JULY 1959 TO JAN 1960

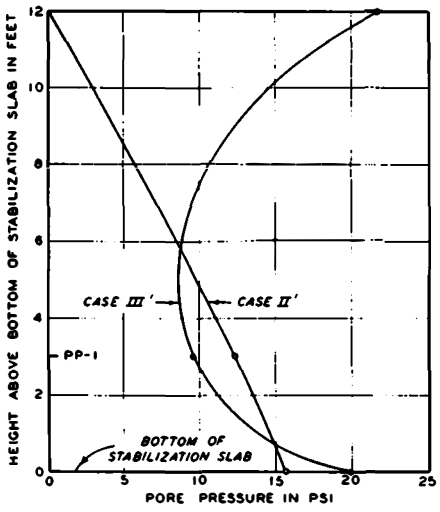

ESTIMATED DISTRIBUTION OF PORE PRESSURES FOR CASE II' AND CASE III'

DATA FROM PORE PRESSURE CELL PP-1

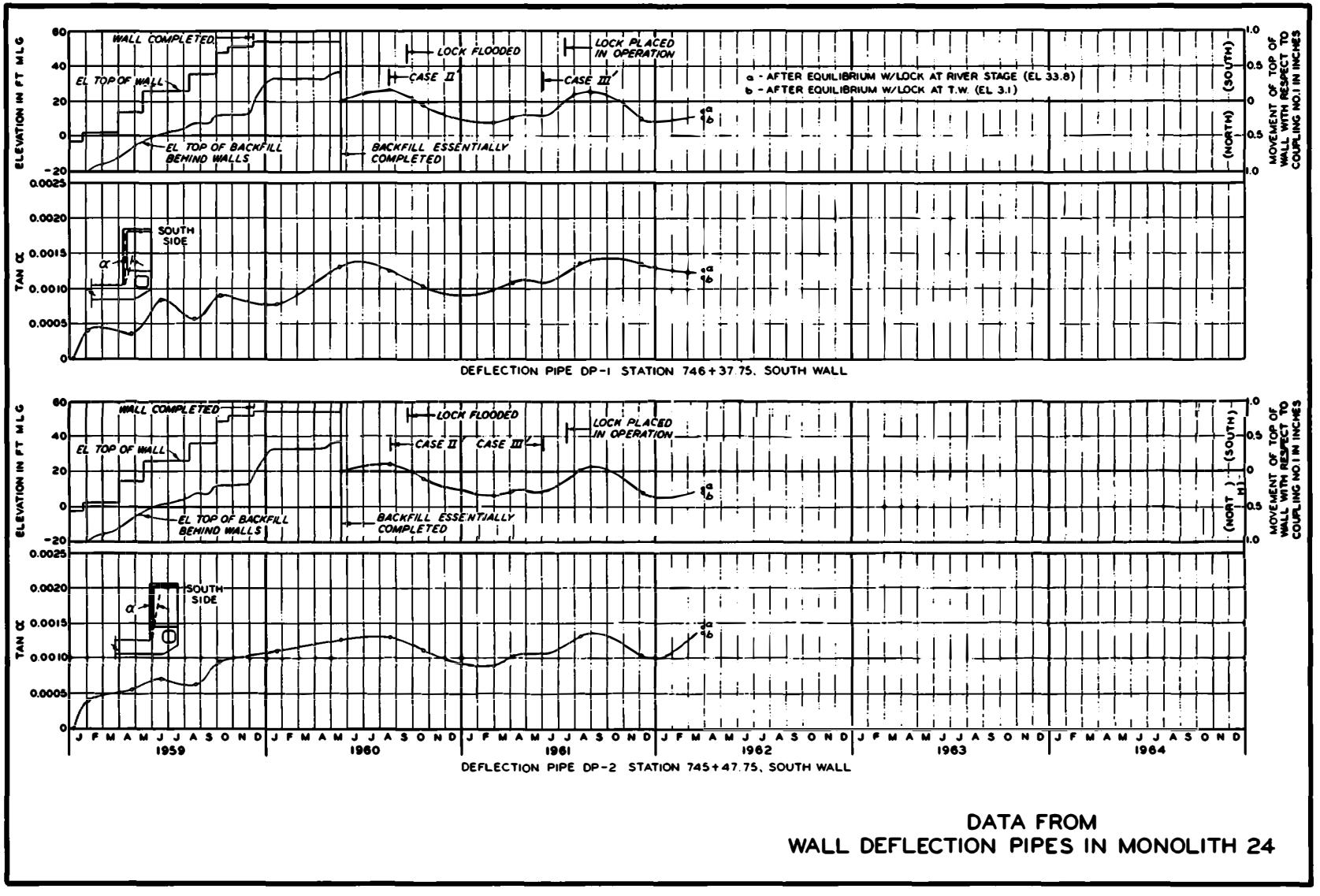

DATA FROM
WALL DEFLECTION PIPES IN MONOLITH 24

PLATE 55

PLATE 56

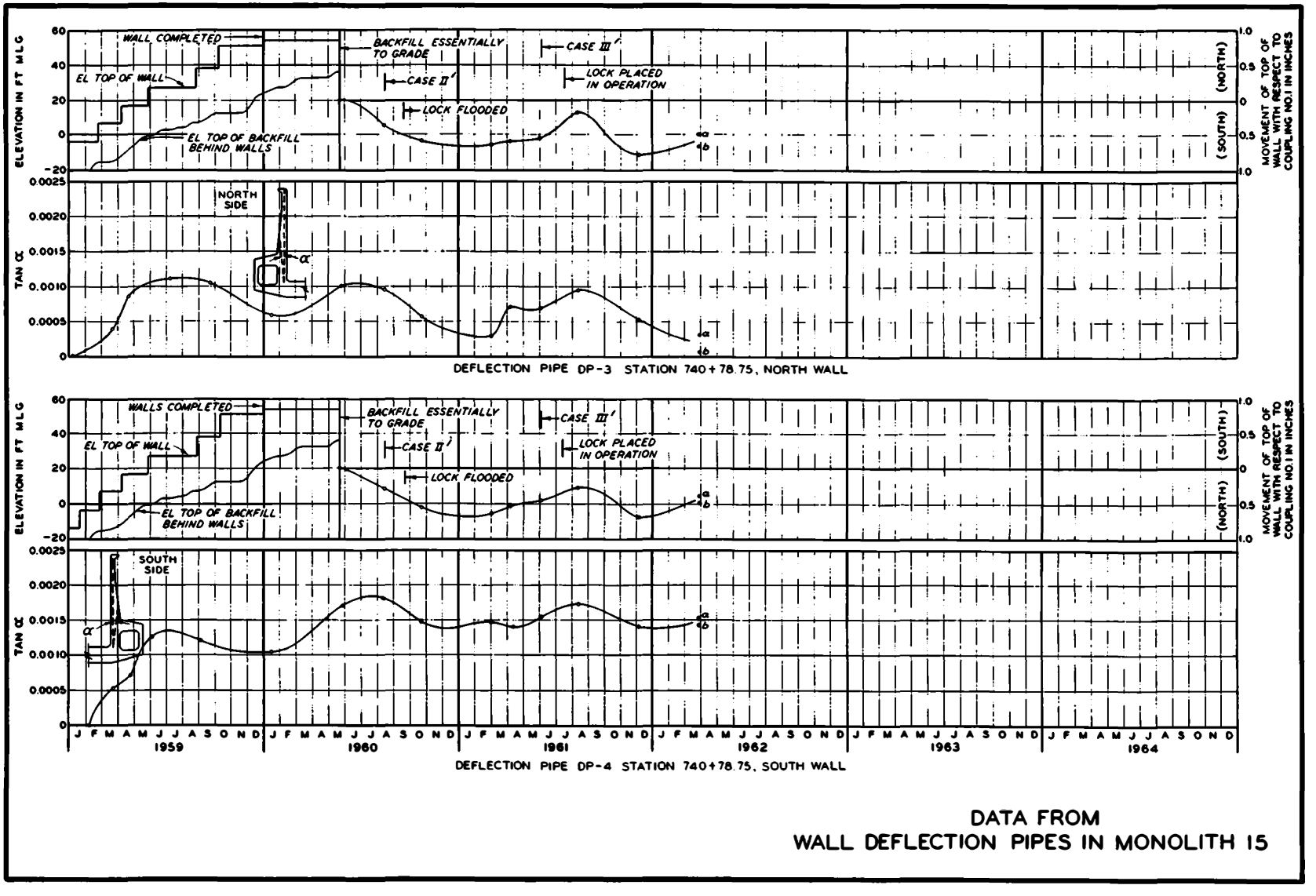

DATA FROM
WALL DEFLECTION PIPES IN MONOLITH 15

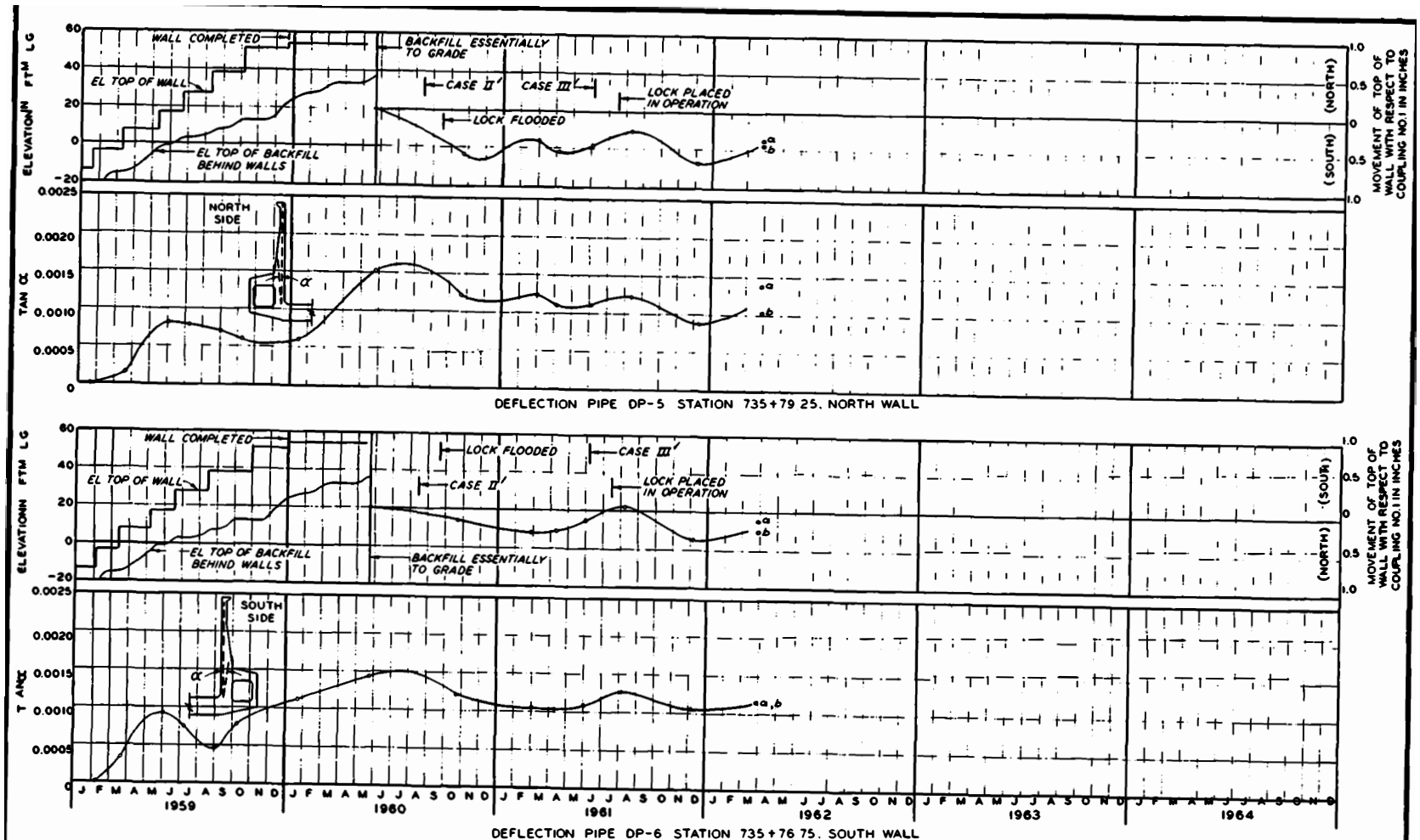

DATA FROM
WALL DEFLECTION PIPES IN MONOLITH 6

PLATE 57

PLATE 58

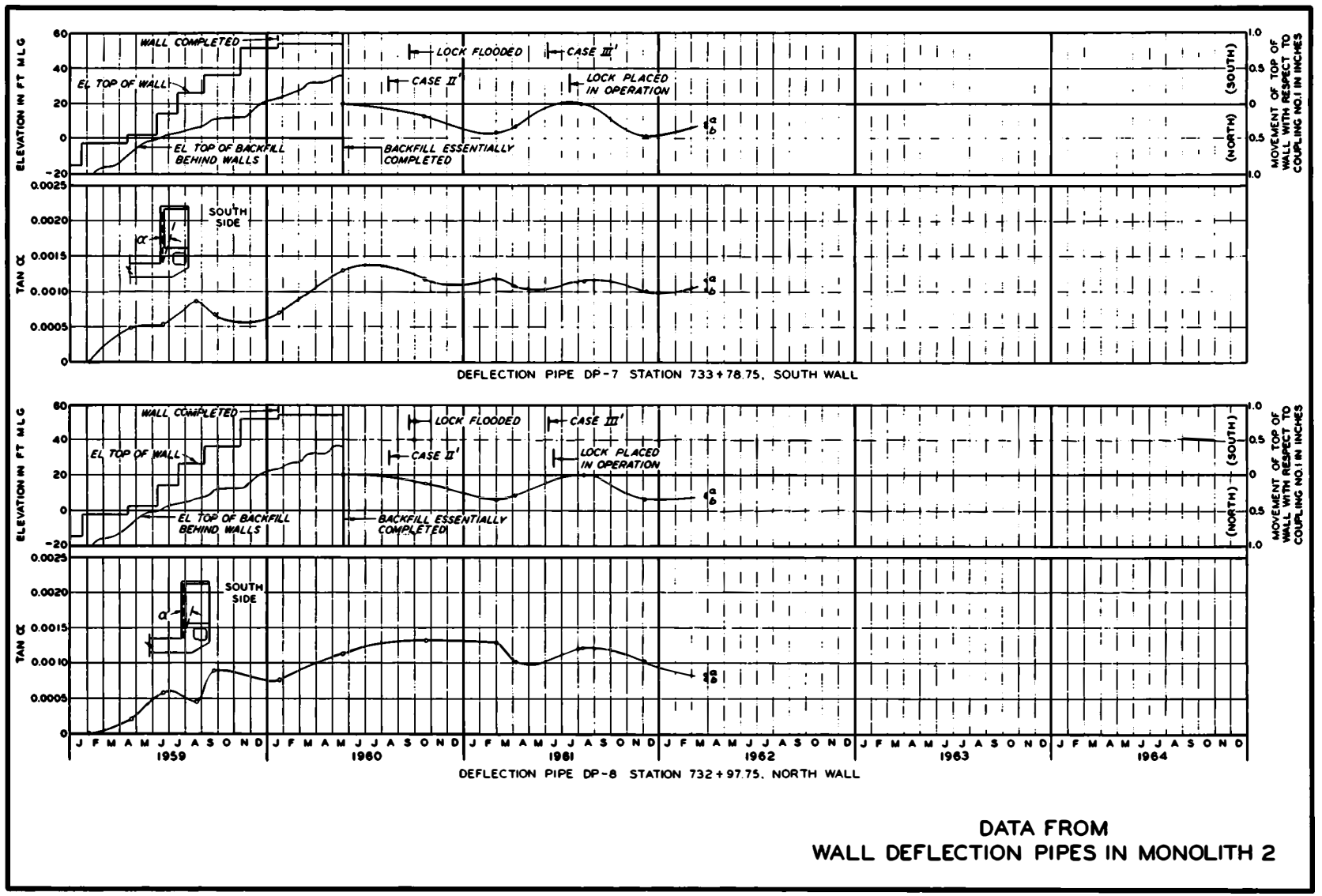

DATA FROM
WALL DEFLECTION PIPES IN MONOLITH 2

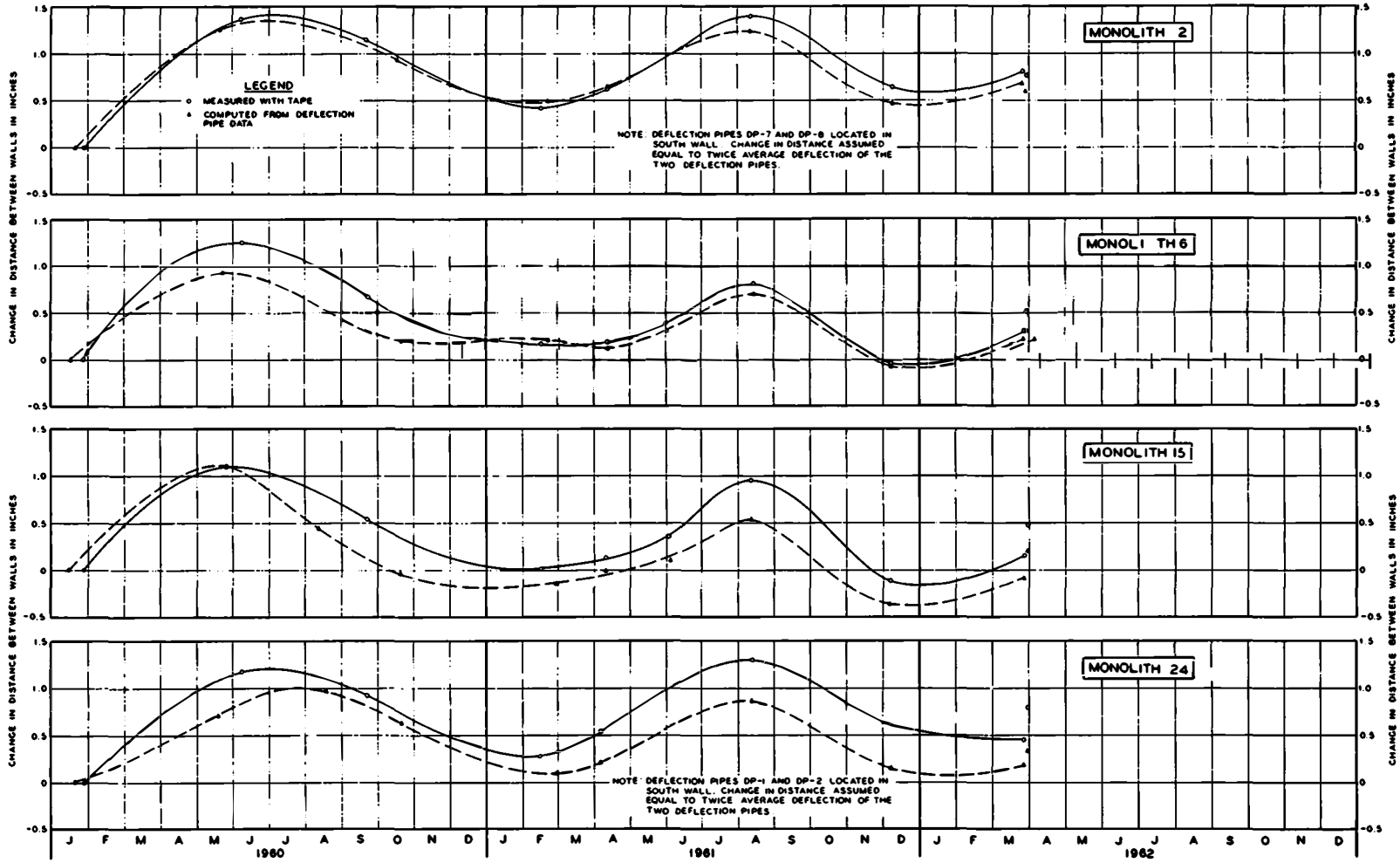

CHANGE IN DISTANCE BETWEEN WALLS VS TIME

PLATE 59

PLATE 60

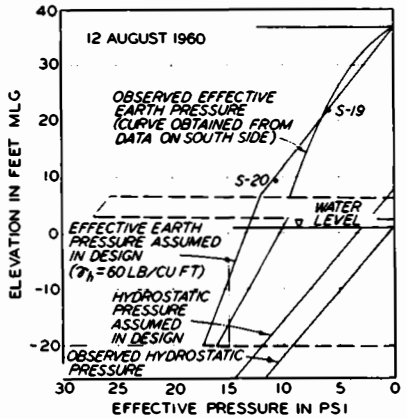

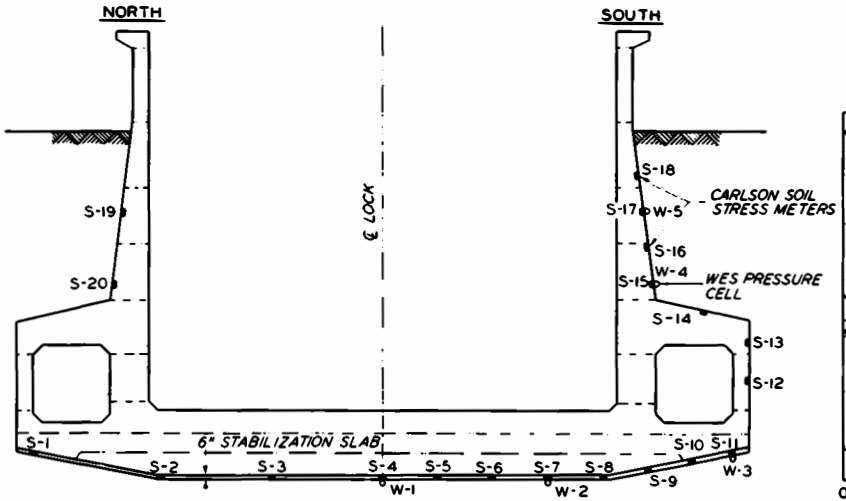

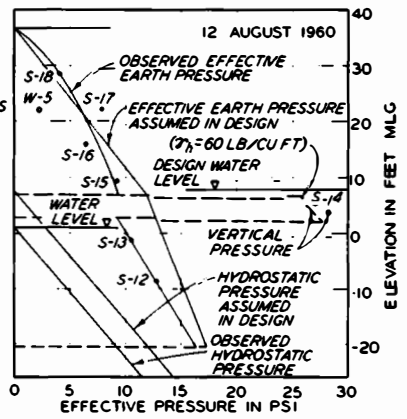

NOTE W-4 IS INOPERATIVE

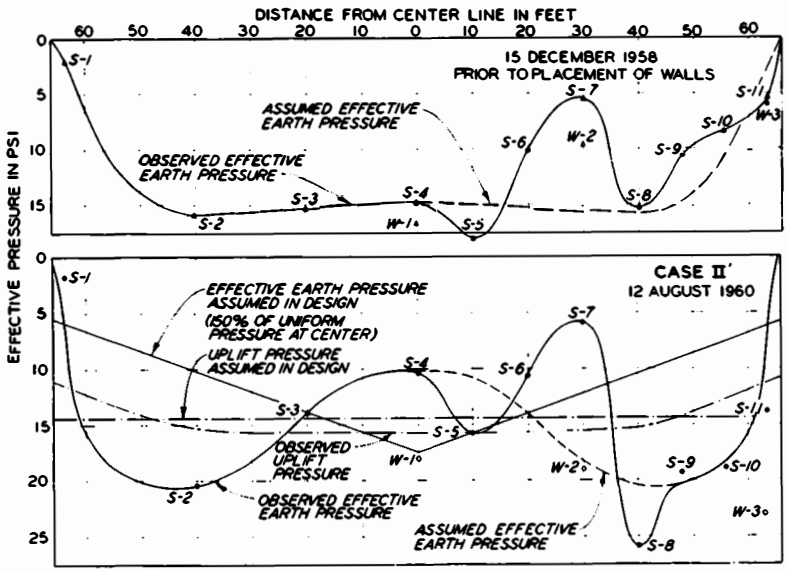

CASE II LOADING CONDITIONS

LOCK COMPLETED
BACKFILL IN PLACE
NO WATER IN LOCK

EFFECTIVE EARTH PRESSURES

MONOLITH 15 PRIOR TO PLACING WALLS AND CASE II'

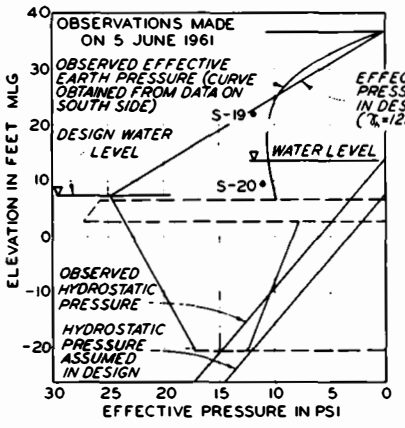

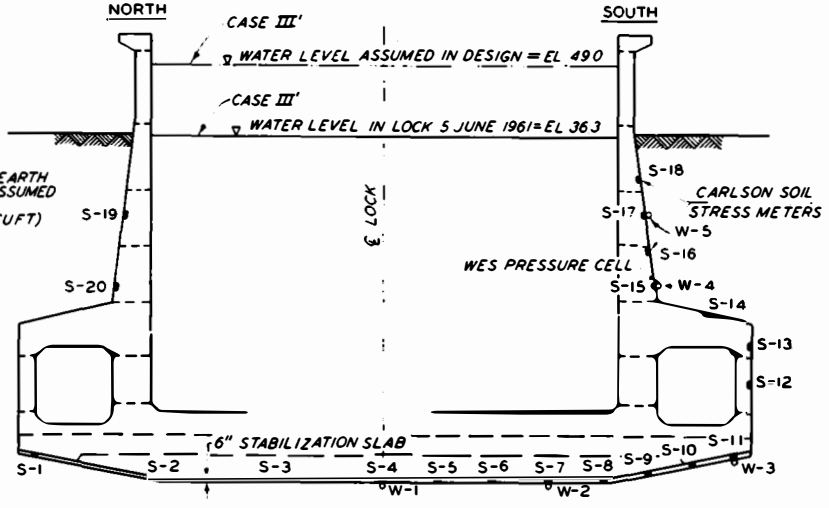

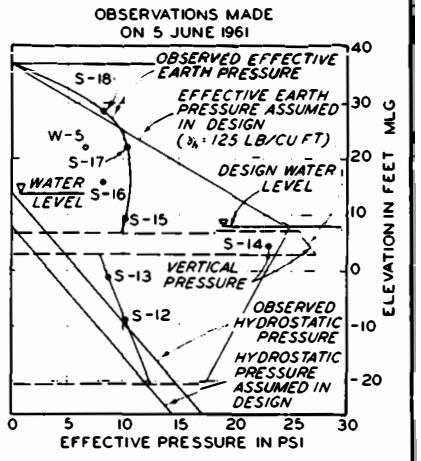

NOTE: W-4 IS INOPERATIVE

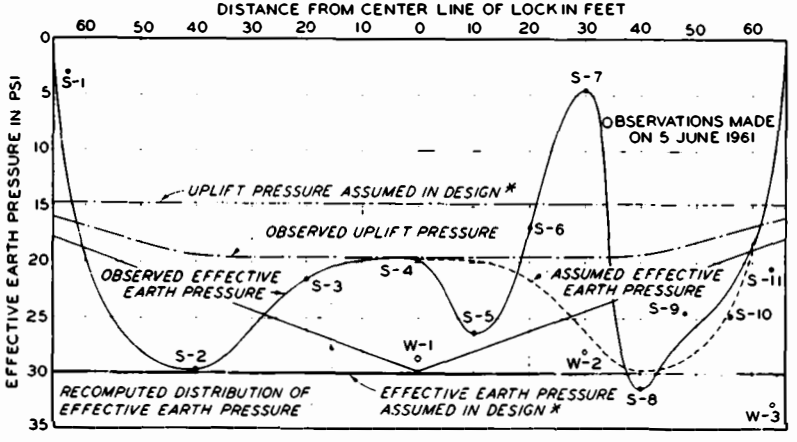

* DESIGN VALUES SHOWN FOR CASE III LOADING IN FIG 7

CASE III LOADING CONDITIONS

LOCK COMPLETED
BACKFILL IN PLACE
MAXIMUM WATER LEVEL IN LOCK = EL 490

EFFECTIVE EARTH PRESSURES

MONOLITH 15, CASE III'

PLATE 61

PLATE 62

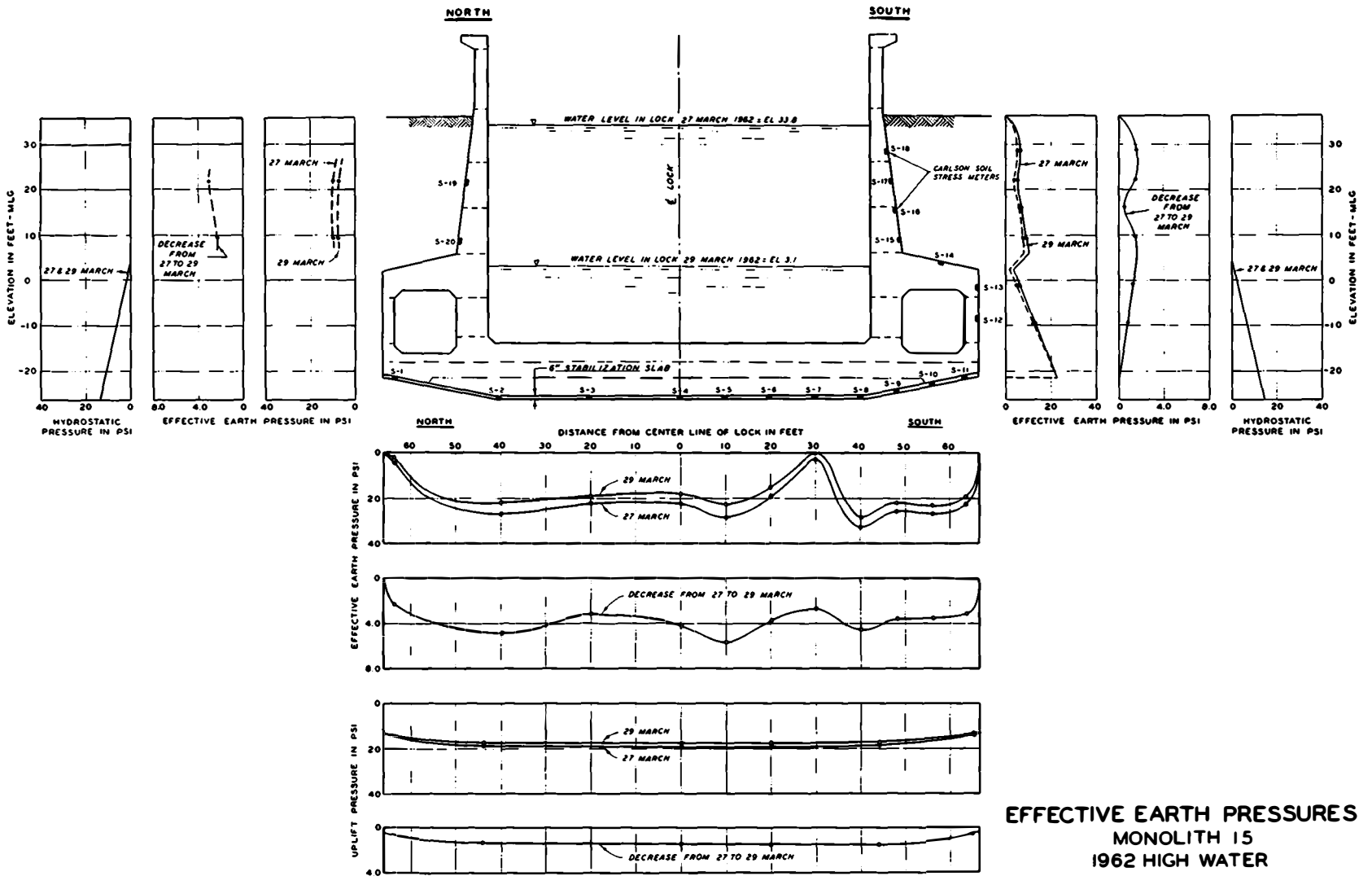

EFFECTIVE EARTH PRESSURES
MONOLITH 15
1962 HIGH WATER

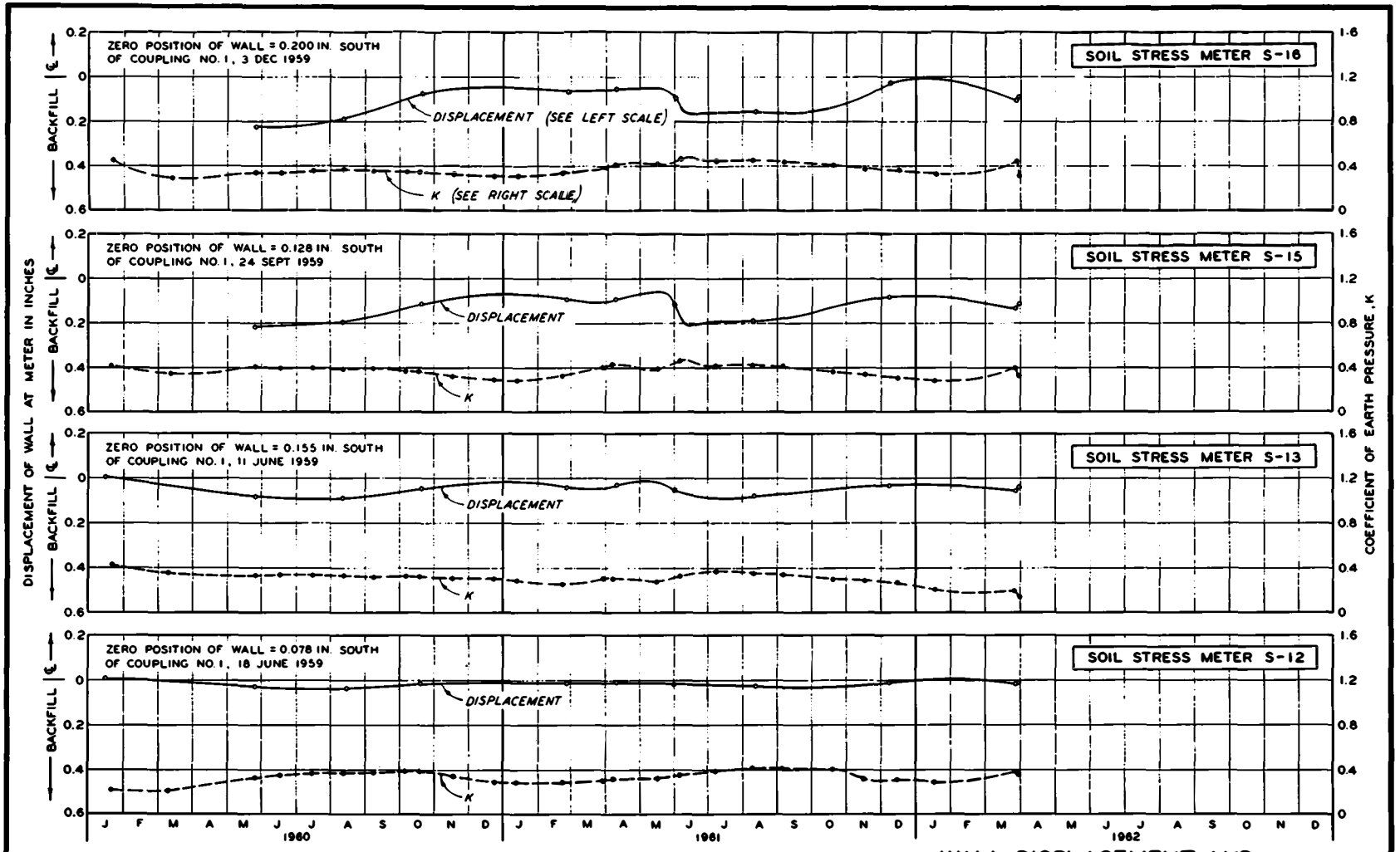

NOTE : ZERO DISPLACEMENT BASED ON POSITION OF WALL AT TIME TOP OF BACKFILL REACHED ELEVATION OF METER

WALL DISPLACEMENT AND COEFFICIENT OF EARTH PRESSURE VS TIME

METERS S-12, S-13, S-15, AND S-16

PLATE 63

PLATE 64

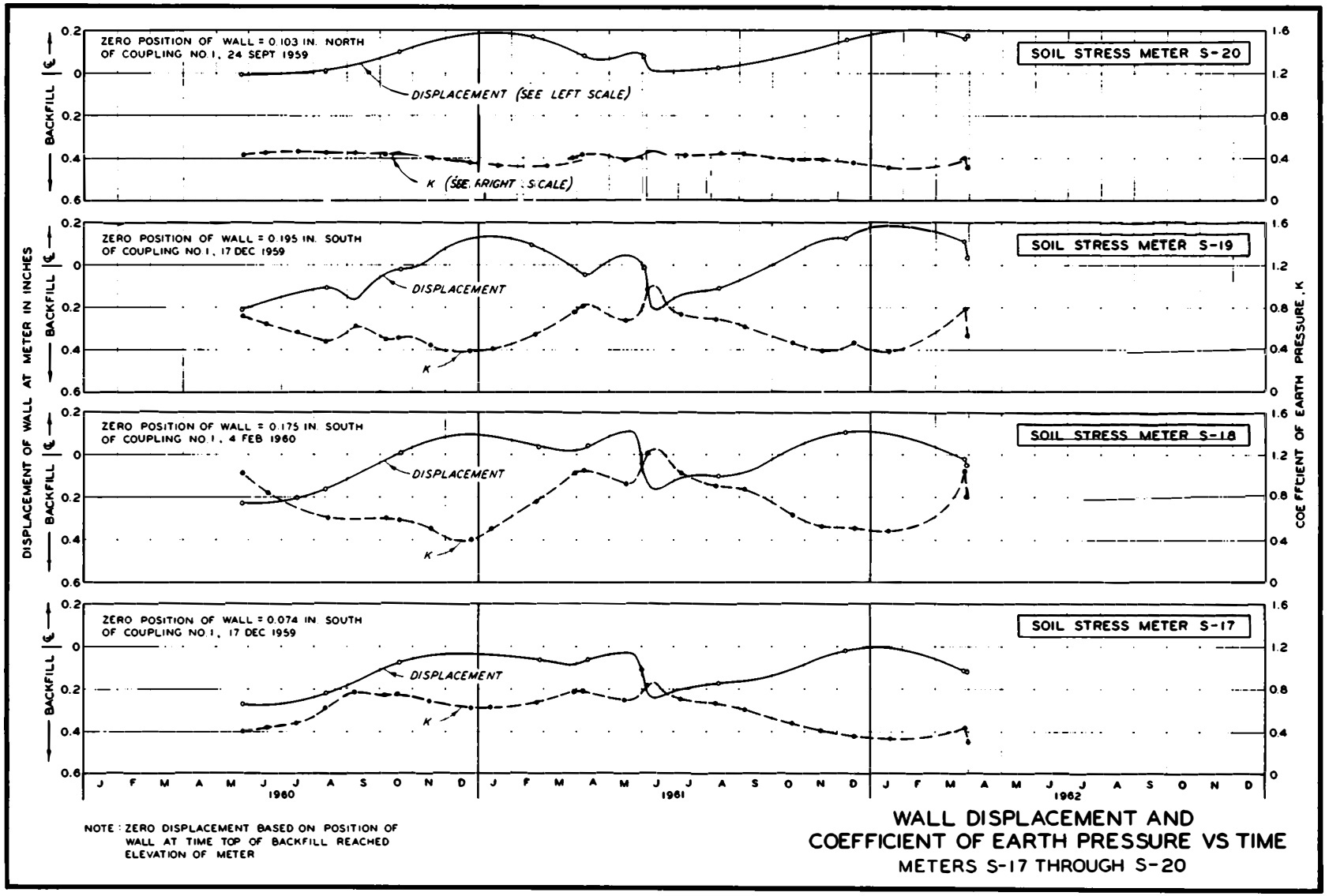

NOTE: ZERO DISPLACEMENT BASED ON POSITION OF WALL AT TIME TOP OF BACKFILL REACHED ELEVATION OF METER

WALL DISPLACEMENT AND COEFFICIENT OF EARTH PRESSURE VS TIME

METERS S-17 THROUGH S-20

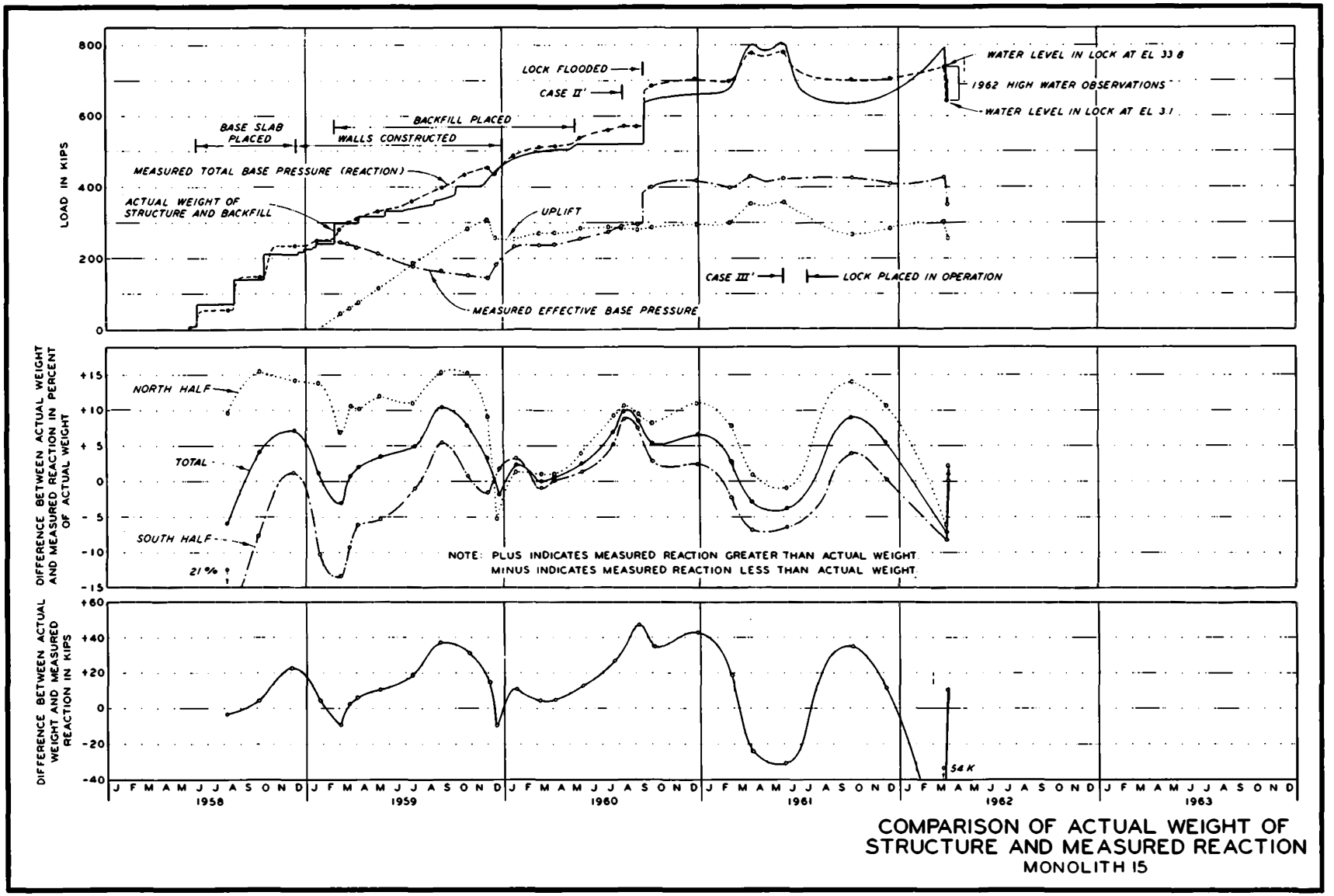

COMPARISON OF ACTUAL WEIGHT OF STRUCTURE AND MEASURED REACTION

MONOLITH 15

PLATE 65

PLATE 66

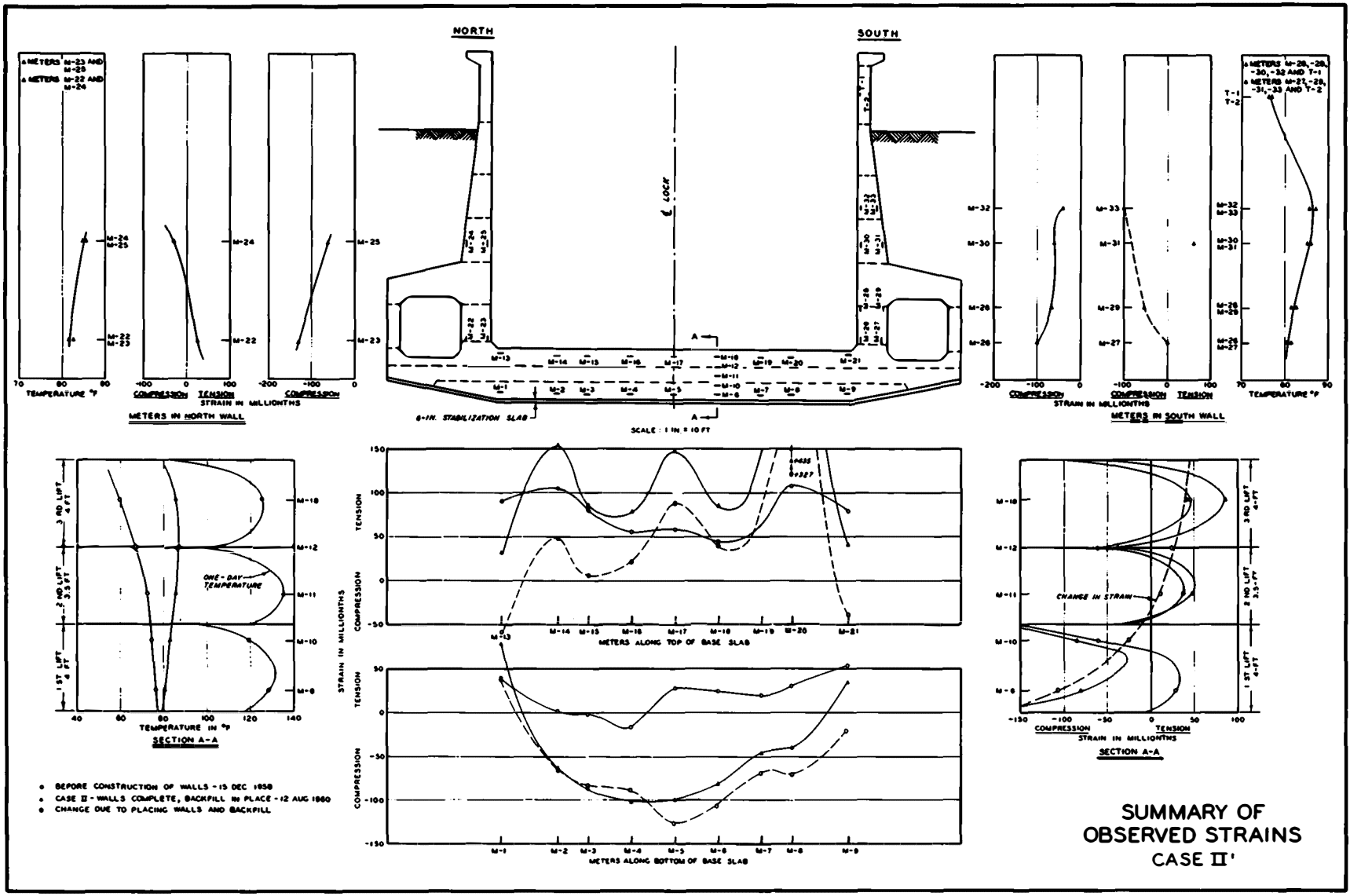

SUMMARY OF OBSERVED STRAINS
CASE II'

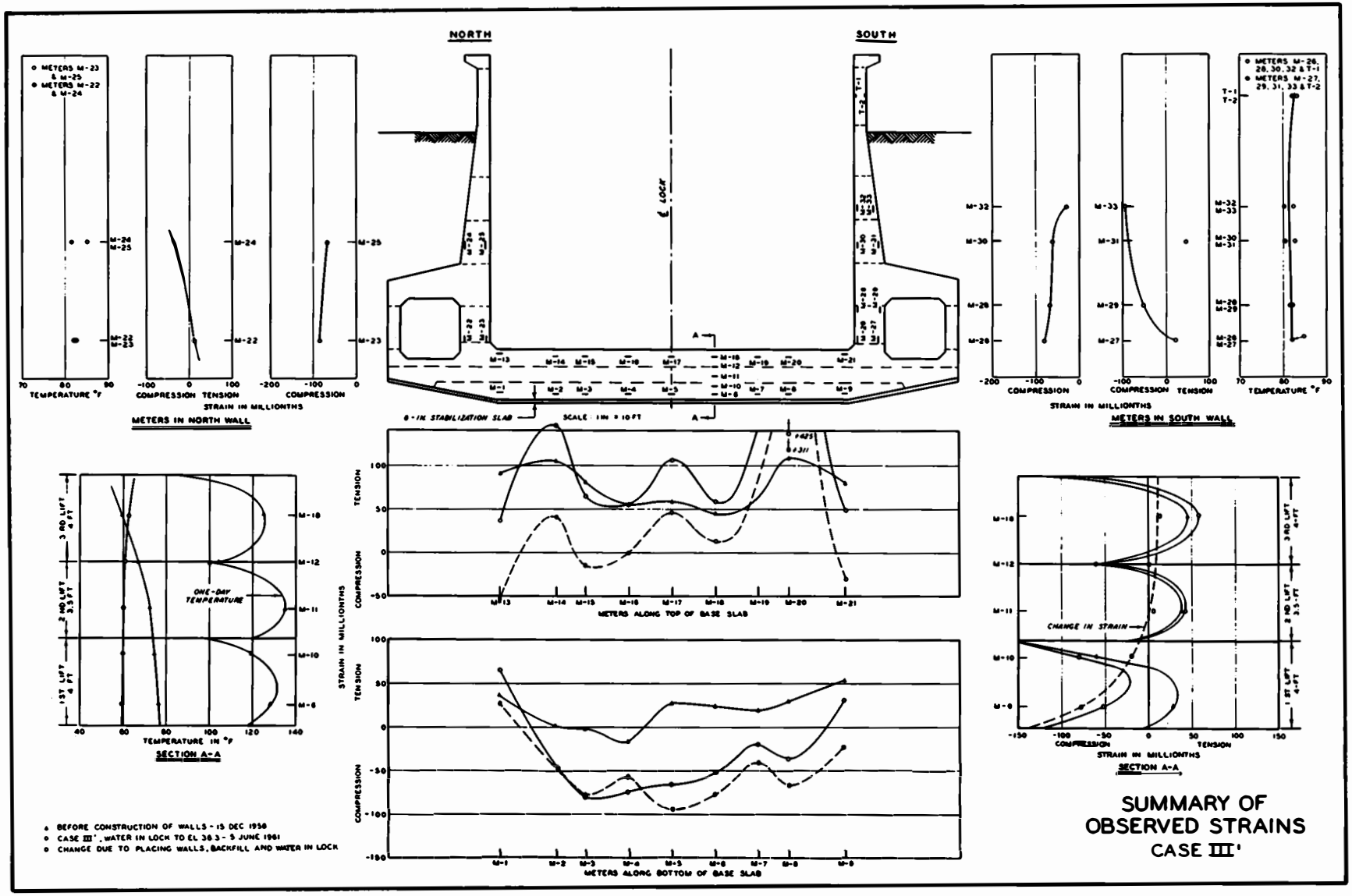

SUMMARY OF OBSERVED STRAINS
CASE III'

PLATE 67

PLATE 68

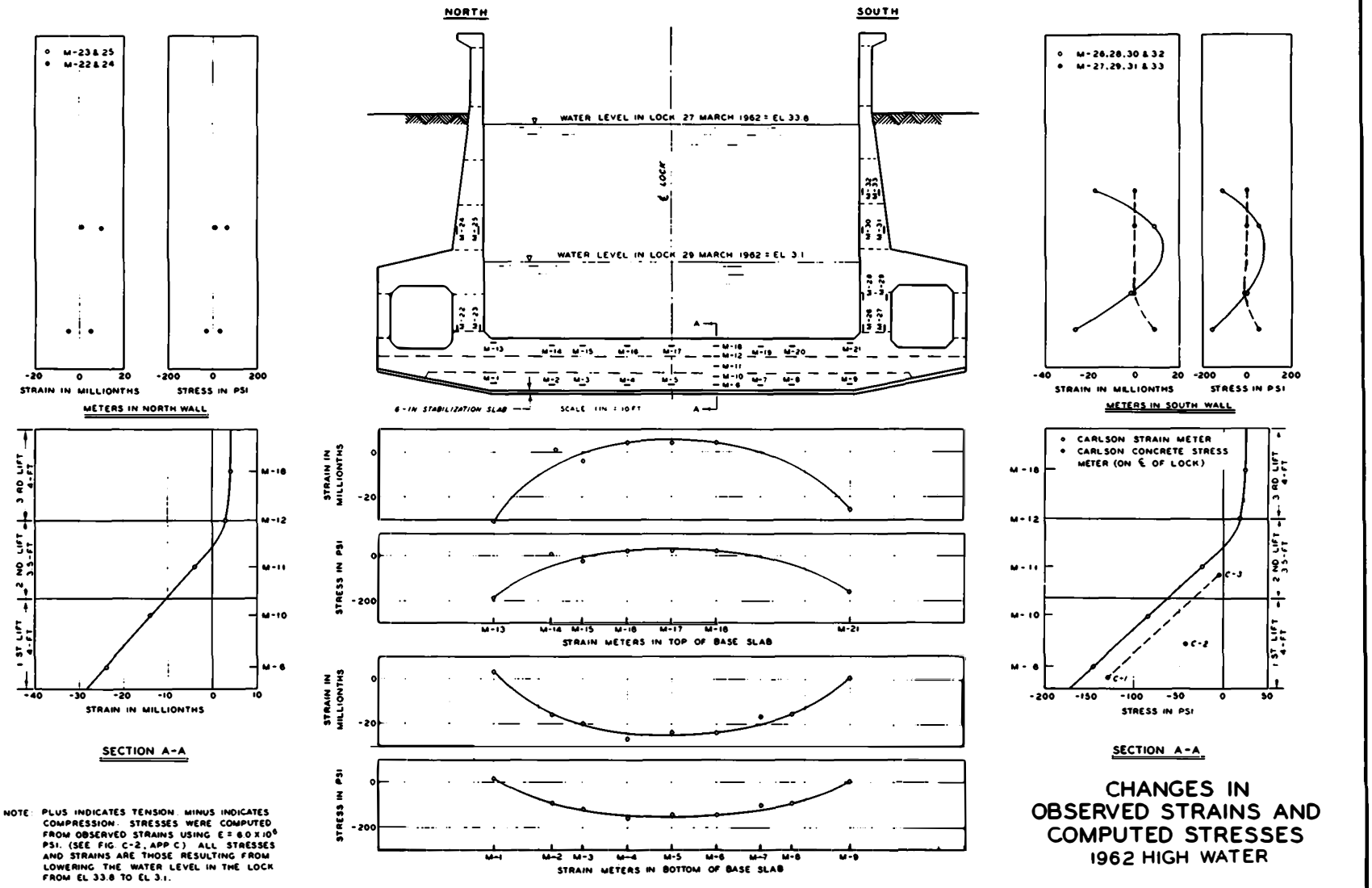

NOTE: PLUS INDICATES TENSION. MINUS INDICATES COMPRESSION. STRESSES WERE COMPUTED FROM OBSERVED STRAINS USING $E = 6.0 \times 10^6$ PSI. (SEE FIG C-2, APP C) ALL STRESSES AND STRAINS ARE THOSE RESULTING FROM LOWERING THE WATER LEVEL IN THE LOCK FROM EL 33.8 TO EL 3.1.

CHANGES IN OBSERVED STRAINS AND COMPUTED STRESSES
1962 HIGH WATER

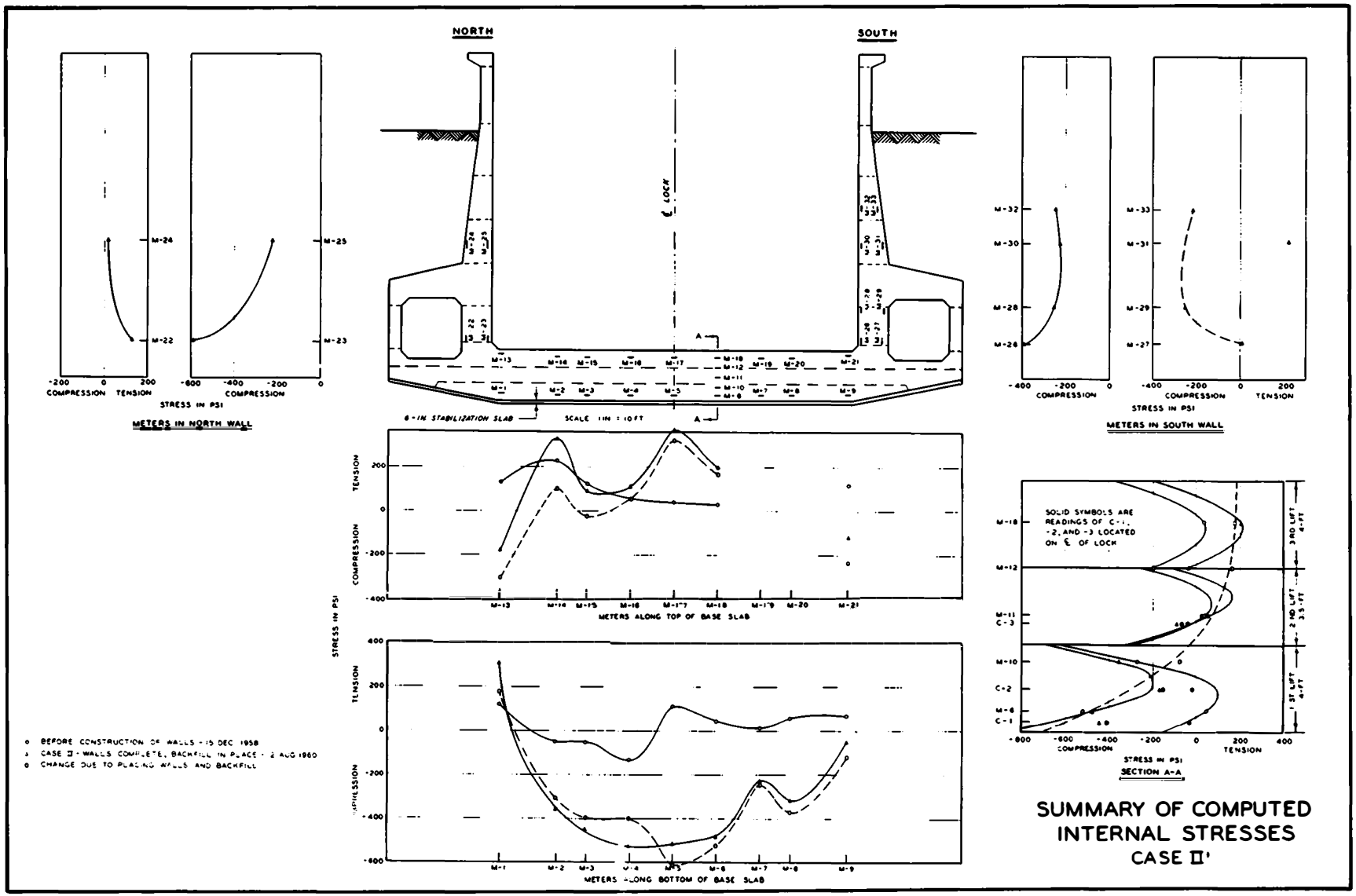

SUMMARY OF COMPUTED INTERNAL STRESSES CASE II'

PLATE 69

PLATE 70

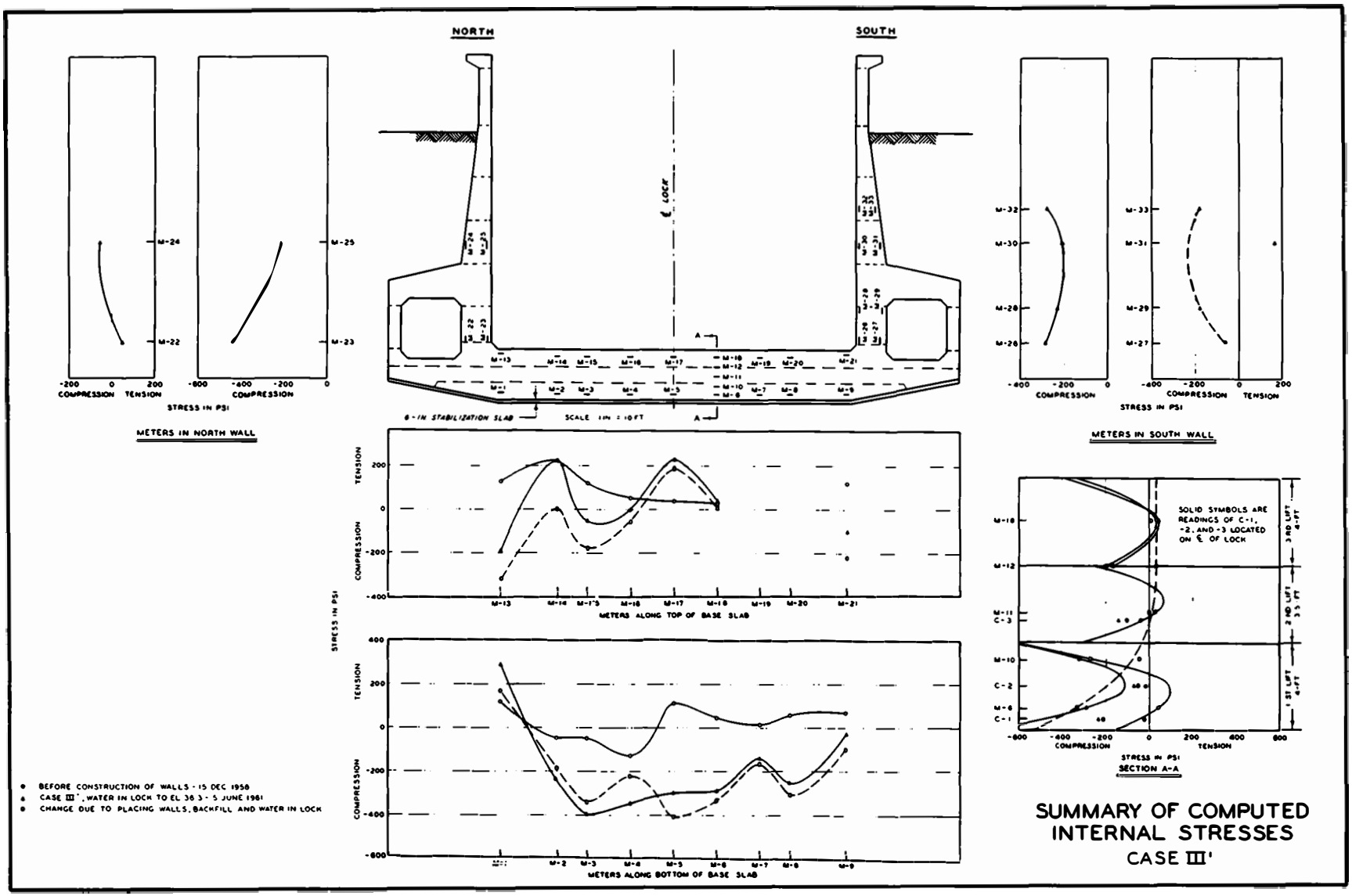

SUMMARY OF COMPUTED INTERNAL STRESSES

CASE III'

APPENDIX A: DESCRIPTION, CALIB RATION,AND INSTAL LATI ON OF ELECTRICAL MEASURING DE VIES

Electrical Measuring Devices

1. Electrical measuring devices consisted of soil stress meters, concrete stress meters, strain meters, a pore pressure cell, and resistance thermometers obtained from Dr. R. W. Carlson, Berkeley, California, and WES pressure cells fabricated at WES. Calibration data for the various types of electrical measuring devices were furnished by Dr. Carlson. All devices were checked at WES for leakage, and additional calibration tests were performed on a number of the devices as an independent check, the results therefrom being compared with the original calibration data. Complete calibration tests were also performed on the WES pressure cells, and the results are presented herein.

2. Each of the Carlson electrical measuring devices had the required length of cable attached. All cable, including that used with the WES pressure cells, consisted of spiral-4 communications cable, having four No. 18 stranded conductors, a foil shield, neoprene jacket, and a steel basket-weave braid. This type of cable was used because of its ability to resist rough treatment. During construction and prior to connecting the cables to a terminal board, a protective housing was attached to the end of each cable.

Carlson soil stress meters

3. Carlson soil stress meters, series PE-50, which measure stresses to the nearest 0.2 psi within a range of 0 to 50 psi in compression, were used. Photographs of the Carlson soil stress meters are shown in fig. A1. A detailed description of the device is given in a previously published report.[18*]

4. The calibration data furnished for each meter are shown in table A1. These data were based on a procedure in which various loads

---

* Raised numbers refers to items listed in the Literature Cited at the end of the main text.

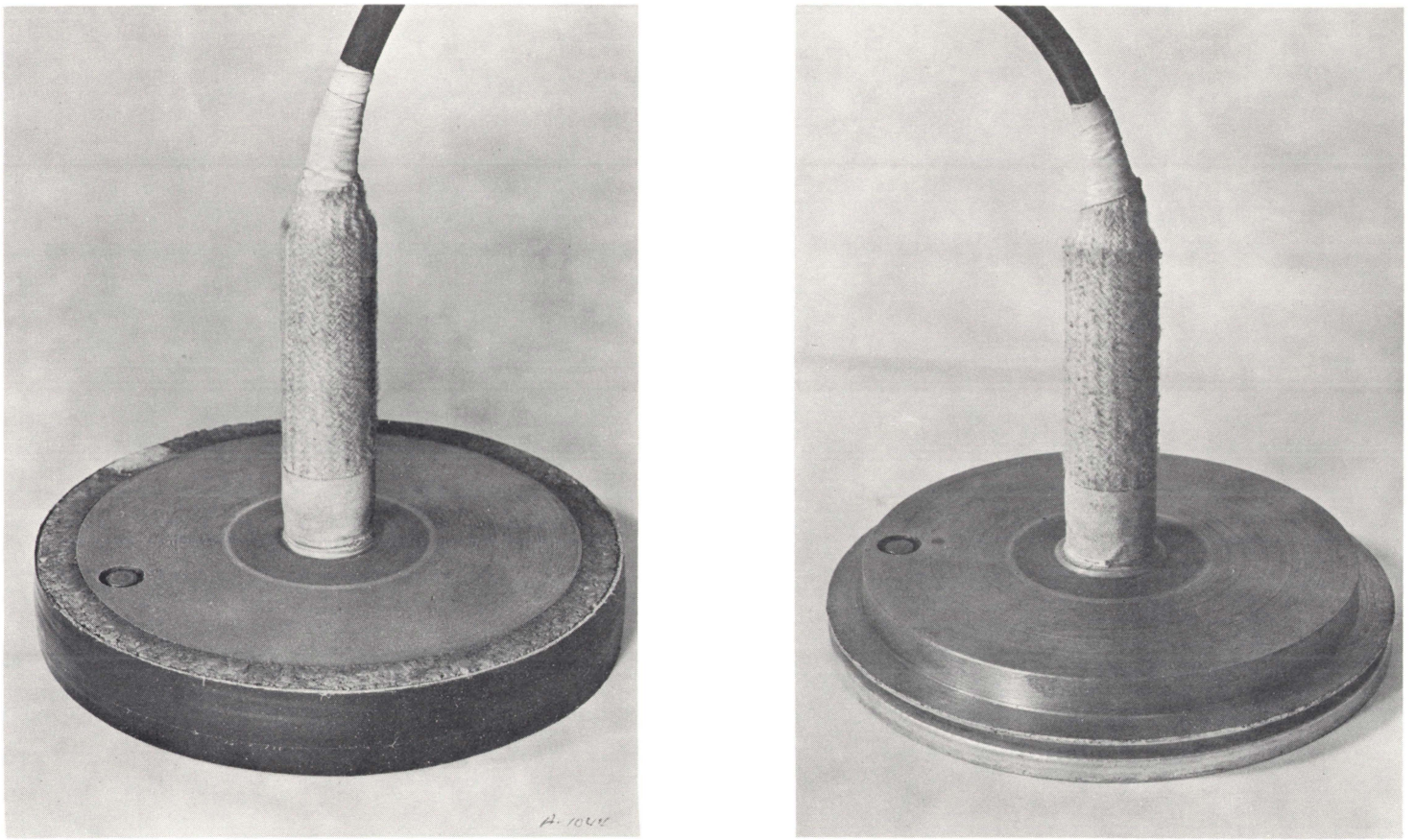

a. As installed

b. Cork and tape removed

Fig. A1. Carlson soil stress meter

were applied through a rigid plate over the effective area of the meter. However, it was believed that field loading conditions would be simulated more closely if the calibration loadings were applied as a uniform pressure through a flexible diaphragm. Consequently, all soil stress meters were calibrated at WES by means of diaphragm loading. The soil stress meters were further calibrated by means of hydrostatic pressure. The procedures used in the three types of load calibration are shown schematically in fig. A2. There is a difference between the diaphragm and hydrostatic loadings. In the diaphragm loading, the load is distributed uniformly over the entire faceplate, whereas in the hydrostatic pressure loading the load acting on the faceplate is partially balanced by reaction components existent in the peripheral slot. Direct loading through the diaphragm corresponds to loading in the field under total pressures (intergranular plus hydrostatic pressures). The hydrostatic pressure calibrations were performed to permit computation of intergranular pressures acting on the face of the meter.

5. Leakage tests and hydrostatic calibration. When received at WES, the meters were placed in a pressure tank and calibrated under hydrostatic pressure. The resistance ratio was generally determined at pressures of 0- and 17-psi air pressure, with the total resistance of the meter observed for each load. After it was established that the meter did not leak under air pressure, water was allowed to enter the pressure tank to immerse the meters and cable connections. The test was repeated to check the devices for cable-entry leaks and defective cables. The latter were indicated by low insulation resistance between the cable conductors and/or meter case. The meters were subjected to a maximum hydrostatic pressure of 17 psi for at least 20 hr during immersion. None of the soil stress meters leaked, but six developed low insulation resistances during the calibration tests and subsequently were replaced or repaired by Dr. Carlson.

6. When received in the laboratory, the periphery of each stress meter was covered with friction tape (see fig. A1). The purpose of the tape was to prevent concrete from bonding to the rim or entering the peripheral groove on the meter. After the initial leakage tests, it was discovered that corrosion had occurred inside the groove beneath the tape.

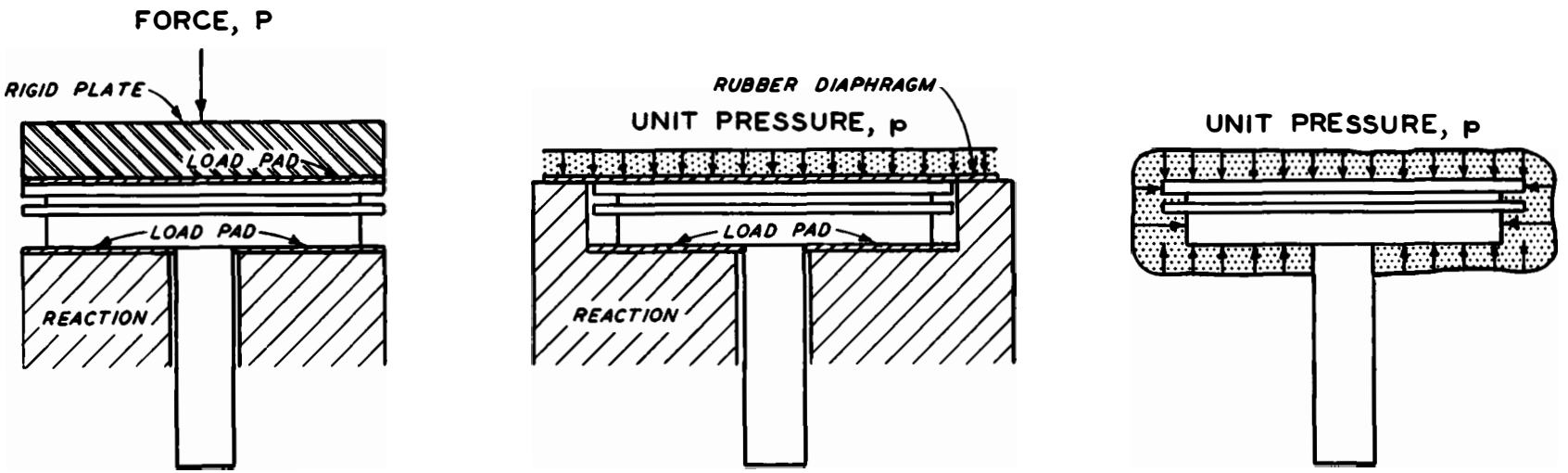

(A) RIGID PLATE CALIBRATION

(B) WES DIAPHRAGM PRESSURE CALIBRATION

(C) HYDROSTATIC PRESSURE CALIBRATION

Fig. A2. Methods used in calibrating Carlson soil stress meters

The grooves were cleaned, and all stress meters were dipped in zinc chromate paint to protect them against corrosion. It was thought that the tape supplied with the meters was not sufficiently rigid to prevent entrance of concrete into the indentation formed by the peripheral groove, and the tape was replaced by a strip of cork approximately 0.055 in. thick. The cork was held in place by electrician's plastic tape. It was felt that the cork was sufficiently porous to allow entrance of water into the groove and thus provide a true hydrostatic pressure on the loading diaphragm.

7. Load calibration of diaphragm. In the diaphragm-loading method, a uniform pneumatic load was applied in a chamber to the faceplate of the stress meter through a single rubber diaphragm. The back of the stress meter was supported by a thin cork load pad on an accurately machined steel reaction plate forming part of the chamber. The meters were calibrated by increasing the load in increments of 10 to 50 psi, then reducing the load in decrements of 10 to 0 psi, repeating the process three times. Calibration constants were computed based on the average slope of the curve for increasing pressures.

8. Comparison of calibration constants. Calibration constants furnished by Dr. Carlson are shown in table A1. In order to compare these constants with those obtained by WES with the meters having the leads attached, the calibration constants furnished by Dr. Carlson were corrected for the resistance of the leads. The equation used for this correction was:

$$C' = C + \frac{YC(0.89)}{R}$$

where

C' = revised calibration constant, psi/0.01 percent

C = original calibration constant, psi/0.01 percent

Y = resistance in ohms of a pair of leads = 0.013 × cable length, ft

R = meter resistance in ohms at 0 F

9. The corrected calibration constants vary between 96 to 100 percent of the calibration constants determined by WES. The differences are

insignificant, and in subsequent calculations the WES values were used. The hydrostatic calibration constants determined by WES were considerably greater than either the calibration constant that Dr. Carlson obtained from the rigid plate test or the WES diaphragm load calibration constant. A conservative estimate was made of the required length of cable for each device. Consequently, when terminal leads were installed in the instrumentation houses and it became necessary to shorten the cables, the calibration constants were revised to take into account the change in resistance of the cables.

Carlson strain meters

10. Thirty-three series SA-10 Carlson strain meters were obtained initially. These meters can measure strains between 400 millionths in expansion and 800 millionths in contraction. Two more meters of this type were obtained later to serve as replacements in case any of the original 33 meters were damaged or became inoperative prior to installation. A photograph of the Carlson strain meter is shown in fig. A3. A detailed description of the devices is given in reference 18.

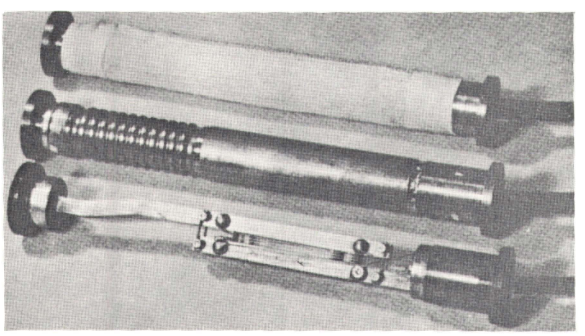

Fig. A3. Carlson strain meter; complete assembly (top), assembly with fabric cover removed (middle), and assembly with flexible brass cover tube removed (bottom)

11. Upon receipt at WES, all the strain meters were checked for cable-entry leaks and defective cables, as previously described for the soil stress meters. None of the meters leaked, although two meters developed low insulation resistances and one became inoperative during the check tests. These three meters were replaced with new meters. The calibration data furnished by Dr. Carlson are shown in table A2. These constants were corrected to take into account the cables attached to the meters, using the equation given previously. Also shown in table A2 are the results of the acceptance tests by WES. The tests included the measurement of resistance ratio at zero strain to check whether it fell near the midrange of the resistance ratios furnished by Dr. Carlson, and the

measurement of total resistance and computation of temperature therefrom to check whether the meters gave reasonably satisfactory readings in this respect. On the basis of test data presented by Dr. Carlson, the calibration curves for the strain meters are linear and are the same for temperatures within the range of 44 to 98 F. The calibration constants furnished by Dr. Carlson were accepted for use. When it was necessary to shorten the cables, the calibration constants were revised accordingly.

Carlson concrete stress meters

12. Three series PC-800 Carlson concrete stress meters were utilized. These meters measure stresses within a range of 0 to 800 psi in compression. The calibration constants furnished by Dr. Carlson are shown in table A3 together with constants corrected for the effect of attached cable. A photograph of a Carlson concrete stress meter is shown in fig. A4. The cork ring around the periphery of the meter is not shown in the photograph. The concrete stress meter operates basically the same as the soil stress meter described above. The effective modulus of elasticity of all the concrete stress meters is approximately 3-1/2 million psi. All of the meters were checked for leakage and low insulation and were found to be satisfactory. Equipment was not available at WES to check the calibration constants in the range of stresses expected, and the calibration constants furnished by Dr. Carlson were accepted. The calibration constants were corrected when it was necessary to shorten the cables.

Carlson pore pressure cell

13. One series TP-50 Carlson pore pressure cell was utilized. This cell, which is used to measure pore pressures within the concrete, has a range of 0 to 50 psi. A photograph of the cell is shown in fig. A5. The device consists of a porous plug, steel diaphragm, and strain meter unit. In operation, the water pressure being measured deflects the diaphragm and the deflection is measured by the strain meter unit.

14. The calibration constant furnished by Dr. Carlson and corrected for the resistance of the leads was equal to 0.186 psi/0.01 percent (see table A3). A calibration check at WES indicated considerable hysteresis and deviation from the calibration constant furnished by Dr. Carlson. It

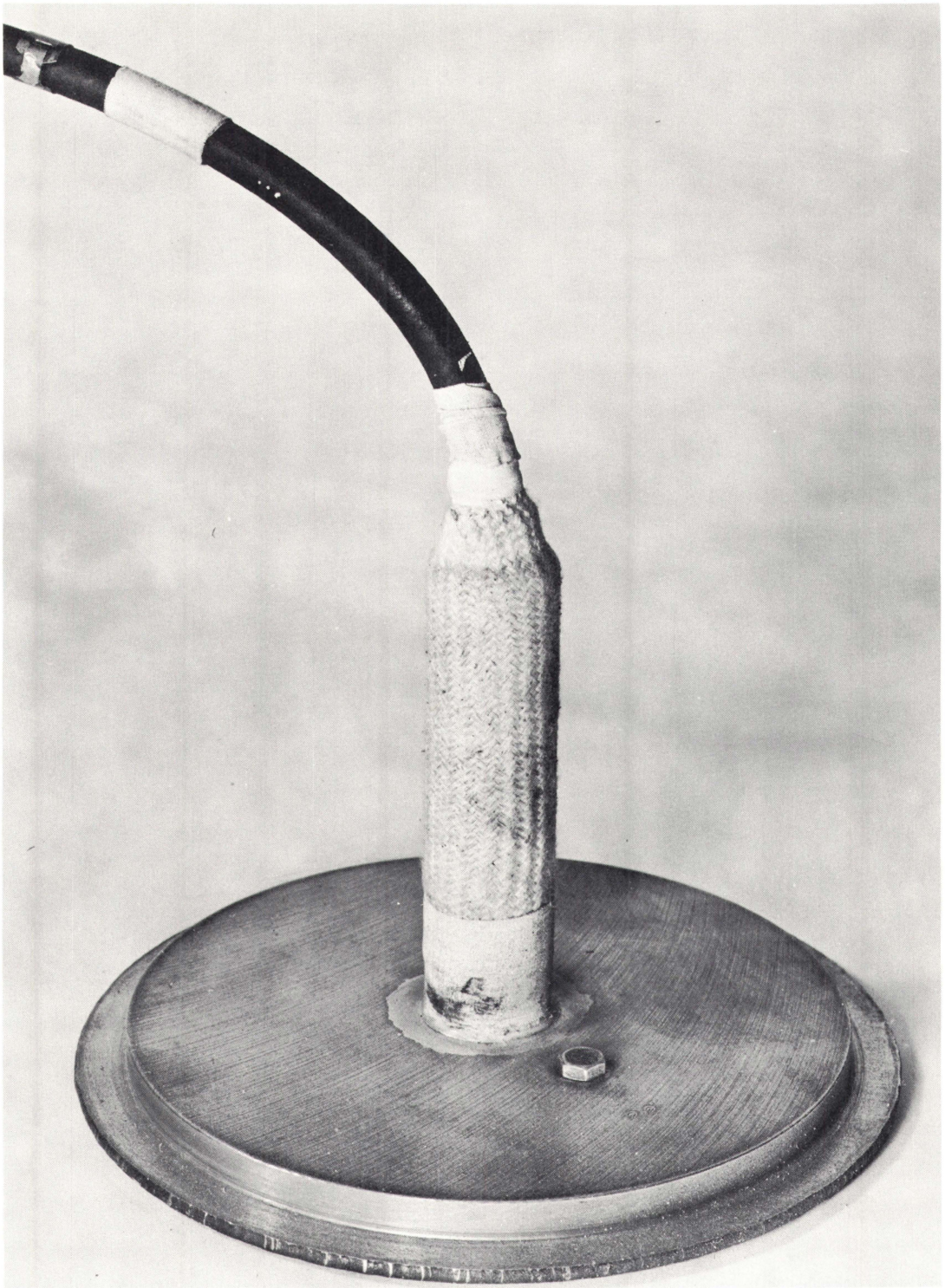

Fig. A4. Carlson concrete stress meter (peripheral cork ring removed)

was decided that the hysteresis was due to the presence of petroleum jelly that had been introduced between the porous plug and diaphragm to reduce the time lag. Therefore, the porous plug was cleaned of all petroleum jelly, and the tip of the pore pressure cell was filled with oil. The cell was recalibrated and no hysteresis was noted. After calibration, the cell was kept in an upright position to avoid loss of the oil. The calibration constant obtained in the final tests at WES (C'_H = 0.198 psi/0.01 percent) was adopted for the pore pressure cell. The calibration constants were revised on the basis of the actual length of cable employed.

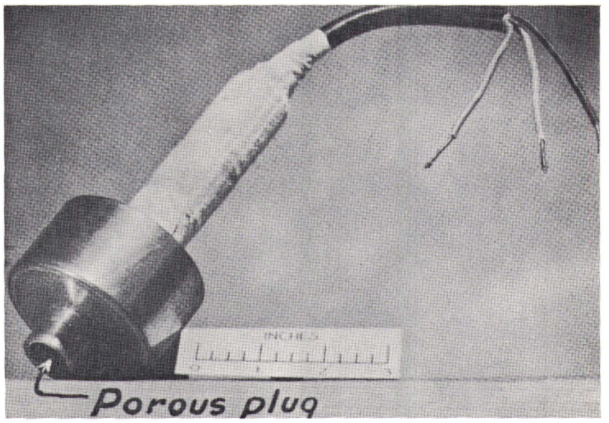

Fig. A5. Carlson pore pressure cell

Carlson resistance thermometers

15. Carlson Type TM-1 resistance thermometers were used. The resistance thermometer consists of a noninductively wound coil of enameled copper wire inside a brass case. A photograph of the device is shown in fig. A6. Calibration data furnished by Dr. Carlson are shown in table A3. Because the length of cable has no effect on the calibration constant, no revisions to the calibration data were necessary when the cables were shortened. The thermometers were checked at WES for leakage and loss of insulation and were found to be satisfactory. The calibration data furnished by Dr. Carlson were utilized for these instruments.

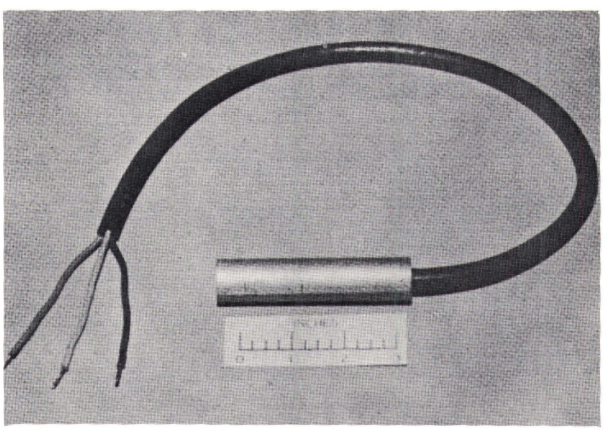

Fig. A6. Carlson resistance thermometer

WES pressure cells

16. Five WES earth pressure cells were provided for installation in

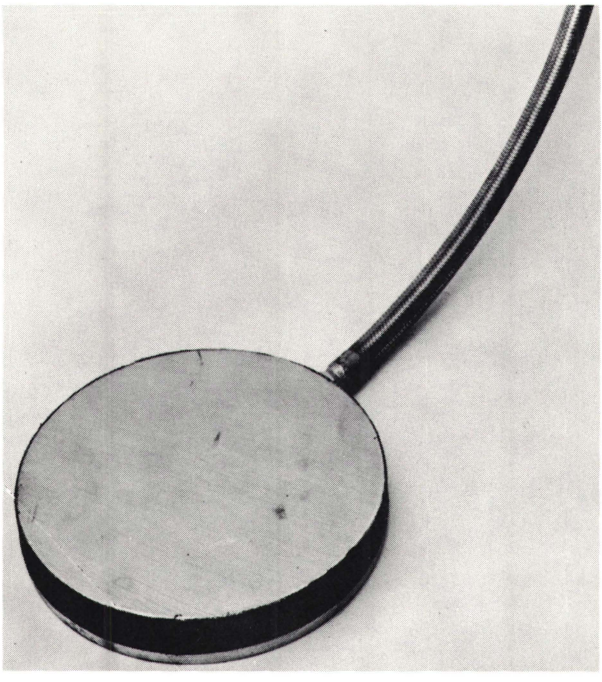

Fig. A7. WES earth pressure cell

the base and walls of the lock. The WES pressure cell (fig. A7) is a bonded strain gage and is made of stainless steel. A detailed description of the device is given in a previously published WES bulletin.[25]

17. The WES pressure cells were calibrated by applying various pressures through a thin rubber diaphragm to the faceplate of the cell and recording the strain gage readings. As in the case of the soil stress meter, a difference exists between diaphragm and hydrostatic loading because of hydrostatic pressures acting in the peripheral slot. Consequently, the cells were also calibrated under hydrostatic pressure. These calibrations were performed in the same manner as described for the Carlson soil stress meter.

18. The WES pressure cell is provided with plastic tape along its rim to prevent entrance of concrete or foreign material into the peripheral slot (the tape is not shown in fig. A7). The slot is not as wide as that of the Carlson soil stress meter and is located closer to the faceplate surface. Consequently, it was not considered necessary to provide a cork strip along the rim beneath the tape to permit entrance of water to the slot.

Installation of Electrical Measuring Devices

19. The electrical measuring devices were installed essentially as prescribed in WES Instruction Report No. 3.[3] Departures from the prescribed procedures were found to be necessary in some instances, and the revised procedures together with photographs and pertinent features of

the installation are presented below. The actual locations of all electrical measuring devices as installed are also described.

Carlson soil stress meters and
WES pressure cells below base slab

20. The soil stress meters and pressure cells beneath the structure were installed in recesses formed in the 6-in. stabilization slab. The stabilization slab consisted of essentially the same concrete as used for the overlying structure but did not contain steel reinforcements. The foundation area between sta 740+75.75 from the north side of the north culvert to the south side of the south culvert was trimmed carefully to final grade prior to placing the stabilization slab. At positions shown in fig. A8, recesses 4 ft square were formed in the stabilization slab for installation of the stress meters. A photograph of the recesses before installation of the devices is shown in fig. A9. Where a WES pressure cell was to be installed adjacent to a stress meter, a 4- by 6-ft recess was provided in the stabilization slab, and both devices were installed in the same recess.

21. The recesses were kept covered by panels of marine plywood 3/4 in. thick and by tarpaulins to protect the surface of the underlying soil until the cells and meters were installed. However, it was found that curing water had entered some of the recesses prior to installation of the devices, and in removing this water it was necessary to remove some of the soil in order to have an undisturbed surface on which to place the devices. As a result, it was necessary to place some of the devices slightly below the bottom of the base slab. Installation data for the devices, including the thickness of the stabilization slab at the recess, the depth of the meters, and a description of the conditions within the recess areas, are given in table A4. In some instances it was found that, if located as planned, the devices would be too close to the heave and settlement points previously installed in drill holes below the subgrade, and some slight changes in location were made to correct this situation.

22. Inspection of soil conditions in the recesses indicated that the foundation soils were very heterogeneous, consisting primarily of a dark gray silt with layers of fat clay and silty clay. It had been

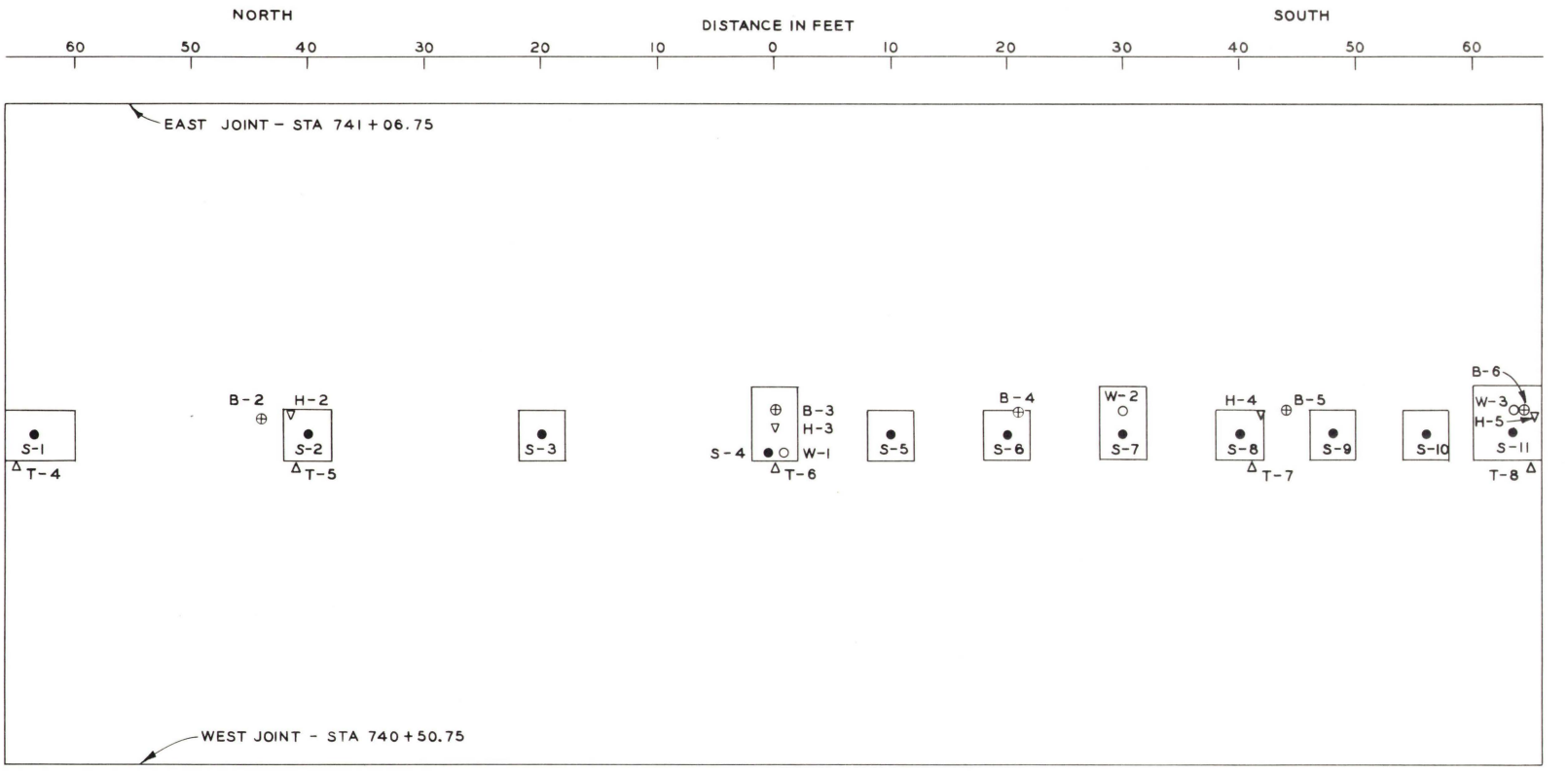

Fig. A8. Locations of soil stress meters and pressure cells

Fig. A9. Recesses in stabilization slab of monolith 15 prior to installation of devices

planned to place both the stress meters and pressure cells on a thin layer of silt, but a sufficient amount of suitable silt was not available, and the devices were placed instead on a layer of very fine sand. Because of the heterogeneous nature of the foundation soils and because the bottoms of the recesses generally were somewhat below the bottom of the stabilization slab, it was decided to cover the entire recess area with a 1/8-in. layer of fine sand. In the case of the WES pressure cell a cylindrical hole 3/8 in. deep was excavated, a 1/8-in. layer of sand was placed in the hole, and the cell was bedded on the sand. The WES pressure cell therefore protruded 3/8 in. below the concrete instead of 1/4 in. as originally planned. However, it was considered that the effect on the readings would not be significant. Details of the installation and procedures followed for both devices are shown in fig. A10. The thickness of sand beneath the instruments was determined by taking elevations at the instrument locations before and after the sand layer was placed. Photographs of various stages of installation are shown in fig. A11 (a), (b), and (c). Each instrument

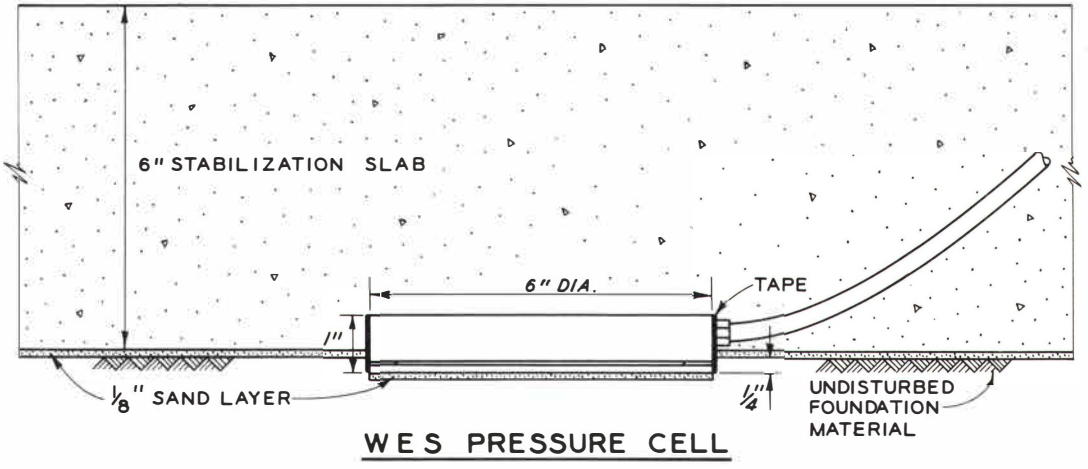

WES PRESSURE CELL

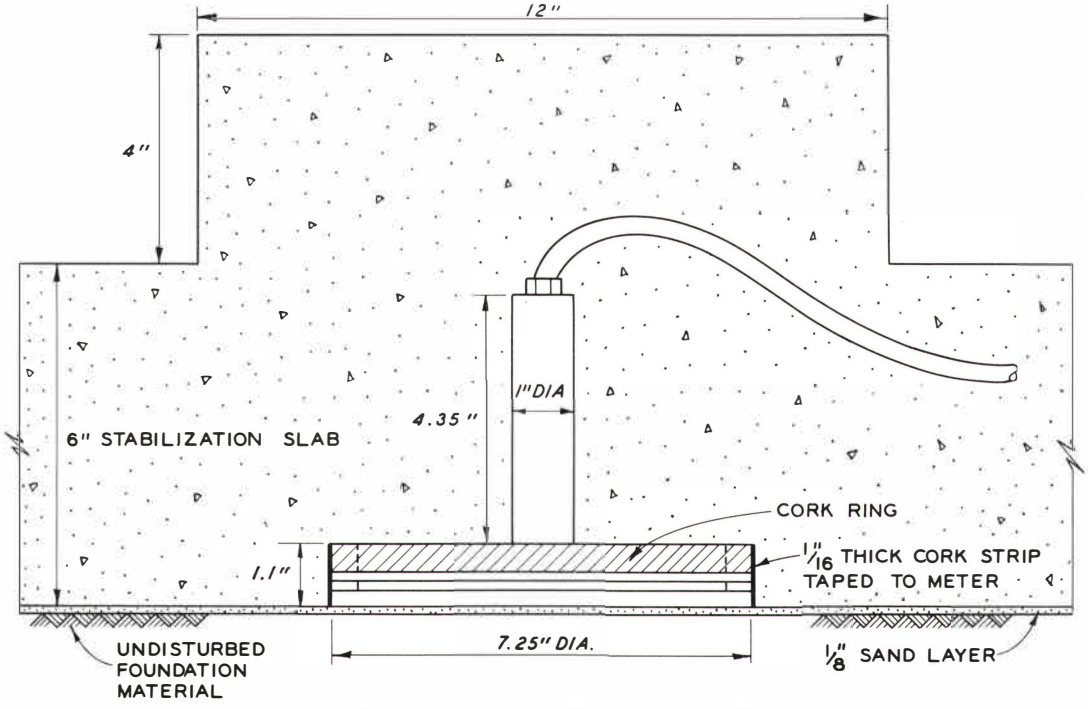

CARLSON SOIL STRESS METER

PROCEDURE:

1. FOUNDATION SOILS IN RECESS AREAS ARE TRIMMED AND LEVELED BY HAND.
2. A CYLINDRICAL HOLE, 3/8 IN. DEEP, AND HAVING THE SAME DIAMETER AS THE WES PRESSURE CELL IS CARVED IN THE FOUNDATION SOIL AT THE LOCATION OF THESE CELLS.
3. A LAYER OF SAND, 1/8 IN. THICK, IS PLACED IN THE BOTTOM OF THE HOLE.
4. THE WES PRESSURE CELL IS BEDDED ON THE SAND LAYER IN THE CYLINDRICAL HOLE.
5. A LAYER OF SAND, 1/8 IN. THICK, IS PLACED OVER THE WHOLE RECESS AREA EXCEPT FOR THAT AREA OCCUPIED BY THE WES PRESSURE CELLS.
6. THE CARLSON SOIL STRESS METER IS BEDDED ON THE SAND LAYER IN ITS PROPER POSITION.
7. THE RECESS AREA IS CAREFULLY BACKFILLED WITH CONCRETE.

Fig. A10. Procedure for installation of electrical measuring devices in stabilization slab

(a) Soil stress meter S-5 in position on layer of sand at bottom of recess in stabilization slab prior to placement of concrete

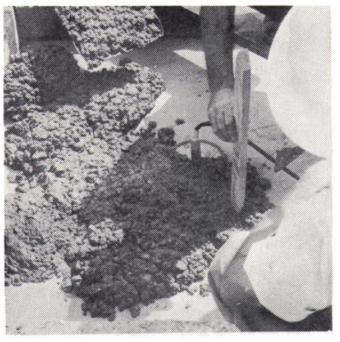

(b) Hand placement and compaction of concrete in recess for soil stress meter S-5

(c) Recess in stabilization slab filled with concrete. Note protruding block to protect top of stress meter

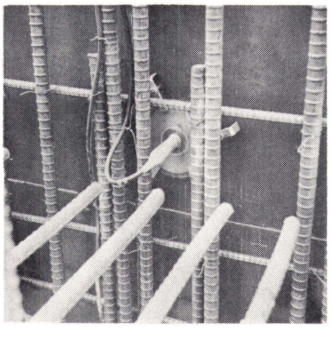

(d) Soil stress meter S-13 attached to inside of form prior to placement of concrete

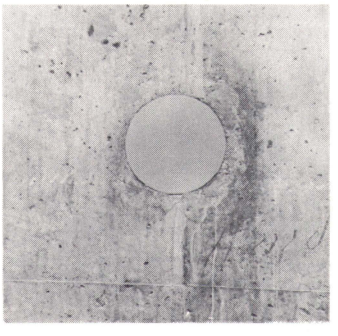

(e) Acting face of soil stress meter S-12 after removal of form and prior to placement of backfill

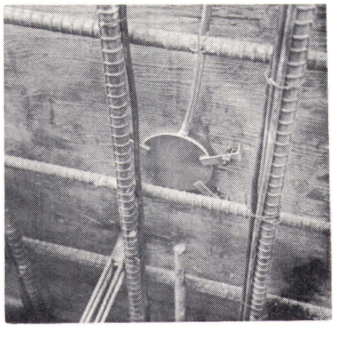

(f) WES pressure cell W-5 attached to inside of form prior to placement of concrete

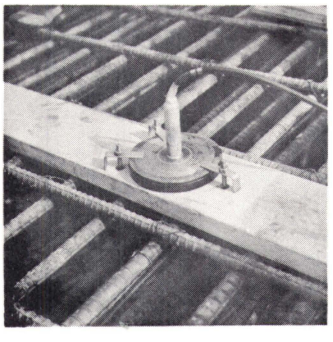

(g) Soil stress meter S-14 to be located on top of conduit shown attached to temporary timber support. Meter and support are in an inverted position

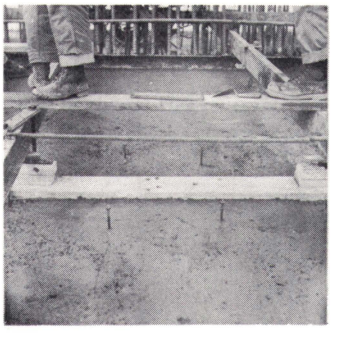

(h) Timber support, with soil stress meter S-14 attached, in position immediately after top lift of concrete in conduit was brought to grade

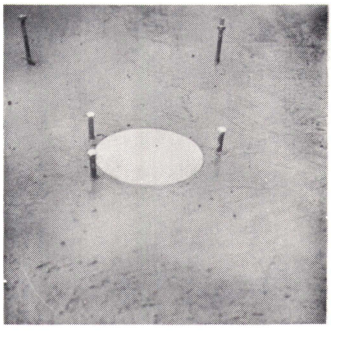

(i) Acting face of soil stress meter S-14 after removal of temporary timber support. Bolts attached to clamps will be removed and holes filled with concrete

Fig. A11. Installation of Carlson soil stress meters and WES pressure cells

was read just before it was installed, and a set of readings was taken on all instruments after the installation had been completed.

Carlson soil stress meters and WES pressure cells along sides of walls

23. The stress meters and pressure cells on the backfill side of the lock walls and culvert were attached to the concrete forms so that after placement of the concrete and removal of the forms, the acting face of the device was flush with the lock wall or culvert. The stress meters were attached to the forms as shown in fig. A12. The meters were centered between the four clips to provide space for the concrete to enter on all sides of the meter. Subsequently, it was found that three clips were sufficient to hold the meters to the wall frame. After the concrete had set and before the forms were removed, the bolts holding the stress meter clips to the form were removed. The holes left by the bolts were backfilled carefully with mortar after removal of the forms. Data on installation of the stress meters and pressure cells on the walls are shown in table A5. Photographs of the installation of the devices in the walls are shown in fig. A11 (d), (e), and (f).

24. Soil stress meter S-14 on the top of the culvert was attached to a 2- by 8-in. supporting timber in the same manner that the meters in the walls were attached to the wall forms. The timber then was attached to two channel irons that extended above the top of the culvert so that the face of the meter was at the same elevation and slope as the top of the culvert. About three hours after placement of concrete in the top lift of the culvert, the timber was removed, and the concrete in the vicinity of the face of the meter was finished. The bolts holding the meter clips were removed after the concrete had set, and the holes left by the bolts were filled with mortar. Photographs of the installation of stress meter S-14 are shown in fig. A11 (g), (h), and (i). A protective cover was placed over the meter until backfill was placed over the device.

25. The sand backfill immediately adjacent to the meters was placed in 4-in. layers, each layer being compacted by hand tamping. The remaining sand backfill close to the walls was placed in 8-in. layers and compacted with vibratory compactors and rollers.

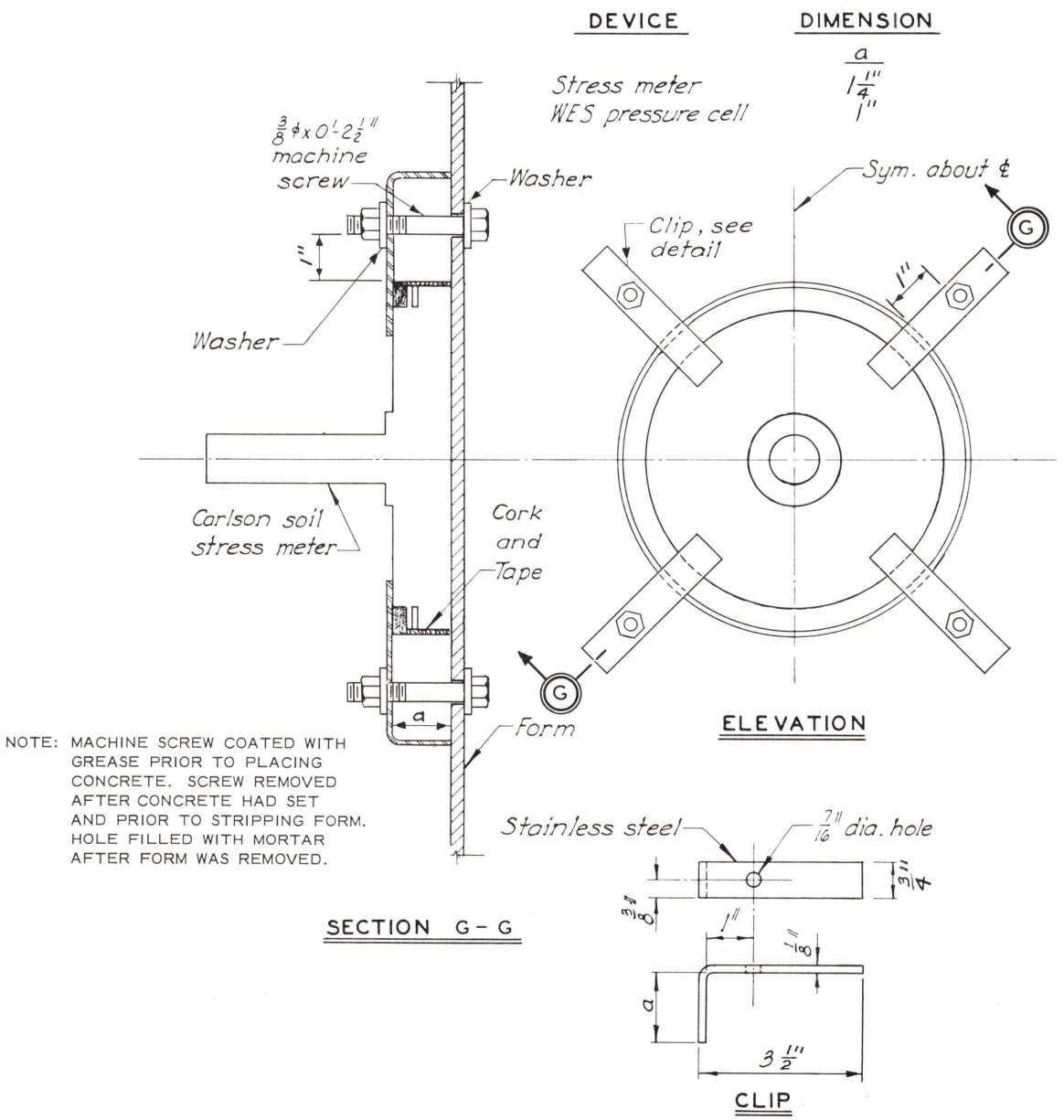

Fig. A12. Attachment of measurement devices to wall forms

Installation of concrete
stress meters and pore pressure cell

26. The concrete stress meters were installed in the base slab with the face of each meter vertical and parallel to the center line of the lock. The locations of the three concrete stress meters and the pore pressure cell were controlled by using two transits and a level. One transit was set up on the lock center line and the other on the station at which the instrument was to be installed. In addition to locating the three meters with surveying instruments, the proper alignment of the faceplates also was checked. The concrete stress meters and the pore pressure cell were installed during concrete placement operations in concrete that had set sufficiently to support the instruments but not to such extent as would preclude working the concrete. A photograph of concrete stress meter C-2 is shown in fig. A13 (e). Particular care was taken to see that the concrete was well vibrated by hand along the cable for pore pressure cell PP-1 and within 3 to 4 ft from the cell. The locations of the concrete stress meters and the pore pressure cell are tabulated below:

	As Installed		
Meter No.	Station	Elevation ft mlg	Date Installed
C-1	740+80.00	-24.75	13 June 1959
C-2	740+80.00	-23.25	13 June 1959
C-3	740+80.00	-20.25	21 August 1959
PP-1	740+78.50	-22.75	13 June 1959

Strain meters

27. All strain meters were checked prior to installation to ensure that they were set at approximately the midpoint of the potential strain range. All strain meters in the base slab, except for M-12, were supported by brackets constructed of No. 2 bars welded to the reinforcing steel. Details of the supports for the strain meters are shown in figs. A14 and A15. A dummy cylinder of wood of the same size and shape as the strain meter was used in the position of the meter when welding the bars in place. The bars were welded in place after the dummy cylinder had been leveled and aligned properly. Strain meter M-12 was installed on the surface of the second lift of the base slab after the second lift had been placed

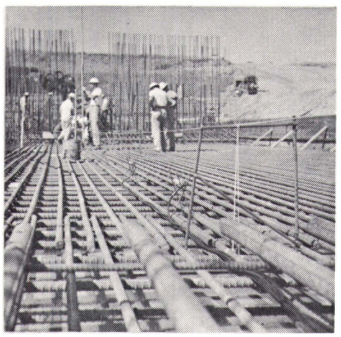

a. Strain meters M-2, M-3, M-4, and M-5, in first lift of base slab in place prior to placement of concrete

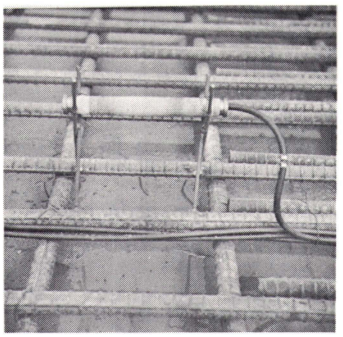

b. Strain meter M-2 in place prior to placement of concrete

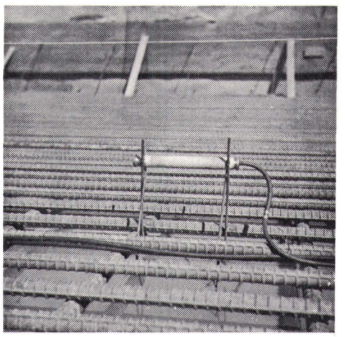

c. Strain meter M-3 in place prior to placement of concrete

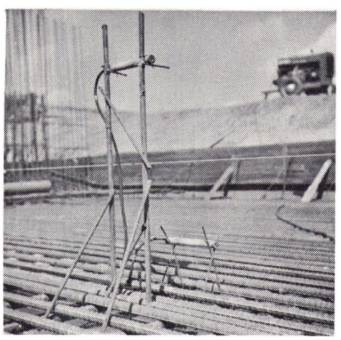

d. Strain meters M-6 and M-10 in first lift of base slab in place prior to placement of concrete. Strain meter M-10 offset and elevated above M-6

e. Concrete stress meter C-2 during hand placement of concrete around meter

f. Strain meter M-12 on surface of second lift of base slab. This meter was installed after the second lift was placed and the concrete had set sufficiently to support the meter

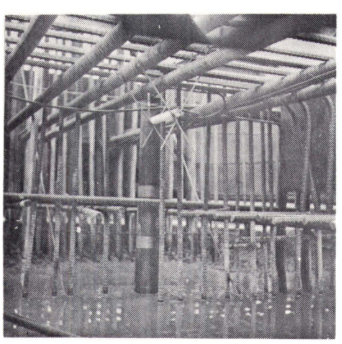

g. Strain meter M-21 in third lift of base slab, in place prior to placement of concrete

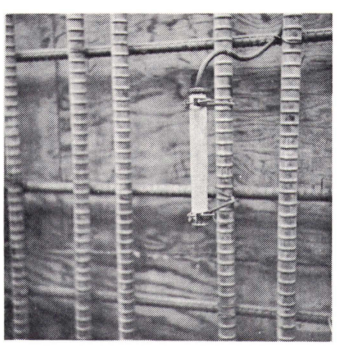

h. Strain meter M-25 in north wall in place prior to placement of concrete

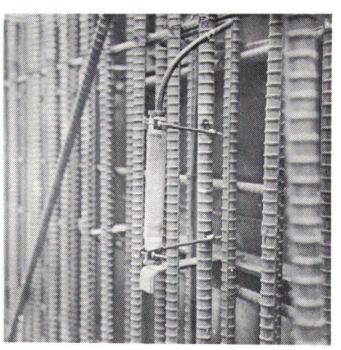

i. Strain meter M-32 in south wall in place prior to placement of concrete

Fig. A13. Installation of concrete stress meters and strain meters

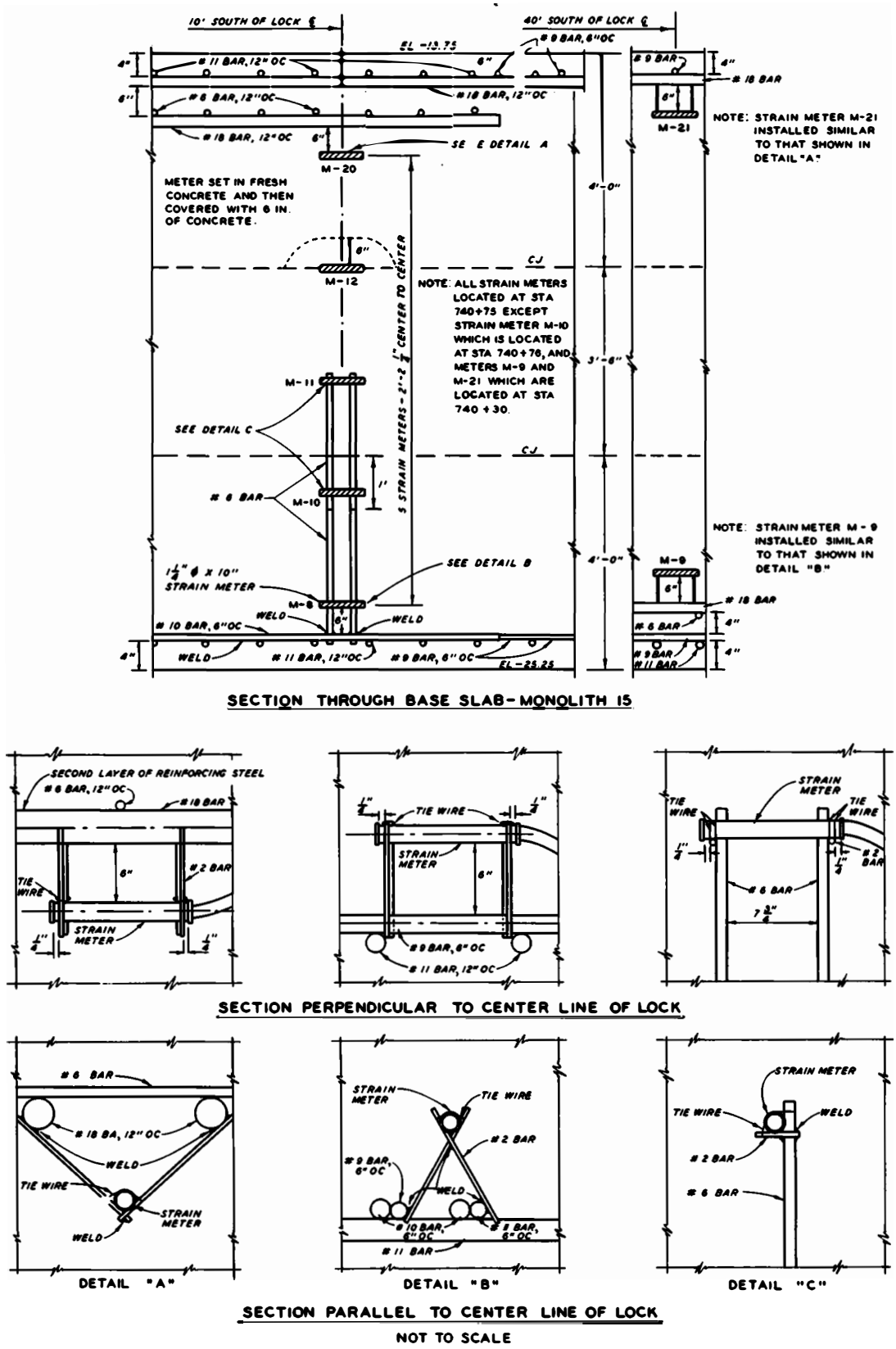

SECTION THROUGH BASE SLAB - MONOLITH 15

SECTION PERPENDICULAR TO CENTER LINE OF LOCK

DETAIL "A" DETAIL "B" DETAIL "C"

SECTION PARALLEL TO CENTER LINE OF LOCK

NOT TO SCALE

Fig. A14. Support of strain meters in base slab

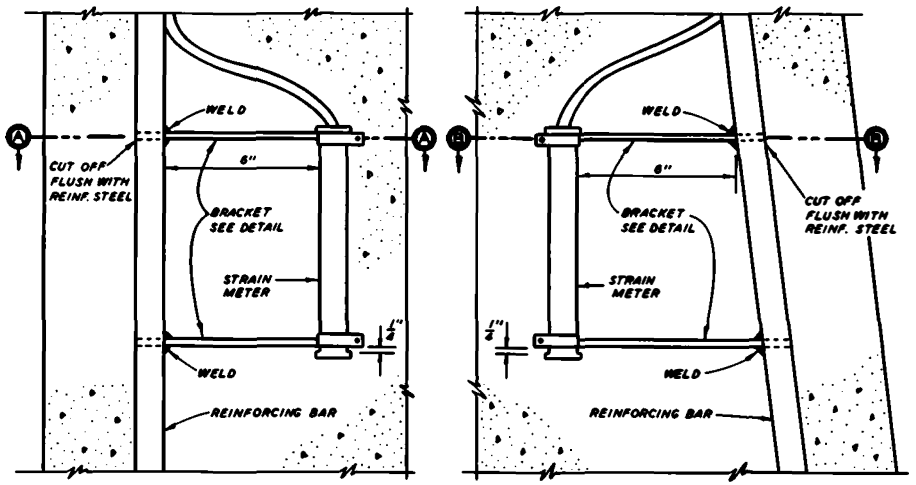

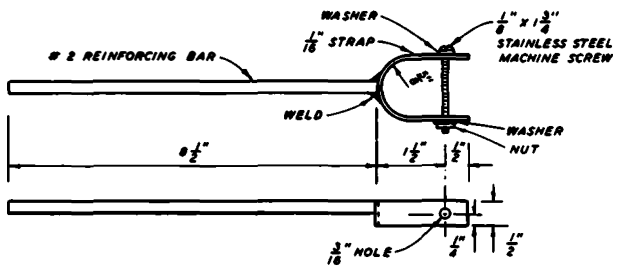

NOTE: ALL WELDING AND CUTTING DONE PRIOR TO INSERTING STRAIN METER IN BRACKETS.

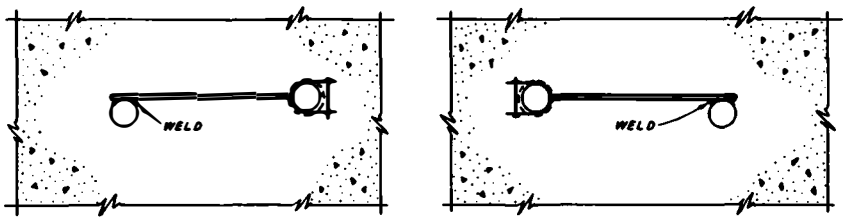

NOT TO SCALE

Fig. A15. Support of strain meters in walls

and the concrete had set sufficiently to support the meter (see fig. A13 (f)). Photographs of the strain meters attached to the reinforcing steel in the base slab and walls of the structure prior to placement of concrete are shown in fig. A13. Installation data for the strain meters are shown in table A6.

Resistance thermometers

28. The two resistance thermometers were fastened securely in proper position by wires fastened to the reinforcing steel. Installation data for these instruments are as follows:

Meter No.	Station	Elevation ft mlg	Distance from Inside face of Wall, ft	Date Installed
T-1	740+78.50	44.89	0.37	9 October 1959
T-2	740+78.50	44.89	2.75	9 October 1959

Table A1

Calibration Data for Carlson Soil Stress Meters

WES Meter No.	Carlson Meter No.	Cable Length ft	Data Furnished by Carlson: Calibr Constant C psi per 0.01%	Calibr Constant C' psi per 0.01%	Resistance at 0 F R_I ohms	Resistance Ratio at 0 psi RR %	ΔRR % per 1 F Temp Rise	WES Diaphragm Load Calibration: Calibr Constant C'_W psi per 0.01%	RR at 0 psi %	Total Resistance R ohms	Computed Temp F	WES Hydrostatic Calibration: Calibr Constant C'_H psi per 0.01%	Total Resistance R ohms	Computed Temp F	RR at 0 psi %
S-1	V-11	100	0.134	0.137	60.18	102.4	0.0036	0.139	102.36	68.70	72.2	0.159	69.78	81.4	102.39
S-2	V-6	150	0.133	0.137	59.88	103.6	0.0034	0.145	103.44	68.07	69.4	0.165	66.87	59.2	103.41
S-3	V-5	175	0.133	0.137	60.19	103.0	0.0036	0.141	102.77	68.94	74.1	0.160	69.62	80.0	102.81
S-4	V-4	175	0.135	0.140	60.21	103.3	0.0036	0.147	103.11	68.80	72.9	0.165	69.65	80.0	103.15
S-5	V-1	175	0.138	0.143	60.20	104.4	0.0028	0.146	104.21	69.60	79.8	0.168	69.89	82.1	104.20
S-6	V-3	175	0.128	0.132	60.37	103.3	0.0034	0.140	103.21	68.97	73.0	0.158	70.14	82.9	103.25
S-7	V-2	175	0.145	0.150	59.91	102.5	0.0028	0.153	102.36	69.03	77.4	0.174	69.62	82.3	102.38
S-8	V-8	150	0.135	0.139	59.91	104.2	0.0031	0.144	103.99	68.00	68.5	0.162	66.95	59.6	103.96
S-9	V-9	150	0.113	0.116	59.90	103.6	0.0040	0.118	103.47	68.87	76.1	0.130	69.53	81.7	103.57
S-10	V-10	150	0.134	0.138	60.07	103.2	0.0028	0.144	102.82	69.28	78.2	0.159	69.22	77.3	103.06
S-11	V-7	150	0.143	0.147	60.34	103.1	0.0028	0.153	102.97	69.53	78.0	0.177	68.36	68.0	102.94
S-12	V-12	100	0.146	0.149	59.88	103.3	0.0036	0.153	103.31	68.30	71.5	0.174	69.03	77.5	103.34
S-13	V-15	100	0.127	0.130	59.96	103.6	0.0038	0.130	102.24	---	75.0*	0.148	69.09	77.3	102.32
S-14	V-14	100	0.137	0.140	60.18	103.2	0.0042	0.143	103.09	69.07	75.4	0.162	69.33	77.5	103.13
S-15	V-13	100	0.140	0.143	60.23	103.6	0.0032	0.150	103.47	68.61	71.0	0.168	67.26	59.6	103.45
S-16	V-16	50	0.143	0.144	59.99	102.7	0.0030	0.146	102.66	---	75.0*	0.174	69.15	77.6	102.64
S-17	V-17	50	0.123	0.124	60.09	103.3	0.0036	0.129	103.12	68.44	70.7	0.153	67.14	59.8	103.10
S-18	V-18	50	0.134	0.135	60.15	103.3	0.0038	0.141	103.19	68.39	69.9	0.159	67.25	60.2	103.15
S-19	V-19	50	0.133	0.134	60.10	102.5	0.0038	0.139	102.37	68.83	74.1	0.156	69.72	81.5	102.41
S-20	A-1	50	0.178	0.180	60.15	102.0	0.0035	0.188	102.11	69.24	77.1	0.230	68.30	69.1	102.07

Note: WES diaphragm load calibration performed by applying air pressure to the loading face of the meter by means of a rubber diaphragm.
WES hydrostatic calibration performed by applying a hydrostatic pressure to the meter while submerged under water.
Calibration constant is the stress in pounds per square inch required to reduce the resistance ratio by 0.01% (or one least reading on the test set).
The temperature in °F is determined by subtracting R_I from the measured resistance, R, and multiplying by K_I (8.48 F per ohm).
The resistance ratio is measured directly by the testing set.
C = calibration constant furnished by Carlson. The area used to determine the calibration constant was 42.0 sq in.
C' = calibration constant furnished by Carlson corrected for cable resistance.
C'_W = calibration constant obtained at WES using direct loading (cable resistance included).
C'_H = calibration constant obtained at WES using hydrostatic loading (cable resistance included).
R_I = meter resistance at 0 F. Meter resistance is the total resistance of the meter exclusive of cable resistance. The meters are provided with 4-conductor cable which permits a direct determination of meter resistance.
RR = approximate resistance ratio at 0 psi; ΔRR = change in resistance ratio in per cent due to a temperature change of the meter.
* Estimated.

Table A2

Calibration Data for Carlson Strain Meters

WES Meter No.	Carlson Meter No.	Cable Length ft	Data Furnished by Carlson: Calibr Constant C	Calibr Constant* C'	Resistance at 0 F R_I	Degrees per ohm K_I	Range of Resistance Ratio	Approximate Resistance Ratio When Shipped	WES Acceptance Data: RR at 0 psi	Total Resistance R ohms	Computed Temp F
M-1	P-16	150	3.74	3.86	55.92	8.58	0.973 - 1.027	1.002	1.0027	64.95	77.5
M-2	P-15	150	3.78	3.90	56.10	8.56	0.972 - 1.027	1.000	1.0015	65.21	78.0
M-3	P-10	175	3.78	3.92	56.41	8.51	0.966 - 1.019	0.991	0.9924	66.05	82.0
M-4	P-9	175	3.74	3.88	56.08	8.56	0.975 - 1.030	1.003	1.0046	65.65	81.9
M-5	P-8	175	3.78	3.92	56.04	8.56	0.970 - 1.020	0.999	1.0009	65.60	81.8
M-6	P-6	175	3.78	3.92	56.03	8.57	0.973 - 1.027	1.008	1.0110	65.52	81.2
M-7	P-7	175	3.74	3.88	56.02	8.57	0.975 - 1.029	1.005	1.0028	65.54	81.6
M-8	P-14	150	3.76	3.88	56.13	8.55	0.968 - 1.023	1.004	1.0044	65.22	77.7
M-9	P-13	150	3.78	3.90	56.16	8.55	0.971 - 1.024	1.000	1.0013	65.32	78.3
M-10	P-12	150	3.78	3.90	56.07	8.56	0.968 - 1.019	0.999	1.0000	65.17	77.9
M-11	P-11	150	3.70	3.81	56.15	8.55	0.971 - 1.027	1.002	1.0022	65.21	77.4
M-12	P-17	150	3.76	3.86	56.12	8.55	0.973 - 1.028	1.006	1.0085	65.21	77.7
M-13	P-18	150	3.80	3.91	55.99	8.57	0.968 - 1.021	0.998	0.9986	65.05	77.7
M-14	P-19	150	3.74	3.85	56.15	8.55	0.969 - 1.024	0.998	0.9989	65.23	77.5
M-15	P-1	175	3.74	3.88	56.13	8.55	0.965 - 1.020	0.999	0.9986	65.75	82.2
M-16	P-3	175	3.80	3.94	56.11	8.55	0.969 - 1.024	1.003	1.0037	65.70	82.0
M-17	P-4	175	3.78	3.92	56.22	8.54	0.968 - 1.023	1.002	1.0028	65.70	81.0
M-18	P-5	175	3.78	3.92	56.09	8.56	0.979 - 1.009	1.009	1.0102	65.62	81.4
M-19	A-1	175	3.74	3.88	56.01	8.57	0.978 - 1.033	1.006	1.0050	63.66	65.5
M-20	P-20	150	3.78	3.90	55.81	8.60	0.974 - 1.028	1.006	1.0060	64.80	77.4
M-21	A-2	150	3.78	3.90	55.97	8.57	0.973 - 1.024	1.003	1.0029	63.61	65.5
M-22	P-22	80	3.76	3.82	56.15	8.55	0.969 - 1.021	1.001	1.0018	65.38	78.8
M-23	P-23	80	3.76	3.82	56.04	8.56	0.972 - --	1.000	0.9997	65.27	79.0
M-24	A-3	55	3.72	3.76	56.21	8.54	0.964 - 1.020	1.000	0.9978	63.95	66.1
M-25	P-29	55	3.78	3.82	56.07	8.56	0.974 - --	1.000	1.0003	65.19	78.0
M-26	P-26	80	3.78	3.84	55.96	8.58	0.975 - --	1.007	1.0069	65.11	78.5
M-27	P-27	80	3.78	3.84	55.88	8.59	0.982 - --	1.013	1.0130	65.05	78.8
M-28	P-24	80	3.78	3.84	55.99	8.57	0.976 - --	1.004	1.0041	65.20	78.9
M-29	P-25	80	3.78	3.84	55.78	8.60	0.974 - --	1.004	1.0038	64.95	78.9
M-30	P-30	55	3.74	3.78	56.00	8.57	0.976 - --	1.007	1.0072	65.12	78.1
M-31	P-31	55	3.76	3.80	56.06	8.56	0.971 - 1.022	1.002	1.0018	65.18	78.1
M-32	P-32	55	3.76	3.80	56.13	8.55	0.968 - 1.022	1.001	1.0004	65.26	78.0
M-33	P-33	55	3.78	3.82	56.16	8.55	0.975 - 1.030	1.006	1.0063	65.30	78.0
M-34	A	175	3.78	3.92	55.93	8.58	0.973 - 1.028	1.011	1.0015	63.87	68.1
M-35	B	175	3.72	3.87	56.12	8.55	0.972 - 1.008	1.008	1.0083	64.20	69.0

Note: Definition of terms presented in table A1.
* C' = calibration constant corrected for cable resistance.

Table A3

Calibration Data for Miscellaneous Electrical Instruments

Device No.	Cable Length ft	Carlson Calibration Data: Calibr Constant C	Calibr Constant C'	Resistance at 0 F R_I ohms	Change in Resistance per °F ohms	Degrees F per ohm	Approximate RR at 0 psi, ℉	Mercury Thickness T, in.	Composite Thickness D, in.	80 T/D	RR Increase per °F Temp Rise	WES Calibration Data: Calibr Constant C'_W	Calibr Constant C'_H
Carlson Concrete Stress Meters													
C-1	175	5.65	5.84	60.53	--	8.48	103.2	0.012	0.525	1.8	--	--	--
C-2	175	5.65	5.84	60.21	--	8.48	103.9	0.009	0.530	1.4	--	--	--
C-3	175	5.15	5.32	60.28	--	8.48	104.3	0.010	0.525	1.5	--	--	--
Carlson Pore Pressure Cell													
PP-1	175	0.180	0.186	60.32	--	8.48	102.1	--	--	--	0.0025	--	0.198
Carlson Resistance Thermometers													
T-1	30	--	--	39.40	0.10	--	--	--	--	--	--	--	--
T-2	30	--	--	39.40	0.10	--	--	--	--	--	--	--	--
WES Pressure Cells													
W-1	175	--	--	--	--	--	--	--	--	--	--	0.0191	0.0224
W-2	150	--	--	--	--	--	--	--	--	--	--	0.0186	0.0217
W-3	150	--	--	--	--	--	--	--	--	--	--	0.0186	0.0227
W-4	50	--	--	--	--	--	--	--	--	--	--	0.0202	0.0236
W-5	35	--	--	--	--	--	--	--	--	--	--	0.0212	0.0248

Note: T is the thickness of the mercury film in inches; D is the thickness of the composite diaphragm in inches.
The value 80 T/D is used in the equation for temperature correction.
Definitions of other terms presented in table A1.

Table A4

Installation Data for Electrical Measuring Devices in Stabilization Slab

Meter No.	As Installed Station	As Installed Distance from ℄, ft	Avg Thickness of Stabilization Slab at Recess, in.	Depth of Meter Face Below Bottom of Slab, in.	Soil Conditions in Recessed Area
S-1	740+78.75	63.5 north	6.25	1.50	Dark gray silt with lenses and areas of blue fat clay. Soil on east and west sides of recess were eroded to a depth of 1/2 to 1 in. prior to installation. Backfilled with damp silt.
S-2	740+78.75	40.0 north	6.25 on 3 sides 4.00 on north side	0.50	Finely stratified gray silt with small pockets of gray lean clay. Surface area rather rough due to rain wash.
S-3	740+78.75	20.0 north	5.75	0	Finely stratified gray silt with a few small areas and lenses of lean gray silt.
S-4	740+77.35	0.75 south	5.50	1.0 to 2.5	Thin, stratified layers of gray silt interspersed with small areas of gray medium clay.
W-1	740+77.35	0.75 north	5.50	1.0 to 2.5 0.25 in. below S-4	
S-5	740+78.75	10 south	6.25	1.0	Finely stratified gray silt. Portions of box-out not immediately under meter are interspersed with thin lenses and areas of gray lean clay.
S-6	740+78.75	20 south	5.00 to 6.00	1.0 to 2.0	Finely stratified gray silt interspersed with a few thin lenses and areas of lean gray clay.
S-7	740+78.75	30 south	6.25	0.75 to 1.25	Finely stratified gray silt interspersed with a few thin lenses and areas of lean gray clay.
W-2	740+80.75	30 south	6.25	0.75 to 1.25 0.25 in. below S-7	Finely stratified gray silt interspersed with a few thin lenses and areas of lean gray clay.
S-8	740+78.75	40 south	6.25	0.25 to 0.50	Gray silt with areas of gray fat clay.
S-9	740+78.75	48 south	6.00	0	Finely stratified gray silt under meter. Remaining portion contains thin lenses and areas of gray lean clay. Clay areas had dried and cracked slightly.
S-10	740+78.75	56 south	6.75	0.75	Two thin layers of medium clay parallel to center line of lock and terminate under meter. Area heavily pocketed with areas and lenses of fat to lean clay.
S-11	740+78.75	63.5 south	6.25	1.50	Area under meters finely stratified gray silt. One small area of fat clay under S-11. Area badly washed out due to heavy rains. Backfilled to instrument elevation with hand-tamped damp silt.
W-3	740+80.75	63.5 south	6.25	0.25 in. below S-11	

Note: Stabilization slab for monolith 15 placed on 15-16 May 1958. Electrical measuring devices in stabilization slab installed on 28-29 May 1958.

Table A5

Installation Data for Electrical Measuring Devices on Walls

Meter No.	Station*	Elevation* ft mlg	Location	Date Installed
S-12	740+78.67	-8.75	South wall	14 Jan 1959
S-13	740+78.50	-1.23	South wall	28 Feb 1959
S-14	740+78.75	+4.38	Top of culvert south wall	28 Feb 1959
S-15	740+77.85	+9.25	South wall	9 Apr 1959
W-4	740+79.85	+8.45	South wall	9 Apr 1959
S-16	740+77.95	+15.80	South wall	9 Apr 1959
S-17	740+78.00	+21.99	South wall	27 May 1959
W-5	740+76.05	+22.05	South wall	27 May 1959
S-18	740+79.48	+28.52	South wall	29 Aug 1959
S-19	740+78.00	+22.00	North wall	29 May 1959
S-20	740+79.45	+9.40	North wall	7 Apr 1959

Note: All meters except S-14 were installed with face of meter flush with outside of wall, S-14 was installed in top of culvert 57.57 ft from center line of lock, with face of meter flush with top of culvert.

* Station and elevation of center of face of meter

Table A6

Installation Data for Strain Meters

Meter	Station	Distance from Inside Face of Wall ft	Offset from Center Line of Lock ft	Elevation ft mlg	Location		Date Installed
					Wall	Lift	
			Strain Meters in Base Slab				
M-1	740+75.0	--	40.0 N	-29.97		First	13 Jun 58
M-2	740+75.0	--	27.0 N	-24.53		First	13 Jun 58
M-3	740+75.0	--	20.0 N	-24.55		First	13 Jun 58
M-4	740+75.0	--	10.0 N	-24.52		First	13 Jun 58
M-5	740+75.0	--	center line	-24.54		First	13 Jun 58
M-6	740+75.0	--	10.0 S	-24.25		First	13 Jun 58
M-7	740+75.0	--	20.0 S	-24.18		First	13 Jun 58
M-8	740+75.0	--	27.0 S	-24.24		First	13 Jun 58
M-9	740+80.0	--	40.0 S	-24.76		First	13 Jun 58
M-10	740+76.0	--	10.0 S	-21.99		First	13 Jun 58
M-11	740+75.0	--	10.0 S	-19.87		Second	20 Aug 58
M-12	740+75.0	--	10.0 S	-17.69		Second	20 Aug 58
M-13	740+75.0	--	40.0 N	-14.80		Third	16 Oct 58
M-14	740+75.0	--	27.0 N	-15.51		Third	16 Oct 58
M-15	740+75.0	--	20.0 N	-15.56		Third	16 Oct 58
M-16	740+75.0	--	10.0 N	-15.54		Third	16 Oct 58
M-17	740+75.0	--	center line	-15.55		Third	16 Oct 58
M-18	740+75.0	--	10.0 S	-15.59		Third	16 Oct 58
M-19	740+75.0	--	20.0 S	-15.49		Third	16 Oct 58
M-20	740+75.0	--	27.0 S	-15.54		Third	16 Oct 58
M-21	740+80.0	--	40.0 S	-14.93		Third	16 Oct 58
			Strain Meters in Walls				
M-22	740+70.0	5.42	--	-11.38	North	First	30 Dec 58
M-23	740+70.0	0.92	--	-11.38	North	First	30 Dec 58
M-24	740+70.0	5.42	--	+11.21	North	Third	7 Apr 59
M-25	740+70.0	1.42	--	+11.17	North	Third	7 Apr 59
M-26	740+75.0	1.00	--	-11.40	South	First	20 Jan 59
M-27	740+75.0	5.50	--	-11.43	South	First	20 Jan 59
M-28	740+75.0	1.00	--	-4.36	South	First	20 Jan 59
M-29	740+75.0	6.00	--	-4.31	South	First	20 Jan 59
M-30	740+75.75	1.42	--	+11.30	South	Third	9 Apr 59
M-31	740+74.75	5.40	--	+11.28	South	Third	9 Apr 59
M-32	740+76.0	1.42	--	+19.29	South	Fourth	27 May 59
M-33	740+76.0	4.20	--	+19.29	South	Fourth	27 May 59

APPENDIX B: DESCRIPTION, CALIBRATION, AND INSTALLATION OF WALL DEFLECTION PIPES

Description and Calibration

Description of equipment

1. The wall deflection pipes and deflectometer consisted of 5-in.-ID pipe set vertically in the lock wall and a deflectometer consisting of a compound vise and dial gages to measure movement of a plumb bob attached to the vise. Fig. B1 is a schematic diagram of the equipment used to measure wall deflections. In measuring deflections, the plumb bob is lowered into the pipe, and the positions of reference points in the pipe with respect to the bottom of the wall are determined by means of an electrical circuit. It may be noted that for each coupling the positions of two contact points are determined so that the center of each coupling is established. In this manner, any inherent errors in determining the points of contact are partially compensable. Changes in the relative positions of the centers of the couplings based on subsequent measurements indicate the lateral movements that have occurred during the period between the two observations. Details of the wall deflection pipes and deflectometer are shown in fig. B2. Fig. B3 is a photograph of the deflectometer, plumb bob, and pipe coupling used as a reference point. The apparatus was designed to measure changes in alignment of the wall from the vertical of ± 2 in. with an accuracy of ± 0.01 in. over a height of 68 ft. Extensive calibration tests were conducted on the deflectometer before using it in the structure.

Wall deflection pipes

2. Sections of the 5-in.-ID steel wall deflection pipe are joined by couplings that contain four 1/2-in. stainless steel (No. 302) contact rods set at right angles to each other, each pair of rods being approximately 4.75 in. apart. It was found that commercially available pipe and couplings were not aligned with sufficient accuracy and would result in displacements from the vertical considerably in excess of tolerable limits. For this reason, the couplings were specially made and both the

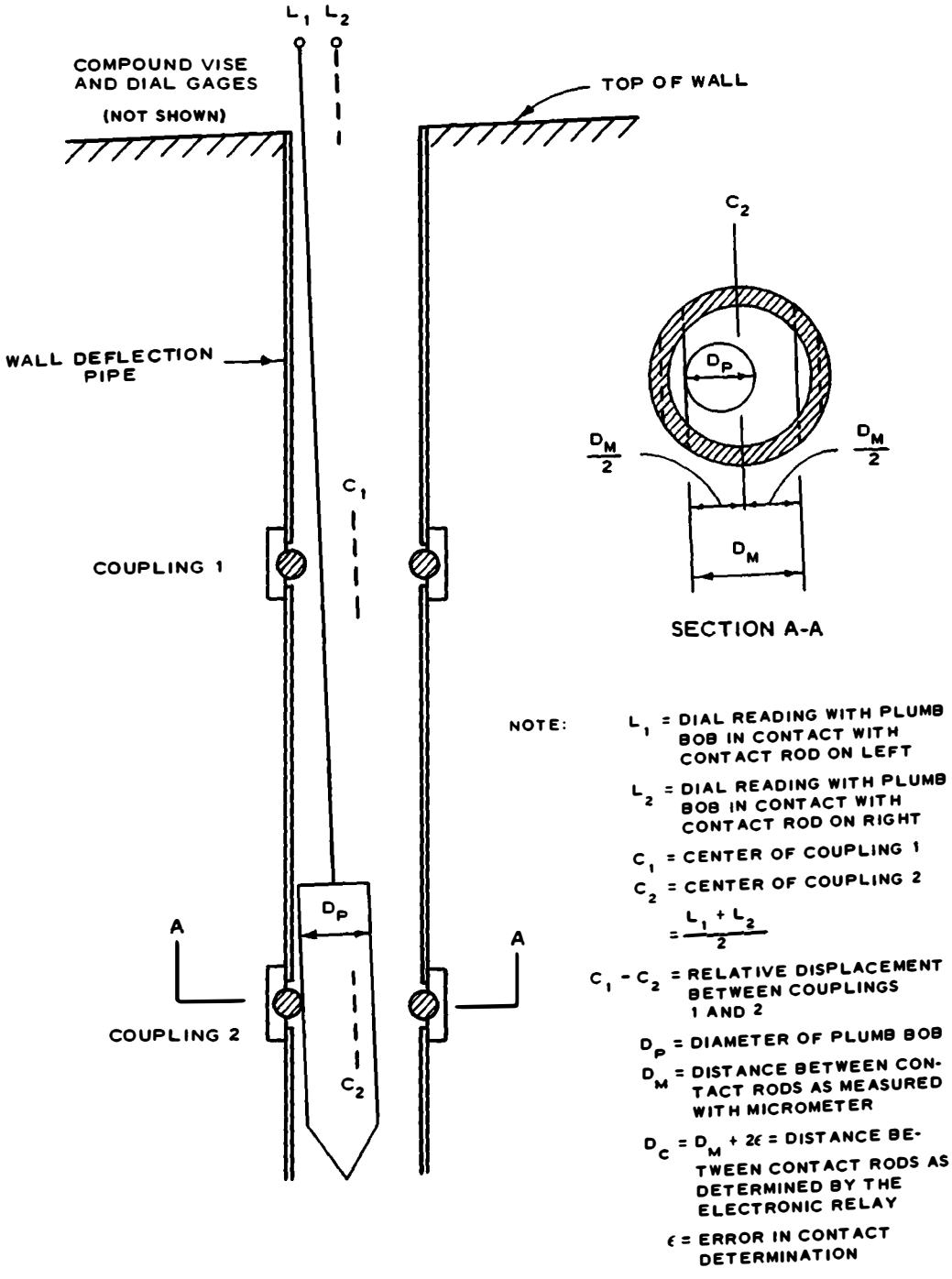

Fig. B1. Schematic diagram of equipment used for measuring wall deflections

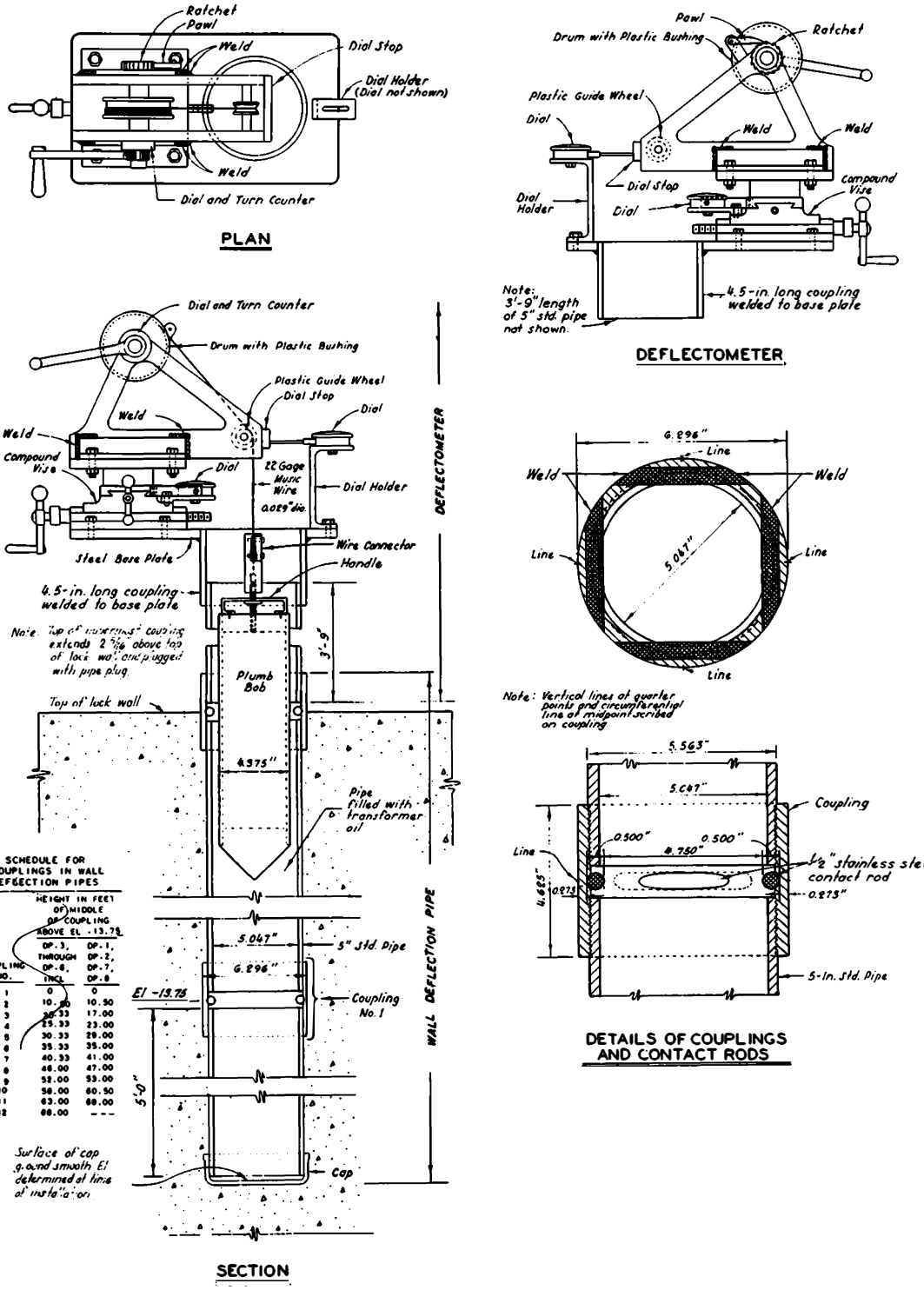

Fig. B2. Details of wall deflection pipes and deflectometer

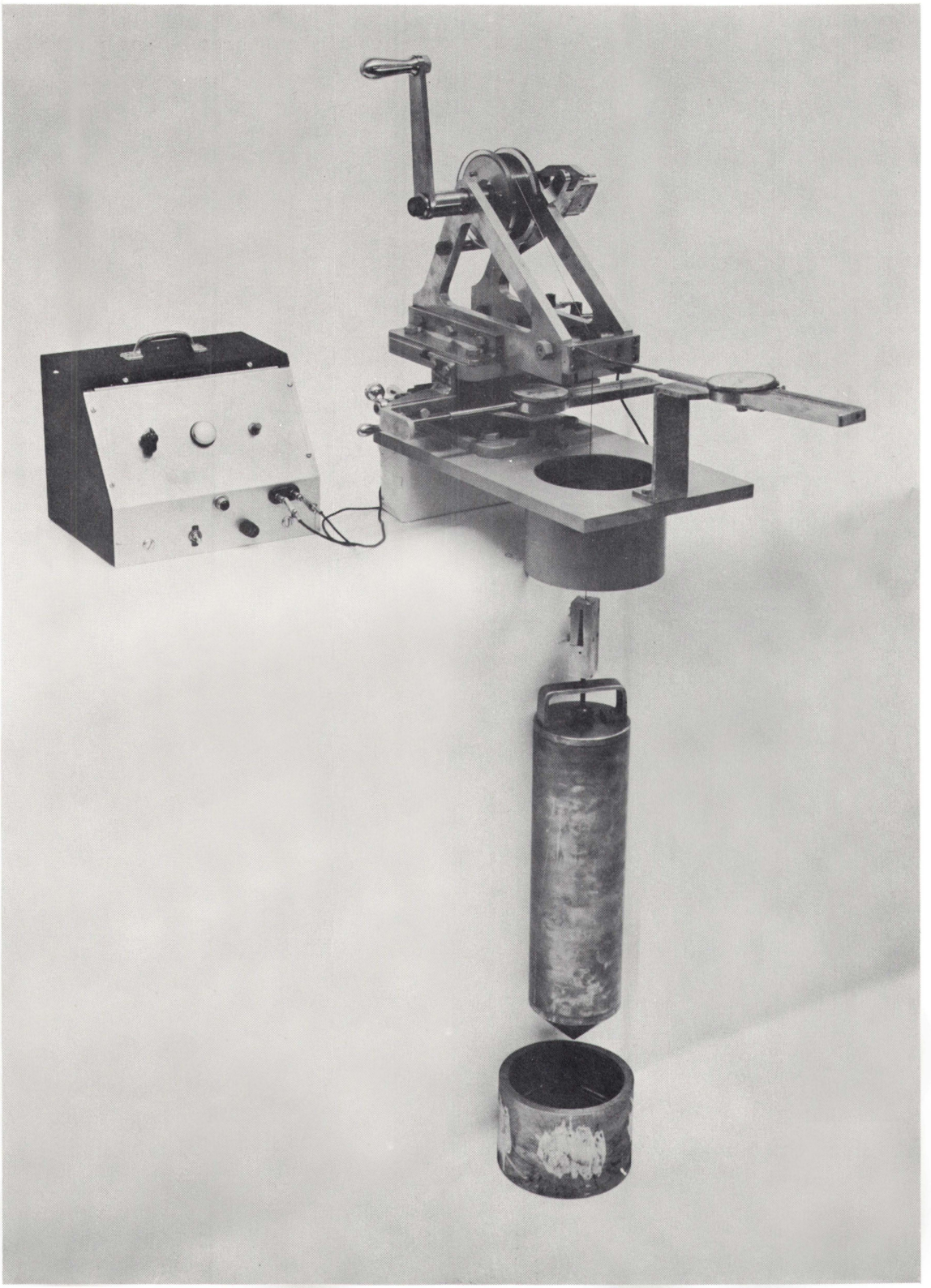

Fig. B3. Deflectometer and coupling

couplings and commercially available pipe were threaded in a precision lathe. However, in the field it was difficult to install the deflection pipes because of the close tolerance of the precision threads and their susceptibility to damage during handling. A micrometer was used to measure the distance between contact rods in each coupling. The deflection pipes were filled with transformer oil after installation to dampen movement of the plumb bob, as subsequently described, and to reduce the tendency for corrosion to develop. Computations indicated that the presence of the wall deflection pipes would not alter the deflection of the wall by more than 1 percent.

Deflectometer

3. The deflectometer, shown in figs. B2 and B3, consists of a bronze-faced plumb bob weighing approximately 30 lb and suspended by 22-gage (0.029-in.-diam) music wire from a crank-operated drum mounted on a compound vise. The plumb bob can be raised or lowered by rotating the drum and can be fixed at a given elevation by a pawl and ratchet. The diameter of the plumb bob and position of contact rods are such that the plumb bob cannot come in contact with the walls of the deflection pipe when it is suspended at the location of one of the couplings; contact is made only with the contact rods. A turn counter is provided on the drum to permit measurement of vertical distances. The base of the compound vise is attached to a baseplate which in turn is attached to the deflection pipe. The deflectometer is always positioned so that movement of the compound vise is perpendicular and parallel to the contact rods in the couplings.

4. The relative position of one coupling to another is determined by moving the compound vise, and thus the attached plumb bob, laterally in a direction perpendicular to the face of the wall at the elevation of each coupling until it comes into contact with the contact rods in the coupling. The movement required for the plumb bob to make contact with the contact rods is determined by a dial gage having a 4-in. travel and reading direct to 0.001 in. A similar dial gage is provided on the deflectometer to center the plumb bob between contact rods perpendicular to the face of the wall. The point of contact between the plumb bob and

contact rods is determined by means of an electrical circuit and indicator.

Electrical circuit

5. The indicator, which has one wire lead attached to the deflection pipe and the other to the music wire and plumb bob by means of a brush contact on the rim of the drum, indicates an electrical contact when the plumb bob touches the contact rods. The drum contains a plastic bushing to insulate the music wire from the rest of the deflectometer assembly. An electronic relay connected to a signal light indicates when contact is made, contact being defined as the point at which the total resistance across the indicator terminal is reduced to a predetermined level. The system initially required a 115-v, a-c power source; however, a portable, battery-powered indicator was developed. A battery-powered ohmmeter is available for use in the field in case of malfunctioning of the electronic relay. Consistent results also can be obtained with the ohmmeter; however, more time is generally required for the measurements. In addition, the signal light on the electronic relay presents a more positive indication of contact and thus there is less need for interpretation.

Installation of Wall Deflection Pipes

6. The wall deflection pipes were installed essentially as prescribed in Instruction Report No. 3.[3] Locations of all deflection pipes as installed are presented in table B1.

7. A steel plate (not shown in fig. B2) equipped with three setscrews threaded through it was used to establish a base for each pipe to facilitate installation of the pipe at the proper elevation. A depression 2 to 3 in. lower than the final elevation of the base of the deflection pipe was formed in the concrete. The steel plate was placed in this depression and adjusted to the correct elevation by means of the setscrews. Grout then was placed beneath and around the plate to hold it in position. After alignment, the bottom sections of the deflection pipes were braced to steel angles embedded in the concrete. Subsequent sections of the deflection pipes were also braced after early measurements

indicated that significant displacement of the pipe occurred during placement of concrete when the pipe was not braced.

8. By means of three transits with lines of sight intersecting at the center of the pipe (two parallel and one perpendicular to the lock center line) the position of the bottom section of the deflection pipe was adjusted so that the vertical scribe marks on the first and second couplings were in a vertical line and perpendicular and parallel to the lock center line. From the third coupling up, the transits could not be used because of variations in construction lifts on adjoining monoliths and obstructions such as forms and reinforcing steel. Instead of the transits, two plumb bobs suspended from the top of the added sections of pipe were used to plumb and orient the added sections with respect to the top couplings of the previously placed sections. The couplings were oriented with respect to an X mark inscribed on the couplings. The final position of X was noted; that is, whether the diametric line passing through X was perpendicular or parallel to the center line of the lock. Based on this observation and micrometer measurements made prior to installation, the measured distance between contact rods was established perpendicular and parallel to the center line of the lock. These distances are shown in table B1. The horizontal distances in a N-S direction are perpendicular to the center line of the lock; the distances in an E-W direction are parallel to the center line of the lock.

Table B1

Installation Data for Wall Deflection Pipes

Deflection Pipe No.	Coupling No.	Height Above Coupling No. 1 ft	Horizontal Distance Between Contact Rods* in. N-S	Horizontal Distance Between Contact Rods* in. E-W	Date Concrete Placed Around Coupling
DP-1	1	0	4.709	4.730	19 Nov 58
	2	10.5	4.706	4.718	19 Nov 58
(Mono. 24	3	17.0	4.709	4.726	26 Jan 59
South wall	4	23.0	4.735	4.748	2 Apr 59
Sta	5	29.0	4.734	4.715	2 Apr 59
746+37.75)	6	35.0	4.706	4.729	16 May 59
	7	41.0	4.700	4.732	16 May 59
	8	47.0	4.722	4.733	11 Aug 59
	9	53.0	4.729	4.710	11 Aug 59
	10	60.5	4.694	4.717	2 Oct 59
	11	68.0	4.730	4.740	8 Oct 59
DP-2	1	0	4.694	4.720	19 Nov 58
	2	10.5	4.725	4.713	19 Nov 58
(Mono. 24	3	17.0	4.712	4.735	26 Jan 59
South wall	4	23.0	4.733	4.716	2 Apr 59
Sta	5	29.0	4.738	4.722	2 Apr 59
745+47.75)	6	35.0	4.712	4.731	16 May 59
	7	41.0	4.730	4.752	16 May 59
	8	47.0	4.715	4.690	11 Aug 59
	9	53.0	4.693	4.720	11 Aug 59
	10	60.5	4.707	4.727	2 Oct 59
	11	68.0	4.712	4.726	8 Oct 59
DP-3	1	0	4.704	4.729	30 Dec 58
	2	10.5	4.712	4.726	30 Dec 58
(Mono. 15	3	20.3	4.725	4.698	25 Feb 59
North wall	4	25.3	4.705	4.730	8 Apr 59
Sta	5	30.3	4.704	4.724	8 Apr 59
740+78.75)	6	35.3	4.732	4.717	29 May 59
	7	40.3	4.734	4.716	29 May 59
	8	46.0	4.717	4.698	29 Aug 59
	9	52.0	4.713	4.728	29 Aug 59
	10	58.0	4.694	4.717	6 Oct 59
	11	63.0	4.732	4.737	6 Oct 59
	12	68.0	4.705	4.723	31 Dec 59
DP-4	1	0	4.738	4.723	20 Jan 59
	2	10.5	4.723	4.691	20 Jan 59
(Mono. 15	3	20.3	4.721	4.729	27 Feb 59
South wall	4	25.3	4.750	4.727	9 Apr 59
Sta	5	30.3	4.721	4.706	9 Apr 59
740+78.75)	6	35.3	4.712	4.725	27 May 59
	7	40.3	4.704	4.716	27 May 59
	8	46.0	4.690	4.712	28 Aug 59
	9	52.0	4.712	4.700	28 Aug 59
	10	58.0	4.702	4.717	9 Oct 59
	11	63.0	4.694	4.716	9 Oct 59
	12	68.0	4.758	4.726	31 Dec 59
DP-5	1	0	4.732	4.716	19 Jan 59
	2	10.5	4.733	4.717	19 Jan 59
(Mono. 6	3	20.3	4.732	4.735	10 Mar 59
North wall	4	25.3	4.694	4.720	12 May 59
Sta	5	30.3	4.728	4.715	12 May 59
735+79.25)	6	35.3	4.723	4.756	23 Jun 59
	7	40.3	4.732	4.711	23 Jun 59
	8	46.0	4.742	4.724	11 Aug 59
	9	52.0	4.710	4.733	11 Aug 59
	10	58.0	4.744	4.728	6 Oct 59
	11	62.0	4.699	4.729	6 Oct 59
	12	68.0	4.727	4.708	19 Dec 59
DP-6	1	0	4.706	4.737	5 Feb 59
	2	10.5	4.729	4.749	5 Feb 59
(Mono. 6	3	20.3	4.725	4.713	13 Mar 59
South wall	4	25.3	4.729	4.715	6 May 59
Sta	5	30.3	4.711	4.730	6 May 59
735+76.75)	6	35.3	4.715	4.743	17 Jun 59
	7	40.3	4.704	4.729	17 Jun 59
	8	46.0	4.701	4.679	14 Aug 59
	9	52.0	4.738	4.713	14 Aug 59
	10	58.0	4.705	4.729	30 Sep 59
	11	62.0	4.715	4.698	30 Sep 59
	12	68.0	4.731	4.709	29 Dec 59
DP-7	1	0	4.709	4.734	3 Dec 58
	2	10.5	4.723	4.704	3 Dec 58
(Mono. 2	3	17.0	4.721	4.742	15 Apr 59
South wall	4	23.0	4.680	4.704	9 Jun 59
Sta	5	29.0	4.722	4.697	9 Jun 59
733+87.75)	6	35.0	4.712	4.732	17 Jul 59
	7	41.0	4.719	4.737	17 Jul 59
	8	47.0	4.706	4.689	5 Sep 59
	9	53.0	4.731	4.719	5 Sep 59
	10	60.5	4.704	4.733	11 Nov 59
	11	68.0	4.736	4.717	20 Jan 60
DP-8	1	0	4.704	4.679	3 Dec 58
	2	10.5	4.722	4.708	3 Dec 58
(Mono. 2	3	17.0	4.711	4.721	15 Apr 59
South wall	4	23.0	4.727	4.709	9 Jun 59
Sta	5	29.0	4.725	4.707	9 Jun 59
732+97.75)	6	35.0	4.728	4.705	17 Jul 59
	7	41.0	4.720	4.694	17 Jul 59
	8	47.0	4.706	4.723	5 Sep 59
	9	53.0	4.713	4.734	5 Sep 59
	10	60.5	4.713	4.735	11 Nov 59
	11	68.0	4.711	4.734	20 Jan 60

*Measured with micrometer in WES Machine Shop.

APPENDIX C: RESULTS OF TESTS ON CONCRETE, REINFORCING STEEL, AND SAND BACKFILL

Purpose of Tests

1. Laboratory tests were performed to determine pertinent engineering properties of the concrete and reinforcing steel used in monolith 15. The data obtained from these tests are used to interpret data obtained from the instruments embedded in the concrete base slab and walls of the lock. The data are also used to check certain assumptions made in the design of the lock. Laboratory tests were made to determine the coefficient of thermal expansion, volume change in water, autogenous growth, Poisson's ratio, modulus of elasticity, creep, and compressive and tensile strength of concrete, and modulus of elasticity and tensile strength of reinforcing steel. Additional laboratory tests were performed on cylinders of concrete obtained in the field during construction of monolith 15 to permit a qualitative comparison of the concrete actually used in the structure with that used in the laboratory testing program. In-place density determinations were made of the sand backfill used behind the lock walls, and representative samples were tested in the laboratory to determine the relative density and shear strength of the backfill material.

Laboratory Tests on Concrete

Mixture proportions

2. Concrete specimens were fabricated in the laboratory from materials that were to be used in monolith 15, and the mixture proportions used were those selected for that monolith. The mixture proportions were as follows:

Maximum size of aggregate, in.	1
Sand/total aggregate ratio by weight, %	36
Fineness modulus	2.86
Cement factor, bags per cu yd	5.0

Water-cement ratio by weight	0.48
Water-cement ratio, gal/bag	5.4
Air content, %	5.8
Slump, in.	2-3/4
Bleeding, %	1.8
Portland cement, type (No. 25 C-1)	II
Air-entraining admixture (Air-in, double strength) ml/bag	30

Coefficient of
thermal expansion

3. Five 3-1/2- by 4-1/2- by 16-in. prisms were fabricated for tests to determine linear coefficient of thermal expansion. The tests were conducted at the age of 90 days at a temperature range of 40 to 140 deg F, using Method CRD-C 39.* Each specimen was subjected to ten cycles of heating and cooling. Test results are as follows:

Linear Coefficient of Thermal Expansion (Millionth per deg F)

Specimen No. 3272	Specimen No. 3273	Specimen No. 3274	Specimen No. 3275	Specimen No. 3276	Avg
6.29	6.33	6.22	5.26	6.36	6.30*

* Excluding results of specimen No. 3275 because data were erratic.

The average value of 6.3×10^{-6} per deg F is the value normally expected for concrete of this type, i.e., concrete containing chert coarse aggregate and siliceous sand fine aggregate. Based on the test results shown above, a coefficient of thermal expansion value of 6.3×10^{-6} per deg F was selected to correct data from the strain meters.

4. The coefficient of thermal expansion was also determined on two autogenous length change specimens (6- by 16-in. cylinders) with embedded Carlson concrete strain meters, which were tested in conjunction with creep tests. An average value of 7.2×10^{-6} per deg F was obtained; however, it was considered that this value was not as reliable as that determined using Method CRD-C 39.

---

* All CRD-C test methods mentioned herein can be found in reference 26.

Volume change

5. Six 3-1/2- by 4-1/2- by 16-in. prisms were fabricated for volume (length) change tests. The specimens were measured at ages of 1, 3, 7, 28, 90 days, and one year. Test Method CRD-C 25 and applicable portions of Method CRD-C 56 were used. Volume changes of the specimens are listed below:

Volume Change, Percent (Based on Linear Measurement)					
Specimen No.	3 Days Age	7 Days Age	28 Days Age	90 Days Age	357 Days Age
3267	0	+0.0020	+0.0013	+0.0007	-0.0042
3268	0	-0.0040	0.0000	-0.0146	-0.0063
3269	0	-0.0020	+0.0033	+0.0033	-0.0087
3270	0	-0.0000	-0.0007	-0.0020	-0.0129
3271	0	-0.0007	+0.0020	+0.0020	-0.0042

The test results were somewhat erratic and showed no definite trend either to increase or to decrease with time.

Poisson's ratio

6. Poisson's ratios of five prism specimens were determined at the ages of 3, 7, 28, 90, and 180 days (at the same time that the lengths of specimens were measured). Poisson's ratio was calculated from Young's dynamic modulus of elasticity and the dynamic modulus of rigidity of the specimens, since the value of Poisson's ratio is believed to be independent of the method used. The dynamic (sonic) method, as described in CRD-C 18, was used to determine values of modulus of elasticity and modulus of rigidity. Test results are shown in table C1.

7. Values of Poisson's ratio shown in table C1 fall within the range of values that are usually obtained for this type of test. Poisson's ratio averaged 0.12 at 3 days and 7 days, 0.13 at 28 days, 0.16 at 90 days, and 0.18 at 180 days. The variation in test results may be due to experimental error. A value of Poisson's ratio of 0.18 was selected for use in the analysis of data obtained from the electrical measuring devices.

Modulus of elasticity and compressive strength

8. Thirteen 6- by 12-in. concrete cylinders were fabricated for tests to determine the static modulus of elasticity and compressive

strength. Two specimens were tested at each age of 3, 7, 28, 90, and 180 days. The modulus of elasticity was determined from stress-strain curves using the secant method at a strain of 300 μin./in. Values of modulus of elasticity and compressive strength obtained in the tests are shown in table C1.

9. Values of compressive strength are plotted versus time in fig. C1, and values of modulus of elasticity are plotted versus time in fig. C2. Values of compressive strength vary from about 1400 psi at 3 days to about 4600 psi at 180 days. Also shown for comparison in figs. C1 and C2 are the values obtained from tests on the field cylinders. These values are discussed later in this appendix.

Tensile strength

10. The tensile strength of the concrete was determined by the tensile splitting test on 6- by 12-in. concrete cylinders using Method CRD-C 77. The tensile splitting strengths of two cylinders were determined at each age of 3, 7, 28, 90, and 180 days. Results of the tests are shown in table C1 and are plotted versus time in fig. C1.

Permeability

11. Permeability tests were performed on six 6- by 6-in. concrete cylinders when the cylinders were 90 days old. The tests were performed according to Method CRD-C 48-55. The permeability varied from 120 to 240 ft per min with an average value of 160 ft per min. On the basis of experience with other concretes, the Port Allen Lock concrete was concluded to be of excellent quality as regards permeability.

Creep test

12. Creep tests were performed using Method CRD-C 54 on concrete cylinders 6 in. in diameter by 16 in. long with embedded Carlson concrete strain meters. Creep tests were performed on duplicate sealed specimens at each age of 1, 7, 28, and 90 days. In general, tests were conducted by applying loads of 200 psi to the specimens and measuring the unit length change at various intervals of time by means of the embedded strain meters. Results were reported in terms of unit length change per psi as a function of time. After a test had been completed, a curve of best fit was determined for the test results, the curve being in the form of the equation:

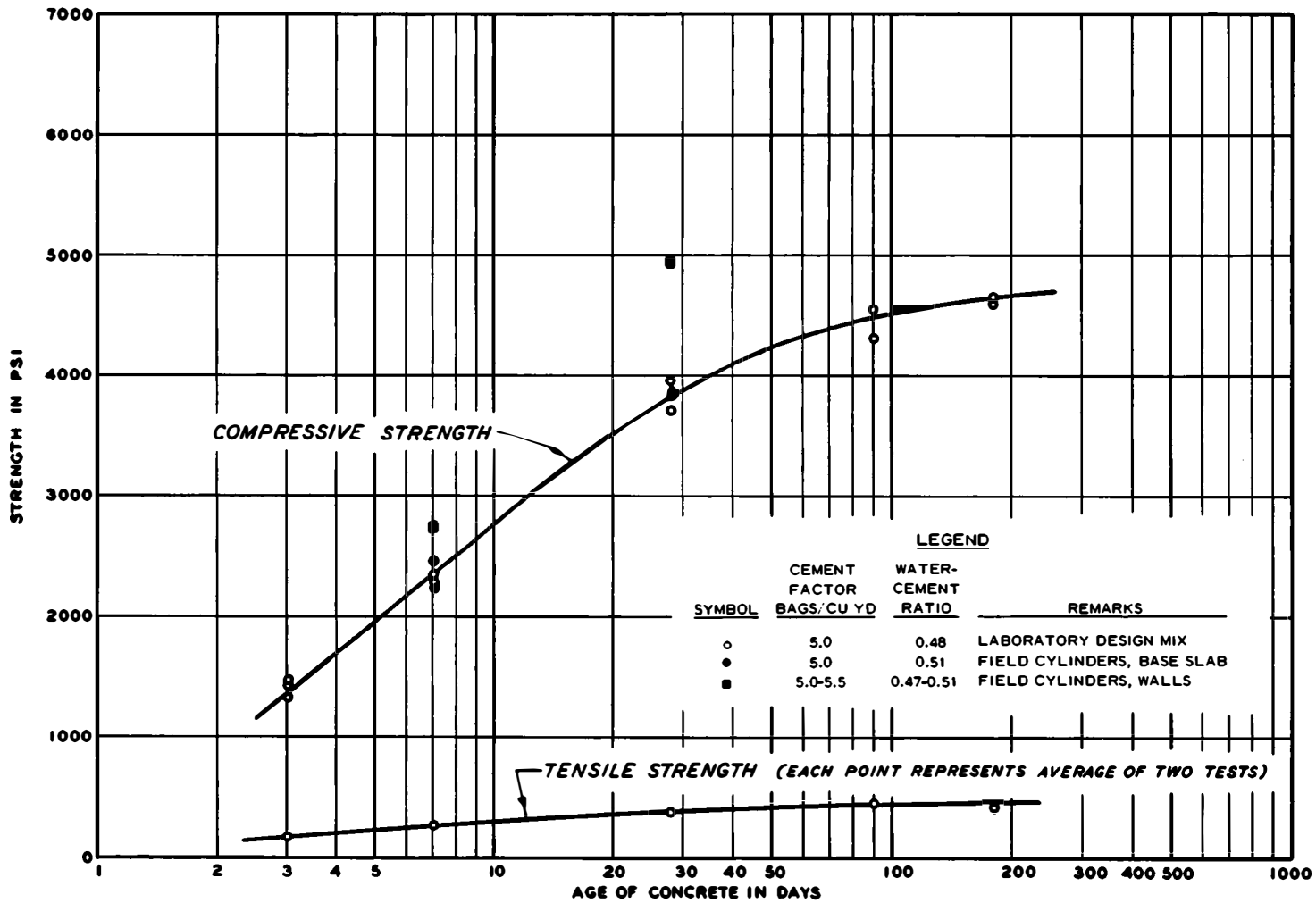

Fig. C1. Compressive strength of concrete versus time

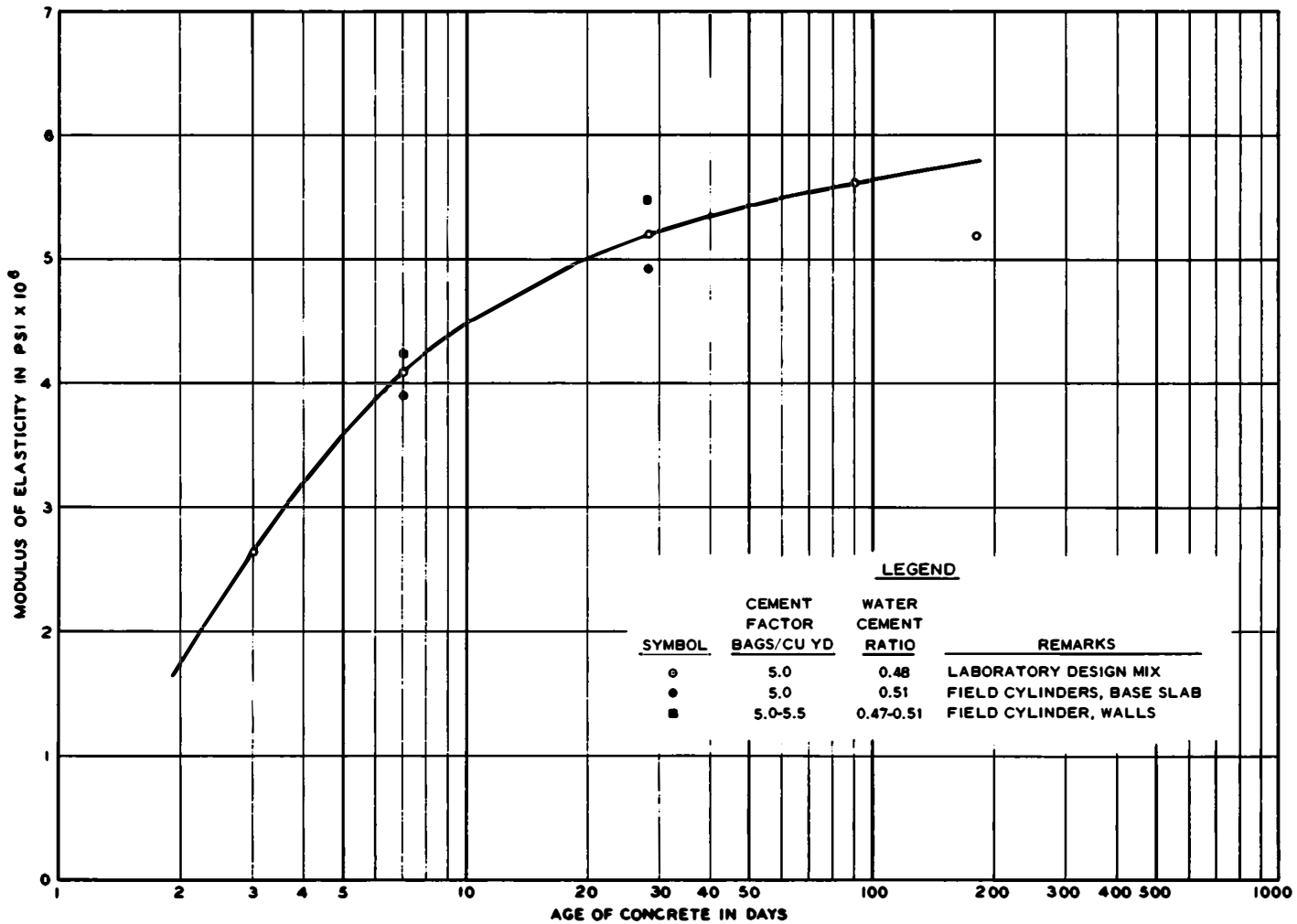

Fig. C2. Modulus of elasticity of concrete versus time

$$\epsilon = 1/E + F(K) \ln (t + 1)$$

where

ϵ = unit length change per psi

$1/E$ = elastic deformation, μin./in.

$F(K)$ = creep constant

t = time after loading in days

13. Autogenous length change measurements were made on two specimens similar to the creep specimens (6- by 16-in. concrete cylinders) on the same days that creep measurements were made so that creep data could be corrected for autogenous length change. Length change measurements were used to correct creep data.

14. Values of $1/E$ and $F(K)$ obtained from each creep test are shown in table C2. Values obtained from tests on similar concrete (sealed and saturated) for Old River Lock are shown for comparison. Arrangements were made for the University of California to conduct similar creep tests (sealed) on concrete containing the same materials as those used at Old River Lock. The results of this independent series of tests are also shown in table C2. All of the test results discussed above are plotted versus time in fig. C3. As can be seen in fig. C3, test results on Port Allen Lock concrete are in good agreement with test results from sealed specimens of Old River Lock concrete and also agree with results of tests conducted by the University of California. Values of $1/E$ for saturated specimens were slightly lower than those for sealed specimens. Values of $F(K)$ were somewhat erratic, and one curve of best fit was drawn for all data. The equations for the curves shown in fig. C3 are as follows:

$$1/E = 0.13 + 0.17K^{-0.75} \text{ (for saturated specimens)}$$

$$1/E = 0.15 + 0.20K^{-0.75} \text{ (for sealed specimens)}$$

$$F(K) = 0.034K^{-0.16} \text{ (for all specimens)}$$

These equations were used to compute stress in the concrete from strain meter readings at Port Allen Lock.

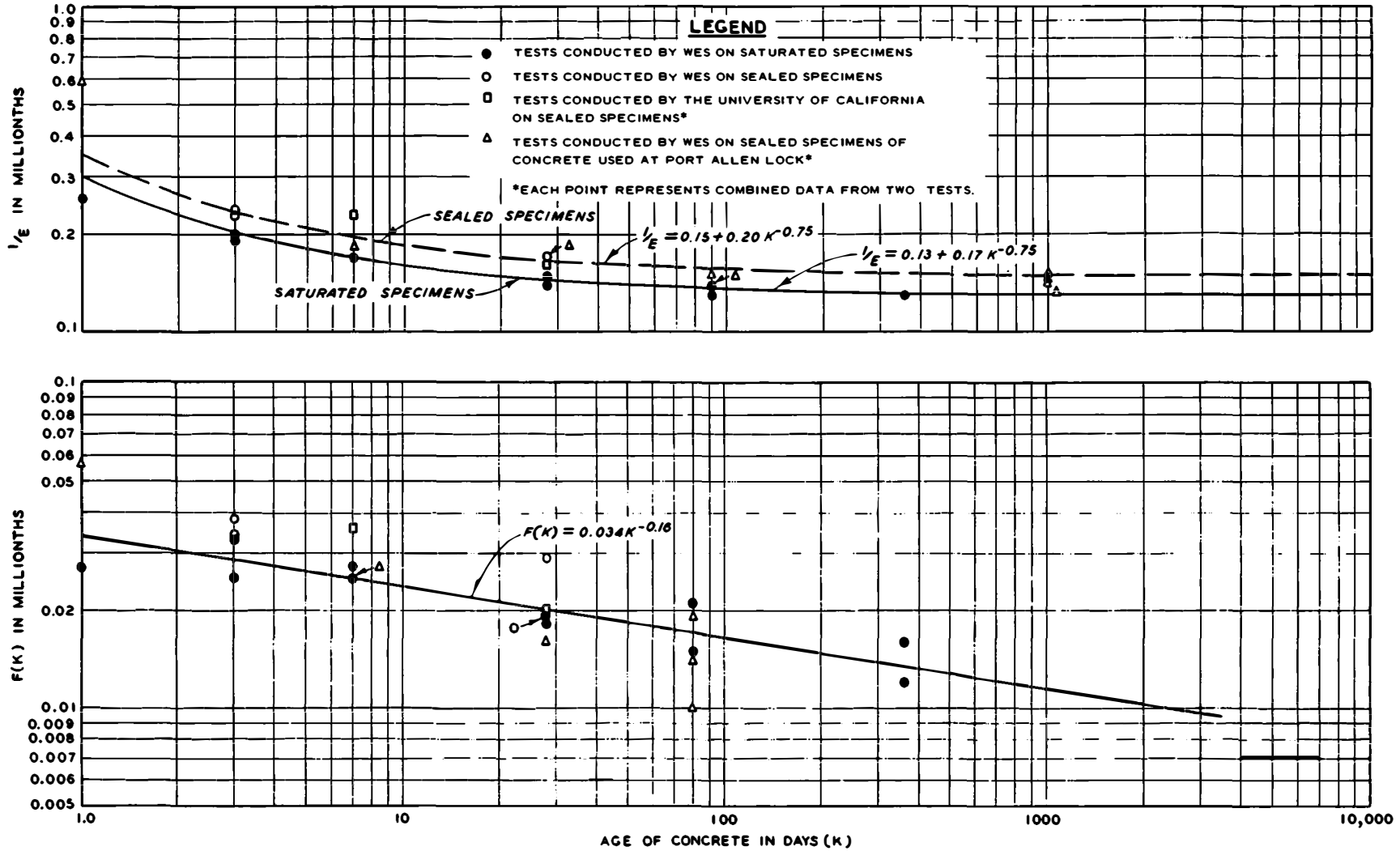

Fig. C3. Laboratory creep data on concrete cylinders

Tests on Reinforcing Steel

15. A limited number of laboratory tests were performed to develop tensile stress-strain data and to determine the modulus of elasticity of the reinforcing steel used in monolith 15 of Port Allen Lock. Six representative samples, two No. 9 bars, two No. 10 bars, and two No. 18 bars, were tested. The steel was turned down to conform with ASTM Designation E-8 and tested in accordance with ASTM Methods A-15 and E-8. Values of tensile strength, yield point, and elongation obtained in the tests are shown in table C3. Values obtained in the modulus of elasticity tests are shown in table C4. The average secant modulus for all specimens was 29.3×10^6 psi. The average chord modulus for all specimens was 29.1×10^6 psi. In analyzing data from electrical measuring devices in the structure, a value of 29.3×10^6 psi was selected for the modulus of elasticity of reinforcing steel.

Tests on Concrete Cylinders

Concrete design

16. Concrete for the base slab and walls of Port Allen Lock was designed for a 28-day compressive strength f'_c of 3000 psi. Materials used in the concrete were as follows:

a. Type II portland cement purchased from the Ideal Cement Company, Baton Rouge, La.

b. Coarse and fine aggregate purchased from the Jahncke Service Company, Buffalo, La., and obtained from the Bluff Creek pit near Clinton, La.

c. An air-entraining admixture, Air-in, purchased from the Hunt Process Company, Ridgeland, Miss.

The maximun size of coarse aggregate used in monolith 15 was 1-1/2 in. The specified gradations of aggregate were as follows:

Fine Aggregate		Coarse Aggregate	
Sieve Size	% Passing by Weight	Sieve Size	% Passing by Weight
No. 4	95-100	1-1/2 in.	100
No. 8	80-90	1 in.	90-97

(Continued)

Fine Aggregate		Coarse Aggregate	
Sieve Size	% Passing by Weight	Sieve Size	% Passing by Weight
No. 16	55-75	1/2 in.	40-60
No. 30	30-60	No. 4	0-6
No. 50	12-30		
No. 100	3-10		

The basic design mixture for the concrete in monolith 15 was as follows:

Cement factor, bags per cu yd	5.0
Water-cement ratio by weight	0.48
Sand/total aggregate ratio by weight, %	36

The design mixture utilized in preparing concrete cylinders for the laboratory tests is described in paragraph 2 of this appendix. Prior to actual construction, the water-cement ratio was increased to 0.51 to provide for better placeability with the equipment used.

Sample preparation

17. Two sets of concrete test cylinders were obtained from each lift of concrete in the base slab of monolith 15 and from each of the first wall lifts. One set of cylinders was obtained from the second, third, fifth, and seventh wall lifts of monolith 15. Each set of cylinders consisted of six 6- by 12-in. standard test cylinders. Information pertinent to the concrete in each set of cylinders was recorded at the structure site. This information, summarized in table C5, included air content, slump, cement factor, and water-cement ratio.

18. Excess bleeding of the concrete was observed during placement of the first wall lift; therefore, beginning with the second wall lift, the water-cement ratio of concrete was reduced to about 0.47 to prevent this condition. Beginning with the third wall lift, the cement factor was increased from 5.0 to 5.5 bags per cu yd in order to produce a more workable concrete to facilitate placement of concrete in the thinner sections of wall.

Laboratory tests

19. Compressive strength and modulus of elasticity. The compressive strength and modulus of elasticity were determined on each concrete

cylinder. The locations of the cylinders are shown in table C5. In each set of six cylinders, three cylinders were tested at the age of 7 days and the other three at 28 days, with the exception of the cylinders from the first lift of the north wall. These latter cylinders apparently were affected by freezing temperatures during storage (see table C5) and, therefore, were not tested for the 28-day strength.

20. Compressive strength and modulus of elasticity determinations are shown in table C5. Results of the 7-day compressive strength tests for the entire monolith, excluding data on cylinders from the first lift of the north wall, range from 2120 to 3140 psi, with an average of 2600 psi and a standard deviation of 256 psi. The results of the 28-day compressive strength tests range from 2860 to 6000 psi, with an average of 4350 psi and a standard deviation of 849 psi.

21. As shown in table C5, the compressive strength and modulus of elasticity values of the concrete in the base slab are somewhat lower than those of the concrete in the walls. Average values are as follows:

	Compressive Strength psi		Modulus of Elasticity psi x 10^{-6}	
	7-day	28-day	7-day	28-day
Concrete in base slab	2483	3489	3.91	4.93
Concrete in wall	2739	4946	4.24	5.49

The reasons for the differences in the values for strength and modulus of elasticity of the concrete in the base slab and wall may be due to (a) the reduction in water-cement ratio and increase in the cement factor in the concrete for the walls, (b) the variation in strength-producing characteristics of different shipments of concrete, or (c) the difference in temperature at the time the concrete was made. Concrete made in cool weather, if cured properly, generally will show higher strengths than concrete made in hot weather. The 28-day compressive strengths for both the walls and the base slab are well above the 28-day compressive strength (f'_c = 3000 psi) assumed for design.

22. The 7- and 28-day compressive strengths of the laboratory prepared cylinders were 2290 and 3850 psi, respectively. Although the water-cement ratio of the laboratory cylinders (0.48) was about equal to that of

the field cylinders from the wall mixture (0.47), higher compressive strength values were obtained for the latter. The field cylinders from the base slab mixture with an average water-cement ratio of about 0.51 indicated compressive strengths somewhat closer to those determined for the laboratory prepared cylinders. In general, however, the compressive strength values of the laboratory and field cylinders are in good agreement. On the basis of the tests described above, it is concluded that the concrete used in the structure is essentially similar to that used in the program of laboratory tests to establish specific properties of the concrete. Therefore, these properties can be applied with confidence to the in-place concrete.

23. Density. The densities of the concrete cylinders from the lock walls were determined to establish a proper value for use in the analytical studies. Density determinations were made prior to conducting other tests. The density was computed from the bulk specific gravity determined in accordance with CRD-C 23-48. The densities determined are shown in table C1 and indicate an average value of 145.8 pcf. In the analytical studies, a value of 146 pcf was used for the concrete throughout monolith 15. Adjustments were made where necessary for the presence of reinforcing steel in the concrete.

Tests on Sand Backfill

Sand backfill

24. A wedge-shaped section of sand backfill was placed behind the walls of the lock structure. The original specifications required that the sand contain less than 5 percent passing the No. 100 sieve. However, sufficient amounts of the specified material could not be obtained locally. Therefore, sand having less than 5 percent passing the No. 200 sieve was used. It was believed that this requirement would also provide a free-draining material. Materials for this backfill consisted of a fine sand obtained from the Mississippi River.

Field compaction

25. Except for the area adjacent to the wall, the backfill was placed in 8-in. layers, and each layer was compacted by two passes of a crawler-type tractor, which was usually a D-7, although a D-8 and D-6 with blade

were used some of the time. Each layer was saturated before it was compacted. Below about el +15, the sand was saturated by flooding and the water level in the sand backfill was adjusted by controlling the downstream outlet of the collector pipe for the backfill drainage system. Sand placed above el +15 was saturated by sprinkling. Backfill within 2 ft of the concrete walls was placed in 8-in. layers and compacted with one of the following three types of compactors: (a) a Wacker "Vibro-Rammer," Model GVR 100-6; (b) an Essick Vibrating Roller (tractor-drawn), Model VR-54-T; and (c) a Jackson Electric Vibratory Compactor. Backfill was placed adjacent to soil stress meters in the walls in 4-in. lifts and compacted by hand-tamping.

Samples obtained

26. During construction, in-place density determinations were made of the sand backfill behind the walls of monoliths 2, 6, 15, and 24. The exact locations from which the samples were taken are shown in fig. C4. Two samples were taken at each location with a 2-in.-OD, 1-7/8-in.-ID by 3-9/32-in.-long drive sampler. Representative material from near the center of the excavation was taken for grain-size analysis by WES. The water content and density of one drive sample were determined in the field laboratory at the lock site. The second sample was sealed in a jar and sent to the New Orleans District (NOD) soils laboratory for water content and density determinations.

27. In addition to the samples mentioned above, two 50-lb sack samples of the sand backfill were sent to WES for shear strength tests.

Laboratory tests

28. Grain-size analysis. Grain-size analyses of all samples were performed in the WES soils laboratory and the results are shown in fig. C5. The grain-size curves fall within a narrow range, indicating a relatively homogeneous backfill. The specifications required that the sand backfill contain not more than 5 percent passing the No. 200 sieve. All but three samples fell within the specified limit.

29. Density and water content determinations. The results of the water content and density determinations made on the 2-in. drive samples by the field laboratory and the NOD soils laboratory are shown in table C6.

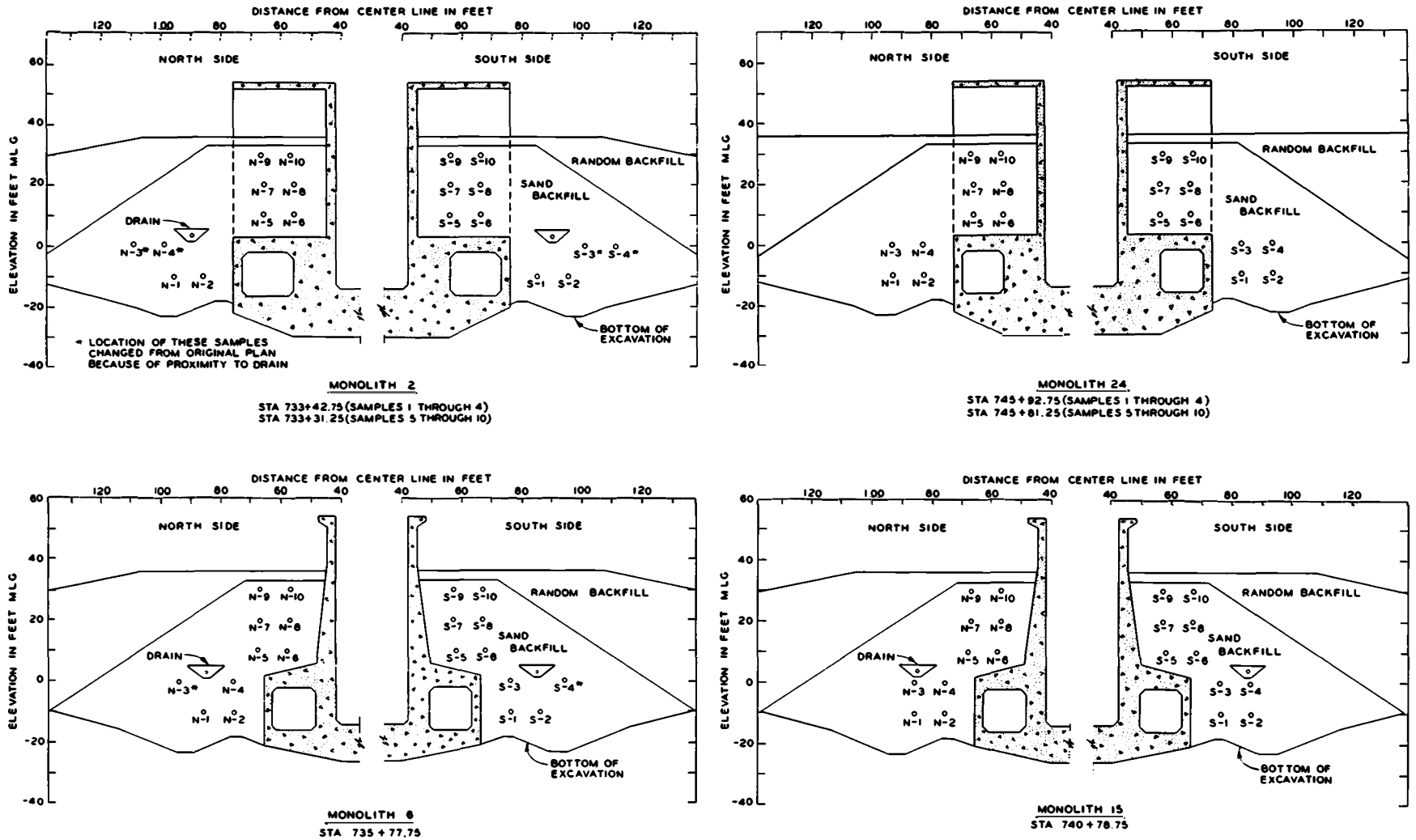

Fig. C4. Locations of sand backfill record samples

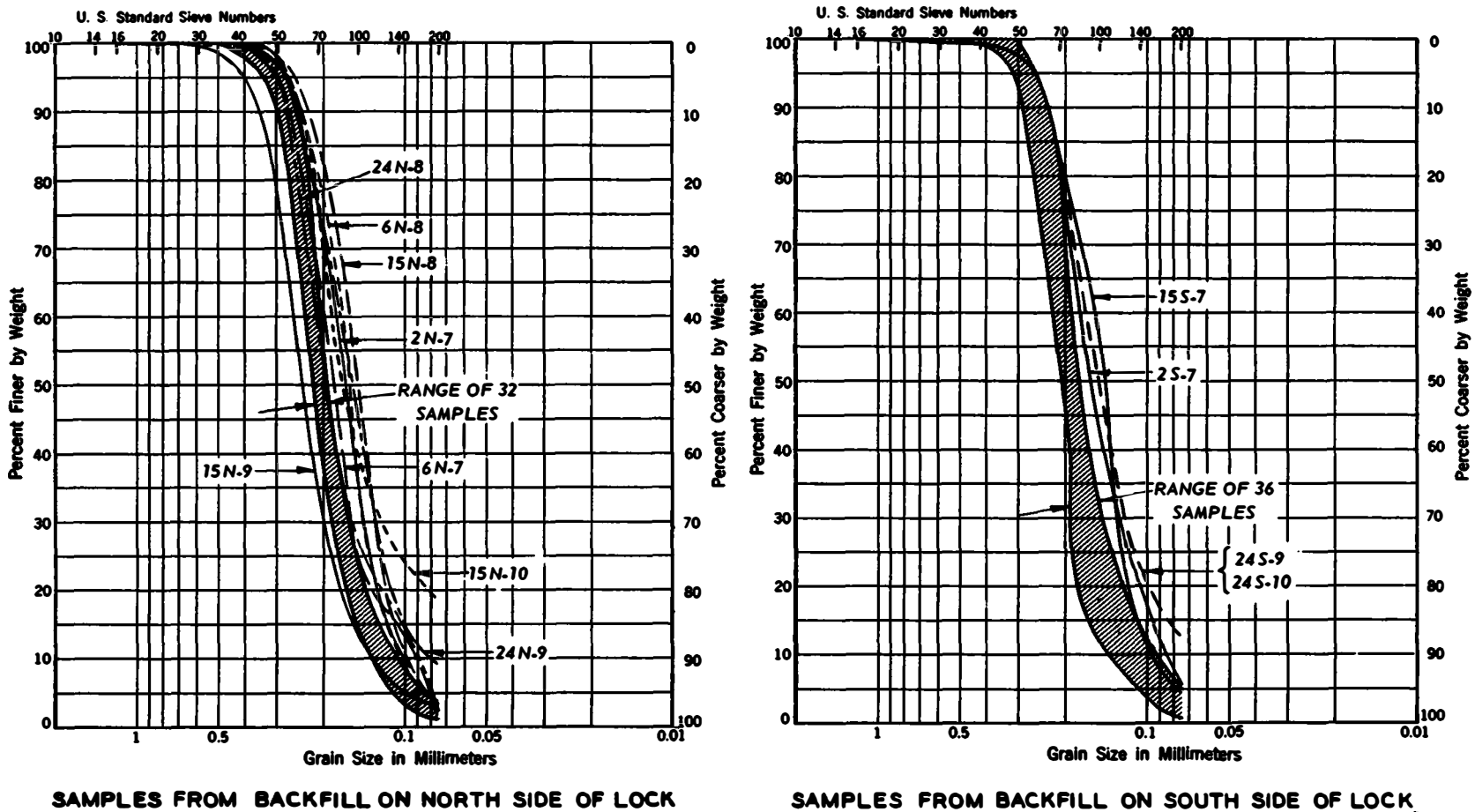

Fig. C5. Grain-size curves

The water content values varied from 6 to 22 percent, and the density values varied from 91 to 106 pcf. The water content values have very little significance for the sands tested inasmuch as the material was free draining. Density values versus elevation are plotted in fig. C6. Also shown

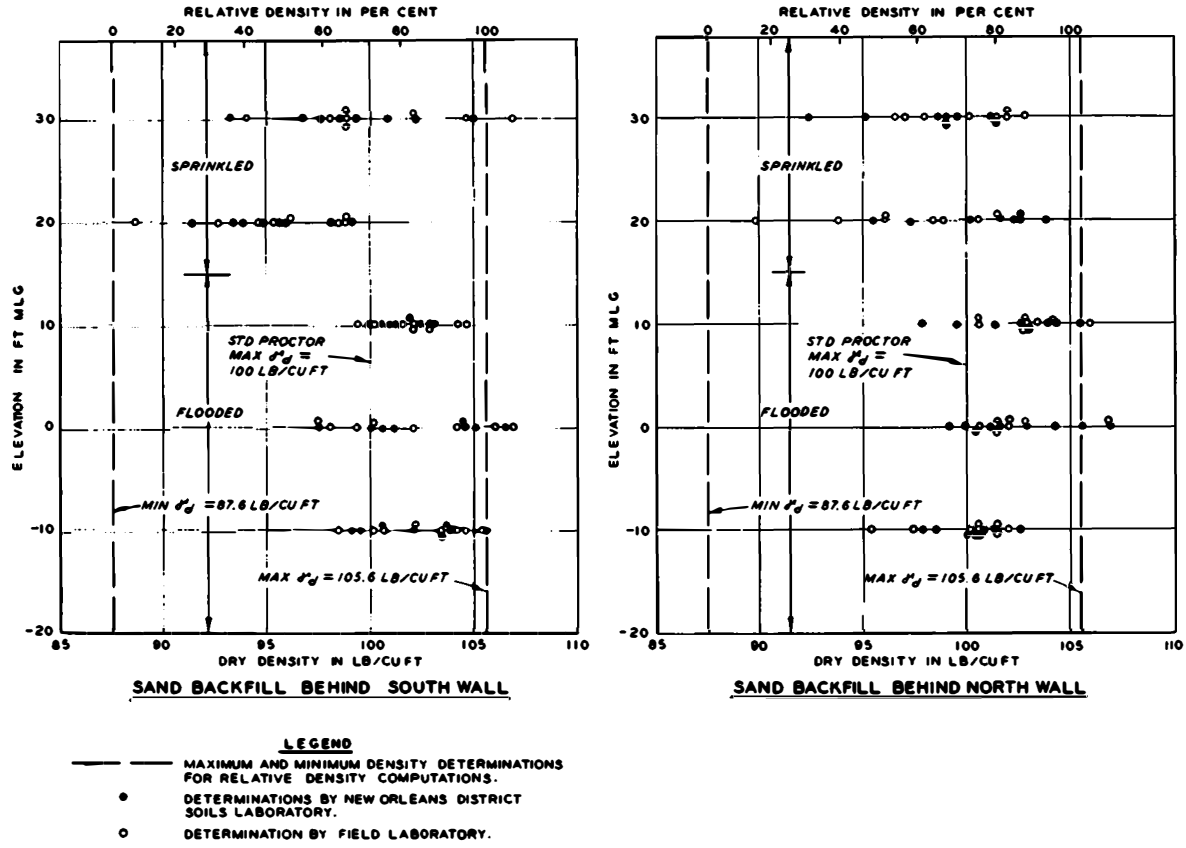

Fig. C6. Density versus elevation

in fig. C6 are the maximum and minimum density values from relative density determinations and the maximum density based on the standard Proctor compaction tests described below. In general, the density values of material below el +15 were substantially higher than those of material above el +15, which indicates that saturation by flooding resulted in somewhat better compaction than sprinkling. The average density of the sand backfill at monolith 15 is about 100 pcf. Comparative tests at Old River Lock indicated that the density obtained by the drive sampler was in the order of 5 pcf less than that obtained by more refined techniques. It is not

known whether this difference would also apply to the sands from Port Allen Lock.

30. Compaction test. A standard Proctor compaction test performed on a representative sample (see fig. C7) indicated a maximum density of

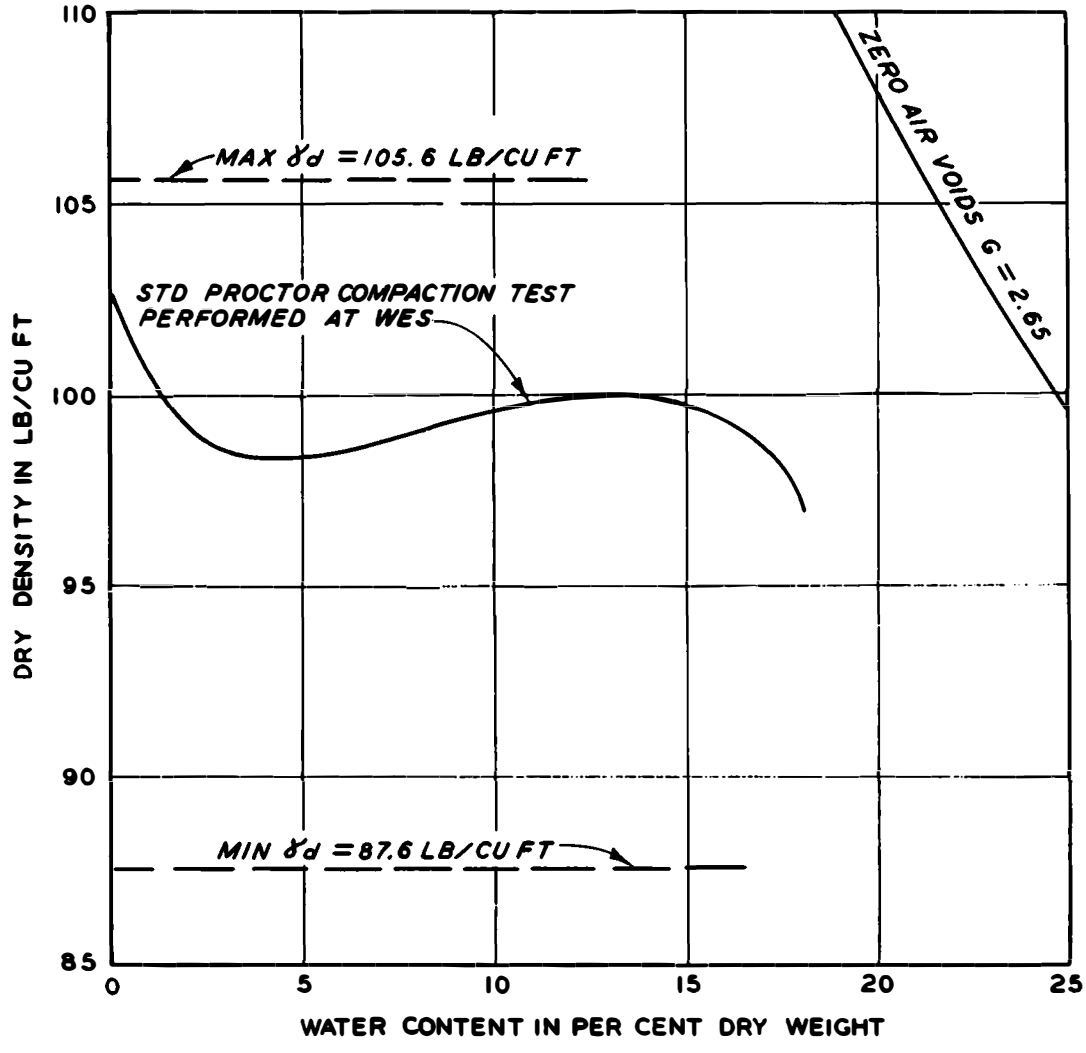

Fig. C7. Results of compaction and maximum and minimum density tests

100 pcf. The percent compaction achieved in the field based on densities determined by the NOD soils laboratory is shown in table C6. The average percent compaction for all the backfill samples was 100. The percent compaction for the samples of backfill behind monolith 15 also averaged 100.

31. Relative density determinations. Maximum and minimum relative

density values were determined on a representative sample of the sand backfill. As shown in fig. C7, the maximum and minimum density values were found to be 105.6 and 87.6 pcf, respectively. The maximum dry density was obtained by compacting ovendry material in three layers of 100 g each in a mold 2 in. in diameter and 4 in. high. Each layer was compacted by 25 blows of a 4-lb hammer that was dropped 12 in. The minimum dry density was obtained by pouring ovendry material through a funnel into the same size mold, keeping the bottom of the funnel approximately 1 in. above the material in the mold. The relative densities computed for the backfill using the field densities determined by the NOD soils laboratory are shown in table C6. The average relative density for all the backfill samples was 74 percent. The average relative density for the samples of backfill behind monolith 15 was 71 percent. Assuming that the actual density is 5 pcf more than that indicated by the drive sampler method, the resulting relative density of the sand backfill behind monolith 15 would be 97 percent.

32. Shear strength tests. Consolidated-drained (S) triaxial compression tests were performed by WES on remolded specimens from the two sack samples of representative sand backfill. The specimens were prepared at dry densities of 95, 100, and 105 pcf. The specimens, which were 2.8 in. in diameter, were saturated under a low confining pressure by allowing water to enter under a low head, and then were tested under drained conditions. The stress-strain curves and Mohr's envelopes for each test are shown in fig. C8. The shear strengths ranged from $\phi = 38.5$ deg for a dry density of about 95.6 pcf to $\phi = 43$ deg for a dry density of about 105.1 pcf.

Shear strength of sand backfill

33. Shear strength (angle of internal friction) versus relative density is plotted in fig. C9. The shear strengths of all field density samples were estimated from this plot, and the results are shown in table C6. The estimated shear strengths of the samples varied from $\phi = 37.5$ deg to $\phi = 43.5$ deg , with an average of 40.5 deg. In computations involved in the analysis of data from the instrumentation program, a shear strength of $c = 0$, $\phi = 40$ deg was selected for the sand backfill behind the walls.

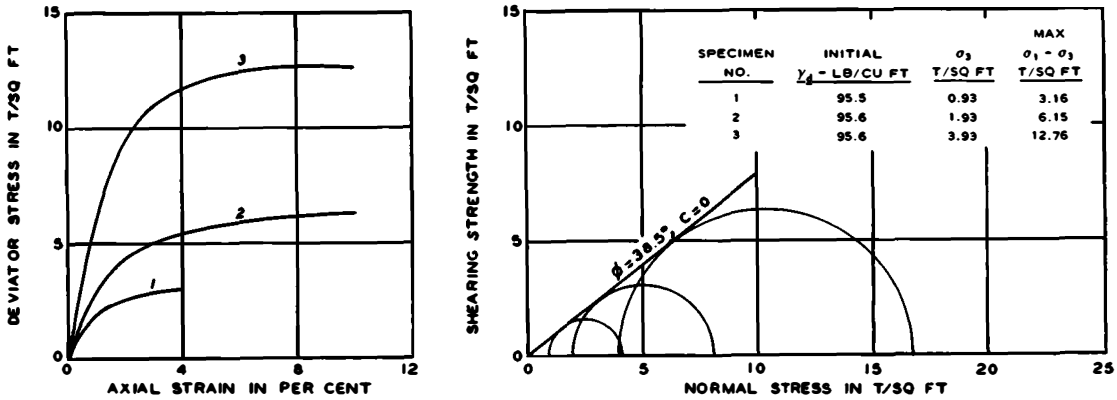

SHEAR STRENGTH AT RELATIVE DENSITY=49.0 PER CENT (95.6 LB/CU FT)

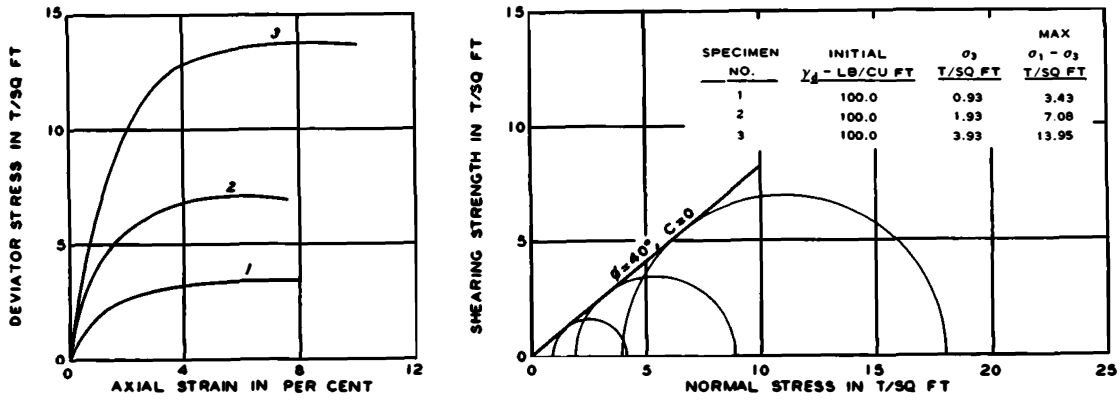

SHEAR STRENGTH AT RELATIVE DENSITY=72.6 PER CENT (100.0 LB/CU FT)

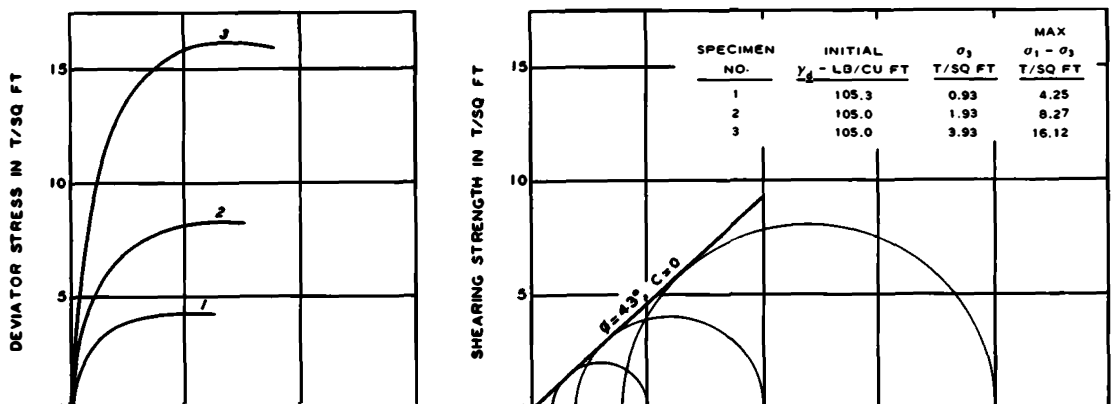

SHEAR STRENGTH AT RELATIVE DENSITY=97.5 PER CENT (105.1 LB/CU FT)

NOTE: ALL TESTS PERFORMED ON SATURATED SPECIMENS UNDER DRAINED CONDITIONS.
SPECIMENS WERE 2.8 IN. DIAM BY 6.5 IN. HIGH.

Fig. C8. Shear strength test data

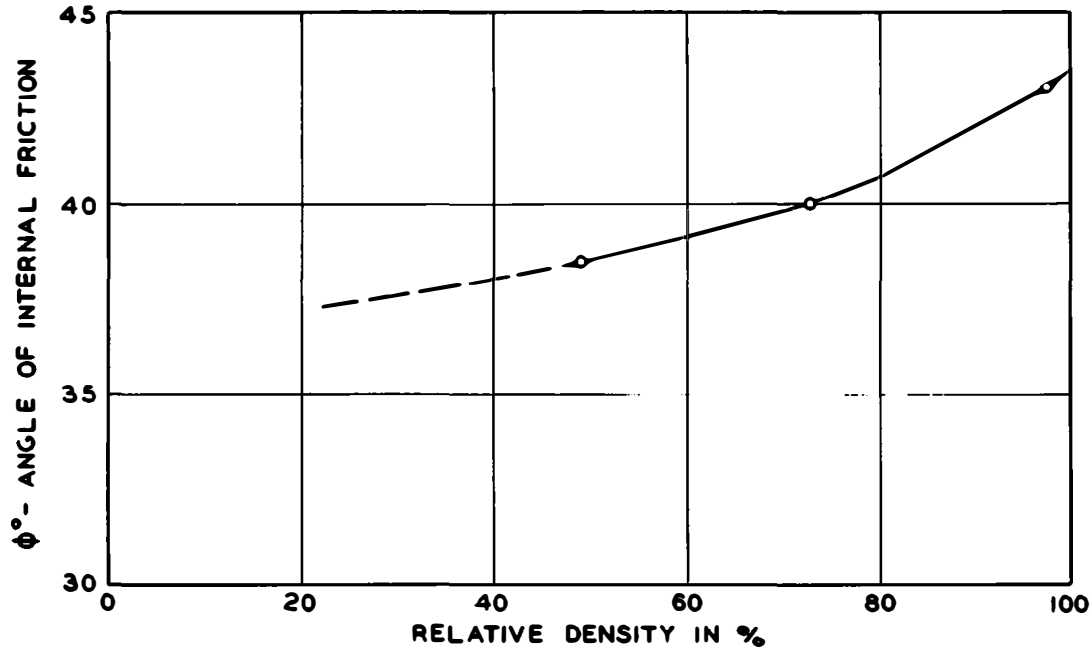

TEST	AVG γ_d	RELATIVE DENSITY	$\phi°$
1	95.6	49.0	38.5°
2	100.0	72.6	40.0°
3	105.0	97.5	43.0°

Fig. C9. Relation between shear strength and relative density

Table C1

Results of Laboratory Strength Tests on Concrete

Specimen No.	3 Days Age			7 Days Age			28 Days Age			90 Days Age			180 Days Age		
	E	G	μ	E	G	μ	E	G	μ	E	G	μ	E	G	μ
Results of Dynamic Tests															
3277	4.96	2.19	0.13	5.69	2.52	0.13	6.53	2.83	0.15	6.86	2.91	0.18	6.94	2.92	0.19
3278	5.00	2.28	0.10	5.76	2.65	0.09	6.58	3.00	0.10	6.93	3.02	0.15	6.92	2.96	0.17
3279	4.90	2.19	0.12	5.65	2.59	0.09	6.44	2.88	0.12	6.82	3.02	0.13	6.85	2.95	0.16
3280	4.99	2.21	0.13	5.74	2.57	0.12	6.58	2.95	0.12	6.89	3.03	0.14	6.97	3.01	0.16
3281	5.14	2.26	0.14	6.03	2.62	0.15	6.79	2.94	0.15	7.15	3.04	0.18	7.23	2.99	0.21
Avg	5.00	2.23	0.12	5.77	2.59	0.12	6.58	2.92	0.13	6.93	3.00	0.16	6.98	2.97	0.18

Results of Static Compression and Tension Splitting Tests

	Compression Tests			Tension Splitting Tests	
Age, Days	Specimen No.	Modulus of Elasticity 10^6 psi	Compressive Strength, psi	Specimen No.	Tensile Strength psi
3	9135	2.65	1460	--	--
	9136	2.75	1410	9125	175
	9137	2.60	1310	9126	175
7	9138	4.20	2350	--	--
	9139	3.95	2280	9127	255
	9140	4.15	2240	9128	270
28	9141	5.10	3870	--	--
	9142	5.20	3710	9129	385
	9143	5.33	3970	9130	400
90	9144	5.67	4310	9131	455
	9145	5.58	4550	9132	455
180	9146	5.15	4640	9133	390
	9147	5.25	4590	9134	420

Note: For dynamic tests, E denotes dynamic modulus of elasticity in 10^6 psi; G denotes dynamic modulus of rigidity in 10^6 psi; and μ denotes dynamic Poisson's ratio.

Table C2

Results of Laboratory Creep Tests

Age of Concrete at Time of Loading days	Load psi	1/E in Millionths: Old River Concrete WES*	1/E in Millionths: Old River Concrete Univ of Calif**	1/E in Millionths: Port Allen Concrete WES**	F(K) in Millionths: Old River Concrete WES*	F(K) in Millionths: Old River Concrete Univ of Calif**	F(K) in Millionths: Port Allen Concrete WES**
			Sealed Specimens				
1	200	--	--	0.60	--	--	0.057
3	200	0.23	--	--	0.038	--	--
		0.24	--	--	0.034	--	--
7	200	--	0.23	0.18	--	0.036	0.025
28	200	0.17	0.16	0.17	0.029	0.020	0.016
		0.17	--	--	0.019	--	--
90	200	--	--	0.14	--	--	0.010
90	400	--	--	0.14	--	--	0.019
90	600	--	--	0.15	--	--	0.014
			Saturated Specimens				
1	200	0.26	--	--	0.027	--	--
		0.26	--	--	0.027	--	--
3	200	0.19	--	--	0.025	--	--
		0.20	--	--	0.025	--	--
7	200	0.17	--	--	0.025	--	--
		0.17	--	--	0.027	--	--
28	200	0.14	--	--	0.019	--	--
		0.15	--	--	0.018	--	--
90	200	0.13	--	--	0.015	--	--
		0.14	--	--	0.021	--	--
360	200	0.13	--	--	0.016	--	--
		0.13	--	--	0.012	--	--

* Functions were computed independently for each of two specimens.

** Functions were computed using combined data on duplicate specimens.

Table C3

Strength Tests of Reinforcing Bars

Bar No.	Turned Diameter in.	Area sq in.	Yield Point psi	Ultimate Stress psi	Elongation in 8 in. percent
9-A	1.064	0.8866	47,400	86,300	17.2
9-B	1.000	0.7854	47,600	80,600	18.0
10-A	1.125	0.9940	45,600	84,200	16.4
10-B	1.125	0.9940	43,800	82,400	16.4
18-A	2.000	3.1416	39,800	76,700	25.0
18-B	2.000	3.1416	41,400	76,700	25.0

Table C4

Modulus of Elasticity Determinations for Reinforcing Bars

Total Load, lb	Stress psi	Modulus* Secant	Modulus* Chord	Total Load, lb	Stress psi	Modulus Secant	Modulus Chord
	No. 9-A Bar				No. 9-B Bar		
10,000	11,280	30.2	30.2	5,000	6,365	28.7	28.7
20,000	22,560	31.1	32.0	10,000	12,730	29.1	29.5
30,000	33,840	30.0	28.1	15,000	19,100	29.4	29.7
40,000	45,115	29.4	27.8	20,000	25,465	29.6	30.6
				25,000	31,830	29.7	30.0
				30,000	38,200	29.7	30.0
				35,000	44,565	29.6	28.7
	Avg	30.2	29.5			29.4	29.6
	No. 10-A Bar				No. 10-B Bar		
5,000	5,030	30.3	30.3	5,000	5,030	29.6	29.6
10,000	10,060	30.5	30.7	10,000	10,060	29.8	29.9
15,000	15,090	29.9	28.9	15,000	15,090	29.9	30.3
20,000	20,120	29.8	29.2	20,000	20,120	29.8	29.2
25,000	25,150	29.3	27.9	25,000	25,150	29.9	30.7
30,000	30,180	--	--	30,000	30,180	30.2	31.8
35,000	35,210	--	--	35,000	35,210	20.2	29.8
40,000	40,240	28.8	--	40,000	40,240	30.1	29.6
	Avg	29.8	29.4			28.7	30.1
	No. 18-A Bar				No. 18-B Bar		
20,000	6,365	30.3	30.3	20,000	6,365	29.6	29.6
40,000	12,730	29.9	29.5	40,000	12,730	29.5	29.5
60,000	19,100	30.0	30.3	60,000	19,100	29.3	28.9
80,000	25,465	29.1	26.7	80,000	25,465	28.9	27.9
100,000	31,830	28.6	26.5	100,000	31,830	28.8	28.2
120,000	38,200	27.7	23.9	120,000	38,200	27.7	23.5
	Avg	29.3	27.9			29.0	27.9

* Modulus of elasticity in 10^6 psi.

Table C5

Summary of Compressive Strength Tests on Concrete Placed in Monolith 15

Lift Location	Date Placed	Cement Factor bags/yd	Water Cement Ratio	Air Content, %	Slump, in.	7-Day Strength				28-Day Strength			
						Cylinder No.	Density pcf	Elastic Modulus psi x 10^{-6}	Compressive Strength psi	Cylinder No.	Density pcf	Elastic Modulus psi x 10^{-6}	Compressive Strength psi
Base Slab													
1st lift	13 June 58	5.0	0.51	5-1/4 to 5-3/4	3 to 3-1/4	1	--	4.20	2290	2	--	4.50	2860
						3	--	3.85	2170	4	--	4.45	2960
						5	--	3.85	2190	6	--	4.85	3230
						9	--	3.55	2120	8	--	4.70	3360
						11	--	3.75	2320	10	--	4.65	3450
						13	--	3.85	2180	12	--	4.95	3430
2d lift	21 Aug 58	5.0	0.51	5-1/4 to 5-1/2	2-3/4 to 3	5	--	3.45	2680	8	--	5.15	3550
						6	--	3.50	2480	9	--	4.70	3750
						7	--	3.80	2480	10	--	4.60	3680
						15	--	3.65	2620	18	--	5.00	3910
						16	--	3.30	2510	19	--	4.80	4180
						17	--	3.80	2500	20	--	4.80	4040
3d lift	16 Oct 58	5.0	0.51	5-1/2 to 5-3/4	2 to 2-3/4	5	--	4.17	2430	8	--	5.03	4230
						6	--	4.03	2430	9	--	5.03	3800
						7	--	4.13	2640	10	--	5.27	4300
						15	--	4.24	2860	18	--	5.27	5110
						16	--	4.53	2710	19	--	5.50	4870
						17	--	4.77	3090	20	--	5.40	4570
					Avg			3.91	2483			4.93	3849
Walls													
1st lift north (inside)	30 Dec 58	5.0	0.51	5-3/4	3-1/2	5	147.0	2.90*	1490*	-	--	--	--
						6	146.4	3.33*	1620*	-	--	--	--
						7	147.0	3.12*	1660*	-	--	--	--
						8	146.4	2.97*	1460*	-	--	--	--
						9	146.4	2.95*	1530*	-	--	--	--
						10	145.8	2.90*	1480*	-	--	--	--
1st lift south (inside)	20 Jan 59	5.0	0.51	5-1/4	3	5	146.4	4.33	2880	8	146.4	5.73	5300
						6	146.4	4.30	2520	9	145.8	5.87	5450
						7	146.4	4.20	2690	10	147.0	5.73	5230
2d lift north	26 Feb 59	5.0	0.48	5-1/4	3	5	146.5	4.47	2820	8	146.9	5.71	5800
						6	147.2	4.50	2840	9	147.2	6.09	5930
						7	146.8	4.37	2700	10	147.4	5.95	6000
3d lift north	8 Apr 59	5.5	0.47	5	3	5	145.3	4.35	2720	8	146.9	5.69	4520
						6	145.7	4.40	2780	9	145.8	5.62	4610
						7	145.6	4.46	3140	10	146.5	5.91	4640
5th lift south	28 Aug 59	5.5	0.47	5	3	5	145.3	4.37	3000	8	145.0	4.92	3710
						6	145.9	4.19	2700	9	145.0	4.94	3800
						7	145.4	4.17	2770	10	145.1	5.04	4010
7th lift north	31 Dec 59	5.5	0.47	5-1/2	3-1/4	5	144.8	3.65	2440	8	143.7	4.97	4980
						6	142.8	4.10	2610	9	143.9	5.18	5070
						7	142.6	3.80	2480	10	144.3	5.00	5140
					Avg		145.8	4.24	2739		145.8	5.49	4946

* Samples subjected to freezing temperatures during storage and therefore they are not included in averages.

Table C6

Results of Tests on Sand Backfill Record Samples

Sample No.	Station	Offset from ℄ ft*	Elevation ft mlg	D_{10} Size mm	In Place γ_d, pcf **	In Place γ_d, pcf †	Water Content % **	Water Content % †	Percent Compaction	Relative Density %	Est Shear Strength ∅
					Monolith 2						
N-1	733+42.75	96-N	-10.0	0.12	102.6	100.7	18.2	18.7	103	86	41.3
N-2	733+42.75	86-N	-10.0	0.12	97.8	97.4	22.0	22.2	98	61	39.3
N-3	733+42.75	109-N	0	0.12	101.6	102.0	17.6	15.8	102	80	40.7
N-4	733+42.75	99-N	0	0.12	105.6	106.9	17.9	16.4	106	100	43.0
N-5	733+31.25	66-N	10.0	0.11	105.5	106.0	14.5	8.9	106	100	43.0
N-6	733+31.25	56-N	10.0	0.11	104.3	104.2	19.3	16.9	104	93	42.3
N-7	733+31.25	66-N	20.0	0.10	103.8	93.9	15.7	8.6	104	91	42.0
N-8	733+31.25	56-N	20.0	0.11	102.6	93.4	17.4	7.2	103	86	41.3
N-9	733+31.25	67-N	30.0	0.14	101.2	102.0	18.1	17.1	101	79	40.6
N-10	733+31.25	57-N	30.0	0.12	98.6	94.7	11.9	14.3	99	65	39.5
				Average	102.4	100.1	17.3	14.6	103	84	41.3
S-1	733+42.75	86-S	-10.0	0.14	105.6	105.5	17.3	17.9	106	100	43.5
S-2	733+42.75	96-S	-10.0	0.12	102.1	103.4	13.9	13.0	102	83	41.0
S-3	733+42.75	101-S	0	0.12	105.1	104.2	15.9	16.9	105	98	43.0
S-4	733+42.75	111-S	0	0.13	106.5	106.0	15.8	15.2	106	102	44.0
S-5	733+31.25	56-S	10.0	0.12	103.1	104.2	18.0	15.6	103	88	41.6
S-6	733+31.25	66-S	10.0	0.11	102.8	102.0	17.4	17.1	103	87	41.5
S-7	733+31.25	56-S	20.0	0.08	93.4	94.7	13.7	10.0	93	36	37.8
S-8	733+31.25	66-S	20.0	0.11	95.9	95.3	10.2	7.0	96	50	38.6
S-9	733+31.25	57-S	30.0	0.12	96.7	98.8	19.0	19.2	97	54	38.8
S-10	733+31.25	67-S	30.0	0.07	102.2	104.7	18.2	15.4	102	83	41.0
				Average	101.3	101.9	15.9	14.7	101	78	41.1
					Monolith 6						
N-1	735+77.75	86-N	-10.0	0.13	98.5	100.7	19.8	20.0	98	64	39.4
N-2	735+77.75	76-N	-10.0	0.14	100.5	100.1	19.0	18.9	100	75	40.2
N-3	735+77.75	94-N	0	0.11	102.9	102.8	17.2	18.4	103	87	41.5
N-4	735+77.75	76-N	0	0.12	104.3	106.9	16.7	15.2	104	94	42.5
N-5	735+77.75	68-N	10.0	0.11	102.7	102.8	21.5	17.1	103	86	41.3
N-6	735+77.75	58-N	10.0	0.10	97.8	100.7	16.2	12.0	98	61	39.2
N-7	735+77.75	67-N	20.0	0.10	95.5	89.9	5.6	7.5	96	48	38.5
N-8	735+77.75	57-N	20.0	0.10	100.2	96.1	12.2	7.0	100	73	40.0
N-9	735+77.75	67-N	30.0	0.07	99.1	102.0	8.8	5.3	99	67	39.1
N-10	735+77.75	57-N	30.0	0.06	99.1	101.5	13.5	9.3	99	67	39.1
				Average	100.1	100.3	15.0	13.1	100	72	40.1
S-1	735+77.75	76-S	-10.0	0.12	103.8	104.2	17.5	15.6	104	91	42.0
S-2	735+77.75	86-S	-10.0	0.12	103.5	100.7	17.7	16.9	104	90	41.8
S-3	735+77.75	76-S	0	0.11	100.0	106.9	20.6	13.9	100	72	40.0
S-4	735+77.75	94-S	0	0.12	104.6	99.3	14.7	18.8	105	95	42.6
S-5	735+77.75	58-S	10.0	0.13	102.3	104.7	16.4	17.9	102	84	41.1
S-6	735+77.75	68-S	10.0	0.13	99.9	100.1	14.1	13.5	100	72	40.0
S-7	735+77.75	57-S	20.0	0.11	94.8	96.1	10.0	5.6	95	44	38.2
S-8	735+77.75	67-S	20.0	0.11	91.4	88.6	10.0	7.6	91	24	37.4
S-9	735+77.75	57-S	30.0	0.09	98.5	98.8	12.7	12.3	98	64	39.4
S-10	735+77.75	67-S	30.0	0.09	97.6	98.0	11.7	9.8	98	60	39.2
				Average	99.6	99.7	14.5	13.2	100	70	40.2

(Continued)

Note: Percent compaction based on standard Proctor maximum dry density of 100 pcf. Estimated shear strength based on shear strength plot in fig. C9. Percent compaction, relative density, and estimated shear strength were computed using dry density determinations made by New Orleans District Laboratory.

* N and S denotes north and south side of lock, respectively.

** Determined in New Orleans District Laboratory.

† Determined in field laboratory.

Table C6 (Concluded)

Sample No.	Station	Offset from ℄ ft*	Elevation ft mlg	D_{10} Size mm	In-Place γ_d, pcf **	In-Place γ_d, pcf †	Water Content % **	Water Content % †	Percent Compaction	Relative Density %	Est Shear Strength ∅
					Monolith 15						
N-1	740+78.75	86-N	-10.0	0.12	100.6	101.5	18.2	14.7	101	75	40.2
N-2	740+78.75	76-N	-10.0	0.14	101.3	95.3	18.9	23.9	101	79	40.6
N-3	740+78.75	86-N	0	0.12	101.2	100.7	19.0	18.7	101	79	40.6
N-4	740+78.75	76-N	0	0.11	99.9	101.5	20.6	21.3	100	72	40.0
N-5	740+78.75	68-N	10.0	0.10	101.4	102.8	17.8	15.8	101	80	40.7
N-6	740+78.75	58-N	10.0	0.12	99.6	100.7	14.1	14.7	100	70	39.8
N-7	740+78.75	67-N	20.0	0.12	97.3	93.9	8.2	7.1	97	58	38.5
N-8	740+78.75	57-N	20.0	0.11	102.3	96.1	12.0	9.8	102	84	41.1
N-9	740+78.75	67-N	30.0	0.13	95.1	96.6	8.4	5.6	95	46	38.3
N-10	740+78.75	57-N	30.0	--	101.4	102.8	14.3	14.5	101	80	40.7
				Average	100.0	99.2	15.2	14.6	100	72	40.0
S-1	740+78.75	76-S	-10.0	0.12	99.1	100.1	19.2	20.3	99	68	39.7
S-2	740+78.75	86-S	-10.0	0.12	103.7	104.7	17.7	16.7	104	90	41.8
S-3	740+78.75	76-S	0	0.13	100.6	100.1	19.4	18.9	101	75	40.2
S-4	740+78.75	86-S	0	0.12	104.4	102.0	16.7	19.7	104	94	42.5
S-5	740+78.75	58-S	10.0	0.13	100.5	102.0	18.5	19.7	100	75	40.2
S-6	740+78.75	68-S	10.0	0.12	101.2	101.5	16.7	12.0	101	79	40.6
S-7	740+78.75	57-S	20.0	0.10	99.7	98.8	11.2	8.2	96	49	38.5
S-8	740+78.75	67-S	20.0	0.11	93.8	92.7	9.5	8.7	94	38	38.0
S-9	740+78.75	57-S	30.0	0.10	105.0	106.9	9.0	10.1	105	97	42.9
S-10	740+78.75	67-S	30.0	0.09	93.2	94.0	10.8	8.6	93	35	37.8
				Average	99.7	100.3	15.1	14.3	100	70	40.2
					Monolith 24						
N-1	745+92.75	93-N	-10.0	0.12	100.0	102.0	19.0	18.4	100	72	40.0
N-2	745+92.75	83-N	-10.0	0.12	100.7	101.5	16.9	16.0	101	76	40.3
N-3	745+92.75	93-N	0	0.12	99.1	102.1	19.4	17.1	99	68	39.7
N-4	745+92.75	83-N	0	0.12	100.5	101.5	18.4	18.7	100	75	40.2
N-5	745+81.25	66-N	10.0	0.12	103.0	103.4	18.5	16.9	103	88	41.6
N-6	745+81.25	56-N	10.0	0.11	103.9	102.8	18.5	19.7	104	92	42.1
N-7	745+81.25	66-N	20.0	0.12	101.6	100.7	16.6	10.7	102	80	40.7
N-8	745+81.25	56-N	20.0	0.10	102.6	101.5	16.7	12.0	103	85	41.2
N-9	745+81.25	67-N	30.0	0.08	99.6	98.0	14.2	10.9	100	70	39.8
N-10	745+81.25	57-N	30.0	0.09	92.4	100.1	12.6	10.8	92	30	37.6
				Average	100.3	101.4	17.1	15.1	100	74	40.3
S-1	745+92.75	83-S	-10.0	0.12	100.5	98.4	18.9	20.8	101	75	40.2
S-2	745+92.75	93-S	-10.0	0.12	99.5	102.0	18.7	18.4	100	70	39.8
S-3	745+92.75	83-S	0	0.12	97.5	97.4	20.8	20.8	98	59	38.5
S-4	745+92.75	93-S	0	0.12	101.2	98.0	19.9	20.5	101	78	40.5
S-5	745+81.25	56-S	10.0	0.13	100.8	102.8	15.4	17.1	101	77	40.4
S-6	745+81.25	66-S	10.0	0.12	101.8	99.3	17.2	17.6	101	82	40.9
S-7	745+81.25	56-S	20.0	0.12	98.1	98.8	15.8	19.2	98	62	39.3
S-8	745+81.25	66-S	20.0	0.11	99.1	98.0	14.9	19.2	99	68	39.7
S-9	745+81.25	57-S	30.0	0.09	99.3	98.8	17.1	13.7	99	69	39.8
S-10	745+81.25	67-S	30.0	0.06	100.8	102.0	17.3	14.5	101	77	40.4
				Average	99.9	99.6	17.6	18.2	100	72	40.0

** Determined in New Orleans District Laboratory.
† Determined in field laboratory.

Distribution List

Address	No. of Copies
Lower Mississippi Valley Division	60
Office Chief of Engineers	60

Unclassified

Security Classification

DOCUMENT CONTROL DATA - R & D

(Security classification of title, body of abstract and indexing annotation must be entered when the overall report is classified)

1. ORIGINATING ACTIVITY (Corporate author)
U. S. Army Engineer Waterways Experiment Station
Vicksburg, Mississippi

2a. REPORT SECURITY CLASSIFICATION
Unclassified

2b. GROUP

3. REPORT TITLE

ANALYSIS OF DATA FROM INSTRUMENTATION PROGRAM, PORT ALLEN LOCK

4. DESCRIPTIVE NOTES (Type of report and inclusive dates)
Final report

5. AUTHOR(S) (First name, middle initial, last name)
Walter C. Sherman, Jr.
Charles C. Trahan

6. REPORT DATE	7a. TOTAL NO. OF PAGES	7b. NO. OF REFS
September 1968	239	26

8a. CONTRACT OR GRANT NO.	9a. ORIGINATOR'S REPORT NUMBER(S)
b. PROJECT NO.	Technical Report S-68-7
c.	9b. OTHER REPORT NO(S) (Any other numbers that may be assigned this report)
d.	

10. DISTRIBUTION STATEMENT
This document has been approved for public release and sale; its distribution is unlimited.

11. SUPPLEMENTARY NOTES	12. SPONSORING MILITARY ACTIVITY
	Office, Chief of Engineers Washington, D. C.

13. ABSTRACT

Port Allen Lock is a reinforced concrete U-frame structure located on the west bank of the Mississippi River near Baton Rouge, La. The lock chamber was designed for a trapezoidal distribution of base pressure. This distribution was determined by a trial method in which the plastic and elastic deformation of the base slab and the corresponding deformation of soil foundation were computed for various assumed base pressure distributions until the desired agreement between structure and soil deformations was obtained. The lock chamber was instrumented to obtain engineering data for use in design of similar structures and to determine the validity of the design assumptions. Measurements were made of earth and hydrostatic pressures beneath the base slab and along the walls of the lock and of stresses and strains within the base slab and walls of the lock. The settlement of the lock was determined at various locations, and deflections of the walls were determined by means of wall deflection pipes and a deflectometer. Observed rebounds were greater than those predicted in design; observed settlements were less than those predicted in design. Observed base pressures differed from the total structure load, and the difference was attributed to frictional soil forces acting on the outer sides of the lock. Computations of base pressures and moments from theoretical consideration of a beam on an elastic foundation were in poor agreement with actual base pressures and moments computed from observed loads.

DD FORM 1 NOV 68 1473 REPLACES DD FORM 1473, 1 JAN 64, WHICH IS OBSOLETE FOR ARMY USE.

Unclassified

Security Classification

14. KEY WORDS	LINK A		LINK B		LINK C	
	ROLE	WT	ROLE	WT	ROLE	WT
Foundations						
Locks						
Port Allen Lock						
Instrumentation						
Pressure measurement						
Soils--Settlement						